Injury Criteria for the THOR 50th Male ATD

Matthew Craig, Daniel Parent, Ellen Lee, Rodney Rudd, Erik Takhounts

Human Injury Research Division
National Highway Traffic Safety Administration

Vikas Hasija

Bowhead Logistics Solutions

TABLE OF CONTENTS

SUMMARY

HEAD – NHTSA intends to use the head injury criterion (HIC_{15}) as a metric for assessing head injury risk in frontal crashes. It is currently in use in FMVSS No. 208 and frontal NCAP tests (Eppinger et al. 1999, NHTSA, 2008). As described in the 2008 NCAP Final Decision Notice, the risk curve associated with HIC_{15} in frontal NCAP testing represents a risk of AIS 3+ injury. However, while HIC_{15} injury assessment values in frontal NCAP testing have continued to decrease over time as have the field incidence of skull and facial fractures, the incidence of traumatic brain injury in frontal crashes has not decreased at a similar rate (Takhounts et al. 2013). This may be because the HIC_{15} criterion only addresses linear acceleration of the head, which does not completely describe the motion of and subsequent injury risk to the brain. To assess the risk of brain injury due to rotation of the head, Takhounts et al. (2013) developed a kinematically-based brain injury criterion (BrIC). BrIC is calculated by combining the angular velocities of the head about its three local axes compared to directionally dependent critical values. BrIC was one of many brain injury correlates that were considered and was found to have the highest correlation to two strain metrics measured in the brain. These strain metrics, cumulative strain and maximum principal strain, are the mechanical measures that have been shown to be directly associated with brain injury potential (Takhounts et al. 2003, Takhounts 2015).

Injury Criterion: HIC_{15}

$$p(AIS \geq 2) = \Phi\left[\frac{\ln HIC_{15} - 6.96362}{0.84687}\right] \quad (1)$$

$$p(AIS \geq 3) = \Phi\left[\frac{\ln HIC_{15} - 7.45231}{0.73998}\right] \quad (2)$$

where:

$$HIC_{15} = \left.\left|(t_2 - t_1)\left[\frac{1}{t_2 - t_1}\int_{t_1}^{t_2} a(t)dt\right]^{2.5}\right|\right|_{max} \quad (3)$$

$$for\ t_2 - t_1 \leq 15\ milliseconds$$

Injury Criterion: $BrIC$

$$P(AIS\ 3+) = 1 - e^{-\left(\frac{BrIC - 0.523}{0.531}\right)^{1.8}} \quad (4)$$

$$P(AIS\ 4+) = 1 - e^{-\left(\frac{BrIC - 0.523}{0.647}\right)^{1.8}} \quad (5)$$

where:

$$BrIC = \sqrt{\left(\frac{\omega_x}{\omega_{xC}}\right)^2 + \left(\frac{\omega_y}{\omega_{yC}}\right)^2 + \left(\frac{\omega_z}{\omega_{zC}}\right)^2} \quad (6)$$

$$\omega_{xC} = 66.25\,rad/s,\ \omega_{yC} = 56.45\,rad/s,\ \omega_{zC} = 42.87\,rad/s$$

NECK – NHTSA intends to use a modified, THOR-specific version of the neck injury criterion (Nij) as a metric for assessing neck injury in frontal crashes. In addition, a tension-only risk function is being presented. The formulation of Nij will be retained, but the critical values have been updated to specifically represent the THOR-50M anthropomorphic test device (ATD). Based on a comprehensive review of available experimental data, the current effort is proposing a human cadaver-based set of critical intercepts that have been adjusted based on the enhanced biofidelity of the THOR-50M ATD. These critical values are based on measurements from the upper neck load cell alone: 4200 N in tension, 6400 N in compression, 88.1 Nm in flexion, and 117 Nm in extension. As the cadaver-based values

represent a “relaxed” human, this is a conservative estimate of injury risk because it does not account for additional resistance to tension provided by neck musculature (Dibb et al., 2006).

Injury Criterion:
Peak Neck Tension

$$p(AIS \geq 3) = \frac{1}{1 + e^{(5.5763 - 0.00132 F_T)}} \quad (7)$$

Injury Criterion:
Nij

$$p(AIS \geq 2) = \frac{1}{1 + e^{(4.3085 - 5.4079 N_{ij})}} \quad (8)$$

$$p(AIS \geq 3) = \frac{1}{1 + e^{(4.9372 - 4.5294 N_{ij})}} \quad (9)$$

CHEST – NHTSA intends to use a multi-point thoracic injury criterion to predict chest injury for the THOR-50M ATD. A relationship was sought between the measurements available in the thorax of the THOR and PMHS-observed injury through a series of matched-pair sled tests conducted in 14 conditions. Incidence of injury was quantified as AIS 3+ skeletal thoracic injury to the PMHS, which represents three or more fractured ribs based on the 2005 (update 2008) version of AIS. The matched set of post-mortem human surrogate (PMHS) tests included 18 non-injury observations and 30 injury observations. Of the available thoracic measurements, the peak resultant deflection, calculated using the maximum of the peak resultant chest deflections from the four 3D IR-TRACC assemblies in the THOR rib cage, was selected as the most reasonable predictor. Age was determined to be a significant covariate in the prediction of injury, but not mass, stature, or sex. The resulting risk function, assuming an age of 40 to represent the mean age of exposed male drivers in frontal crashes, is shown in Equation (10).

Injury Criterion:
Peak Resultant Chest Deflection

$$p(AIS \geq 3) = 1 - e^{-\left(\frac{R_{max}}{59.865}\right)^{2.7187}} \quad (10)$$

ABDOMEN – NHTSA intends to use a measurement of peak abdominal deflection measured by the abdomen IR-TRACC instrumentation to predict abdominal injury for the THOR-50M ATD. This injury criterion is based on testing of porcine surrogates by Kent et al. (2008), who found percent compression to be the best injury discriminator out of the considered metrics. A risk function was developed to relate the peak compression of the THOR-50M ATD abdomen, measured using bi-lateral 3D IR-TRACC assemblies in the lower abdomen, to the risk of AIS 3+ abdomen injury (see Equation (11)).

Injury Criterion:
Peak Abdomen Compression

$$p(AIS \geq 3) = \frac{1}{1 + e^{(7.849 - 0.0886 \delta_{max})}} \quad (11)$$

PELVIS – NHTSA intends to use an acetabulum load criteria to assess potential pelvis injuries with the THOR-50M ATD. Rupp et al. (2009) developed a post-mortem human surrogate (PMHS) injury risk function to relate the force transmitted to the hip, the stature of the occupant, the hip flexion angle, and the hip abduction angle to the risk of a hip fracture. The data used to develop this risk function were re-evaluated herein, and it was confirmed that either sex or stature have a significant contribution to the risk function, and while hip flexion angle is confirmed as a significant covariate, abduction angle was not. The relationship between the force transmitted to the hip of the PMHS and the acetabulum force measured in the THOR-50M ATD is developed based the ratio of applied force at the knee to measured force at the femur load cell and the ratio of measured force at the femur load cell and the resultant force measured at the acetabulum load cell. The proposed risk function considers both stature and flexion angle as covariates, and relates the peak resultant acetabulum force measured with the THOR-

50M ATD to the risk of hip fracture. The resulting risk function is shown in Equation (12), assuming stature of 178 centimeters to represent a 50th percentile male and a flexion angle of 15 degrees to represent the nominal flexion angle in a belted frontal crash for both PMHS and THOR.

Injury Criterion:
Peak Resultant Acetabulum Force

$$p(Hip\ Fracture) = \Phi\left[\frac{\ln 1.429F_{AR} - 1.6058}{0.2339}\right] \quad (12)$$

KNEE/FEMUR – NHTSA intends to use peak femur axial force as a metric for assessing knee/femur injury risk in frontal crashes. As currently used in FMVSS No. 208 and frontal NCAP, the injury risk function does not account for the difference between the applied force at the knee of the PMHS used to develop the risk function and the peak axial compression force measured at the femur load cell of the ATD. A correction factor is applied to the peak axial compression force measured at the femur load cell of the THOR-50M ATD to account for this difference, resulting in the risk of AIS 2+ knee and knee/femur injury shown in Equation (13).

Injury Criterion:
Peak Axial Femur Force

$$p(AIS\ 2+) = \frac{1}{1 + e^{5.7949 - 0.6748F_{LC}}} \quad (13)$$

LEG – NHTSA intends to use injury risk curves developed for the human lower extremity and applied to the lower extremity hardware of the THOR-50M ATD. NHTSA developed injury risk curves for the prediction of tibia plateau fractures using the axial force measured by the upper tibia load cell; tibia/fibula shaft fractures using the resultant moment calculated using measurements from the upper and lower tibia load cells; and distal tibia, calcaneus, talus, ankle, and midfoot fractures using the axial force measured by the lower tibia load cell. The axial load criteria address the most common injury mechanism for many of the leg structures. The combined stress approach represented by the Tibia Index and Revised Tibia Index was not pursued for the THOR-50M ATD because the simplified approach of using only the resultant moment was deemed sufficient for predicting mid-shaft fracture given the existence of the proximal and distal axial load criteria. Assessing fracture risk based on the resultant moment will address bending occurring in the leg from external loading sources and ankle rotation.
The upper tibia axial force risk function is:

Injury Criterion:
Upper Tibia Axial Force

$$p(AIS \geq 2) = \frac{1}{1 + e^{(5.6654 - 0.8189F_{upper\ tibia})}} \quad (14)$$

Where $F_{upper\ tibia}$ is the largest compressive z-axis force, in kN, measured in the left and right upper tibia of the THOR-50M ATD.
The lower tibia axial force risk function is:

Injury Criterion:
Lower Tibia Axial Force

$$p(AIS \geq 2) = \frac{1}{1 + e^{(3.9121 - 0.48F_{lower\ tibia})}} \quad (15)$$

Where $F_{lower\ tibia}$ is the largest compressive z-axis force, in kN, measured in the left and right lower tibia of the THOR-50M ATD.

The tibia bending moment risk function is:

Injury Criterion:
Tibia Bending Moment

$$p(tibia\ fracture) = 1 - e^{-e^{\left(\frac{lnM_{RES} - 5.8492}{0.2965}\right)}} \quad (16)$$

Where M_{res} is the largest resultant moment, in Nm, calculated from the x-axis and y-axis moments measured in the left and right upper and lower tibia of the THOR-50M ATD.

Table S1. Summary of THOR-50M Injury Measures and Values at 10, 25 and 50% Risk.

Injury Measure	AIS Severity Level	10% Risk	25% Risk	50% Risk
BrIC	2	0.62	0.69	0.79
	3	0.68	0.79	0.96
	4	0.71	0.85	1.05
HIC_{15}	2	357	597	1,057
	3	668	1,046	1,724
Neck Tension (N)	3	2,704	3,397	4,090
Nij	2	0.39	0.59	0.80
	3	0.60	0.85	1.09
Chest Deflection (mm)*	3	26.2	37.9	52.3
Abdomen Deflection (mm)	3	63.8	76.2	88.6
Acetabulum Force (N)	2	2,583	2,977	3,486
Femur Force (N)	2	5,331	6,960	8,588
Upper Tibia Force (N)	2	4,235	5,577	6,918
Lower Tibia Force (N)*	2	3,573	5,861	8,150
Tibia Moment (Nm)	2	178	240	311

*Age set to 40 per GES/CDS analysis of front row occupant age trends

1 INTRODUCTION

This report describes in detail the methods and results for deriving injury measures and associated injury risk functions planned for use with the *T*est device for *H*uman *O*ccupant *R*estraint (THOR) 50th percentile male anthropomorphic test device (ATD), here forward referred to as THOR-50M. The THOR-50M is frontal crash test dummy that the National Highway Traffic Safety Administration (NHTSA) has planned for use in NHTSA's New Car Assessment Program (NCAP) (NHTSA,2015b).

1.1 Real-world Data

Vehicle safety performance assessment and associated predictions for injury and fatality risk are influenced by three main areas: (1) the condition the vehicle is tested in; (2) the quality of the tools (e.g. test dummies) used in the testing and how well they represent humans; and (3) the injury measures used to estimate the risk of different injuries as applied together with (1) and (2). Item (3) is the focus of this report as it relates to the THOR-50M.

Despite prior/current efforts (standardized tests, test devices or ATDs, injury measures), significant societal harm remains in frontal crashes. Figure 1.1 shows the last 15 years of fatality data sourced from NHTSA's Fatal Analysis Reporting System (FARS). FARS provides an annual nationwide census of fatalities resulting from motor vehicle crashes.

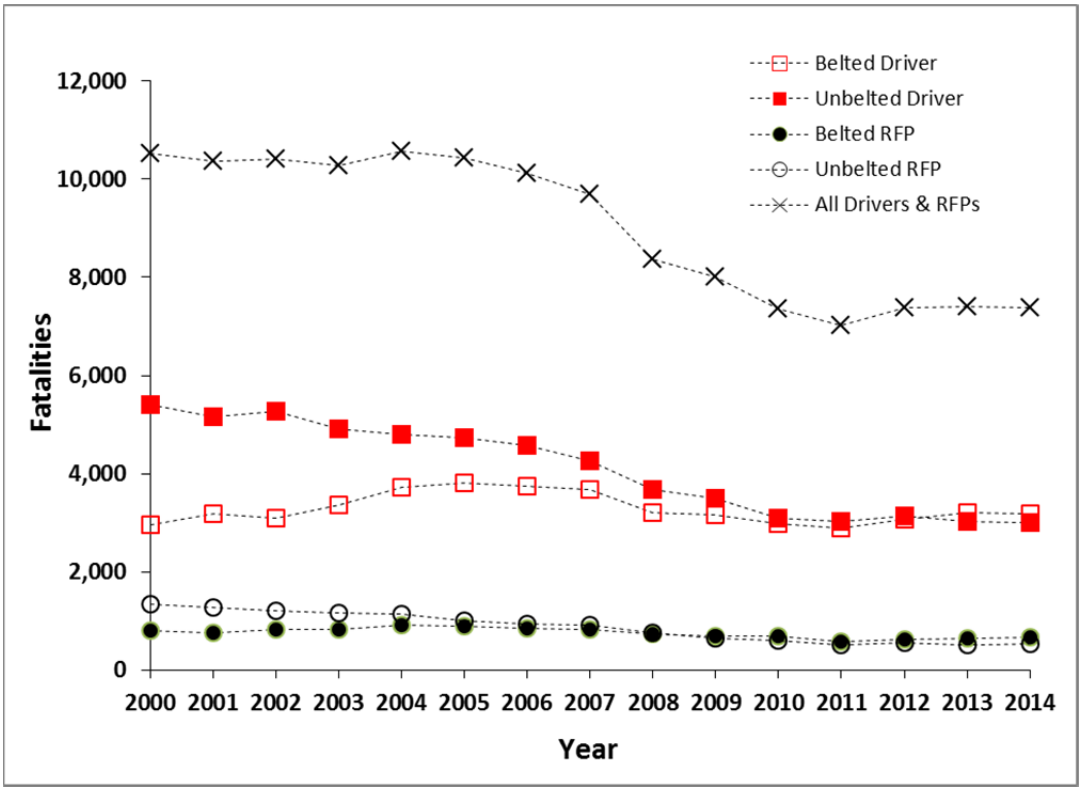

Figure 1.1. Frontal crash fatalities - belted and unbelted drivers and right front passengers (*belted cases coded as wearing lap and shoulder belt; unbelted includes cases coded as no belt, shoulder or lap belt only, incorrect use and unknown use); FARS 2000-2014*

The National Automotive Sampling System – Crashworthiness Data System (NASS-CDS) was queried for case years 2000 to 2014 in summarizing the total number of injuries by body region at the maximum Abbreviated Injury Scale (MAIS) 2+ and 3+ severity level for AIS version 1990 (1998 update) (AAAM, 1998) by occupant (Table 1.1). Each occupant is only counted once per body region as appropriate and can be counted more than once if multiple body regions are injured at the 2+ and/or 3+ severity level. The results are presented for all occupants and then separately by driver and right front passenger. Driver and right front passenger is further broken down by belted and unbelted occupants. Table 1.2 presents the same type of data but shows total injury counts for each body region. In this case, occupants could have multiple injuries represented at the 2+ and 3+ severity level for a body region/injury grouping.

Table 1.1. NASS-CDS 2000 to 2014 Frontal Crashes – Weighted MAIS totals by Body Region.

		Frontal Crashes - NASS-CDS 2000-2014[1]								
		Body Region MAIS Counts								
		All Occupants[2]			Belted Drivers / Right Front Passengers[3]			Unbelted Drivers / Right Front Passengers[3]		
Severity	Body Region	*Pt*	*Lwr*	*Upr*	*Pt*	*Lwr*	*Upr*	*Pt*	*Lwr*	*Upr*
	TOTAL	1,151,211	791,001	1,511,421	695,351	524,001	866,702	271,366	140,745	401,987
	Head/Face	389,732	236,020	543,444	159,072	110,807	207,338	131,953	62,399	201,506
	Skull/Facial Fracture	83,480	56,734	110,226	18,800	14,618	22,982	32,856	23,206	42,506
	Brain	331,440	192,391	470,489	145,369	99,814	190,923	109,118	41,943	176,294
	Neck	62,471	34,468	90,475	29,663	14,438	44,888	17,612	6,067	29,157
	Spinal Cord	6,489	3,360	9,617	2,288	1,094	3,481	2,689	494	4,883
	Osteoligamentous	52,607	25,438	79,775	24,550	8,368	40,732	14,586	5,591	23,581
	Thorax	256,969	157,338	356,599	155,767	107,187	204,348	58,108	29,924	86,291
	Rib cage/Sternum	204,067	136,950	271,185	132,777	92,288	173,266	45,564	22,415	68,713
	Lungs	73,866	28,327	119,406	30,089	14,365	45,812	20,857	10,833	30,880
	Heart	7,956	5,220	10,691	2,252	920	3,583	4,200	2,517	5,884
MAIS 2+	**Abdomen**	84,125	56,019	112,231	36,396	27,156	45,637	28,973	16,742	41,204
	Vessels/Nerves	2,733	557	4,909	1,073	323	1,823	1,323	0	3,033
	Skin/Tissue/Muscle	163	5	320	119	0	255	21	0	68
	Organs	83,906	56,086	111,726	36,383	27,125	45,641	28,939	16,713	41,164
	Solid	70,816	45,794	95,837	28,045	21,943	34,148	27,004	14,916	39,091
	Hollow	13,515	8,330	18,700	6,920	2,788	11,052	2,983	899	5,067
	Other	12,932	9,417	16,447	7,483	4,853	10,113	3,203	2,069	4,337
	Lower Ext	454,415	298,181	610,648	297,792	177,988	417,597	111,666	76,580	146,752
	Knee/Thigh/Hip	218,653	180,144	257,162	119,791	87,654	151,928	70,553	51,730	89,376
	Tibia/Fibula	164,777	129,277	200,277	107,506	89,912	125,099	39,382	21,450	57,314
	Foot/Ankle	179,337	31,928	326,745	142,717	5,076	280,358	27,846	15,002	40,691
	Upper Ext	291,093	213,159	369,027	185,442	122,001	248,882	62,222	34,577	89,866
	TOTAL	371,277	234,712	507,842	169,402	129,895	208,909	127,180	56,114	198,247
	Head/Face	93,924	40,950	146,898	26,437	16,997	35,876	45,022	3,000	87,044
	Skull/Facial Fracture	26,589	18,195	34,982	5,738	3,986	7,491	10,680	7,324	14,035
	Brain	79,871	32,595	127,148	22,567	13,539	31,595	38,865	0	78,734
	Neck	24,623	10,400	38,846	10,096	4,931	15,261	8,272	559	15,984
	Spinal Cord	6,489	3,360	9,617	2,288	1,094	3,481	2,689	494	4,883
	Osteoligamentous	16,560	4,546	28,574	6,951	733	13,170	4,891	0	9,827
	Thorax	146,908	81,257	212,559	67,266	44,193	90,340	45,401	23,418	67,384
	Rib cage/Sternum	81,891	53,030	110,753	38,568	21,015	56,122	27,957	13,896	42,018
	Lungs	73,290	27,609	118,970	29,998	14,293	45,703	20,419	10,275	30,563
	Heart	6,481	3,221	9,740	2,056	747	3,365	3,184	711	5,657
MAIS 3+	**Abdomen**	29,126	15,608	42,644	14,056	8,386	19,726	8,206	3,976	12,436
	Vessels/Nerves	2,733	557	4,909	1,073	323	1,823	1,323	0	3,033
	Skin/Tissue/Muscle	12	0	37	12	0	37	0	0	0
	Organs	28,091	15,194	40,987	13,599	8,055	19,143	7,931	3,934	11,928
	Solid	22,221	12,514	31,928	9,991	6,954	13,027	6,887	2,618	11,156
	Hollow	5,620	2,517	8,724	2,358	715	4,001	1,574	0	3,440
	Other	2,973	1,334	4,612	1,988	374	3,603	679	177	1,182
	Lower Ext	128,571	101,745	155,396	60,274	50,776	69,773	47,903	34,360	61,445
	Knee/Thigh/Hip	89,579	66,456	112,702	36,943	29,614	44,273	36,552	23,623	49,481
	Tibia/Fibula	49,616	39,867	59,366	29,234	22,460	36,007	15,131	10,792	19,470
	Foot/Ankle	-	-	-	-	-	-	-	-	-
	Upper Ext	62,243	36,620	87,866	35,336	21,564	49,108	17,128	1,946	32,310

1. Unadjusted data, no correction for missing data (e.g. older model year vehicles); restricted to 10-year-old and newer vehicles in each case year
2. All Occupants - any seat position, no restrictions;
3. All frontal/SOI crashes, no rollover, driver/RFP age 15+, 2nd row age 8+

Table 1.2. NASS-CDS 2000 to 2014 Frontal Crashes – Total Weighted Injury Counts.

		Frontal Crashes - NASS-CDS 2000-2014[1]								
		Total Injury Counts								
		All Occupants			Belted Drivers / Right Front Passengers			Unbelted Drivers / Right Front Passengers		
Severity	**Body Region**	*Pt*	*Lwr*	*Upr*	*Pt*	*Lwr*	*Upr*	*Pt*	*Lwr*	*Upr*
AIS 2+	**TOTAL**	2,515,035	1,741,662	3,288,408	1,343,316	1,079,124	1,607,508	695,386	400,597	990,175
	Head/Face	547,672	341,436	753,908	204,758	151,989	257,528	185,133	98,494	271,772
	Skull/Facial Fracture	121,486	88,305	154,668	29,912	24,909	34,915	46,053	32,252	59,854
	Brain	403,745	241,648	565,841	169,077	120,759	217,395	131,884	58,157	205,610
	Neck	89,631	45,341	133,922	40,849	17,741	63,957	26,253	10,317	42,188
	Spinal Cord	6,512	3,382	9,643	2,288	1,094	3,481	2,689	494	4,883
	Osteoligamentous	77,234	34,492	119,976	34,744	10,315	59,172	22,228	9,318	35,138
	Thorax	360,153	238,159	482,147	198,513	142,389	254,638	98,380	59,901	136,860
	Rib cage/Sternum	221,804	152,426	291,182	143,732	102,286	185,178	50,278	25,782	74,775
	Lungs	78,081	30,673	125,489	30,742	14,851	46,633	23,709	11,956	35,462
	Heart	11,522	6,452	16,593	3,209	1,108	5,309	6,122	2,883	9,361
	Abdomen	137,786	91,300	184,273	57,950	41,154	74,745	46,383	26,485	66,281
	Vessels/Nerves	2,947	656	5,238	1,204	314	2,094	1,377	0	3,103
	Skin/Tissue/Muscle	163	5	320	119	0	255	21	0	68
	Organs	134,677	89,519	179,834	56,627	40,513	72,741	44,985	25,799	64,171
	Solid	101,561	64,048	139,074	39,246	29,656	48,835	37,738	19,907	55,569
	Hollow	17,690	10,688	24,693	8,515	4,027	13,003	3,356	1,213	5,500
	Other	15,425	11,046	19,804	8,866	5,439	12,293	3,891	2,486	5,295
	Lower Ext	766,926	530,605	1,003,246	481,671	321,578	641,765	200,844	131,119	270,569
	Knee/Thigh/Hip	296,173	236,223	356,122	153,289	117,418	189,161	100,964	69,772	132,156
	Tibia/Fibula	246,790	190,395	303,186	156,316	128,790	183,842	61,240	33,691	88,789
	Foot/Ankle	223,962	80,079	367,846	172,066	43,348	300,784	38,640	21,427	55,853
	Upper Ext	409,467	307,959	510,975	257,976	179,047	336,904	88,126	45,571	130,681
AIS 3+	**TOTAL**	778,087	501,350	1,054,824	326,276	245,126	407,426	272,559	150,796	394,323
	Head/Face	188,144	118,323	257,965	53,588	39,547	67,629	75,677	32,348	119,005
	Skull/Facial Fracture	35,992	25,216	46,767	7,475	5,691	9,259	14,193	10,290	18,095
	Brain	149,488	89,050	209,925	45,230	32,186	58,274	61,178	18,112	104,243
	Neck	34,115	12,288	55,941	14,148	2,334	25,962	11,374	1,233	21,515
	Spinal Cord	6,512	3,382	9,643	2,288	1,094	3,481	2,689	494	4,883
	Osteoligamentous	25,468	5,655	45,281	10,943	0	23,663	7,826	379	15,273
	Thorax	213,904	128,645	299,162	92,053	61,793	122,312	72,018	43,233	100,804
	Rib cage/Sternum	82,169	53,329	111,009	38,805	21,286	56,323	27,998	13,934	42,063
	Lungs	76,680	29,368	123,993	30,622	14,736	46,507	22,655	11,098	34,213
	Heart	7,014	3,387	10,640	2,145	821	3,470	3,431	858	6,004
	Abdomen	38,260	22,646	53,875	17,205	10,147	24,264	11,570	5,371	17,768
	Vessels/Nerves	2,947	656	5,238	1,204	314	2,094	1,377	0	3,103
	Skin/Tissue/Muscle	12	0	37	12	0	37	0	0	0
	Organs	35,301	21,056	49,547	15,989	9,438	22,540	10,193	5,149	15,237
	Solid	26,076	16,240	35,911	11,288	7,613	14,963	7,875	3,407	12,344
	Hollow	6,150	2,669	9,631	2,713	755	4,671	1,595	0	3,471
	Other	3,075	1,419	4,732	1,988	374	3,603	723	195	1,251
	Lower Ext	168,093	127,943	208,243	79,646	64,899	94,393	61,722	40,948	82,496
	Knee/Thigh/Hip	112,855	79,582	146,128	46,455	35,823	57,087	45,301	27,501	63,102
	Tibia/Fibula	55,238	44,032	66,444	33,191	25,655	40,727	16,421	11,175	21,666
	Foot/Ankle	-	-	-	-	-	-	-	-	-
	Upper Ext	84,406	46,108	122,704	49,323	28,273	70,373	22,415	2,921	41,910

1. Unadjusted data, no correction for missing data (e.g. older model year vehicles); restricted to 10-year-old and newer vehicles in each case year
2. All Occupants - any seat position, no restrictions;
3. All frontal/SOI crashes, no rollover, driver/RFP age 15+, 2nd row age 8+

Eigen and Martin (2005) presented an approach to quantify the cost of injury for different body regions and injuries relative to other body regions. This attributable cost approach was recreated using updated cost data from Blincoe et al. (2015). Blincoe provided data that broke down the cost of injury associated with motor vehicle crashes into body region and injury severity. Table 1.3 presents the sum of medical, wage, and household costs as well as the cost associated with quality-adjusted life years (QALYs) lost. All values are with a 3% discount rate applied. The total cost in these four areas amounts to over 95% of comprehensive cost for AIS 2 through fatal injury severities.

Table 1.3. QALY and Economic Costs Sum by Body Region / Injury Severity.

Total - QALY[1] and Economic Costs (Medical Costs[2], Lost Wages[3], Household Productivity[4])													
	Head		Face		Neck		Chest			Lower Extremities		Upper Extremities	
Severity	No Fracture	Fracture	No Fracture	Fracture	No Fracture[5]	Fracture[6]	No Fracture	Fracture	Abdomen	No Fracture	Fracture	No Fracture	Fracture
AIS 1	$100,296	$12,879	$25,613	$594,740	$462,557	-	$70,194	$175,330	$240,252	$19,643	$15,962	$23,546	$29,860
AIS 2	$567,415	$1,524,384	$979,884	$321,571	$1,183,981	$378,790	$152,895	$343,522	$170,656	$96,741	$369,278	$194,013	$154,930
AIS 3	$1,361,799	$1,941,020	$936,645	$969,900	$2,373,527	$941,343	$297,169	$527,705	$439,262	$711,098	$847,624	$952,755	$992,888
AIS 4	$3,626,768	$2,121,003	-	-	$6,428,249	-	$520,457	$703,772	$626,271	$1,546,776	$1,680,853	-	-
AIS 5	$5,939,398	-	-	-	$7,897,643	-	$960,200	$1,063,954	$652,962	-	$1,755,062	-	-

1. Table B-2 (Blincoe et al. 2015)
1. Table 2-4 (Blincoe et al. 2015)
1. Table 2-5 (Blincoe et al. 2015)
1. Table 2-6 (Blincoe et al. 2015)
5. AIS 1 and 2 are QALY only costs; AIS 3-5 are spinal cord cases
6. Fracture cases assigned cost from Table 4-2 (Blincoe et al. 2015)

In essence, the attributable cost approach looks at the most costly injury sustained by a given occupant and subtracts the cost associated with the next most costly injury. The cost data from Table 1.3 is used for the respective injuries. The difference between the two costs or attributable cost is recorded for that occupant and associated with the most costly body region. This approach can be applied across a target population of interest. In Figure 1.2 this approach has been applied to belted and unbelted drivers and right front passengers involved in frontal crashes for NASS-CDS case years of 2010 to 2014 with the body region data organized to match body regions that map to those of THOR-50M. This is done for all maximum Abbreviated Injury Scale (MAIS) 2+ occupants and associated AIS 2+ injuries. The version of AIS used was AIS 1995/1998 (AAAM, 1998) given the injury coding used in Blincoe et al. (2015) used that version of AIS.

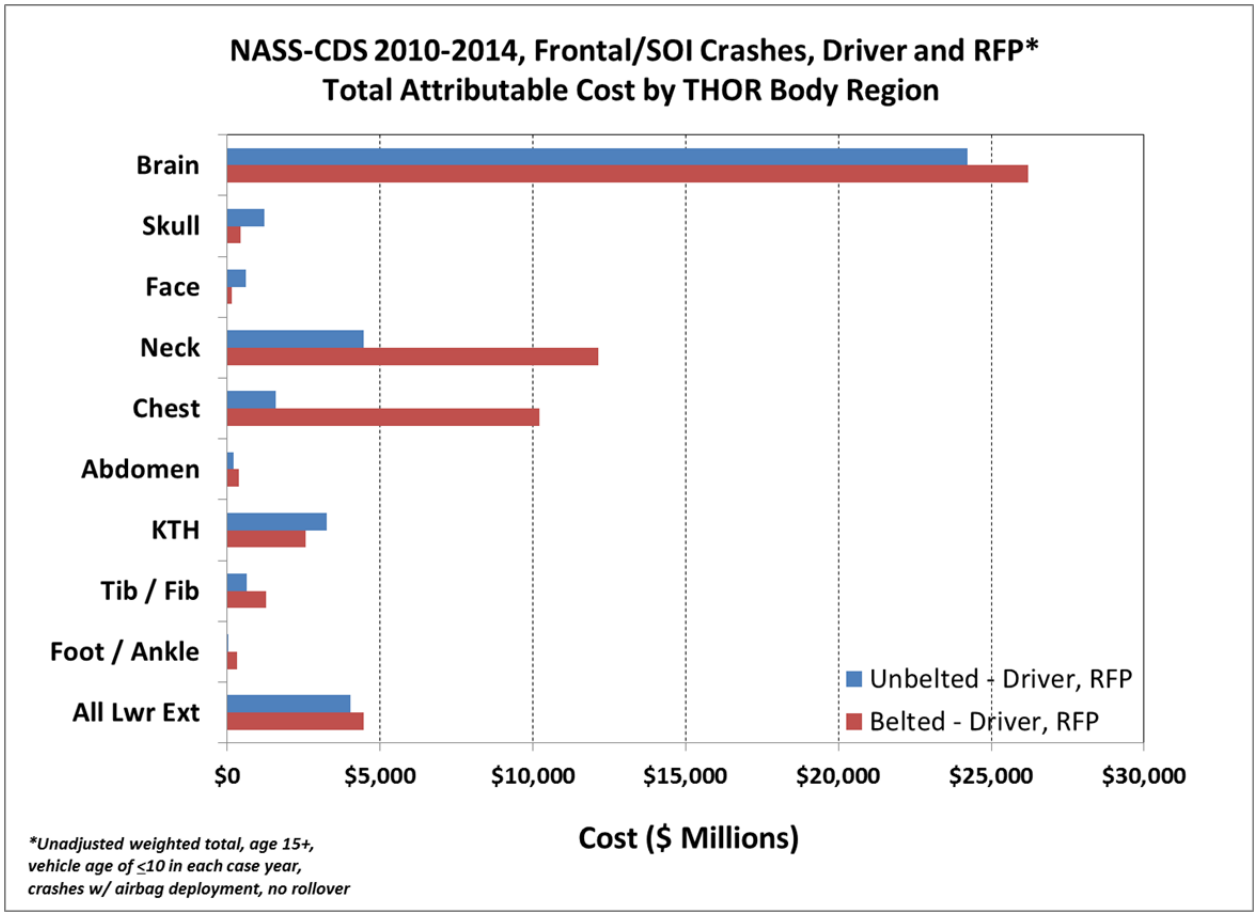

Figure 1.2. Attributable cost by THOR-50M body region for drivers and right front passengers involved in frontal crashes for NASS-CDS 2010-2014 case years.

1.2 Scope

This report describes injury criteria and associated risk function development where both the THOR-50M has available instrumentation and experimental/mathematical injury data exist.

1.3 THOR-50M Technical Documentation

Throughout this document, references to the THOR-50M refer to an ATD described in the September 2015 THOR-50M drawing package (NHTSA, 2015a), for which qualification specifications are defined in the THOR-50M Qualification Procedures Manual (NHTSA, 2015b). Updates to the drawing package between the previous September 2015 release (NHTSA, 2015a) and the docketed drawing package (NHTSA, 2016b), primarily the inclusion of the molded shoe discussed in Section 8, are discussed in later sections of this report where applicable.

The THOR-50M is a physical model of a 50th percentile male motor vehicle occupant. The anthropometry of the THOR-50M was developed to meet the requirements of the Anthropometry of Motor Vehicle Occupants (AMVO) study (Robbins, 1983). The kinematic and dynamic biomechanical performance

requirements of the THOR-50M were developed based on PMHS and volunteer response data, described in more detail in the THOR-50M Biofidelity Report (Parent, 2016).

1.4 **Intended Application**

The THOR-50M is intended for use in development/evaluation of vehicle system/restraint countermeasures and vehicle safety performance in frontal crashes. NHTSA has traditionally used 50th male crash test dummies or ATDs in a variety of frontal crash conditions for rulemaking, consumer metric and/or research purposes in evaluating the performance of passenger cars, light trucks and vans. These conditions include full frontal and small to moderate overlap crashes with those tests being run with various impact angles (collinear and oblique). In these conditions, the dummies are often tested in both belted and unbelted conditions.

2 METHODOLOGY

The following section of the report describes the methods used for collecting and analyzing experimental, real-world crash, and fleet data from crash tests/simulation for the purpose of creating, evaluating and selecting injury criteria and associated risk functions for the THOR-50M ATD.

2.1 Statistical Assessment / Creation of Risk Functions

The following section describes the steps and statistical measures used to describe the respective injury risk functions for the THOR-50M.

2.1.1 Methods for developing risk functions

Hasija et al. (2011) presented a process by which to differentiate between non-correlated and well-correlated datasets when considering the development of injury risk functions. They recommended the use of both logistic regression and survival analysis when using left censored injury data and right censored non-injury data. For a well-correlated dataset with overlapping left and right censored injury and non-injury data, both logistic regression and survival analysis (with Weibull, log-logistic or log-normal) produce nearly identical risk functions. The advantage of survival analysis as compared to logistic regression is that it produces a risk function that presents zero risk with zero stimulus.

For logistic regression-based analyses to be possible, two conditions need to be met. First, the data must include both injury and non-injury data points for the dependent outcome of interest. Second, this dataset must have overlapping injury and non-injury data. As will be described later in this report, it was necessary to consider some datasets that presented only injury data. In these cases where the experimental protocol allowed for the measurement/estimation of load/stimulus magnitude at failure (possibly different than peak stimulus or left censored data where exact failure stimulus is not known), risk functions are presented using survival analysis.

Throughout this report, three main measures of model fit/predictability were used: area under the receiver operating characteristic (ROC) curve, log likelihood and Hosmer and Lemeshow's (Hosmer and Lemeshow, 2000) goodness of fit test.

Area under the ROC curve: The ROC curve is a plot of true positive versus false positive rates. The area under the ROC curve or AUROC can range from 0.5 (no model discrimination) up to 1.0.

Per Hosmer and Lemeshow (2000), AUROC can be interpreted as follows:

- If AUROC=0.5 this suggests no discrimination
- If 0.7 <= ROC < 0.8 this is considered acceptable discrimination
- If 0.8 <= AUROC < 0.9 this is consider excellent discrimination
- If AUROC >= 0.9 this is considered outstanding discrimination

Hosmer and Lemeshow note that "in practice it is extremely unusual to observe areas under the ROC Curve greater than 0.9. In fact…when there is complete separation it is impossible to estimate the

coefficients of a logistic regression model, yet nearly complete separation would be required for the area under the ROC Curve to be >90%."

Log-likelihood (-2 log L or Max Log-likelihood in SAS 9.3, SAS Institute Inc.): Log-likelihood is minimized (or targeted to be as close to zero as possible) in fitting a model to the associated dataset when optimizing for the model coefficients. It is dependent on the sample (content, sample size) and thus should only be used for comparing models (e.g. AIS 2+ or AIS 3+) from the same dataset and not across different datasets.

Goodness of Fit: Hosmer and Lemeshow (2000) described a goodness of fit test that can be used to assess the predictability of model. Hosmer and Lemeshow's goodness of fit statistic groups model observations/probabilities (usually near ten groups) for the purpose of comparing predicted versus observed frequencies. The goodness of fit statistic obtained by calculating the Pearson chi-square statistic Gx2 (G equals number of groups) table of observed versus estimated expected frequencies. If the p value (Pr>ChiSq) is high (> 0.1) then one cannot reject the null hypothesis that the model fits (i.e is correct).

2.2 Injury Severity and Risk Curve Expansion

This report uses the 1990 version (1998) update of the Abbreviated Injury Scale (AAAM, 1998) when considering real-world crash data and experimental data used to develop injury risk functions. As needed, further analysis and/or descriptions are provided when considering some datasets and applications that are based on the 2005 (2008 Update) version of AIS (AAAM, 2008). In these cases, the version of AIS used will be specifically noted. Otherwise all listings of AIS severity (e.g. AIS 2+ or AIS 3+ injured occupants or body regions) will be in AIS 1990 (1998 Update) coding.

Where possible, the risk functions for the respective body regions will be presented for more than one AIS severity level. In some cases (see brain injury) this was simply done through referencing prior expanded curves. In other cases and as the experimental data allows, risk functions are presented for different levels of injury as derived directly from the experimental data (see neck).

2.3 Field Data

This report utilizes various sources of real world or field crash data in analyzing trends of field versus fleet data as well as to present case study results of injury mechanisms.

The following is a brief description of each database:

- **National Automotive Sampling System – Crashworthiness Data System (NASS-CDS)**: NHTSA's NASS-CDS database is a nationally representative sample of crashes on public roadways where at least one vehicle was towed from the crash. NASS-CDS contains detailed, crash investigator collected data related to the crash (scene, vehicle) and occupant/injury (demographics, injury coding, injury sources).
- **Crash Injury Research and Engineering Network (CIREN):** NHTSA's CIREN program dataset is a convenience sample of seriously injured occupants who were admitted to a

Level I trauma center. Vehicle crash data is collected similar to NASS-CDS. CIREN collects additional hospital and medical imaging data and conducts medical/engineering expert team review in assigning sources, causes, and mechanisms of injury.

- **National Automotive Sampling System – General Estimates System (NASS-GES):** NASS-CDS is a nationally representative sample of police reported crashes on a public roadway. NASS-GES collects a larger sample of data as compared to NASS-CDS in an effort to get an overall bigger picture of crashes, but does not have crash investigator collected vehicle crash data or occupant injury data.
- **Fatality Analysis Reporting System (FARS)**: NHTSA's FARS dataset contains a nationwide census of fatal crashes. Like NASS-GES it does not have detailed crash or occupant injury data, but does provide high-level demographic, restraint use and crash type information.
- **Multiple Cause of Death (MCoD):** MCoD is a CDC dataset of national mortality and population data based on death certificates in the U.S. The underlying cause of death (e.g. motor vehicle crash) and associated injury types are documented.

Methods and associated results for comparing rates of injury in field data versus predicted injury risk from use of the THOR-50M in crash tests of fleet vehicles are presented in section 9.

2.4 Fleet Data: THOR-50M

Each injury criteria presented herein is calculated for a set of vehicles which were tested in the frontal rigid barrier (0 degrees, full overlap, 56 km/h) (Keon, 2016) and/or Oblique Moving Deformable Barrier (15 degrees, 35% overlap, 90 km/h barrier speed) (Saunders et al., 2015) crash test procedures. Vehicle selection was limited to those which received a "Good" or "Acceptable" rating in the Insurance Institute for Highway Safety (IIHS) Small Overlap Impact (SOI) crash test and also had side curtain airbags meeting the requirements of Federal Motor Vehicle Safety Standard (FMVSS) No. 226, "Ejection mitigation." These selection criteria were chosen because it is expected that by the time of implementation of these injury criteria in regulations or consumer information testing, a majority of new vehicles will meet both of these vehicle selection criteria. See APPENDIX D for a list of crash tests included in this evaluation. Data, reports, photos, and videos from these crash tests are located in the NHTSA Vehicle Crash Test Database (http://www.nhtsa.gov/Research/Databases+and+Software).

Fleet data from current NCAP testing is also presented for the purpose of comparing trends in fleet testing versus trends in field data.

2.5 Age Considerations – Injury Risk Functions

The National Automotive Sampling System – General Estimates System (NASS-GES) was queried for case years 2005 to 2014 to present the mean age of male drivers involved in frontal crashes. The 10-year trend is seen in Figure 2.1. Extrapolating forward to the potential time frame in which THOR is planned

for application and the estimated mean age for male drivers in frontal crashes is 40-years old. For risk functions presented later in this report that use age as a covariate, 40 will be used as the age as it represents the mean age of exposed male drivers in frontal crashes.

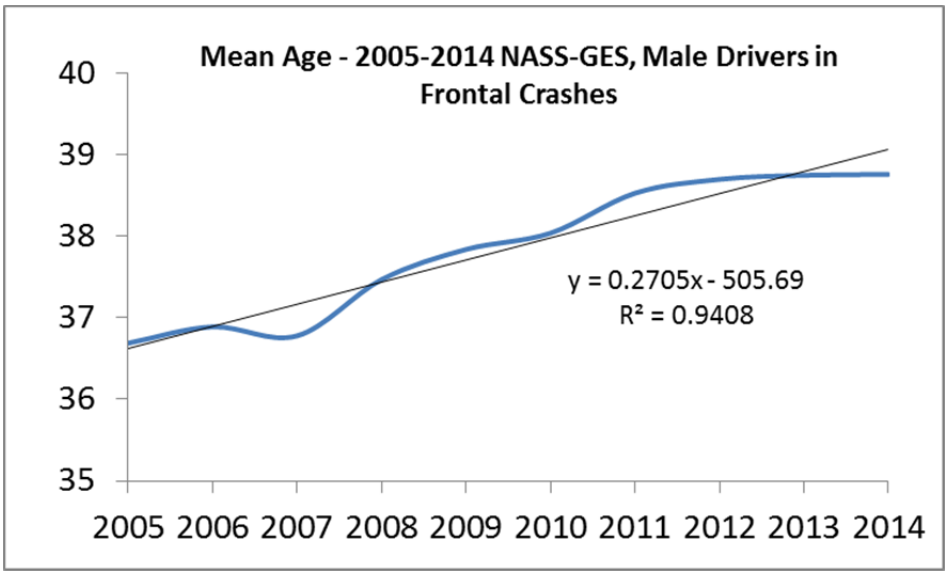

Figure 2.1. NASS-GES mean age for male drivers in frontal crashes, case years 2005-2014.

3 HEAD

3.1 Field and Historical Fleet Data

It can be seen in Table 1.1 that the brain is the most frequently injured body region at the AIS 2+ severity level for all occupants in frontal crashes with knee/thigh/hip, rib cage injuries being the 2nd and 3rd most frequently injured for body regions associated with the THOR-50M. Brain injuries remain prominent when looking at belted and unbelted drivers and right front passengers. Brain injuries are also the most costly injury type per the attributable costs presented in Figure 1.2.

Figure 3.1 shows how the rate of brain injury and skull and facial fractures (both at the AIS 2+ level) have changed in recent model years for belted drivers in frontal crashes where an airbag deployed (no delta V or damage extent filter). The case years included for NASS-CDS were 1993 to 2014. The rate represents a running 3-year average of the percent of injured divided by the total number of cases (e.g. model year 1990 includes the total weighted count of 2+ injuries from 1988, 1989 and 1990, divided by the total number of cases for those years). It appears that while the rate of facial/skull fracture has not changed given belted, airbag restrained drivers in frontal crashes, the rate of brain injury at the AIS 2+ level has increased. In contrast, Figure 3.2 shows a decreasing trend of HIC_{15} values/risk of vehicles tested in the 35-mph full frontal test condition (NCAP, FMVSS No. 208) from model year 1990 to 2016.

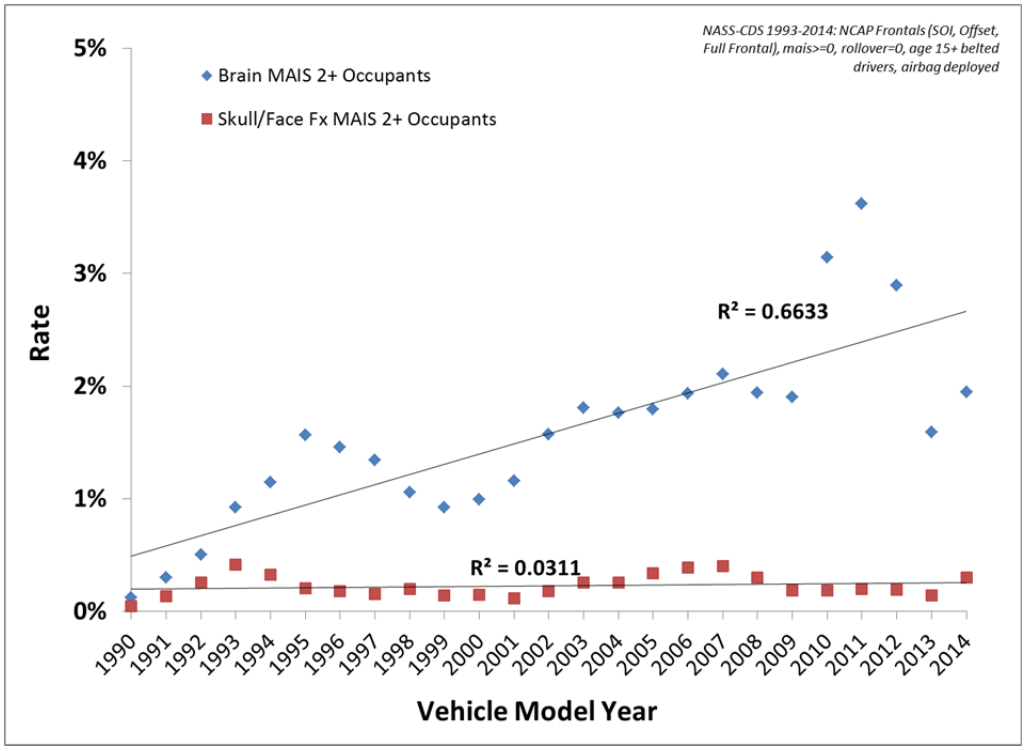

Figure 3.1. Skull/facial fracture MAIS 2+ and brain injury 2+ rate versus model year (1990 to 2014) from NASS-CDS 1993 to 2014.

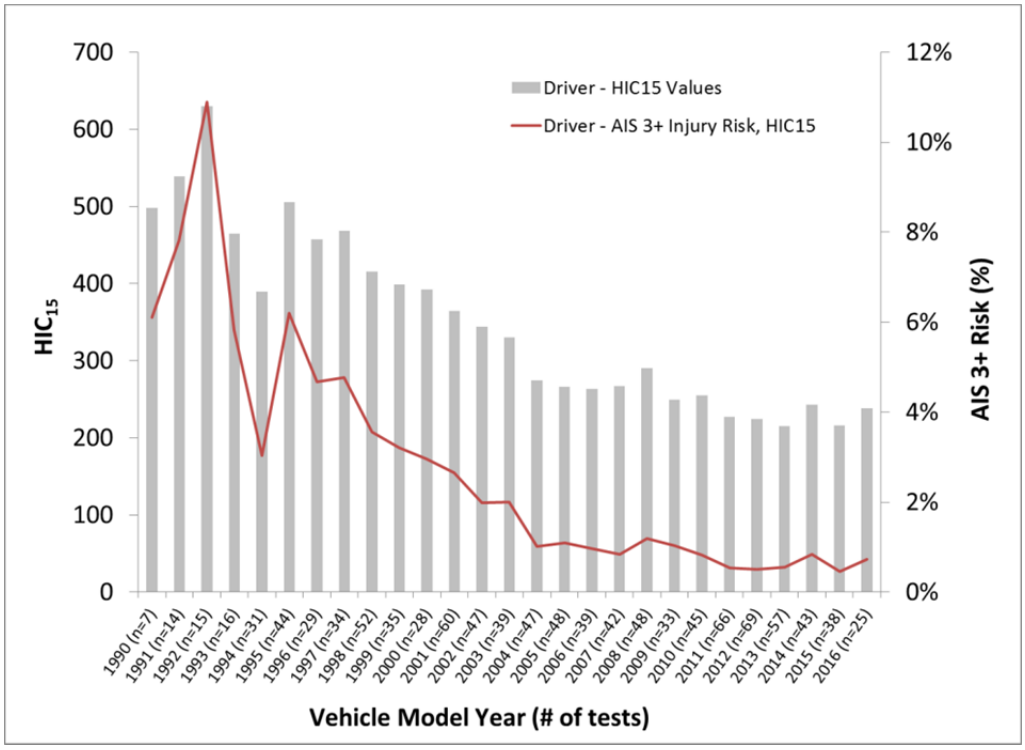

Figure 3.2. Hybrid III 50th percentile driver HIC_{15} values and predicted AIS 3+ risk from model year 1990 to 2016 in 35-mph frontal NCAP tests.

Table 3.1 shows the relative occupant counts of brain injury versus skull/facial fracture for belted drivers in frontal crashes for NASS-CDS case years 2000-2014 where there was a deployed frontal airbag. It can be noted that the majority of occupants with an AIS 2+ or 3+ brain injury are sustaining those injuries in the absence of skull or facial fractures.

Table 3.1. Brain injury versus skull/facial fracture for belted, airbag restrained drivers in frontal crashes (NASS-CDS 2000-2014).

		Skull/Facial Fracture AIS 2+		Skull/Facial Fracture AIS 3+	
		0	1	0	1
Brain AIS 2+	0	5,133,554 (13,290)	6,740 (83)	5,138,102 (13,348)	2,192 (25)
	1	78,538 (614)	4,818 (97)	81,162 (659)	2,195 (52)
Brain AIS 3+	0	5,201,100 (13,735)	8,152 (107)	5,206,721 (13,810)	2,531 (32)
	1	10,993 (169)	3,405 (73)	12,542 (197)	1,856 (45)

Figure 3.3 shows trends for traumatic brain injury (TBI) related fatalities due to motor vehicle crashes (MVC) from the Multiple Cause of Death (MCoD) dataset maintained by the Centers for Disease Control and Prevention (http://wonder.cdc.gov/mcd.html). Also shown are FARS totals for the same years. It can be seen that TBI-related and total fatality counts follow similar trends.

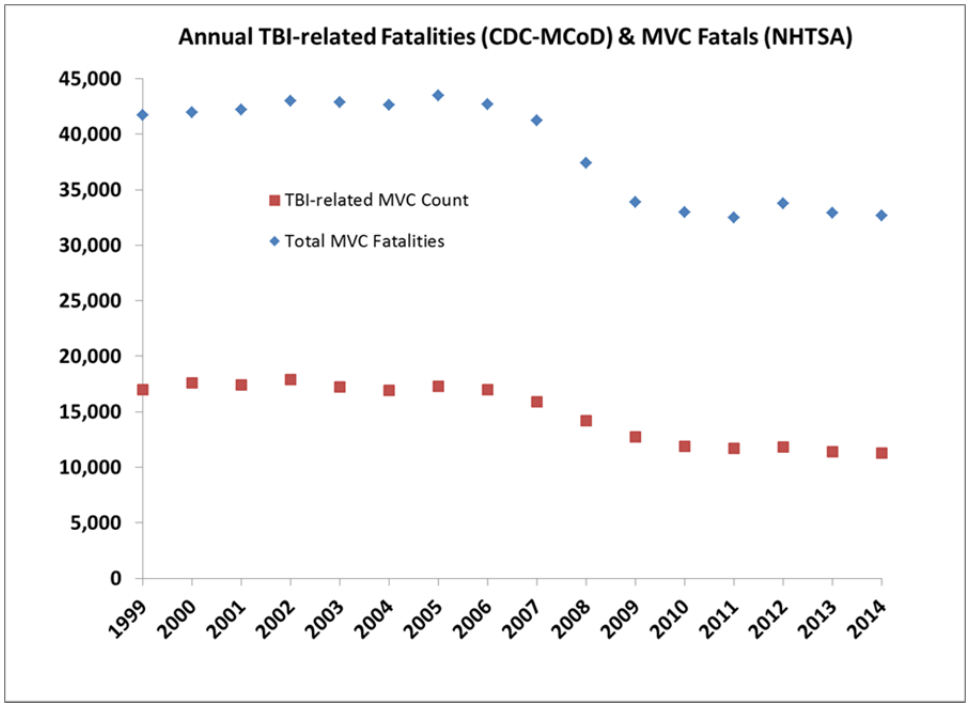

Figure 3.3. TBI-related brain injuries in motor vehicle crashes from MCoD dataset.

The CIREN database includes regional injury mechanism assigned by biomechanical engineers during the case review process. A query of restrained first row occupants sustaining AIS 2+ head and face injuries in frontal crashes was performed to determine the dominant injury-producing mechanisms. Frontal crashes were broadly defined for this query, and include crashes with principal directions of force within 30 degrees of 12 o'clock and any amount of frontal overlap. Only crashes occurring after June 1, 2010 were included in this query. Of 488 occupants in qualifying frontal crashes, 93 sustained an AIS 2+ injury to the head or face, and the mechanisms by the individual injuries by type are shown in Figure 3.4. Fractures were most often coded as the result of compression. Anatomical brain injuries and loss of consciousness (LOC) were assigned regional mechanisms of rotational motion, linear acceleration, and compression. These recorded mechanisms are inferred from the available data and may have been limited to available researcher/published biomechanical knowledge at the time each case was reviewed. Additionally, in brain/LOC injury cases, when the regional mechanism is assigned as "compression" it is generally referring to the type of loading (i.e. contact to a relatively hard component such as the steering wheel or A-pillar) and not an injury that is physically due to compression of the skull or brain tissue. In most of these cases rotational/translational acceleration/velocity was assigned as the secondary regional mechanism.

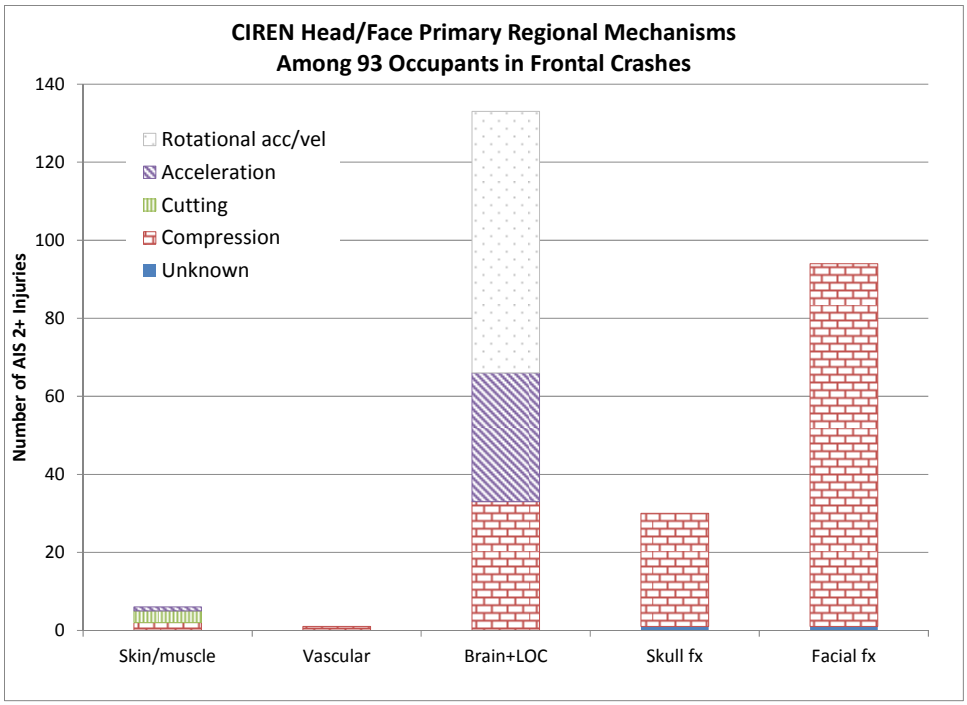

Figure 3.4. Recorded mechanisms of head and face injuries for belted front row occupants involved in frontal crashes from the CIREN database.

3.2 Instrumentation

For measurement of head center of gravity (CG) translational acceleration and angular velocity the THOR-50M is equipped with three uniaxial accelerometers and three angular rate sensors, respectively (Figure 3.5). Five uniaxial face load cells can be installed, though these load cells have not been installed in any vehicle crash tests with THOR-50M ATDs in the NHTSA Vehicle Database. The head also includes a biaxial tilt sensor which measures the quasi-static orientation of the head for pre-test positioning purposes.

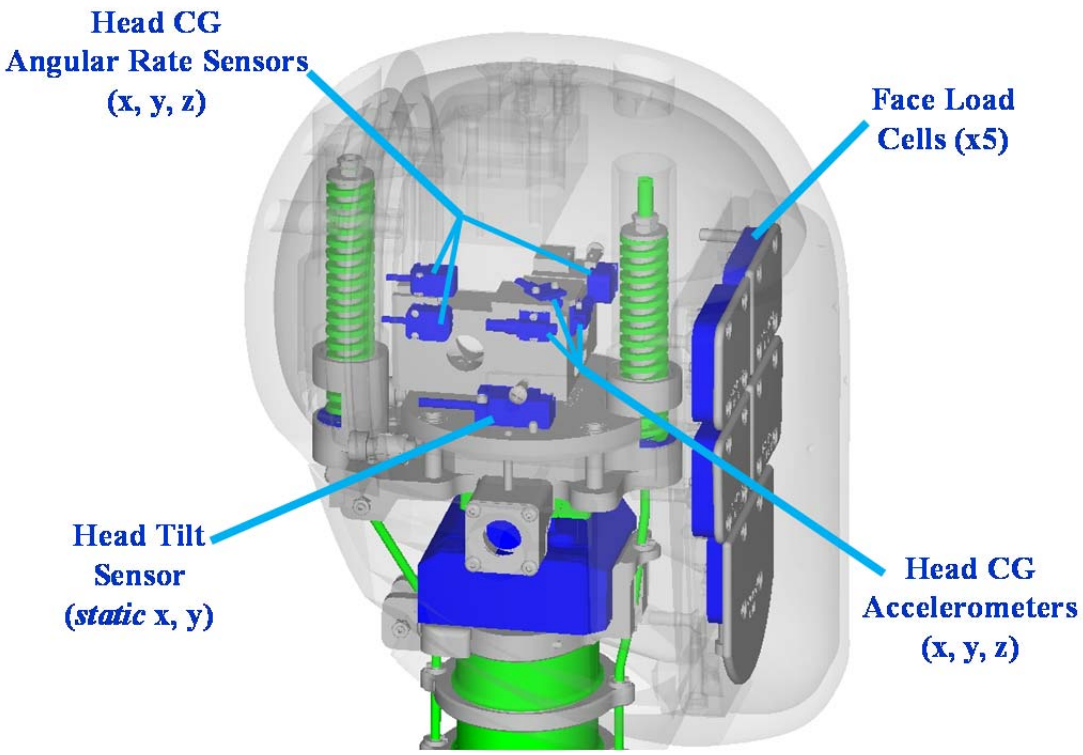

Figure 3.5. THOR-50M head instrumentation.

3.3 **Biofidelity**

The biofidelity of the THOR-50M is described in Parent (2016). For translational motion the response of the THOR-50M headform was evaluated in head drop, whole-body head impact, face rigid bar, and face rigid disk impact conditions. The classified biofidelity performance was excellent for the head drop, whole-body head impact, and face rigid disk impact conditions. The THOR-50M biofidelity performance in the face rigid bar impact condition was marginal, while the Hybrid III 50th male has poor biofidelity in both face rigid bar and face rigid disk impact conditions.

The angular velocity response of the THOR-50M head can be observed in a few experimental conditions. First, head and neck response is measured in a frontal flexion condition. In this condition, biofidelity for the head/neck measures (angle, displacement, resultant acceleration) ranges from good to poor. However, a qualitative comparison of head angular rate time-history data of the THOR-50M versus the referenced biofidelity data shows that the peak value and timing is similar. The THOR-50M was also tested in full-body sled test conditions. Four conditions were evaluated: (1) 40 kph, zero degree with standard/non-force limited three-point seat belts; (2) 30 kph, zero degree with force-limited three-point seat belts; (3) similar to 2nd condition, but with the sled buck rotated 30 degrees to represent a near side condition for the occupant; and (4) far-side oblique condition in vehicle buck with production restraints (seat belts, passenger airbag) tested in a condition meaning to duplicate the full-scale angle/severity of NHTSA's left oblique crash test procedure.

For condition (1), the angular rate biofidelity ranged from excellent to marginal. Excellent biofidelity was found for y-axis rotation (dominant axis of rotation in a zero-degree frontal sled). For condition (2), angular rate biofidelity ranged from good to excellent for the respective axes of rotation. Biofidelity for x- and y-axis rotations in condition (3) were either excellent or good. Biofidelity for z-axis rotation was poor. As was noted by Parent (2016), the cadavers lacked any resistance to z-axis rotation as compared to the THOR-50M and Hybrid III. Additionally, it is noted that this particular oblique condition does not include any head restraint (airbags) and thus does not represent the interactions we see in full-scale fleet testing. Out of all of the conditions, condition (4) is most relevant to the type of airbag loading/restraint we expect for front row seated occupants in frontal/oblique crashes. For the THOR-50M seated in a similar configuration to the three cadavers ("Position C"), the head angular velocity about the x- and y-axes both had good biofidelity while the z-axis angular velocity biofidelity was excellent. In oblique, far-side seated conditions, it is z-axis rotation that contributes most to the angular velocity-based criterion (BrIC) described later in this chapter. BrIC values were also calculated for the respective post-mortem human subjects (PMHS) and paired THOR-50M and Hybrid III 50th Male (H3-50M) (Figure 3.6) in the four sled test conditions. THOR-50M compares well to PMHS in all conditions other than condition (3) (see prior discussion). In looking closer at condition (4), the single THOR-50M test where the lower spine adjustment was changed to allow for THOR-50M to sit in a more slouched position similar to three cadavers resulted in a BrIC value of 1.2, which is closer to the average of 1.1 for the three PMHS.

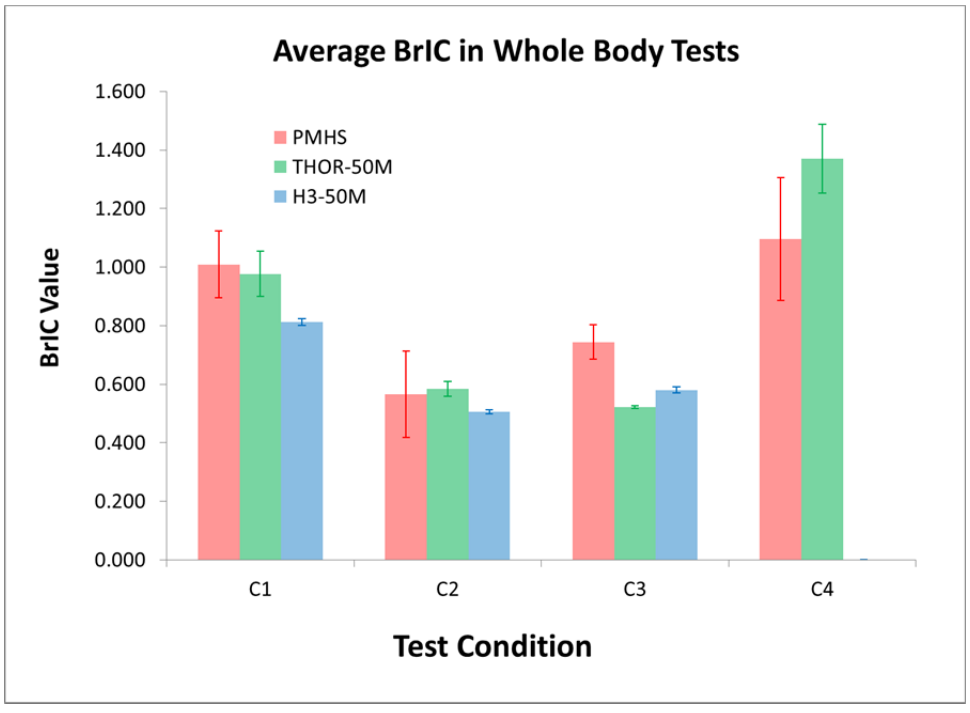

Figure 3.6. Average BrIC values in sled tests of PMHS, THOR-50M and H3-50M.

3.4 **Brain Injuries**

3.4.1 Introduction

Rotational motion of the head as a mechanism for brain injury was suspected as early as 1865 (Alquié, 1865), mentioned by Goggio (1941), clearly explained by Holbourn (1943), and first observed on live monkeys by Pudenz and Sheldon (1946). Since then a number of research studies by various institutions were conducted to confirm/reject this hypothesis (thorough reviews of these studies can be found, for example, in Gurdjian (1972), Hess et al. (1980), Ommaya (1984), Gennarelli et al. (1985), Melvin et al. (1993), Hardy et al. (1994), McLean and Anderson (1997), Goldsmith (2001), Shaw (2002), Goldsmith and Monson (2005), Meaney et al. (2014)). Most of the studies were conducted on animals and concluded that rotational kinematics experienced by the animal's head may cause axonal deformations large enough to induce their functional deficit (Ommaya, 1984). Other studies utilized physical and mathematical models of human and animal heads to derive brain injury criteria based on deformation/pressure histories computed from their models (Gennarelli et al., 1971, 1972, 1985; Margulies and Thibault, 1992; Nusholtz et al., 1984; Zhang et al., 2001; Takhounts et al., 2003, 2008).

All these previous studies along with established scaling techniques were utilized in the development of Brain Injury Criterion (BrIC). First, loading histories of the available animal head kinematics data were digitized and scaled to the size of human head. These loading histories were then applied to two different detailed mathematical models of the human head (SIMon and GHBMC), each validated against various human brain response datasets. Next, physical injury criteria (based on maximum principal strain, or MPS, and cumulative strain damage measure, or CSDM) were established for the human brain based on the injury information obtained from the animal dataset. Since the animal injury data were predominantly for diffuse axonal injury (DAI) type injuries (including severe concussion, subdural hematoma, DAI), which are AIS 4+ in severity, CSDM and MPS risk curves were derived for AIS 4+ injuries. The associated DAI or severe concussion injuries are considered AIS 4+ injuries when looking at both the AIS 1990 (1998 Update) and 2005 (2008 Update) versions of AIS (AAAM, 1998; AAAM, 2008). The AIS 1+, 2+, 3+, and 5+ risk curves for CSDM and MPS were then computed using the ratios between corresponding risk curves for head injury criterion (HIC) at a 50% risk. The risk curves for BrIC were then obtained from CSDM and MPS risk curves using the linear relationship between CSDM - BrIC and MPS – BrIC respectively. The AIS 2+ brain injury risk curve was subsequently verified using angular velocities calculated at a 50% probability of concussion in college football players instrumented with 5 degrees of freedom (DOF) helmet systems. Finally, Anthropomorphic Test Device (ATD) (Hybrid III 50^{th} Male, Hybrid III 5^{th} Female, THOR 50^{th} Male, ES-2re 50^{th} Male, SID-IIs 5^{th} Female, WorldSID 50^{th} Male, and WorldSID 5^{th} Female) test data (NCAP, linear impact, and frontal oblique tests) were used to establish BrIC for all ATDs. A detailed description of the derivation of BrIC is given in Takhounts et al. (2013 and 2011). Briefly, BrIC is a function of the max angular velocities (ω_x, ω_y, and ω_z) computed (at any time) about x-, y-, and z-axes respectively along with the corresponding critical angular velocities ω_{xC}, ω_{yC}, and ω_{zC}:

$$BrIC = \sqrt{\left(\frac{\omega_x}{\omega_{xC}}\right)^2 + \left(\frac{\omega_y}{\omega_{yC}}\right)^2 + \left(\frac{\omega_z}{\omega_{zC}}\right)^2}, \quad \textbf{(3.1)}$$

where ω_{xC}, ω_{yC}, and ω_{zC} are given in Table 3.2 below.

Table 3.2. Critical max angular velocities in each direction.

Critical Max Angular Velocity	Rad/s
ω_x	66.25
ω_y	56.45
ω_z	42.87

Besides angular velocities, other head kinematic parameters, such as angular acceleration (see, for example, Takhounts et al., 2011), the time duration of angular velocity components (see below), and other combinations of kinematic parameters were considered in the developments of the brain injury criteria, but a simple combination of the max angular velocity components (equation 3.1) was sufficient to correlate to the strain-based measures CSDM and MPS.

Figure 3.7 (a) shows the correlation between BrIC and CSDM for all ATDs, while Figure 3.7 (b) shows the correlation between BrIC and MPS – both correlations were based on the 413 data points available at the time of publication (Takhounts et al., 2013). Note: max angular velocity in each direction was calculated irrespective of the time it has occurred as the second approach (max angular velocities at a fixed time of the max of any component) did not improve the correlation between BrIC and CSDM (and MPS). Physically, it makes sense because after the head rotates about one axis and accumulates a certain volume of damaged brain cells (elements in the model exceeding 25% MPS – see definition of CSDM in Takhounts et al., 2003, 2008, 2013), and then starts rotating about another axis, the additional damaged brain cells due to this second rotation will simply add to the previously damaged brain cells (in reality this addition is not simple, but quite complicated – see section below on time duration). This addition is reflected in the formulation of BrIC (equation 1) as a simple addition of the magnitudes of components of angular velocity. The effect of time difference between the peaks of angular velocity components on CSDM was also investigated for up to 150 ms and no significant differences in CSDM were observed.

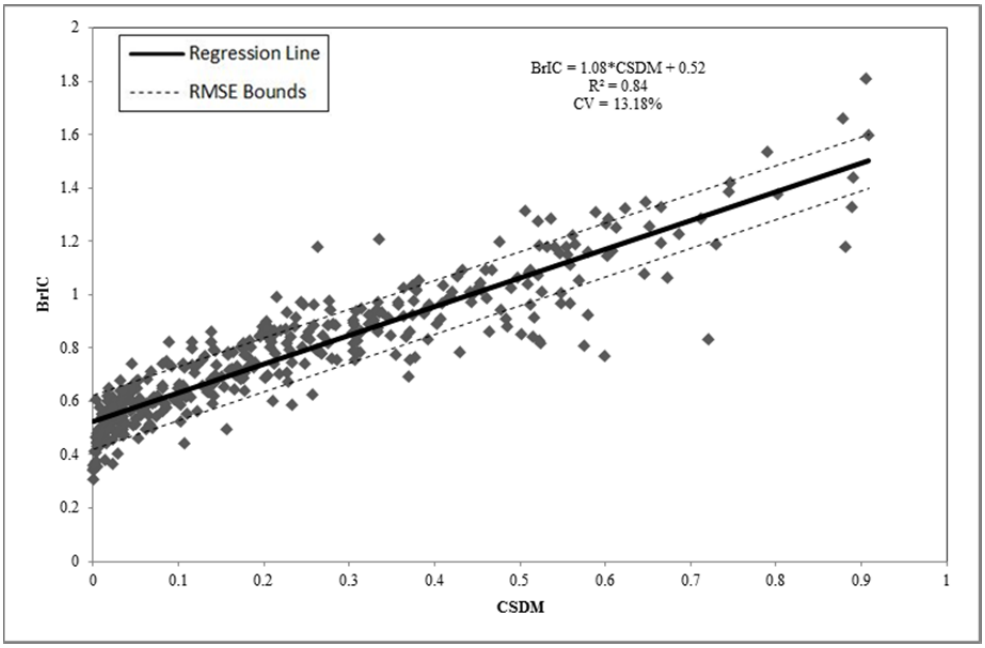

(a)

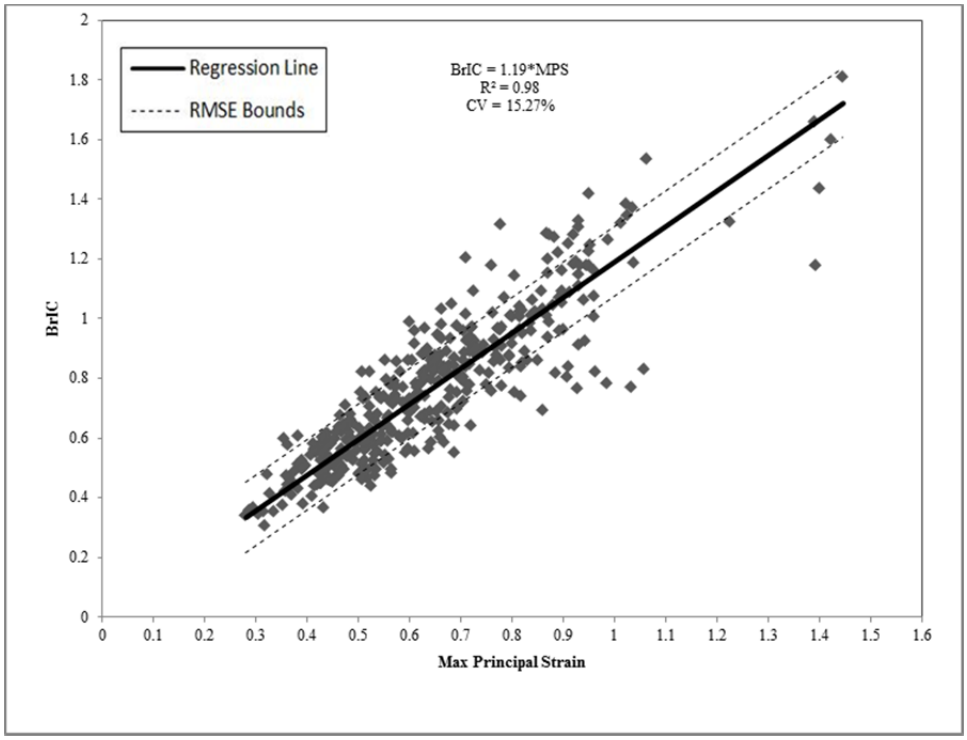

(b)

Figure 3.7. Correlation between (a) BrIC and CSDM and (b) BrIC and MPS for all ATDs in available tests (413 data points); adapted from Takhounts et al. (2013).

The risk curves for CSDM and MPS are given below in Figure 3.6, where AIS 1+, 2+, 3+, and 5+ risk curves were obtained by scaling the AIS 4+ risk curve at a level of 50% probability of injury using coefficients given in Takhounts et al. (2013), while Table 3.3 and Table 3.4 list equations for each of these curves.

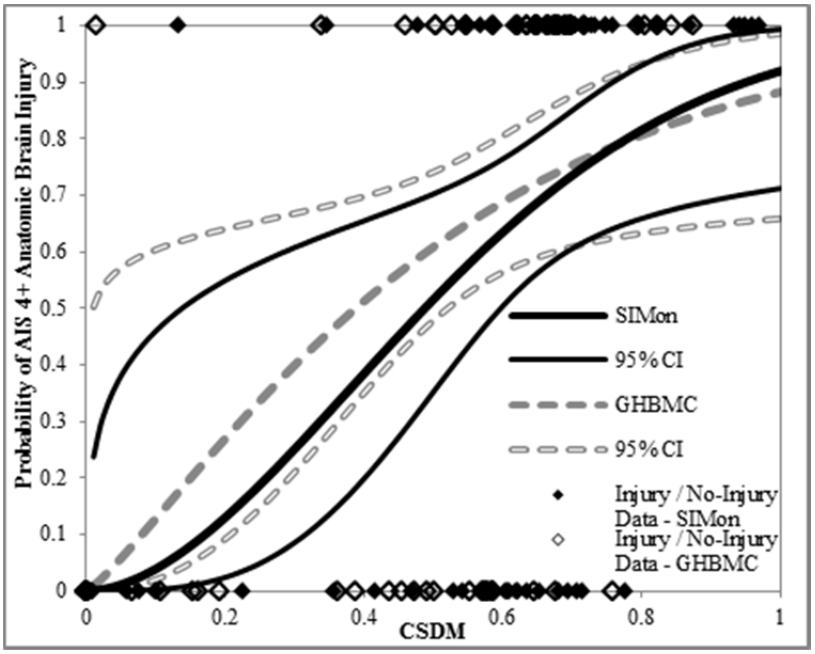

(a)

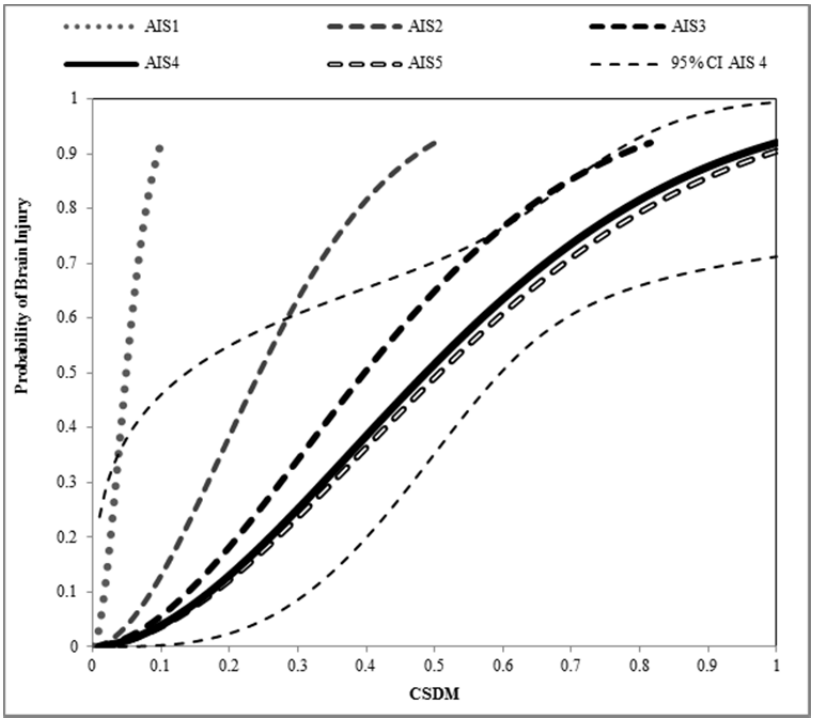

(b)

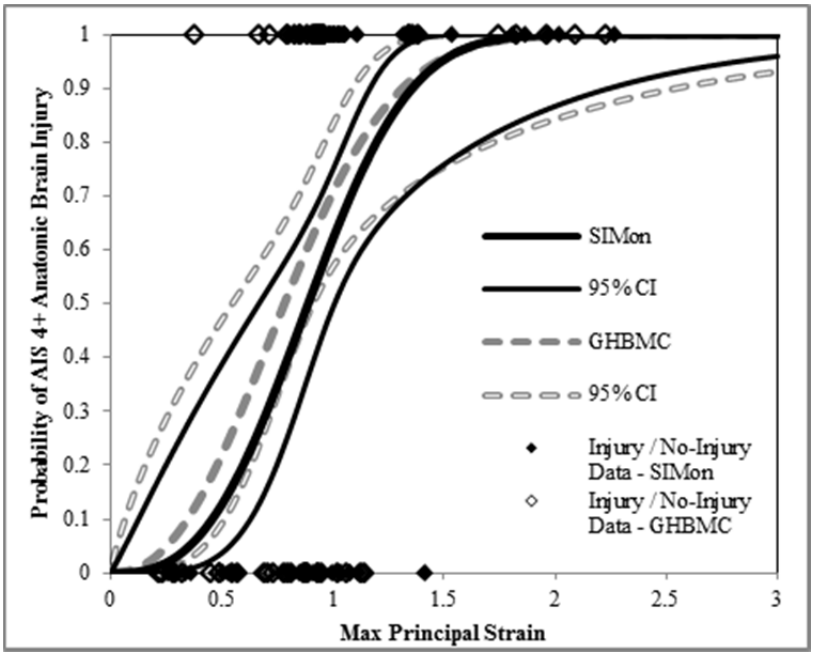

(c)

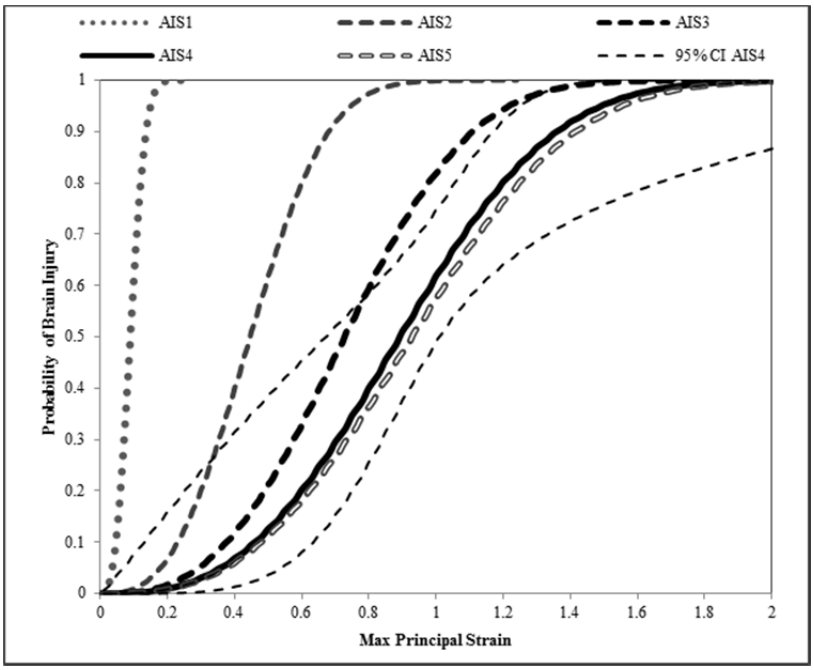

(d)

Figure 3.8. Risk of AIS 4+ anatomic brain injury in scaled animal tests using CSDM (a) and MPS (c) along with the scaled risk curves for various severities based CSDM (b) and MPS (d) – adapted from Takhounts et al. (2013). Note that the areas under the receiver operator characteristic (AUROC) for the AIS 4+ risk curves are 0.83 for CSDM and 0.78 for MPS.

Table 3.3. Risk curve equations for CSDM – adapted from Takhounts et al. (2013).

$$P(AIS\ 1+) = 1 - e^{-\left(\frac{CSDM}{0.060}\right)^{1.8}}$$

$$P(AIS\ 2+) = 1 - e^{-\left(\frac{CSDM}{0.300}\right)^{1.8}}$$

$$P(AIS\ 3+) = 1 - e^{-\left(\frac{CSDM}{0.490}\right)^{1.8}}$$

$$P(AIS\ 4+) = 1 - e^{-\left(\frac{CSDM}{0.600}\right)^{1.8}}$$

$$P(AIS\ 5+) = 1 - e^{-\left(\frac{CSDM}{0.624}\right)^{1.8}}$$

Table 3.4. Risk curve equations for MPS – adapted from Takhounts et al. (2013).

$$P(AIS\ 1+) = 1 - e^{-\left(\frac{MPS}{0.101}\right)^{2.84}}$$

$$P(AIS\ 2+) = 1 - e^{-\left(\frac{MPS}{0.505}\right)^{2.84}}$$

$$P(AIS\ 3+) = 1 - e^{-\left(\frac{MPS}{0.828}\right)^{2.84}}$$

$$P(AIS\ 4+) = 1 - e^{-\left(\frac{MPS}{1.010}\right)^{2.84}}$$

$$P(AIS\ 5+) = 1 - e^{-\left(\frac{MPS}{1.050}\right)^{2.84}}$$

The risk curves for BrIC were then obtained based on the linear relationship between BrIC and CSDM (MPS) as shown in Figure 3.9. Table 3.5 and Table 3.6 list equations for each of these risk curves.

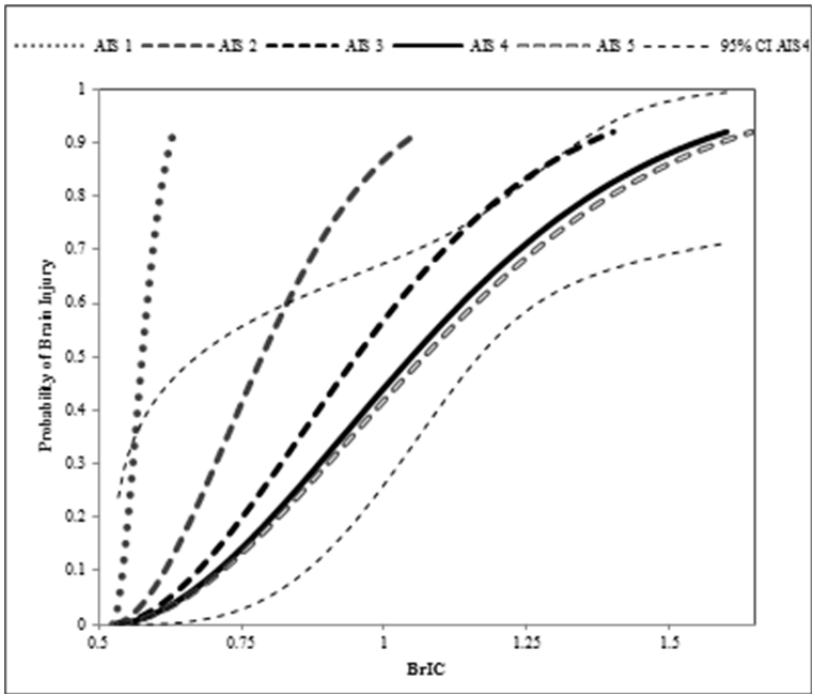

(a)

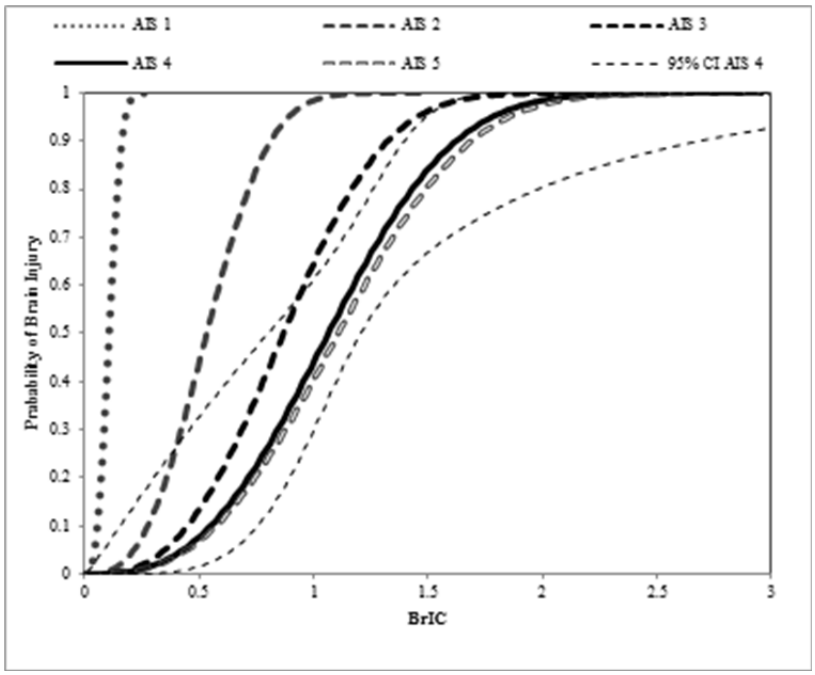

(b)

Figure 3.9. BrIC based on CSDM (a) and MPS (b) obtained from equation 1 with critical angular velocities given in Table 3.2 – adapted from Takhounts et al. (2013).

Table 3.5. Risk curves for BrIC based on CSDM – adapted from Takhounts et al. (2013).

$$P(AIS\ 1+) = 1 - e^{-\left(\frac{BrIC-0.523}{0.065}\right)^{1.8}}$$

$$P(AIS\ 2+) = 1 - e^{-\left(\frac{BrIC-0.523}{0.324}\right)^{1.8}}$$

$$P(AIS\ 3+) = 1 - e^{-\left(\frac{BrIC-0.523}{0.531}\right)^{1.8}}$$

$$P(AIS\ 4+) = 1 - e^{-\left(\frac{BrIC-0.523}{0.647}\right)^{1.8}}$$

$$P(AIS\ 5+) = 1 - e^{-\left(\frac{BrIC-0.523}{0.673}\right)^{1.8}}$$

Table 3.6. Risk curves for BrIC based on MPS – adapted from Takhounts et al. (2013).

$$P(AIS\ 1+) = 1 - e^{-\left(\frac{BrIC}{0.120}\right)^{2.84}}$$

$$P(AIS\ 2+) = 1 - e^{-\left(\frac{BrIC}{0.602}\right)^{2.84}}$$

$$P(AIS\ 3+) = 1 - e^{-\left(\frac{BrIC}{0.987}\right)^{2.84}}$$

$$P(AIS\ 4+) = 1 - e^{-\left(\frac{BrIC}{1.204}\right)^{2.84}}$$

$$P(AIS\ 5+) = 1 - e^{-\left(\frac{BrIC}{1.252}\right)^{2.84}}$$

3.4.2 New Data

Since the publication of original risk curves for BrIC (Takhounts et al., 2013), more data has become available to test the correlation between BrIC and CSDM /MPS. These include NHTSA oblique tests with the THOR-50M (full frontal, right and left oblique), NCAP tests with the Hybrid III 50th male Hybrid III 5th female, ES-2re 50th male and SID-IIs 5th female in side moving deformable barrier (MDB) and vehicle to pole conditions. NHTSA has also run side MDB and side pole tests with the World-SID 50th male. Finally, additional IIHS small and moderate overlap test data with the Hybrid III 50th male has been added. NHTSA conducted, so-called, “airbag tests” where several ATDs were driven into the frontal and side airbags at various initial velocities and angles to simulate many possible interactions between the ATDs heads and the restrain systems. In total, the test dataset is now comprised of 749 tests (instead of the original 413 tests) – see Appendix A for the publicly available test numbers. Figure 3.10 illustrates the correlation of the original BrIC with CSDM for all 749 tests. Neither the correlation coefficient nor the

trend line have changed appreciably (compare with Figure 3.7 a) indicating that new "out-of-sample" data with new test conditions did not affect much the relationship between CSDM and BrIC, thus making this relationship further validated.

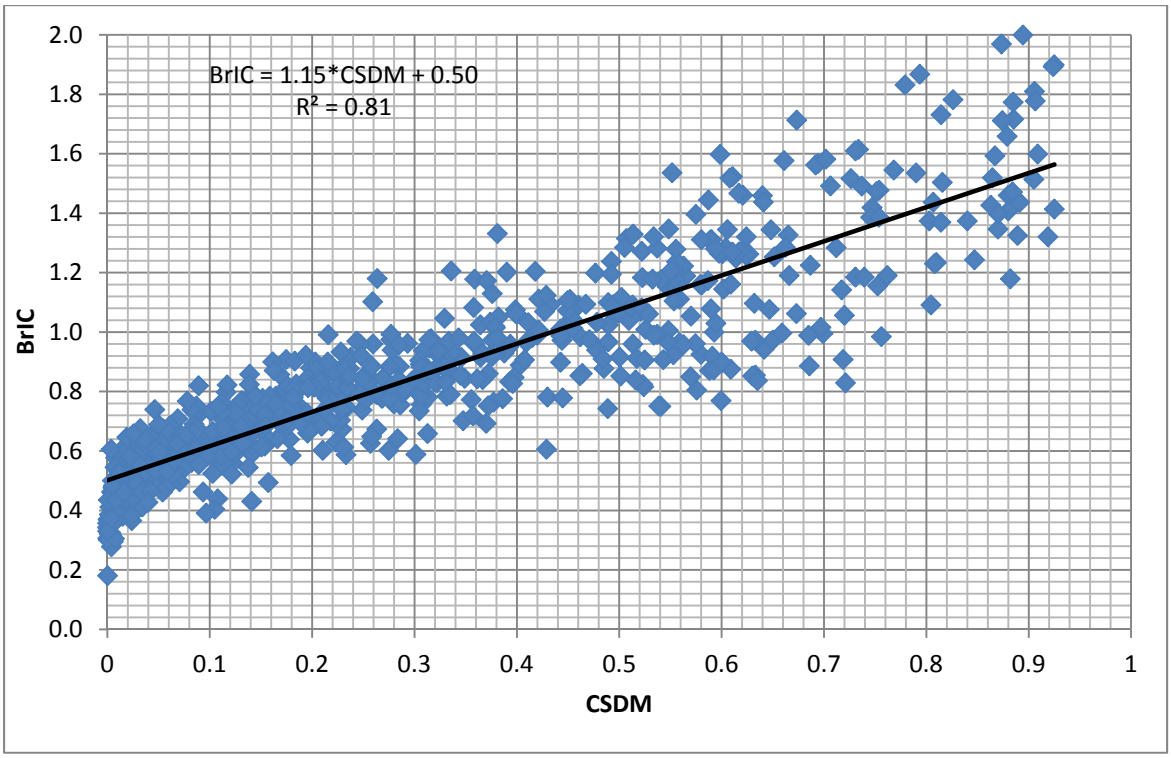

Figure 3.10. Correlation between BrIC and CSDM for all ATDs for all currently available tests (749 total data points).

3.4.3 Relationships for All ATDs vs Individual ATDs

The correlations between BrIC and CSDM given in Figure3.5a and Figure 3.10 are given for all ATDs. Although it is apparent from the high R^2 that such relationships for individual ATDs cannot be statistically different from that given for all ATDs, Figure 3.11a replicates Figure I.8 from Takhounts et al. (2013) of the relationship between CSDM and max angular velocity for all ATDs tested, while Figure 3.11b separates the same data for each individual ATD. It is apparent that no differences can be observed between individual ATDs linear regression lines and that of the combined dataset. It should be noted that the data in Figure 3.9 is from the well-controlled linear impactor tests described in Takhounts et al. (2013), where each ATD was impacted in the direction of the primary use (frontal ATDs were impacted at 0^0 angle, side ATDs – at 90^0 to the SAE's x-axis) as well as at the "oblique" angle of 30^0 from the direction of primary use. Thus the correlations in Figure 3.11 already incorporate out of plane head rotation (combined y- and z-axes rotation for frontal ATDs; and x- and z-axes rotation for side ATDs), consequently reflecting current neck properties (stiffness) of each ATD (including torsional or z-axis stiffness) in the relationship between BrIC and CSDM.

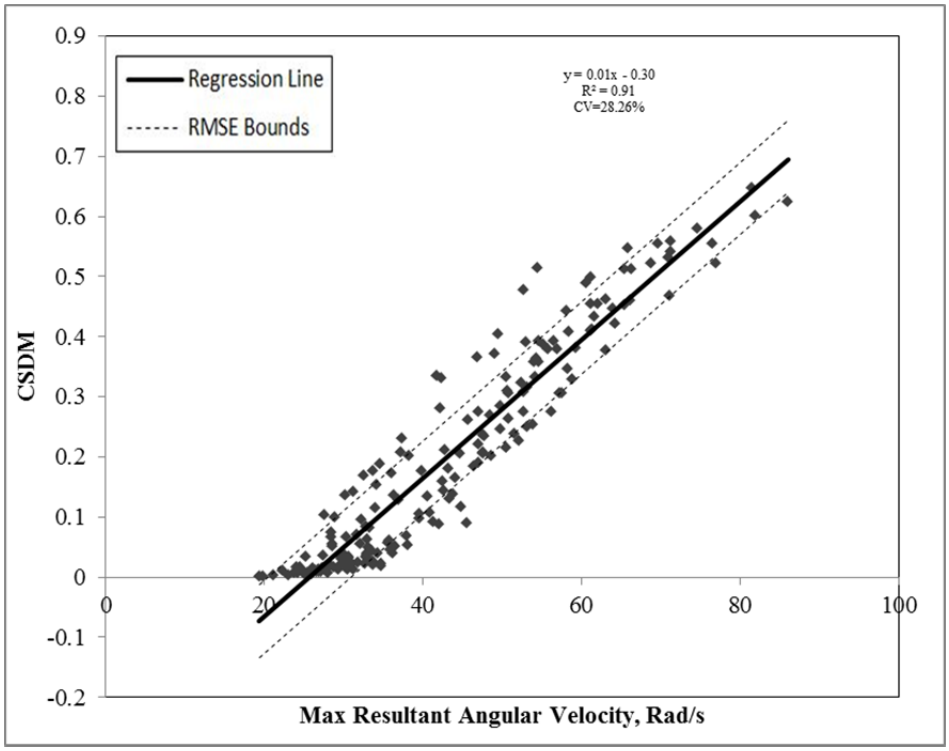

a)

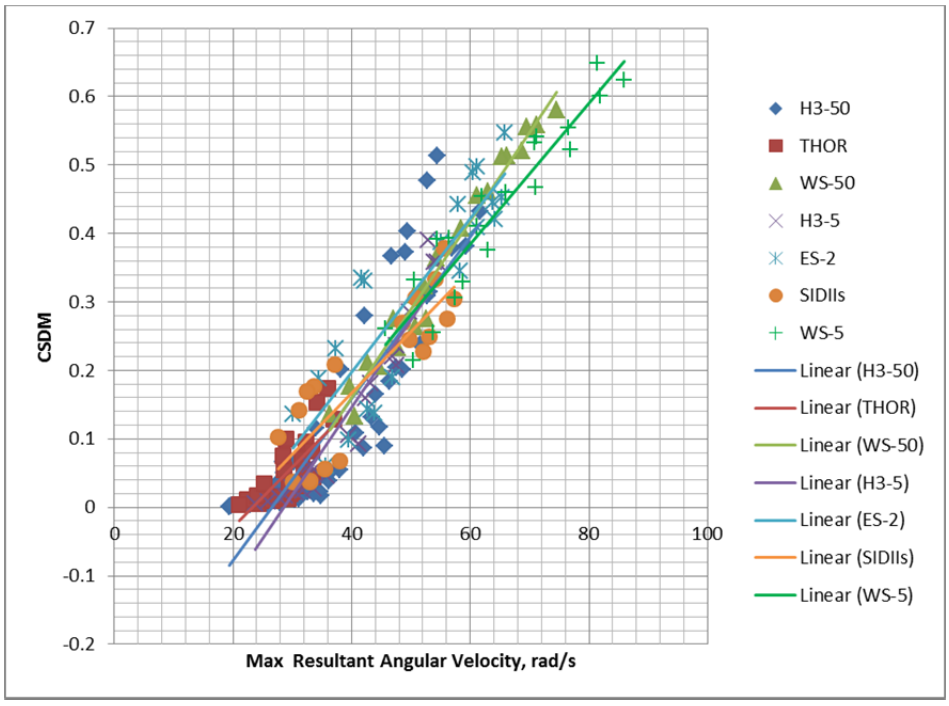

b)

Figure 3.11. CSDM versus max resultant angular velocity for all ATDs (a) and for each individual ATD (b).

3.4.4 Dependence on Time Duration

It has been hypothesized by Holbourn (1943) that "for blows of long duration the shear strains in the brain are proportional to the force, hence the injury is proportional to the acceleration, or the rate of change of velocity of the head… For very short blows the injury is proportional to the force multiplied by the time for which it acts, hence the injury is proportional to the change of velocity of the head…" The switchover occurs somewhere between 2 and 200 ms. Glaister (1975) presented the following chart (Figure 3.12) that was introduced in H.E. von Gierke (1964) demonstrating that the human body response (injury response) when loaded with acceleration pulses of various magnitudes and time durations depends on the velocity change for the first 200 – 300 ms, then on the pulse length (pulse time duration) for up to 2 – 10 s, then for even longer time durations it depends on the peak acceleration. Note that when referring to the signal/pulse time duration, both Holbourn and Glaister (or von Gierke) implied the time duration of the (angular) acceleration pulse (Figure 3.10), and when angular acceleration and time duration are considered together it represents angular velocity upon which BrIC is based. Here, however, the dependence of BrIC on the angular velocity time duration was analyzed.

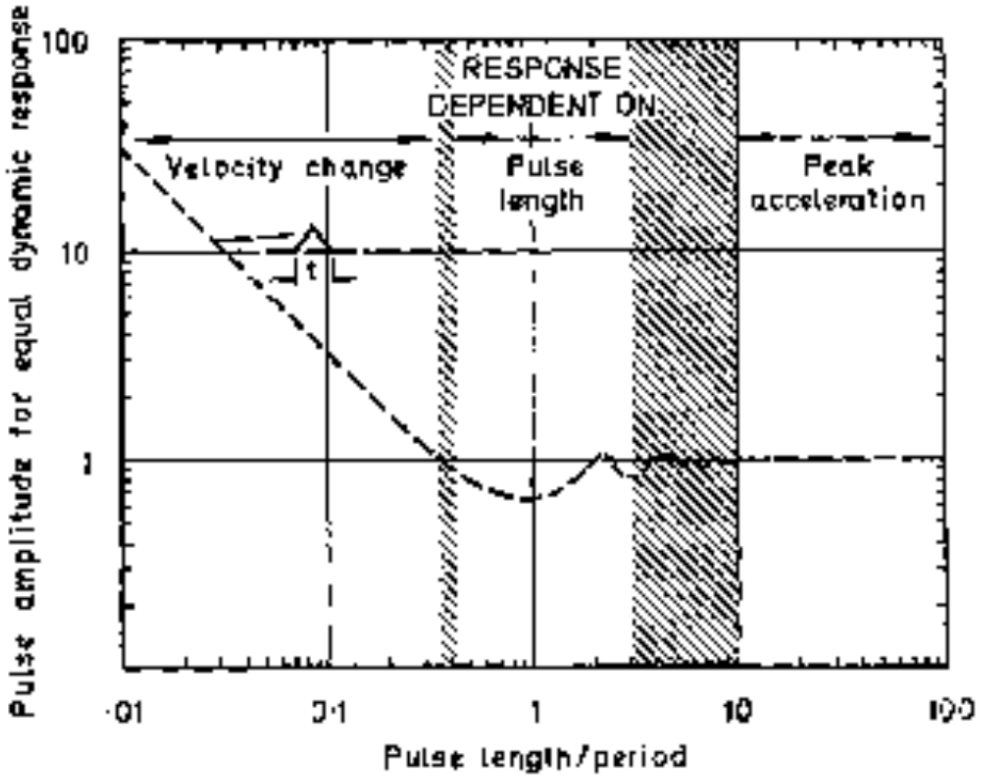

Figure 3.12. Response of human body (injury response) to the applied acceleration pulse of various magnitudes and time durations (copied from Glaister, 1975).

To investigate the potential dependence of BrIC on the angular velocity signal time duration, the haversine type angular velocity time histories shown in Figure 3.13 were applied to the SIMon finite element (FE) head model. The magnitude of the max angular velocity about each rotational axis was

varied from 20 to 120 rad/s at 10 rad/s intervals, while the time duration ranged from 5 to 200 ms with 15 ms time intervals. It can be observed from Figure 3.13 that the slopes of the applied angular velocity signals (or max angular acceleration) are decreasing with increased time duration. Hence, this study of the time duration effect on BrIC/CSDM may also be considered a study of the angular acceleration effect. The values of CSDM for each loading case were calculated and the curves of constant CSDM were plotted as functions of the angular velocity signal time duration. Figure 3.14 illustrates such dependence of CSDM on the signal time duration for rotations about the x-axis (coronal plane rotation). It indicates that up to approximately 30 ms, CSDM is increasing with increased time duration for each magnitude of the max applied angular velocity, and begins to monotonically decrease up until approximately 100 ms, after which it doesn't change. The critical values for angular velocity about the x-axis (x-direction) as functions of the signal time duration can be plotted using two values from the CSDM-based risk curve (Figure 3.15): 0.49 and 0.3, representing 50% and 25 % risk of AIS 4+ brain injury, respectively. These critical angular velocity values decrease for up to approximately 30 ms time duration, after which they begin to increase until approximately 100-120 ms, after which they become relatively constant (independent of the time duration). The current critical value for the x-direction is 66.25 rad/s (Table 3.2), corresponding to approximately 45-ms time duration.

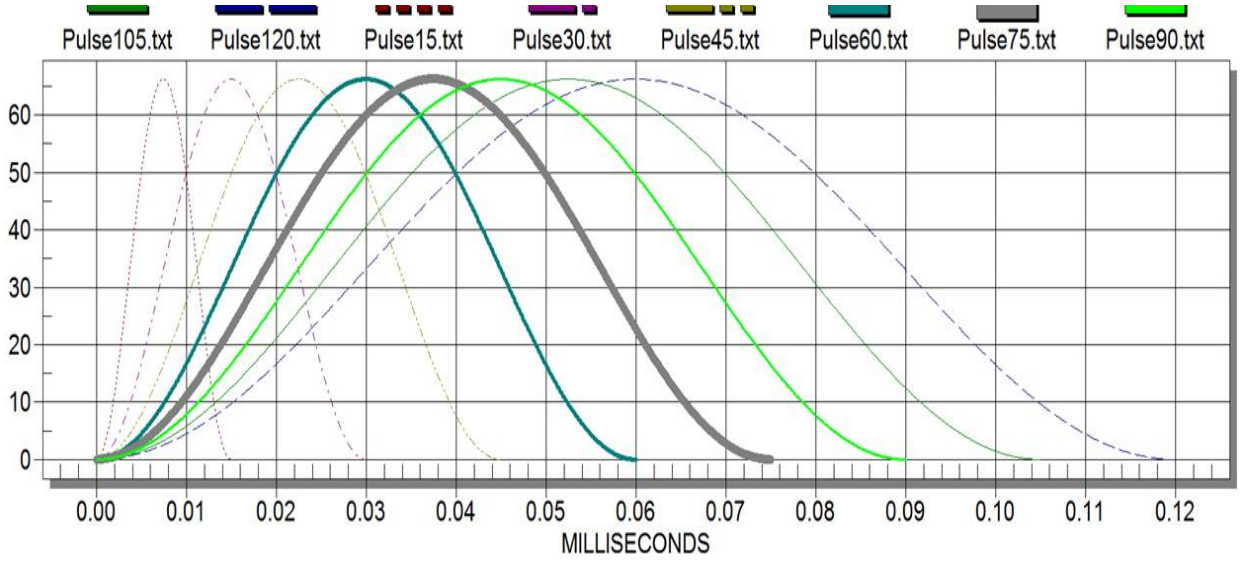

Figure 3.13. Haversine type angular velocity time histories applied to the SIMon head model.

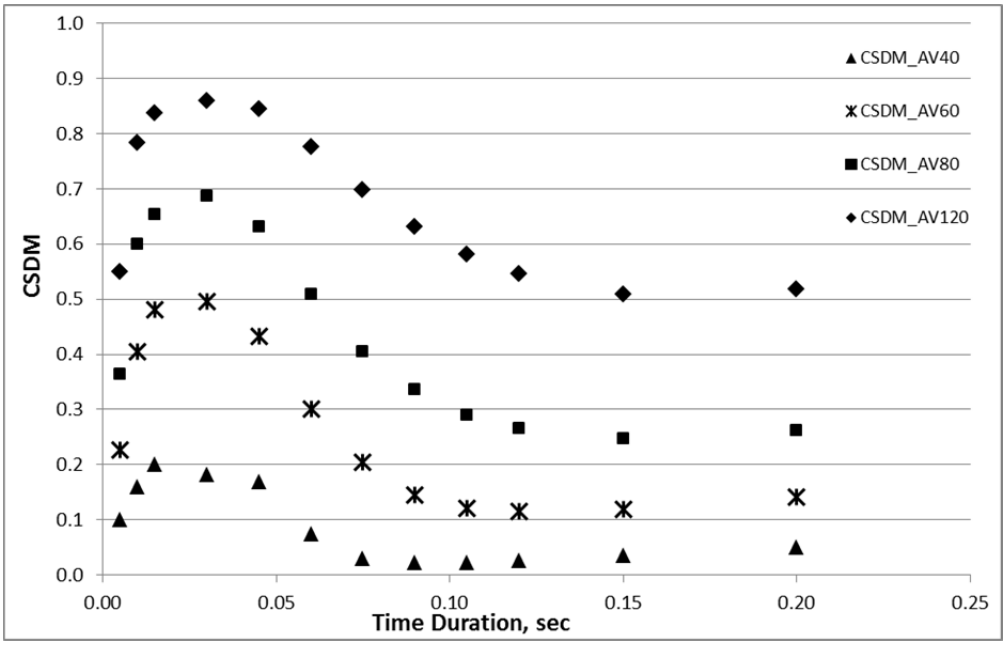

Figure 3.14. CSDM versus x-axis angular velocity signal time duration for four values of the max angular velocity: 40, 60, 80, and 120 rad/s.

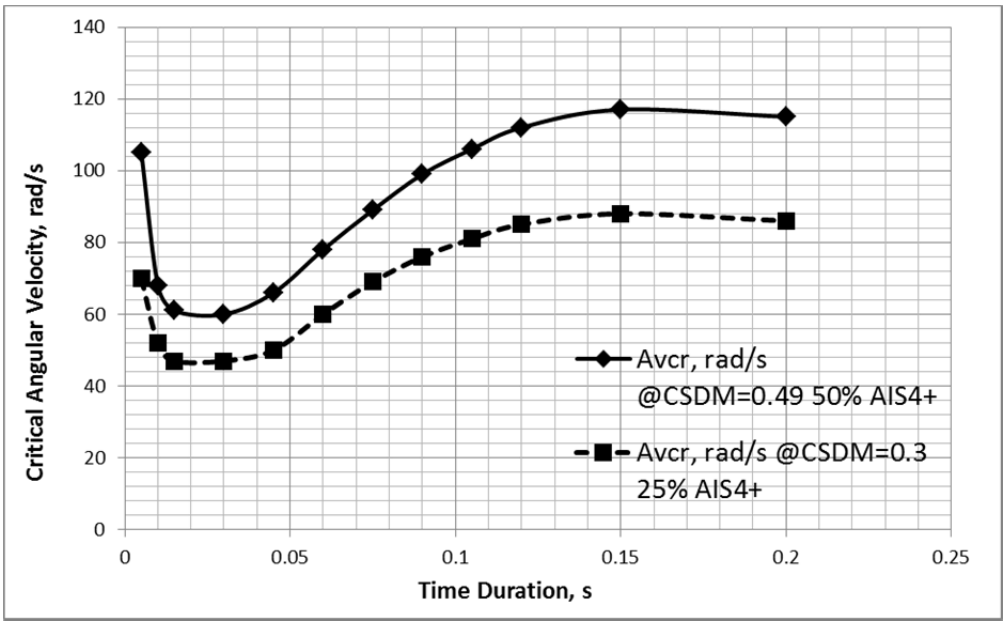

Figure 3.15. Critical angular velocities in x-direction for 50% and 25% risk of AIS 4+ brain injury as functions of signal time duration.

Similar figures for the other two rotational directions (y- and z- directions) were also obtained and their critical values of angular velocity as a function of the signal time duration were plotted and subsequently tabulated (Table 3.7). Table 3.7 can be viewed as a look up table for finding critical angular velocity

when the signal time duration is known. The question now becomes: how to find time duration for an arbitrary angular velocity signal time history?

Table 3.7. Critical angular velocities for each time duration and each rotational direction.

	X-direction		Y-direction		Z-direction	
Time, s	Avcr, rad/s @CSDM=0.49 50% AIS4+	Avcr, rad/s @CSDM=0.30 25% AIS4+	Avcr, rad/s @CSDM=0.49 50% AIS4+	Avcr, rad/s @CSDM=0.30 25% AIS4+	Avcr, rad/s @CSDM=0.49 50% AIS4+	Avcr, rad/s @CSDM=0.30 25% AIS4+
0.005	105	70	92	65	99	57
0.010	68	52	66	52	60	39
0.015	61	47	59	49	46	34
0.030	60	47	58	48	42	32
0.045	66	50	54	46	39	31
0.060	78	60	59	51	50	38
0.075	89	69	68	57	64	49
0.090	99	76	74	62	73	57
0.105	106	81	80	65	81	63
0.120	112	85	84	68	87	68
0.150	117	88	89	70	95	74
0.200	115	86	93	70	100	78

Three methods of estimating time duration for arbitrary signals were devised and the values of BrIC with time adjusted critical values of angular velocities recalculated using Table 3.7 (called “New BrIC”). Only one of the three methods (Appendix B) resulted in an improved R^2 (Figure 3.16) when compared with the “Original BrIC” given in Figure 3.10.

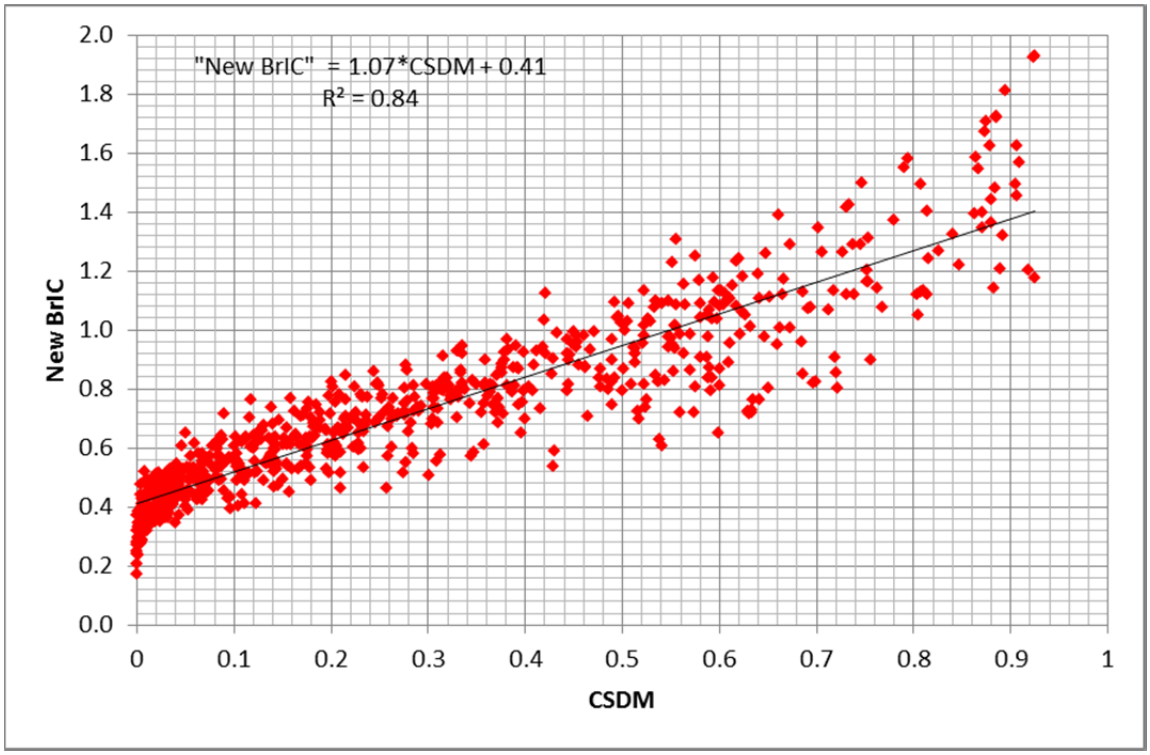

Figure 3.16. Correlation between the "New BrIC" (or time adjusted BrIC) and CSDM.

The R^2 for the "New BrIC" increased to 0.84 from 0.81 for the "Original BrIC," or by 3.7%. The slope and the intercept of the linear regression line are reduced, thus reducing the value of the "New BrIC" corresponding to the 50% risk of AIS 4+ brain injury. From the regression given in Figure 3.10, it can be calculated that a 50% risk of AIS 4+ brain injury (CSDM = 0.49) corresponds to an "Original BrIC" value of 1.06. Out of 749 data points, 160 exceed a BrIC value of 1.06, corresponding to a failure rate of 21.4% for the "Original BrIC." For the "New BrIC," or time adjusted BrIC, the 50% risk of AIS 4+ brain injury at CSDM of 0.49 equals 0.93 as calculated from the regression line given in Figure 3.16. Out of 749 data points, 159 exceed a BrIC value of 0.93, corresponding to a failure rate of 21.2% for the "New BrIC", which is slightly lower than that of the "Original BrIC." The number of cases equal or exceeding the value of CSDM of 0.49 is 189, corresponding to a failure rate of 25.2%. Thus, the failure rate for the "Original BrIC" is closer to that of CSDM.

Figure 3.17 shows histograms of time durations of the head angular velocity for all 749 tests in each direction, calculated using the algorithm given in APPENDIX B. The most frequent time duration in all three rotational directions is 60 ms. From Table 3.7 (for CSDM = 0.49), new critical values for BrIC can be selected to represent the most frequently occurring time duration (Table 3.8).

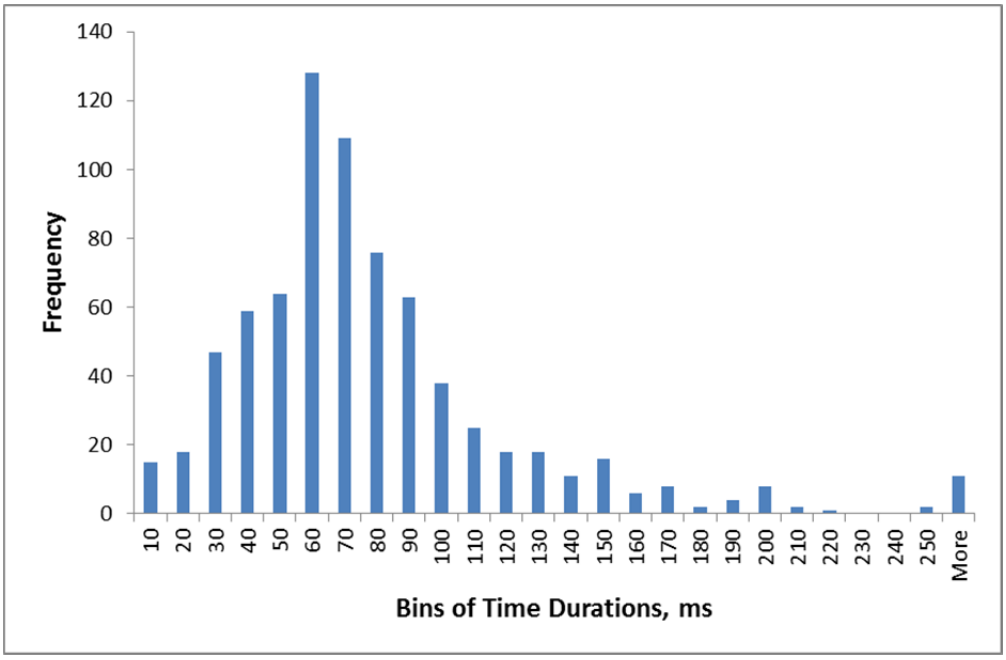
Frequency
140
120
100
80
60
40
20
0
10
20
30
40
50
60
70
80
90
100
110
120
130
140
150
160
170
180
190
200
210
220
230
240
250
More
Bins of Time Durations, ms

a)

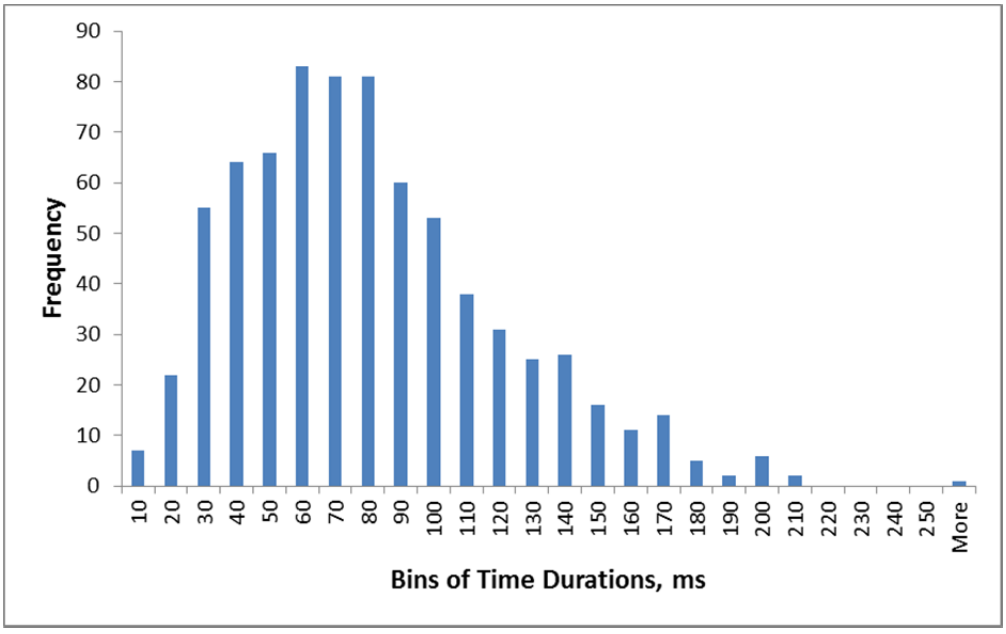
Frequency
90
80
70
60
50
40
30
20
10
0
10
20
30
40
50
60
70
80
90
100
110
120
130
140
150
160
170
180
190
200
210
220
230
240
250
More
Bins of Time Durations, ms

b)

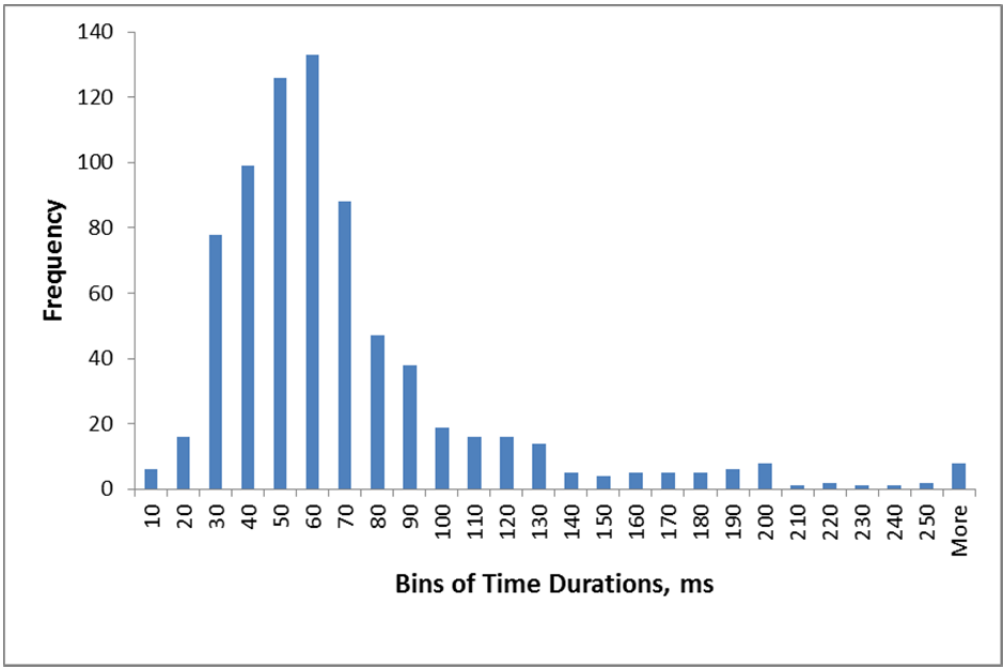

c)

Figure 3.17. Histograms of the angular velocity signal time durations in x-direction (a), y-direction (b) and z-direction (c).

Table 3.8. Critical max angular velocities at the most frequent time durations for each direction.

Critical Max Angular Velocity	Rad/s (Original)	Rad/s (Liberal)
ω_x	66.25	78 @ 60 ms
ω_y	56.45	59 @ 60 ms
ω_z	42.87	50 @ 60 ms

Re-computing BrIC with the critical values of angular velocity shown in the third column of Table 3.8 with higher than original critical values, and replotting another version of the BrIC versus CSDM relationship, gives another version of BrIC, let's call it "Liberal BrIC" (Figure 3.18) due to higher critical values.

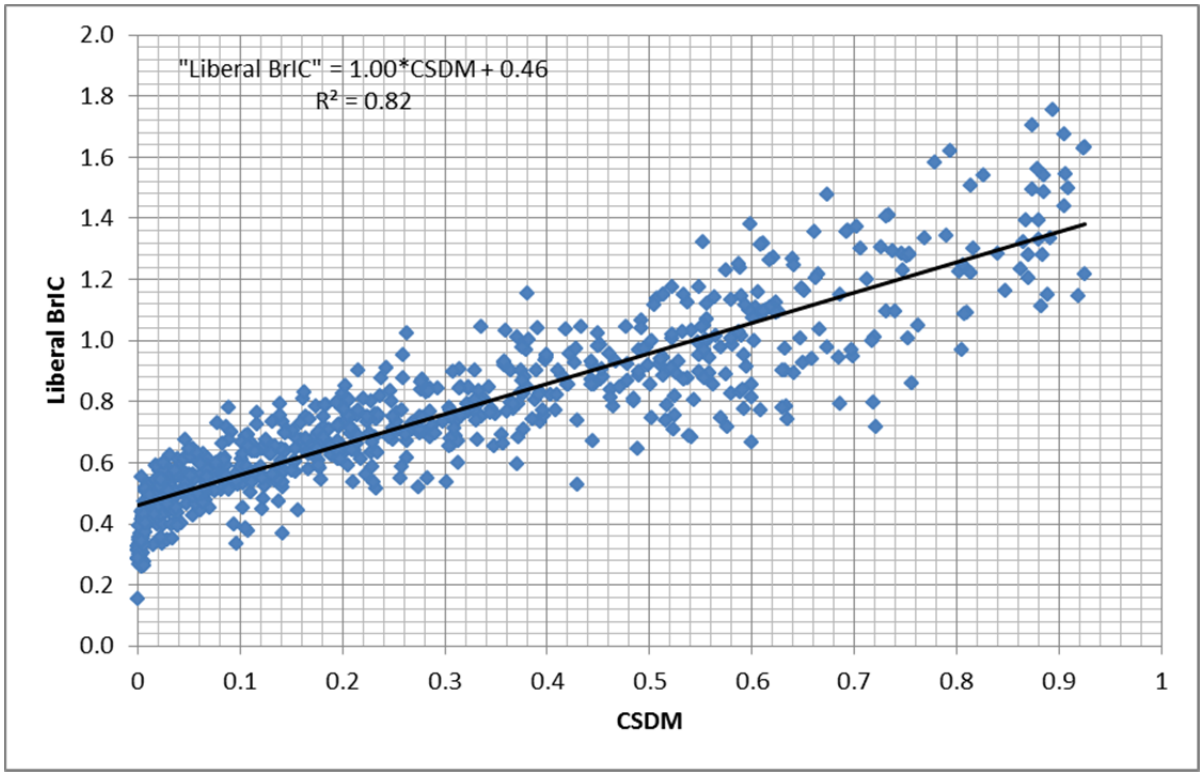

Figure 3.18. BrIC vs CSDM with higher critical values of angular velocities - "Liberal BrIC".

Now, the 50% risk of AIS 4+ brain injury corresponding to CSDM = 0.49 for "Liberal BrIC" equals 0.95 as calculated from the regression equation (Figure 3.18). Little has actually changed compared to the "Original BrIC" given in Figure 3.10; the R^2 values are about the same, but the correlation line moved down by 0.04 with the slight change in slope, giving a lower "Liberal BrIC" number for the same value of CSDM (as compared to the "Original BrIC"). Hence, increasing critical values of angular velocities in BrIC formulation doesn't accomplish anything but shifting the correlation line down with slight decrease in the slope. The "Liberal BrIC" at higher critical values of angular velocity components fails just two fewer cases than the "Original BrIC." Note that CSDM fails the highest number of cases and the number of cases failed by the "Original BrIC" is closer to that of CSDM than the "New BrIC" or "Liberal BrIC."

Figure 3.19 demonstrates the number of true positives (TP), true negatives (TN), false negatives (FN), and false positives (FP) for the "Original BrIC" with the failure level at 1.06 (in blue), "New BrIC" with the failure at 0.93 (in red), and the "Liberal BrIC" with the failure at 0.95 (in green). Overall, the "New BrIC" increases true predictions (based on CSDM = 0.49) from 672 out of 749 for the "Original BrIC" (89.7 % of correct predictions, with the area under the receiver-operator curve AUROC of 0.95 – Figure 3.20) to 677 out of 749 (90.4 % of correct predictions with AUROC = 0.96), or improvement by 0.8% (improvement in AUROC is ~ 1.05%).

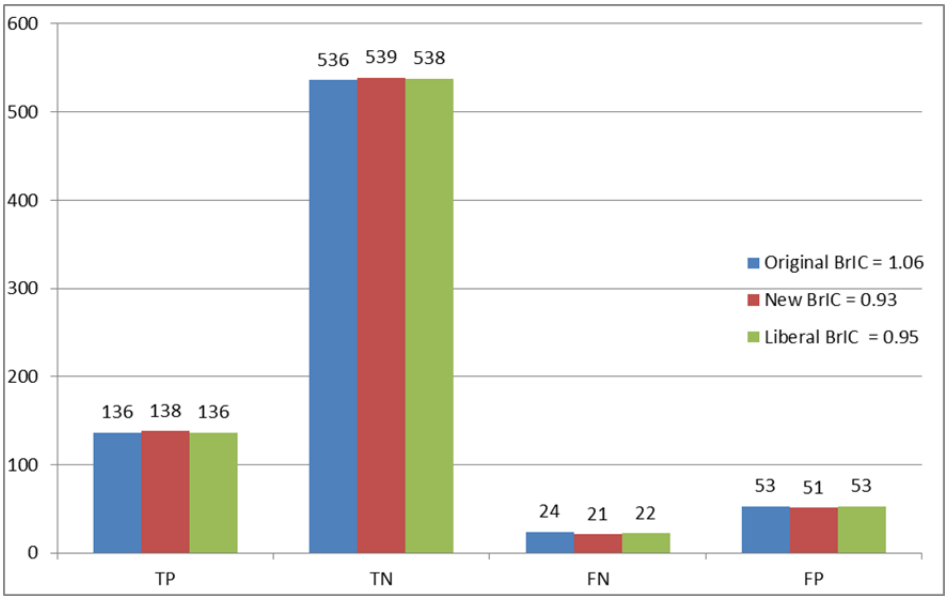

Figure 3.19. Number of true positives (TP), true negatives (TN), false negatives (FN), and false positives (FP) for the "Original BrIC" with the failure at 1.06 (in blue), "New BrIC" with the failure at 0.93 (in red), and the "Liberal BrIC" with the failure at 0.95 (in green).

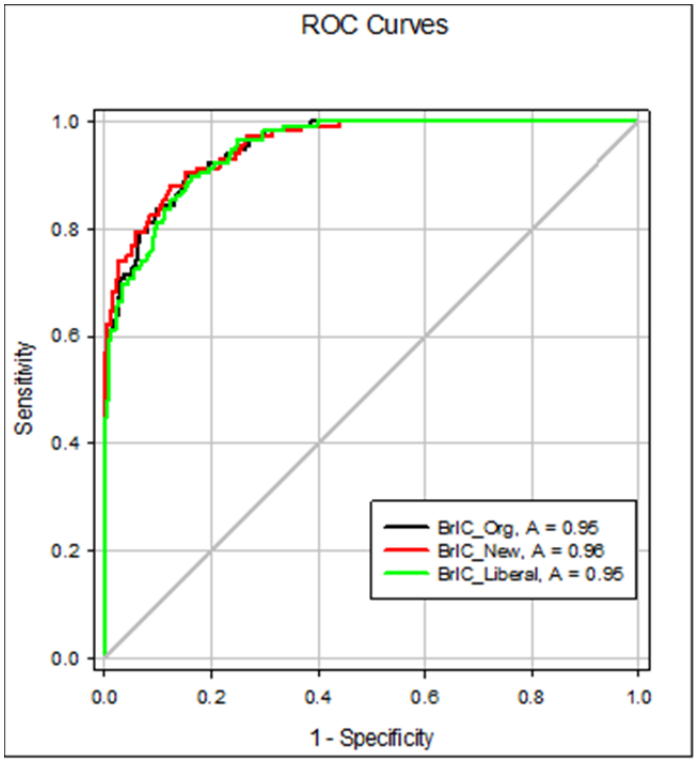

Figure 3.20. Receiver-operator curve (ROC) and the area under the ROC (shown as A) for the "Original BrIC" with the failure at 1.06 (in black), "New BrIC" with the failure at 0.93 (in red), and the "Liberal BrIC" with the failure at 0.95 (in green).

In conclusion, neither adjusting BrIC for the signal time duration nor increasing its critical values offer a clear advantage over the "Original BrIC" when applied for car occupants. A similar conclusion was reached by Gabler et al. (2016). For other loading conditions, such as those seen, perhaps in volunteer tests (or twirling figure skaters) or pedestrians where the time durations are presumably higher than those given in Figure 3.17 – the time adjusted BrIC may be used.

Another study related to the time duration/interval was conducted in which the time "distance" between the peaks of angular velocity components were altered from 0 to 150 ms, and then applied to the SIMon model to calculate CSDM. This study was carried out for three different total time durations of the angular velocity signals (35, 50 and 70 ms). No significant changes in CSDM were observed. In addition, the correlation between BrIC and CSDM was tested for the "instant BrIC," in which angular velocity components were taken at the time of the maximum component of BrIC (the highest ratio of a peak angular velocity component over its critical value). The R^2 for the "instant BrIC" dropped to 0.75. Then, the time window for calculating the max of the other two angular velocity components was expanded to ± 25 ms of the time of peak of the angular velocity component contributing most to the value of BrIC, and the correlation between this "clipped-25 BrIC" and CSDM was tested giving the R^2 value slightly lower than that of the original BrIC. The same process was repeated with a ± 50 ms time window with similar results: the original BrIC had higher R^2 value, although the difference was decreasing with increased time window (note that the original BrIC has an unlimited time window).

3.4.5 Pareto Principle: from Wall Street to BrIC

The current BrIC formulation (equation 3.1) only requires three parameters (maximum absolute values of the head angular velocities in each direction) to be known to calculate the risk of brain injury. One could ask, can the correlation in Figure 3.10 be improved by adding more parameters, such as angular accelerations or time durations? The short answer is – yes, BrIC correlation to CSDM can always be improved as was demonstrated in the section above with the "New BrIC" that takes into account the signal time duration. Among other alternatives, max angular acceleration components may be added to the formulation as independent variables to expand the summation given in equation 3.1. What is the expense, however, of such "improvements?" Is there some sort of a law or principle that can guide the development process with a simple and proven recommendation as to when to stop the "improvements?" Enter the Pareto principle (Pareto, 1896), which is also known as the "80-20 rule," which was originally developed from economic observations. It states that, for many events, roughly 80% of effects come from 20% of the causes (i.e. 80% of land is owned by 20% of population), and later expanded to science, business, occupational health and safety, and other applications (20% of peapods contain 80% of peas, or 80% of all traffic accidents occur during 20% of the time window, etc.). Some argue that the 80/20 ratio is a lot more skewed, and is more like 95/5 (for example, it takes to learn less than 5% of words in a given language to comprehend 95% of conversations; and to get to 98% comprehension (just 3% improvement), would take approximately 12-15 times more effort). The exact 80/20 proportion is not as relevant as the general principle: that a large portion of results come from a small portion of causes, types or circumstances. The principle is also used in Six Sigma – a philosophy and methodology for managing processes and performance. How does this apply to the development of BrIC? Currently, only the knowledge of three parameters is needed (equation 3.1) to calculate BrIC.

These can be easily measured by any ATD with simple instrumentation (angular rate sensors – ARS). However, if angular accelerations are added to the equation 1, then a more complex instrumentation is necessary (nine accelerometer array (NAP) in any configuration, or any other with additional sensors, wiring, channels, etc.), which may increase the risk of measurement failure. The effect of such complication is minimal: perhaps a slight increase in R^2 versus that shown in Figure 3.10 or slightly improved AUROC (see above, for example, 0.8% improvement for the time adjusted "New BrIC"). Is this worth the effort? And if so, then when to stop the improvements as this process is almost infinite with exponentially increasing expense? From the analysis given in the section above combined with the knowledge of Pareto principle, it can be concluded that the current formulation of BrIC is sufficient to correctly capture the vast majority of the occupant cases, and further improvements of the formulation may not be the most efficient way of allocating resources.

3.4.6 Human Volunteer Data: CSDM or MPS?

Human volunteer head rotational data (angular velocities) about the x-axis (Ewing et al., 1977) and y-axis (Ewing et al., 1976) were digitized and applied to the SIMon FE head model. CSDM and MPS were monitored. The values of CSDM ranged between 0.000 and 0.009 for rotations about x-axis (coronal plane rotation for a total of three volunteers) and 0.000 – 0.025 for rotations about y-axis (sagittal plane rotation for a total of nine volunteers), while MPS ranged from 0.29 – 0.41 and 0.15 – 0.59 respectively. The lower values of CSDM are not surprising due to the much longer signal time duration seen in volunteer tests when compared to those measured in the ATDs and FE models (see DOE and Optimization studies below) for occupants in the vehicle crash environment. Using risk curves for CSDM and MPS (Figure 3.8), the risk of sustaining AIS 4+ brain injury under the loading conditions measured in volunteer tests is 0.003% for the max CSDM of 0.025 and 19.3% for the max MPS of 0.59. Given the fact that none of the volunteers sustained any brain injury, it would appear that CSDM is a more appropriate measure of the brain injury risk than MPS. In addition, MPS may be susceptible to potential numerical inaccuracy of a single finite element in the model, while CSDM is an "integral" measure with much smoother response due to the way it is calculated (see Takhounts et al., 2003 for details of calculating CSDM). Given an almost equal number of pros and cons for CSDM and MPS described in Takhounts et al. (2013), in which MPS-based risk curves for BrIC were suggested, this additional volunteer data makes the case for CSDM-based risk curves for BrIC more appealing. For this reason, all of the prior analysis on the signal time duration was given for CSDM only.

It should be noted, however, that the referenced human volunteer data was for healthy young adults. The risk of injury in those young adults may be different than for the average driving population. For example, would the risk of brain injury for 80-90 year olds (who are still driving cars and getting in crashes) exposed to the same loading conditions as the healthy young volunteers have remained as low as was computed by CSDM? Until such data exists or the strains in the "older" brains are compared to those of the "younger" brains under identical loading conditions using computational models, the answer to the question above remains unknown.

3.4.7 Design of Experiments and Optimization Studies

Separately, NHTSA (See APPENDIX C) has completed design of experiment (DOE) and optimization studies of BrIC using the GHBMC 50th male simplified occupant model (version M50_OS_v1.8, Global Human Body Models Consortium, LLC) in a modified sled model of a Toyota Yaris (Reichert et al., 2014). In short, this effort describes in detail the parameters (crash and restraint) that BrIC is most sensitive to and highlighted the correlation between BrIC and these parameters. Additionally, the DOE and optimization studies demonstrate how other injury measures (HIC and chest deflection) change (i.e. are correlated to) with increasing/decreasing BrIC values during optimization studies.

3.2.8. Summary - BrIC

The equation for BrIC as a function of max angular velocity components (equation 3.1) - along with its correlation to CSDM - originally developed in Takhounts et al. (2013) was tested extensively. These tests included:

1. Additional data was added (various NHTSA tests, IIHS tests, and laboratory – airbag tests, etc.) to investigate if the correlation between BrIC and CSDM from the originally published 413 data points (shown in Figure 3.7a) would change with the addition of 336 data points (Figure 3.10). Neither slope nor the intercept have changed significantly (compare Figure 3.7a) and Figure 3.10). The change in R^2 was also insignificant (changed from 0.84 to 0.81). This indicates the "stability" of the BrIC versus CSDM relationship irrespective of the ATD and the test mode.
2. Developing BrIC for individual ATDs is futile as is demonstrated in Figure 3.11.
3. Dependence of critical angular velocities for BrIC (in equation 3.1) on the signal time duration (and/or dependence of CSDM on the signal time duration) was thoroughly investigated and found that such dependence is significant. However, when applied to the occupants of vehicles in various crash conditions, this dependence on signal time duration becomes insignificant as is assessed by the change in R^2 and AUROC. The "New BriC" (time duration dependent BrIC) improved performance (AUROC) of the "Original BrIC" by approximately 1%, which was concluded to be insignificant based on the Pareto principle.
4. For the demonstration purposes, the critical values of the angular velocity components in the BrIC formulation (equations 3.1) were increased significantly (called it "Liberal BrIC") to investigate how such increase will affect the assessment of the brain injury risk. It was demonstrated that such increase in critical values of angular velocity components only shifts the correlation between BrIC ("Liberal BrIC") and CSDM down (reduces the intercept and the value of BrIC corresponding to CSDM= 0.49 - 50 % risk of AIS 4+ brain injury) with no significant changes in R^2 or AUROC (Figure 3.20).
5. Another time duration/interval study was conducted in which the time interval between the peaks of angular velocity components was altered and the effect of such alteration on CSDM was studied. The effect was found to be insignificant. In addition, "instant BrIC" (all angular velocity components values are taken at the same time of the highest component of BrIC), clipped to ± 25 ms, and ± 50 ms were looked at and found that R^2 value decreases with the decreased clipping time with the lowest value for the "instant BrIC."

6. Human volunteer data (Ewing et al., 1976, 1977) was used to compute the risk of injury (or non-injury since none have reportedly sustained any brain injury). It was found that CSDM (showing low risk of brain injury) was more representative of the injury outcome from these volunteer tests. Based on these volunteer tests, the CSDM based risk curves for BrIC were recommended (Figure 3.9a and Table 3.3).
7. To investigate parameters affecting BrIC limited DOE studies were conducted (APPENDIX C) the DOE was limited to the same vehicle dimensions, steering wheel parameters, frontal airbag size, seat position, and occupant parameters including the size, stature, gender and initial position. When delta-V and PDOF were included into the parameters list following conclusions were reached:
    a. Out of nine parameters varied in this study (see Table C.1 for the list of parameters, their nominal values and the varied range), delta-V influences values of BrIC the most (33.3 % influence), followed by PDOF (28.0 % influence).
    b. Increasing PDOF increases the range of values of BrIC, yet it is possible to find a set of parameters with smaller values of BrIC.
    c. When investigating relationships between various parameters, such as BrIC and delta-V, metamodels are more useful than just a scatter plot of the two parameters because various other parameters (for example, when looking at the fleet tests of various vehicles with various sets of restraint parameters) contaminate the relationship (contrast Figures C.8 and C.9) leading to erroneous conclusions about the "true" relationship.
    d. Correlation between the values of BrIC and delta-V and PDOF is the strongest (higher correlation coefficients) and positive (with increased delta-V and PDOF the values of BrIC also increase).
8. When delta-V was fixed to 35 mph and PDOF was fixed at 0^0 (representing full frontal crash mode), -20^0 (representing near side driver oblique crash mode), and $+20^0$ (representing far side driver oblique crash mode) the following parameters were found to be affecting BrIC the most (Table C.9): frontal airbag mass flow rate, load limiter, frontal airbag friction, side airbag friction (for the near side driver oblique crash mode), and frontal airbag firing time (for the far side driver oblique crash mode).
9. DOE studies indicated that it was possible to select many combinations of the investigated parameters yielding values of BrIC corresponding to zero to small risk of brain injury depending on the crash mode.
10. Optimization studies were conducted using a genetic algorithm for the global minimum search, in which BrIC was the objective function subject to constraints in HIC_{15} (constrained to 700), central chest (sternal) deflection (constrained to 63 mm), left and right femur force (both constrained to 10 kN). First, parameters identified as important in the DOE studies (Table C.9) were varied and optimal solution for BrIC was searched for each crash mode separately. It was shown that:
    a. It was possible to obtain low values of BrIC for each crash mode with the highest optimized BrIC in the far side driver oblique crash mode (just under 0.6), and under 0.5 for the full frontal and near side driver oblique crash modes.

b. Decreasing HIC_{15} and/or sternal deflection caused BrIC to increase (and vice versa) indicating that optimizing for just one injury parameter without the knowledge of others may lead to so called "unintended consequences;" for example, currently both – HIC_{15} and sternal deflections are used as injury criteria (but not BrIC), minimization of which without the knowledge of its effects on BrIC may lead to increased risk of brain injuries – the observation that was also confirmed with the field data analysis.

11. When one set of optimization parameters was chosen and ran at various PDOFs (or crash modes), the following observations were made (Table C.12):
    a. The values of BrIC (not optimized) can be kept in a relatively low range for the near side driver oblique runs up until -25^0 PDOF; when the PDOF angle was furthered to -30^0, BrIC significantly increased due to the head almost missing frontal airbag.
    b. The value of BrIC for the far side driver oblique run at PDOF of $+20^0$ was relatively high compared to that when optimized for just this test condition (BrIC was equal to 0.59 – see last column of Table C.10).
    c. HIC_{15} values were relatively low with the highest value of 362 in a full frontal run – this is the crash mode in which BrIC was the lowest.
    d. Similarly to HIC_{15}, the highest value of the sternal deflection of 53 mm was in a full frontal run while the lowest – at -30^0 , in which BrIC was the highest (0.93).
12. To investigate the effect of greater airbag coverage, the frontal airbag volume was scaled up from 50 liters (used in all previous studies) to 98 liters and optimization similar to the described above was run for PDOF = -20^0 only (near side driver oblique crash mode). Then a parameter set was identified (not at a minimal BrIC) to investigate if BrIC can be further reduced for all PDOFs (Table C.16) when compared to that given in Table C.12 (for a smaller size airbag). Significant reduction in the values of BrIC was observed demonstrating conceptually that just increasing the frontal airbag size will reduce the values of BrIC while keeping other injury criteria values below their respective limits.

3.5 **Skull / Facial Injuries**

3.5.1 Injury Criteria

The Head Injury Criterion or HIC is a criterion that has been used by NHTSA and many other safety agencies in regulatory and consumer metric crash testing for decades. The risk function for HIC with 15 ms duration (or HIC_{15}) as applied in the current NCAP rating scheme (NHTSA, 2008) is based on short duration (10 ms and under) linear skull fracture experimental data. Prasad and Mertz (1985) tabulated skull fracture experimental data from other experimental sources showing HIC versus the presence or absence of skull fracture (primarily linear fractures). Hertz (1993) performed regression studies on the fracture data from Prasad and Mertz (1985) to produce the AIS 2+ risk function for HIC_{15} that is presented in Eppinger et al. 1999. NHTSA (NHTSA, 2000) created an expanded set of curves producing the current AIS 3+ risk function used in NHTSA's New Car Assessment Program (NHTSA, 2008). The formulation for HIC_{15} and associated risk functions are presented below.

$$p(AIS \geq 2) = \Phi\left[\frac{\ln HIC_{15} - 6.96362}{0.84687}\right]$$

$$p(AIS \geq 3) = \Phi\left[\frac{\ln HIC_{15} - 7.45231}{0.73998}\right]$$

where:

Φ = Cumulative normal distribution function

HIC_{15} = $\left|(t_2 - t_1)\left[\frac{1}{t_2 - t_1}\int_{t_1}^{t_2} a(t)dt\right]^{2.5}\right|_{max}$

$t_2 - t_1 \leq 15\ milliseconds$

t_1, t_2 = beginning and end of calculation time window (in seconds)

$a(t)$ = Head CG resultant acceleration time-history (in g)

Attempts have been made to relate HIC to concussion/brain injury, but are not supported theoretically based on studies of brain injury mechanisms (Takhounts et al., 2013; Takhounts 2015) nor by observed trends in fleet and field data (see Figure 3.1, Figure 3.2 and Table 3.1). For example, Takhounts et al. (2013) showed how HIC has poor correlation to the strain-based measures that are associated with brain injury (Figure 3.21). Takhounts (2015) presented the results of investigations related to two physical brain injury mechanisms were investigated: strain and pressure. It was demonstrated that based on the mechanical properties of the brain and skull, and the experimental data, pressure doesn't cause brain injuries, while strain does. It was also shown that head translational accelerations (upon which HIC is based) correlate to pressure while causing small strains in the brain compared to those caused by the rotational head motion.

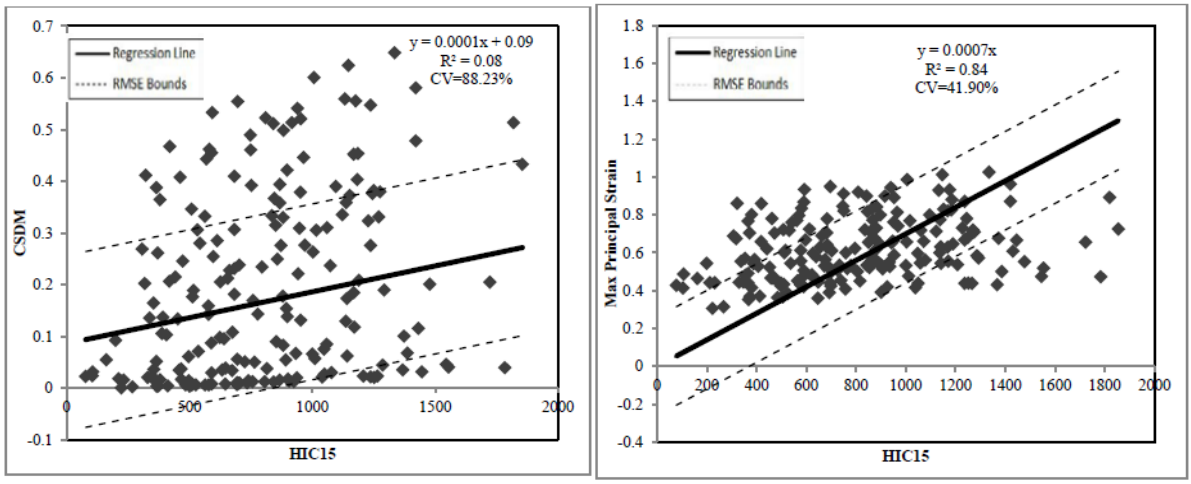

Figure 3.21. CSDM and MPS vs. HIC_{15} (from Takhounts et al., 2013).

The previously mentioned DOE study (APPENDIX C) also found in some cases a negative correlation between BrIC and HIC meaning that optimizing to reduce one measure may result in an increase in the other.

Based on the findings from fleet and field data, the findings from the DOE studies and the fact that the current functions are based on linear skull fractures produced from short duration head impacts to rigid surfaces, NHTSA is planning to use both HIC and BrIC with the THOR-50M. BrIC will be applied for the purpose of mitigating brain injuries while HIC will be used to mitigate against the types of hard contacts that can cause skull and/or facial fractures.

3.6 Fleet Test Data: THOR-50M

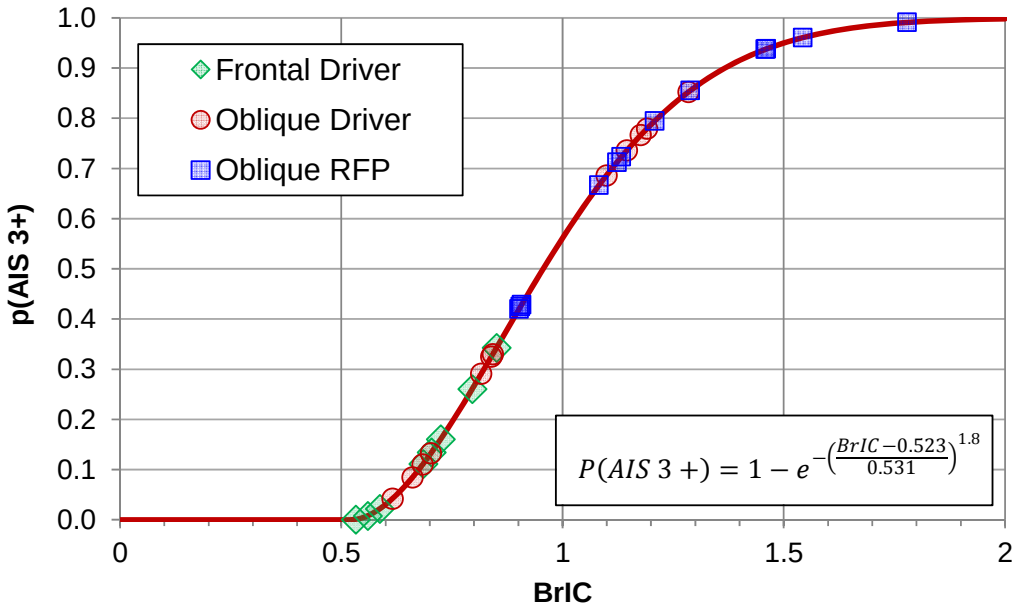

Figure 3.19. Probability of AIS 3+ brain injury predicted using BrIC measured from fleet test results for the driver in the frontal rigid barrier test mode and both the driver and right front passenger in the Oblique MDB test mode.

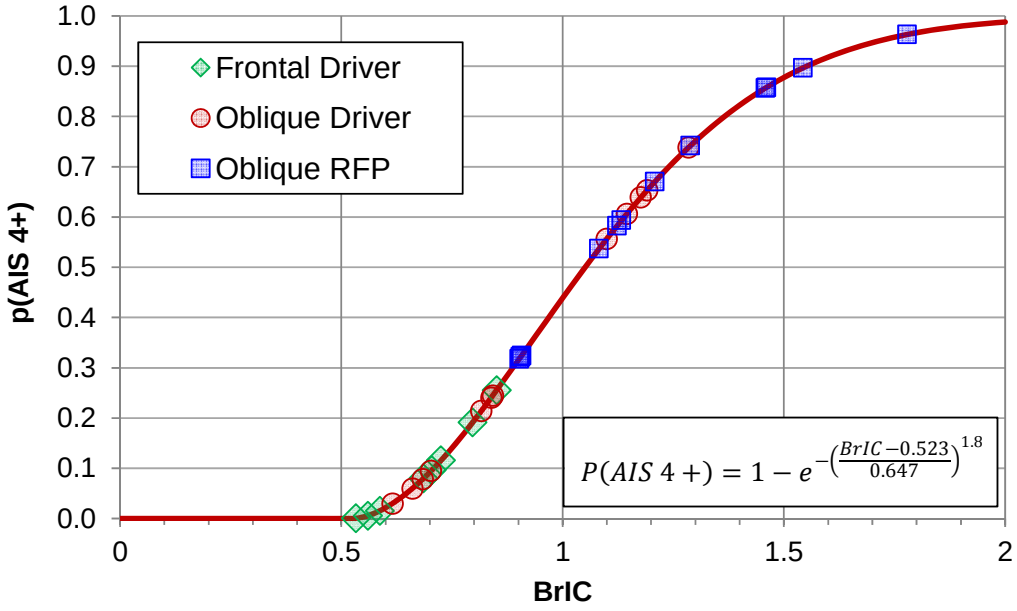

Figure 3.20. Probability of AIS 4+ brain injury predicted using BrIC measured from fleet test results for the driver in the frontal rigid barrier test mode and both the driver and right front passenger in the Oblique MDB test mode.

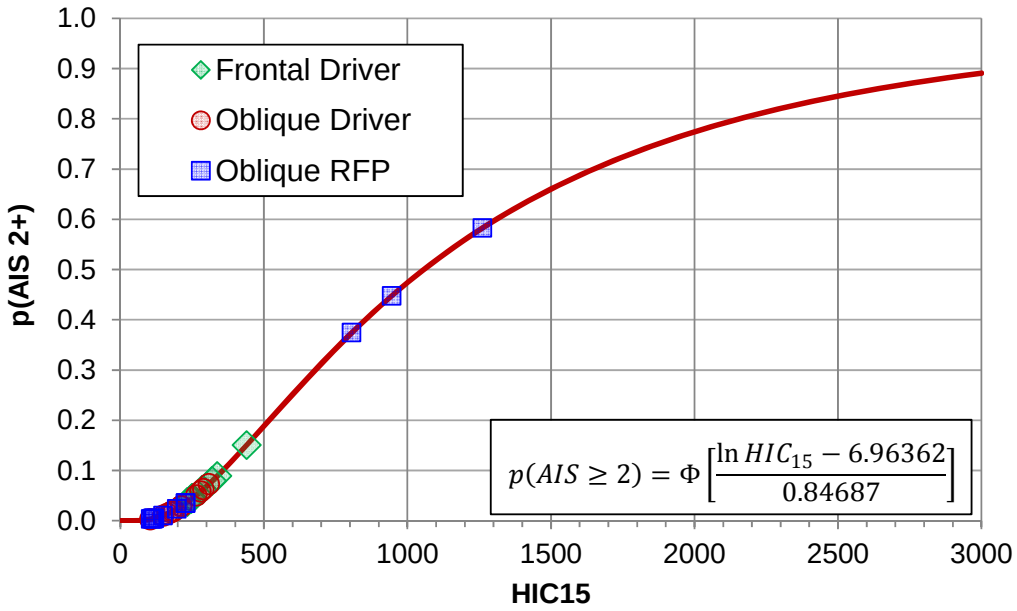

Figure 3.21. Probability of AIS 2+ skull/facial injury predicted using HIC_{15} measured from fleet test results for the driver in the frontal rigid barrier test mode and both the driver and right front passenger in the Oblique MDB test mode.

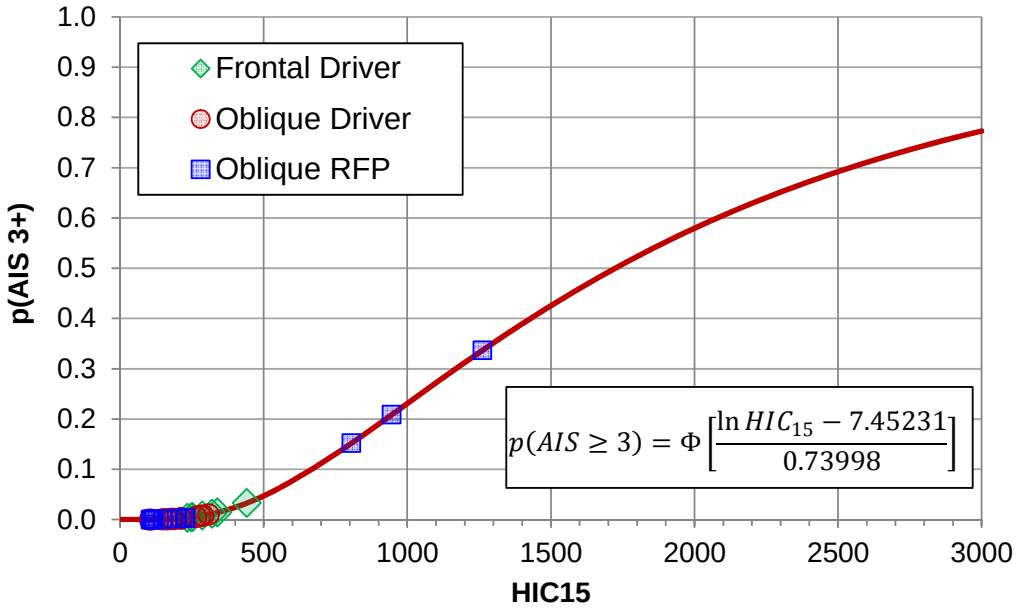

Figure 3.22. Probability of AIS 3+ skull/facial injury predicted using HIC_{15} measured from fleet test results for the driver in the frontal rigid barrier test mode and both the driver and right front passenger in the Oblique MDB test mode.

4 NECK

4.1 Field and Historical Fleet Data

Figure 4.1 presents the regional mechanisms of injury assigned to neck and cervical spine injuries in CIREN front-row belted occupants involved in frontal crashes. While these recorded mechanisms are inferred from the available data and may have been limited to available researcher/published biomechanical knowledge at the time, it can still be concluded from these CIREN cases that neck injuries result from a variety of combinations of loading. It is important to note that the mechanisms shown are regional mechanisms, not organ-specific mechanisms. That is, the chosen mechanism represents the type of loading/motion experienced by the entire neck structure.

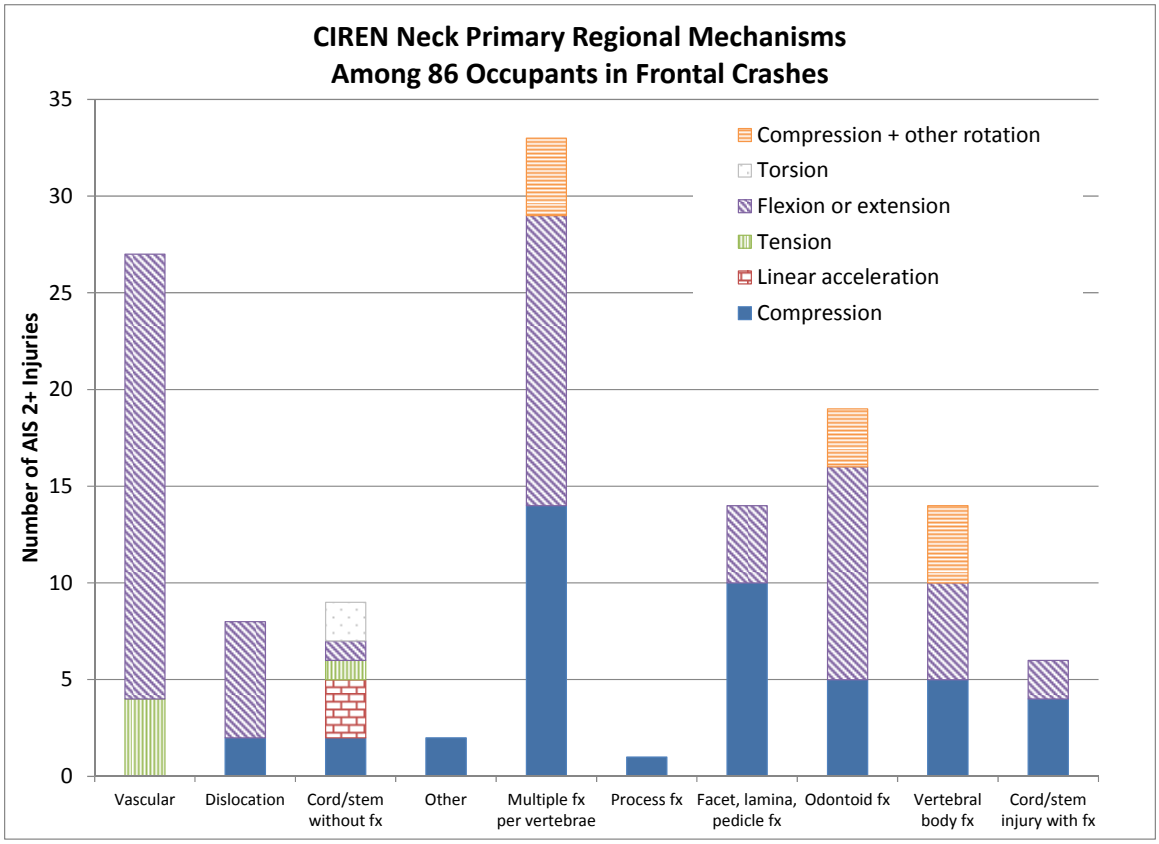

Figure 4.1. Recorded mechanisms of neck and cervical spine injuries for belted front row occupants involved in frontal crashes from the CIREN database.

Figure 4.2 presents the vehicle model year-based trend for AIS 3+ neck injuries for belted drivers in frontal crashes. While there appears to be an increasing trend, the range of percent risk, roughly 0 to 0.3%, is small.

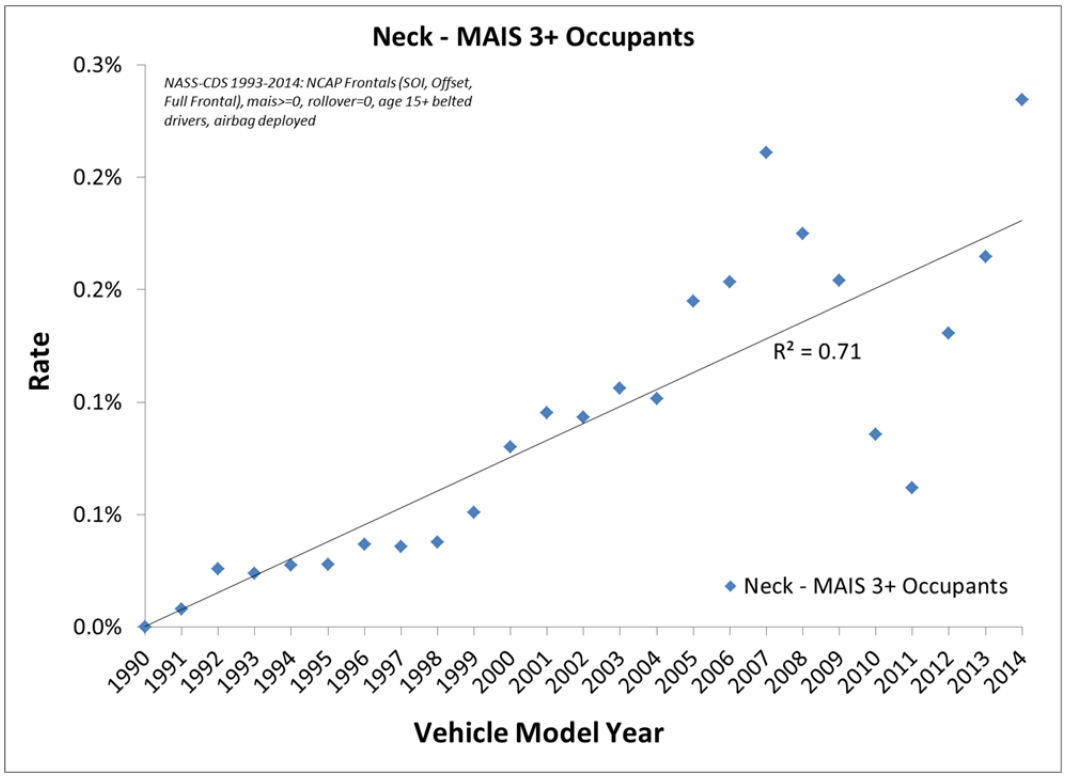

Figure 4.2. Neck injury rate by model year (1993 to 2012) for frontal crashes in NASS-CDS 1993 to 2014.

The trend for Hybrid III 50th male Nij values in 35-mph full frontal tests can be seen in Figure 4.3. Two versions of risk are presented. The first is based on the Nij risk curve that is used in the current NCAP program (NHTSA, 2008). The second uses updated data presented in Mertz and Prasad (2000) and a Weibull curve-based risk function developed using survival analysis.

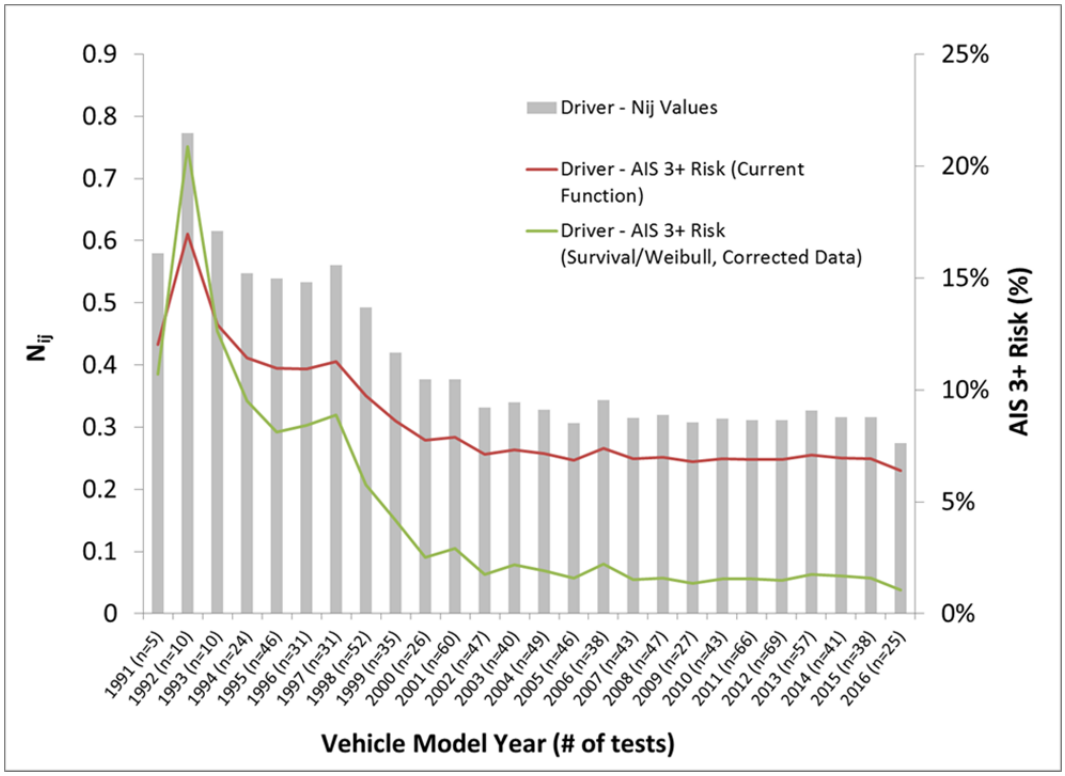

Figure 4.3. Hybrid III 50th percentile driver Nij values and predicted AIS 3+ risk (both current NCAP risk function and revised version based on corrected data and Survival-Weibull function) from model year 1990 to 2016 in 35-mph frontal NCAP tests.

4.2 Literature Review

The risk of neck (i.e. cervical spine, including spinal cord) injury in motor vehicle crashes is important to consider because cervical spine injuries in motor vehicle crashes continue to result in significant morbidity (Wang et al. 2009) and have high attributable cost relative to other body regions (Figure 1.2). In belted front row adults, cervical spine injuries are caused by a variety of mechanisms, including all four primary modes (flexion, extension, tension, compression) as well as combined loading (Figure 4.1). In addition, for the CIREN population shown in Figure 4.1, the most common involved physical components were the belt (flexion/extension of the neck due to restraint of the torso by the belt), A-pillar (head contact), airbag (head/torso restraint by the airbag) and steering rim (head contact). The wide variety of injury causation mechanisms and involved physical components demonstrate the need for either a number of separate injury risk functions, or an inclusive injury measure such as the Nij neck injury criterion.

The Nij neck injury criterion used in Federal Motor Vehicle Safety Standards (FMVSS) No. 208 (Eppinger et al. 1999; Klinich et al. 1996) was originally developed to target out-of-position occupants. The Nij criterion was formulated based on paired tests conducted with anesthetized piglets and baboons, and instrumented 3-year old anthropomorphic tests devices (ATDs) built by General Motors (Mertz et al., 1982) and Ford (Prasad and Daniel, 1984), in typical out-of-position configurations (i.e. with the

occupant close to deploying airbags). The injuries sustained suggested a primary mechanism of high tensile loads in the neck. Based on the paired tests, Prasad and Daniel (1984) proposed that combined tension and bending moments was a better predictor of injury than tensile forces alone. Critical intercepts for the Hybrid III family of dummies were derived from these animal tests, scaled up to adult human level. Other data used in forming the intercepts were from Mertz et al. (1978), where a Hybrid III 50th male ATD was subjected to impacts using a spring-loaded tackling dummy, Nyquist et al. (1980) wherein a Hybrid III 50th ATD was used to reconstruct field crashes (of which only five were injured, and those at the AIS 1 level), and Mertz et al. (1971), wherein flexion and extension bending moment tolerances were described based on volunteers tested up to pain tolerance and cadaver tests that were non-injurious. In short, the intercepts were not based on human adult tolerances, and therefore may not adequately represent the target population of interest. Also given a reliance on the Hybrid III dummy to develop some of the intercepts, they would not be appropriate for use with the THOR-50M dummy.

Since the original formulation of Nij, newer experimental data has been conducted (e.g. Nightingale et al. 2007, Dibb et al. 2009) that expands the knowledge of human tolerances without relying upon scaled animal or dummy data. These data will be described in more depth in upcoming sections. In addition, computational human models have been developed (Chancey et al. 2003) and validated under a wide variety of conditions including pure bending, tension-bending, compressive impact, and volunteer frontal flexion (Dibb et al. 2011). Human models allow estimation of the contribution of muscles to neck response whereas PMHS do not. For an ATD, the THOR-50M is uniquely able to separate muscle and osteoligamentous contributions to neck loads due to its design involving anterior and posterior neck cables, making comparisons to both PMHS and computational models feasible. The availability of new experimental data and the enhanced biofidelity of the THOR neck allow for improved ability to develop a human cadaver based set of neck injury measures for THOR-50M. In contrast to previous efforts that focused heavily on protecting out-of-position occupants who were seated close to a deploying airbag, current injury measures are being developed for normally seated or in-position front row occupants, due to both THOR's intended use applications as well as the current understanding of neck injury causation in the field, as described above.

4.3 **Design**

The THOR-50M neck assembly consists of a series of aluminum disks and rubber pucks which are molded together using an epoxy resin system. The elliptical rubber pucks provide the desired frontal, lateral, and torsional bending responses for the neck assembly. Compression springs are located in the fore and aft regions of the skull. A center safety cable provides durability, while a neoprene spacer at the attachment of the lower neck load cell provides compliance in axial tension. In addition, rubber soft stops at the base of the neck aid in achieving the desired bending characteristics in both front and rear motion.

4.4 Instrumentation

The instrumentation for the neck assembly includes a pair of skull spring load cells, which measure the compression at the front and rear spring locations; six-axis load cells at the top and base of the neck to measure the forces and moments developed at these locations; and a rotary potentiometer at the occipital condyle pin to measure the relative rotation between the head and top of the neck (Figure 4.4).

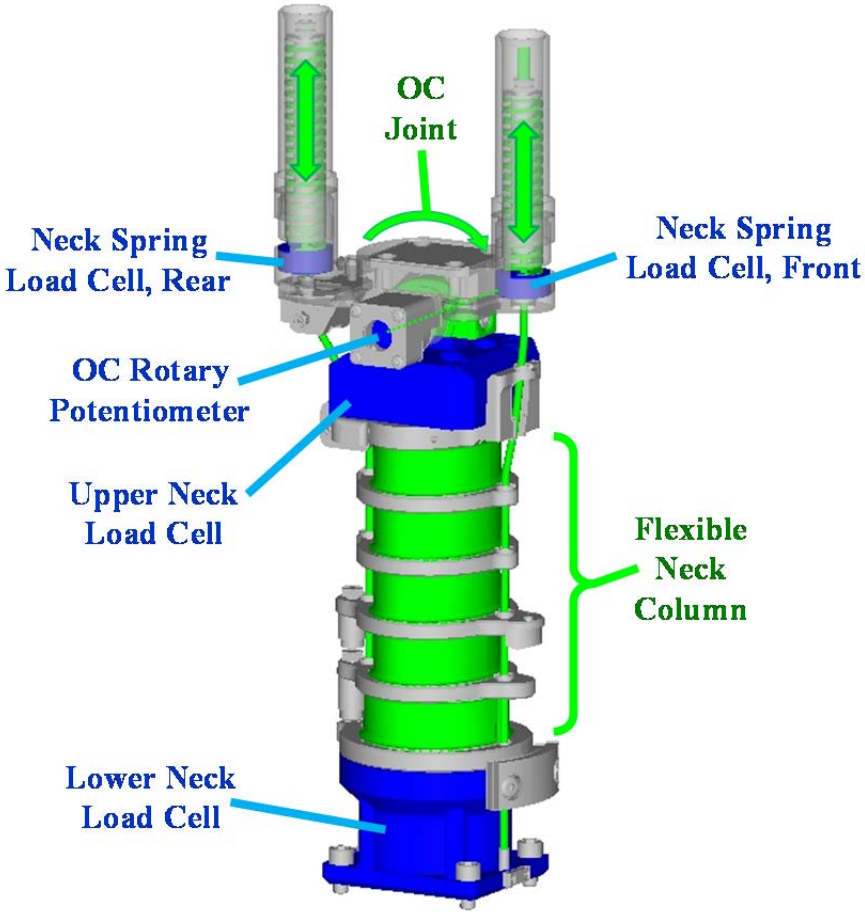

Figure 4.4. THOR-50M neck instrumentation.

4.5 Biofidelity

Biofidelity of the THOR-50M neck was assessed in three conditions (Parent, 2016): frontal flexion, lateral flexion and torsion. In the frontal and lateral flexion conditions, from which the response was based on volunteer testing conducted by the Naval Biodynamics Laboratory (known as the "NBDL" condition), the THOR-50M demonstrated acceptable kinematic and dynamic biofidelity, and was improved compared with H3-50M. In torsion, the THOR-50M response qualitatively showed a similar loading slope to the PMHS response corridor, but did not exhibit the low-moment toe region over the first 50 to 75 degrees of rotation in the human response. The overall neck internal and external BioRank scores were 2.155

and 2.127, respectively. The THOR-50M was quantitatively more biofidelic than the H3-50M (overall BioRank scores of 2.185 and 4.318, respectively).

Despite its improved biofidelity in frontal flexion, the response of the THOR-50M neck still does not exactly replicate the human response. Therefore, transfer functions are required to develop injury risk functions for THOR-50M from human PMHS data. The THOR-50M responses in each loading mode (tension, compression, flexion and extension) are evaluated separately to determine whether transfer functions are required. In general, this is assessed by comparing the load-displacement response in each loading mode to the human response, evaluated with the Duke Adult Head and Neck Model (DAHNM), which is a hybrid multibody and finite element model that consists of an osteoligamentous cervical spine and head, as well as 22 pairs of cervical muscles (Chancey et al. 2003). For the purposes of this analysis, modeling was performed using a relaxed muscle configuration, meaning that muscles were included and exhibited relaxed muscle activation levels. This relaxed condition most closely relates to a condition in the THOR-50M wherein muscle cables are not included.

4.5.1 Tension

Both the DAHNM and the THOR-50M neck were exercised in "pure" tension. The tensile line of action was aligned over the occipital condyles. In this condition, the THOR-50M neck was two (2) times stiffer than the human model, exhibiting 3.3 mm of displacement at 1000N of applied axial load, compared with 6.6 mm in the model.

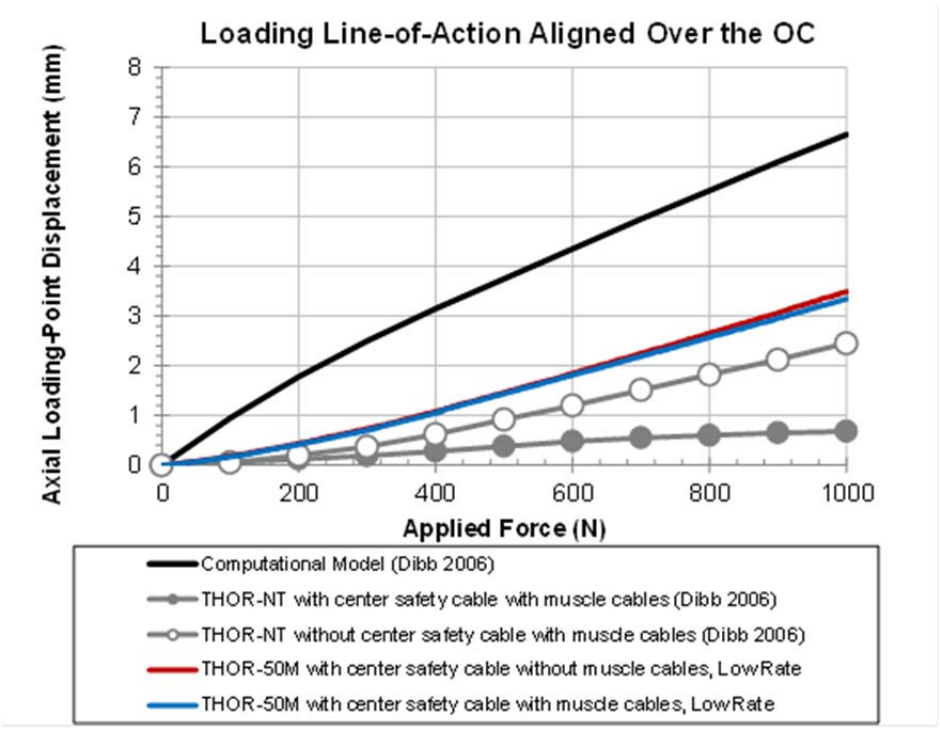

Figure 4.5. Comparison of THOR-50M and human (DAHNM) response in tension.

4.5.2 Flexion/Extension

As noted, the THOR-50M had good overall biofidelity in frontal flexion, as exhibited in the NBDL condition (Parent, 2016). Because the OC moment measured at the upper neck load cell is being considered for application in a THOR-50M injury risk function, an additional comparison between THOR and human at the upper neck load cell is desired. In dynamic flexion and extension, the THOR-50M neck (without cables) closely matched the human model response up to approximately 40 degrees of overall head angular displacement (Figure 4.6), but then diverged from the human model response with increasing angular displacement. To develop a biofidelity transfer function between the THOR-50M and the human model (DAHNM), the difference in rotational stiffness (i.e. the slope of upper neck load cell moment and angular displacement, ΔMy/Δθ) is desired. Figure 4.6 demonstrates the rotational stiffness with respect to the applied moment (applied moment vs. angular displacement, ΔMa/Δθ) and the relationship between applied moment and upper neck load cell moment (ΔMy/ΔMa). These data can be combined to yield the desired rotational stiffness of human and THOR-50M (Table 4.1).

Table 4.1. Moment-angle data for flexion and extension, in THOR-50M (without muscle cables) and the Duke Adult Head and Neck Model (DAHNM).

Study	$\frac{\Delta My}{\Delta Ma}$ (Nm/Nm)	$\frac{\Delta Ma}{\Delta \theta}$ (Nm/deg)	$\frac{\Delta My}{\Delta \theta}$ (Nm/deg)*
THOR-50M	0.64	0.65	0.41
DAHNM	0.26	1.08	0.28

*where $\frac{\Delta My}{\Delta \theta} = \left(\frac{\Delta My}{\Delta Ma}\right)\left(\frac{\Delta Ma}{\Delta \theta}\right)$

Results demonstrate that the THOR-50M is about 1.5 times stiffer than the DAHNM in dynamic flexion and extension.

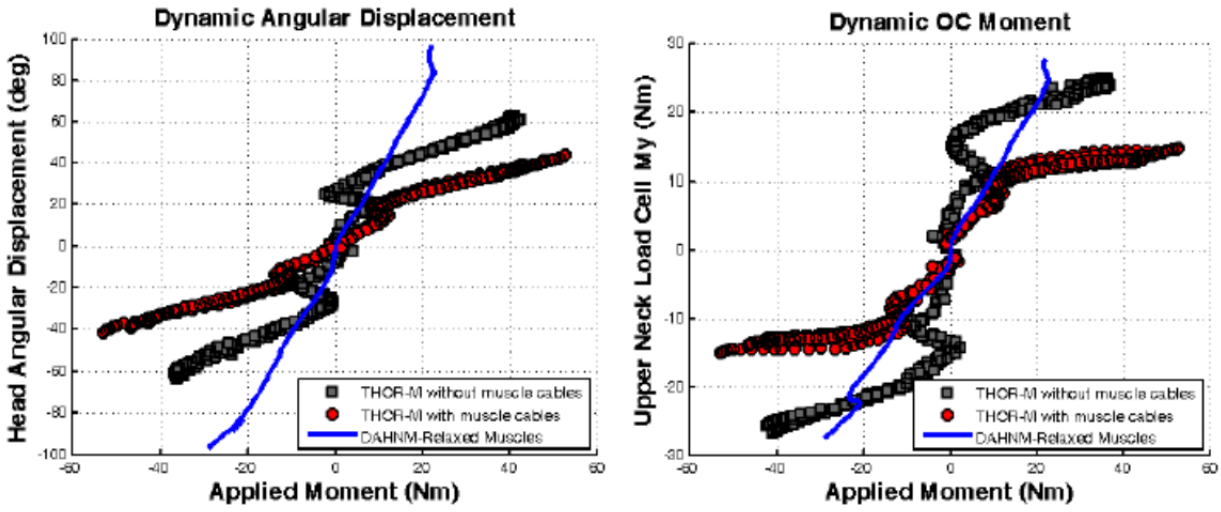

Figure 4.6. THOR-50M neck performance in dynamic flexion-extension, as compared with the human response predicted by the DAHNM.

4.5.3 Compression

In compression, there is insufficient information to develop a transformation for the THOR-50M response. A value of 2 (assume that the compression stiffness ratio is equal to the tension stiffness ratio) will be applied for the transfer function.

4.6 **Data**

As noted above, the data used in the development of the Nij neck injury criterion for use in Federal Motor Vehicle Safety Standards (FMVSS) No. 208 as presented by Eppinger et al. (1999) were not considered to be appropriate for use with the THOR-50M dummy. Instead, human cadaver based data sources, mostly published since Eppinger et al. described the current Nij formulation and risk functions used with the Hybrid III family of dummies, were identified that could be used to develop risk functions in axial loading (tension) and combined loading (Nij). These data sources are described in more detail in the subsection corresponding to each particular loading mode (tension, flexion, extension, compression).

4.6.1 Tension

Dibb et al. (2009) conducted tensile tests on upper cervical spine motion segments both in "pure" tension (loading through the occipital condyles) and combined tension-extension. All specimens were male and all were loaded to failure. Before testing to failure, Dibb et al. conducted non-injurious testing on all specimens (peak loads of about 300 N). This data was not reported in the paper, but the data is available in the NHTSA database. Because the peak loads in the non-injurious testing were so far below those of the failure tests, there was complete data separation and a logistic regression could not be conducted on those datasets alone.

Additional data was therefore sought to determine a tensile injury risk function and tolerance (critical intercept). Due to a lack of additional analogous data using only osteoligamentous neck structures and motion segments, data on whole neck structures was evaluated. Assuming that under tension, the neck acts as a set of springs in series, the tensile tolerance for motion segments is not expected to differ significantly from that of the entire neck. Pintar et al. (2005) conducted high rate tension-extension testing of intact head-neck complexes, using a strap under the chin. Initial non-injurious tests were performed, followed by high speed failure tests. Injuries produced were predominantly C1/2 separations or partial separations. In a similar setup, Yliniemi et al. (2009) conducted high rate tensile testing to failure using intact PMHS head and torso specimens. Tension was applied with a military helmet with an integrated chin-nape strap. There were four females and eight males, and all specimens were tested to failure. Failure loads between these studies (T-1, T-3 and T-4 in Table 4.2) are similar, particularly when considering the loading rates. Tensile failure load is known to increase with loading rate (Nuckley et al., 2005), and thus it is expected that the failure loads in the Dibb et al. (2009) study are below those of the Pintar et al. (2005) and Yliniemi et al. (2009), considering that the loading rate is also lower (Table 4.2).

Table 4.2. PMHS datasets for neck tension risk curve.

	Study	Specimen type	Loading type	Loading rate (and/or displacement rate if provided)	N, injured (AIS 3+)	N, non-injured	Mean (st. dev.) failure load (N)
T-1	Dibb et al. 2009	Motion segments	Pure tension, combined tension-extension, combined tension-flexion	1000 N/s	15	0	2211 (300)
T-2	Duke-unpublished	Motion segments	Pure tension, combined tension-extension, combined tension-flexion	300 N/s	0	24	-
T-3	Pintar et al. 2005	Intact head-neck-torso	Combined tension-extension	4 to 4000 kN/s (1 to 8 m/s)	3	19	2535 (939)
T-4	Yliniemi et al. 2009	Intact head-neck-torso	Tension	0.5 to 0.74 m/s (35-60 kN/s in Hybrid III neck)	12	0	3101 (645)
T-5	Sled tests PMHS-THOR matched pairs	Intact PMHS	Combined tension-flexion	Mean 54,000 N/s (as measured by THOR-50M)	3	45	1182 (604)
T-6	NBDL sled tests-THOR matched pairs	Intact PMHS and volunteers	Combined tension-flexion	Mean 21,900 N/s (as measured by THOR-50M)	0	14	-

As noted in Table 4.2, the tensile testing in Dibb et al. (2009) was performed at approximately 1000 N/s. By contrast, in fleet tests, the THOR-50M experienced loading rates of approximately 54,000 ± 29,000 N/s. Nuckley et al. (2005) developed scaling ratios for baboon spine segments for loading rates between 0.5 mm/s (80 N/s) and 5000 mm/s (1757 kN/s). By interpolation, the baboon failure load at 54,000 N/s is approximately 927 N, which is 1.5 times the failure load at 965 N/s (Table 4.3). To determine the equivalent failure load at 54,000 N/s for the Dibb et al. (2009) specimens, the scaling ratio of 1.5 was applied. This rate-adjusted failure data was used in all subsequent analyses.

Table 4.3. Failure loads based on loading rate, from Nuckley et al. 2005.

Displacement rate (mm/s)	Mean stiffness (N/mm)	Loading rate (N/s)	Baboon mean failure load (N)
0.5	161.4	80.7	468.3
5	193.1	965.5	626.9
50	207.9	10,395	809.3
500	262.6	131,300	1135.3
5000	351.4	1,757,000	2189.5

An additional data source for tension loading is a recent matrix of PMHS sled tests collected by the University of Virginia, consisting of frontal impact sled tests in 12 different velocity or restraint conditions with a total of 42 PMHS observations. In each of these 12 test conditions, at least two THOR-

50M tests were conducted. Later, two additional matched pair test conditions were conducted using both PMHS and THOR-50M, one set with the occupant in a near-side oblique configuration, the other with the occupant in a far-side oblique configuration. A total of 14 test conditions were considered in this matched-pair study, with a total of 48 PMHS observations (Table 5.2). Of the 48 PMHS tested, 3 sustained AIS 3+ cervical spine injury. A limitation to this test series is that PMHS neck loads were not directly measured. Due to this limitation, the matched pair tests are used herein to relate PMHS outcome to THOR measurements in the same test condition. Thus, for this dataset, the THOR-50M neck tensile loads were transformed to equivalent PMHS loads using the biofidelity scaling factor of 2 determined above.

Finally, another data source consists of the volunteers and PMHS run in the NBDL 15 g frontal sled condition. In that condition, there were five volunteers who sustained no injury, and nine PMHS specimens, only one of which sustained an AIS 2 injury (Thunnissen et al. 1995; Wismans et al. 1987). A matched pair test was conducted with THOR-50M in the equivalent condition. As with the UVA sled test series, volunteer and PMHS neck loads were not directly measured. Due to this limitation, the matched pair test is used herein to relate PMHS outcome to THOR measurements in the same test condition. Thus, for this dataset, the THOR-50M neck tensile loads were transformed to equivalent PMHS loads using the biofidelity scaling factor of 2 determined above.

4.6.2 Flexion-Extension

For flexion and extension, the only available data comes from Nightingale et al. 2007, who conducted "pure" bending tests of male upper cervical spine motion segments at a loading rate of approximately 90 Nm/s. Two of the eight specimens tested in flexion sustained AIS 3+ injury, and one sustained AIS 2 injury. In extension, five specimens tested sustained injury. Three additional extension specimens sustained fractures at the fixation; therefore these were excluded from the analysis.

Table 4.4. PMHS data in flexion and extension.

	Study	Specimen type	Loading type	Approximate loading rate	N, injured (AIS 3+)	N, injured (AIS 2)	N, non-injured	Mean (st. dev.) AIS 3+ failure moment (Nm)
F-1	Nightingale et al. 2007	Motion segments	Pure flexion	90 Nm/s	2	1	5	41.9 (8.1)
E-1	Nightingale et al. 2007	Motion segments	Pure extension	90 Nm/s	5	0	0	60.0 (10.2)

Flexion and extension are expected to exhibit similar load rate dependence to that in tension, due to dependence on the same ligaments. Thus, the same scaling ratios developed by Nuckley et al. (2005) apply (Table 4.3). To convert the loading rate from the Nightingale study (90 Nm/s) into the tensile loading rate experienced by the spinal ligaments, one needs to know the distance from the center of rotation (COR) in flexion and extension to the relevant ligaments. While these distances were not known for each specimen tested, representative distances were established for mid-sized males using the Global Human Body Model (GHBMC M50-O v.4.3 50th Percentile Male Occupant Model, Global Human Body Models Consortium, LLC). Using an assumed COR at 2/3 of the distance between the

center of the occipital condyles and the C1/2 joint, the distances from the COR to the anterior and posterior ligaments at C2 were measured on the GHBMC (Figure 4.7).

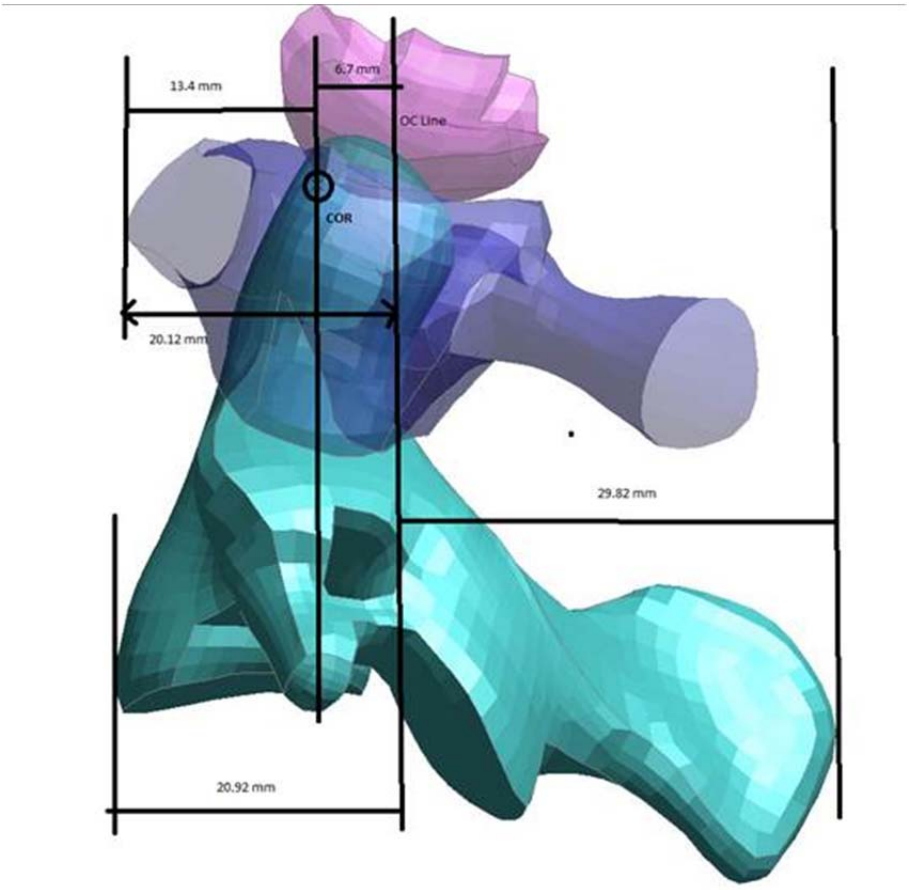

Figure 4.7. Distances from the center of rotation (COR) to the anterior and posterior ligaments at C2, as measured on the 50th percentile GHBMC model.

Table 4.5. PMHS data in flexion and extension.

Loading type	Approximate loading rate	Moment arm to C2 ligaments (mm)	Tensile loading rate (N/s)
Pure flexion	90 Nm/s	36.5	2465
Pure extension	90 Nm/s	14.2	6340

Thus, the specimens tested in flexion and extension testing by Nightingale et al. (2007) experienced tensile loading rates of approximately 2500 to 6300 N/s, respectively. Similar to the rate-adjustment performed on the Dibb et al. (2009) data, this flexion and extension data can be scaled using the Nuckley et al. (2005) loading rate ratios. By interpolation, the baboon failure load at 2565 and 6340 N/s are approximately 656 and 733 N, respectively (Table 4.3). Comparing these values to the interpolated baboon failure load at 54,000 N/s yields scaling ratios of 1.4 and 1.3 that can be applied to transform the

Nightingale et al. (2007) data. This rate-adjusted flexion and extension data was used in all subsequent analyses.

4.6.3 Compression

For compression, studies have been conducted on both motion segments and whole neck structures. Panjabi et al. (1991) conducted pure compression testing on upper cervical spine motion segments (OC-3) using a falling mass impact configuration. Age and sex of individual specimens was not reported, so all specimens were assumed to be male and 61 years (i.e. equal to the mean age). Three specimens sustained no injury to C1, and the results from those specimens were not reported. The remaining eight specimens sustained various types of C1 injuries, four of which were at the AIS 3+ level. Carter et al. (2002) conducted pure compression of lower cervical spine motion segments using a high-rate materials testing fixture. Four males and four females were tested to failure, though none were at the AIS 3+ level. Although an upper cervical spine injury criterion is being targeted, the failure loads in the lower cervical spine motion segments were not significantly different from the upper cervical segments tested by Panjabi. Thus, they were considered for this analysis.

For whole neck structures, Pintar et al. (1995) conducted impact compression testing on intact head-neck complexes that were pre-aligned to remove cervical lordosis. Age and sex, though not reported in the paper, were provided subsequently by the authors. In total, twenty specimens were tested, of which 9 were female and 11 male. Of these, 12 were pre-aligned to produce primarily compression injuries, while eight were pre-aligned to produce flexion or extension injuries. Thus, only the 12 specimens tested in compression are included. The description of the injury was used to categorize "injured" and "non-injured" at the AIS 2+ and 3+ levels. Forces were as measured at the base of spine load cell; OC forces were not provided. Nightingale et al. (1997) conducted head impact experiments using intact head and neck specimens in neutral spine orientation, which included impacts to both compliant and rigid angled surfaces. Neck forces were measured at the base of the spine. In total, 22 specimens were tested, of which 6 sustained AIS 3+injury, 7 sustained AIS 2 injury, and 5 were non-injured. Four male specimens tested with an angled surface of 30° had a lower failure load than the remaining male specimens tested with surfaces angled at 0, +15 and –15 (1650 N vs. 2380 N), due to the confounding (unreported but presumably present) extension moment. These four specimens were excluded from the analysis. Finally, Maiman et al. (1983) conducted axial compression testing on seven male specimens, with preparations ranging from just the cervical spine (C1-T3) to the entire intact head-neck torso, and load applied to the superior aspect of the preparation. Force was as measured at the hydraulic piston. All specimens sustained injury, 2 of which were judged to be at the AIS 3+ level. Differences in test configuration, cervical pre-alignment, and load cell location are known limitations of whole neck test series. However, similarity in reported forces led to these studies being considered herein.

For all datasets combined, females exhibited a significantly lower failure load than males (2202 N vs. 3182 N, $p<0.05$). Thus, for subsequent analysis, only male specimens were used, except in the case of the Panjabi data, which was included despite the sex of each specimen being unknown.

Table 4.6. PMHS datasets for compression.

	Study	Specimen type	Loading	N, injured AIS 3+ (n, males)	N, non-injured (n, males)	Mean Failure load, males (N)
C-1	Panjabi et al. 1991	Upper C-spine motion segment, OC-3	Pure compression (dynamic)	4 (Sex unknown)	4 (Sex unknown)	3029
C-2	Carter et al. 2002	Lower C-Spine motion segments, C5-7	High-rate pure compression	0	8 (4 males)	3447
C-3	Pintar et al. 1995	Head-neck complex with cervical pre-alignment	Compression (with some bending)	12 (6 males)	2 (1 males)	3944
C-4	Nightingale et al. 1997	Head-neck complex with neutral cervical spine position	Compression, (with some bending)	6	12	2377
C-5	Maiman et al. 1983	Differing preparations, ranging from C1-T3 to full head-neck-torso	High rate compression	2 (2 males)	5 (5 males)	3567

4.7 Critical Intercepts for Combined Loading Criterion

4.7.1 Tension

Tension has been established as an injury producing mechanism to the upper cervical spine. In addition, to establish a critical intercept for a combined loading criterion, it is also useful to determine a threshold that corresponds to close to 50% risk for an adult male. The dependent variable used in the development of the tension only criterion was the presence of an Abbreviated Injury Scale (AIS) score of 3 or greater (AIS 3+), based on the AIS 2005 Update 2008 (AAAM, 2008). Using axial tension as the predictor variable, stepwise multiple regression was carried out to assess the sensitivity of occupant-based covariates (age and sex). Neither age nor sex met the significance standard for inclusion in the model ($p<0.1$). Finally, using logistic regression, model significance and goodness of fit were evaluated for four combinations of datasets, to determine which model best fit the data (Table 4.7).

Table 4.7. Goodness of fit statistics for neck tension, AIS 3+ risk curve.

Studies used	Wald Pr>ChiSq	AUROC	Hosmer-Lemeshow Chi-Square	Hosmer-Lemeshow Pr>ChiSq
T-1[1],T-2	Complete data separation – logistic regression not valid			
T-1[1],T-2,T-3,T-4	<0.0001	0.97	7.0	0.53
T-1[1],T-2,T-3,T-4,T-5[2]	<0.0001	0.97	9.6	0.30
T-1[1],T-2,T-3,T-4,T-5[2],T-6[2]	<0.0001	0.97	7.7	0.36

[1]Dibb et al. (2009) data was rate-adjusted

[2]PMHS-equivalent tension = THOR-50M tension divided by 2

For all the logistic regressions, the AUC and model fit statistics were comparable. As such, it is proposed to use the model that included all available data, including the matched pair sled tests. The logistic regression takes the form:

$$p(AIS \geq 3) = \frac{1}{1+e^{(-\beta_0-\beta_1 x)}}$$

where:

β_0	=	Intercept
β_1	=	Independent parameter coefficient
x	=	Neck OC Tension (N)

Table 4.8. Model parameter estimates for neck tension.

Model	β_0	β_1
Neck Tension	-5.5763	0.00264

The risk function and 95% confidence intervals are shown in Figure 4.8. Using the results of the logistic regression (Table 4.8), the critical intercept for a combined loading criterion (e.g. Nij) can be established at the 50% risk level (Table 4.9).

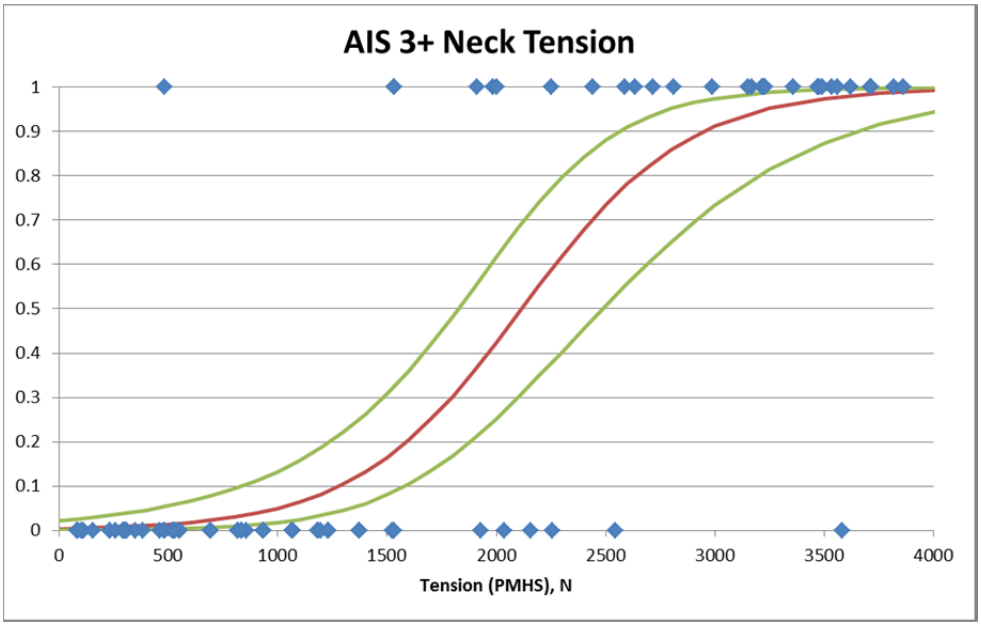

Figure 4.8. Risk function and 95% confidence intervals for neck tension.

Table 4.9. Proposed Nij intercepts for neck tension.

Studies used	PMHS 50% Risk (N)
T-1,T-2,T-3,T-4,T-5, T-6	2100

Once logistic regression was used to determine model goodness of fit, an additional form of the risk function was developed using left/right censored survival analysis. The survival based risk function closely matched the logistic regression curve, but has the advantage of passing through zero at zero stimulus. The survival analysis risk function assumes a Weibull distribution takes the form:

$$p(AIS \geq 3) = 1 - exp\left(exp\left(\frac{\ln(x) - \beta_0}{\alpha}\right)\right)$$

where:

β_0 = Intercept

x = Tension (N)

α = scale

Table 4.10. Model parameter estimates.

Model	β_0	α
T-1,T-2,T-3,T-4,T-5,T-6	7.7727	0.3268

4.7.2 Flexion and Extension

Due to small sample size and insufficient numbers of non-injured specimens, logistic regression was not valid for the available flexion and extension data. Therefore, mean failure loads will define the critical intercepts for the combined loading criterion. However, because the available data was conducted at a slower loading rate than seen in fleet data, and failure load is known to depend on loading rate (Nuckley, 2005), the critical intercepts were rate-adjusted (Table 4.11).

Table 4.11. Proposed Nij intercepts in flexion and extension.

Mode	Quasi-static PMHS intercept	Dynamic load rate scaling factor	Dynamic intercept
Flexion (Nm)	41.9	1.4	58.7
Extension (Nm)	60.0	1.3	78

4.7.3 Compression

Using axial compression as the predictor variable, logistic regression was carried out for different combinations of datasets. Model significance and goodness of fit were evaluated, to determine whether a model could be fit to the available data (Table 4.12). As noted above, females exhibited a significantly lower failure load than males in compression. Thus, for this analysis, only male specimens were used.

None of the combinations of datasets had good model fit, most likely due to the paucity of non-injury data, uncertainties concerning AIS injury level, differences in test configurations, and anatomic considerations (e.g. disc integrity) that affected injury tolerance and resulted in excessive data spread. Therefore, proposed Nij intercepts are based on mean failure loads for males, using all datasets combined (Table 4.13).

Table 4.12. Goodness of fit statistics for neck compression, male specimens only.

Studies used	AIS	Wald Pr>ChiSq	AUROC	Hosmer-Lemeshow Chi-Square	Hosmer-Lemeshow Pr>ChiSq	Overall mean failure load (N)
C-1,C-2,C-3,C-4,C-5	3	0.78	0.58	15.3	0.05	3380
C-1,C-2,C-3,C-4,C-5	2	0.47	0.67	8.5	0.39	3240

Table 4.13. Proposed Nij intercepts in compression.

PMHS intercept	THOR-50M scaling factor	THOR-50M intercept
3200	2	6400

4.7.4 Summary of combined loading criterion intercepts

In summary, each loading mode was assessed separately for determination of critical intercepts. Transfer functions were also developed for each mode to determine THOR-50M intercepts from PMHS data. These intercepts assume a relaxed muscle state. As has previously been done for the Hybrid III ATD, these intercepts could be adjusted by assuming a level of protection provided by muscle tensing. However, the assumed relaxed state is more conservative, and may be more appropriate considering that 40 to 50% of occupants exhibit no pre-impact braking (indicative of being unaware of the impending crash) (Craig et al. 2011).

Table 4.14. Summary of proposed Nij intercepts.

Mode	PMHS intercept	THOR-50M scaling factor	THOR-50M intercept
Tension (N)	2100	2	4200
Compression (N)	3200	2	6400
Flexion (Nm)	58.7	1.5	88.1
Extension (Nm)	78	1.5	117

4.8 Injury Risk Function Formulation

As noted, critical intercepts were developed for the THOR-specific version of the neck injury criterion (Nij) as a metric for assessing neck injury in frontal crashes, based on a comprehensive review of available experimental data. For each specimen, Nij was calculated using instantaneous axial force and y-axis moment data, using the standard formulation and new intercepts (Table 4.15). For tests conducted with the THOR-50M ATD (datasets T-5 and T-6, Table 4.15), loads and moments were obtained directly from the upper neck load cell. This is considered to be more comparable to experimental flexion and extension data conducted on motion segments (Nightingale et al., 2007), from which the flexion and extension critical intercepts were developed, than calculated OC moment. Source data is tabulated in APPENDIX F.

Table 4.15. PMHS datasets for Nij risk curve.

	Study	Specimen type	Loading type	Failure data censoring
T-1	Dibb et al. 2009[1]	Motion segments	Pure tension, combined tension-bending	Peak load reported (left censored)
T-2	Dibb et al. (unpublished)	Motion segments	Pure tension, combined tension-bending	Right censored
T-3	Pintar et al. 2005	Intact head-neck-torso	Combined tension-extension	Peak loads reported (left censored)
T-4	Yliniemi et al. 2009	Intact head-neck-torso	Tension	Failure defined as change in slope in load-displacement curve
T-5	Sled tests (UVA)-THOR matched pair[2]	Intact PMHS	Combined tension-flexion	Peak load reported (left censored)
T-6	NBDL sled tests-THOR matched pair[2]	Intact PMHS and volunteers	Combined tension-flexion	Peak load reported (left censored)
F-1, E-1	Nightingale et al. 2007[1]	Motion segments	Pure flexion and extension	Failure defined as decrease in slope in moment-angle curve
C-1	Panjabi et al. 1991	Upper C-spine motion segment, OC-3	Compression	Peak load reported (left censored)
C-2	Carter et al. 2002	Lower C-Spine motion segments, C5-7	High-rate pure compression, combined compression-bending	Failure defined as a reversal in slope of either axial force or y-axis moment
C-3	Pintar et al. 1995	Head-neck complex with cervical pre-alignment	Compression	Peak load reported (left censored)
C-4	Nightingale et al. 1997	Head-neck complex with neutral cervical spine position	Compression	Failure defined as a reversal in slope of axial force vs. displacement
C-5	Maiman et al. 1983	Differing preparations, ranging from C1-T3 to full head-neck-torso	High-rate compression	Failure defined as the point where force decreased markedly

[1]Data was rate-adjusted

[2]PMHS-equivalent tension = THOR-50M tension divided by 2

The dependent variable used in the development of the neck injury criterion was the presence of an Abbreviated Injury Scale (AIS) score of 2 or greater (AIS 2+) or 3 or greater (AIS 3+), based on the AIS 2005 Update 2008 (AAAM, 2008). Using Nij as the predictor variable, stepwise multiple regression was carried out to assess the sensitivity of occupant-based covariates (age and sex). Finally, using logistic regression, model significance and good of fit were evaluated for four combinations of datasets to determine which model best fit the data (Table 4.16).

Table 4.16. Goodness of fit statistics for Nij risk curve.

Studies used	AIS	Gender included	Wald Pr>ChiSq	AUROC	Hosmer-Lemeshow Chi-Square	Hosmer-Lemeshow Pr>ChiSq
All	3	Males only	<0.0001	0.88	9.6	0.30
T-1[1],T-2,T-3,T-4,T-5[2],T-6[2]	3	Males+Females	<0.0001	0.95	13.8	0.087
T-1[1],T-2,T-3,T-4,T-5[2],T-6[2], E-1, F-1	3	Males+Females	<0.0001	0.94	17.9	0.013
T-1[1],T-2,T-3,T-4,T-5[2],T-6[2]	3	Males only	<0.0001	0.96	7.5	0.48
T-1[1],T-2,T-3,T-4,T-5[2],T-6[2], E-1, F-1	3	Males only	<0.0001	0.96	8.5	0.39
T-1[1],T-2,T-3,T-4,T-5[2],T-6[2], E-1, F-1	2	Males only	<0.0001	0.93	12.8	0.12

[1]Dibb et al. (2009) data was rate-adjusted

[2]PMHS-equivalent tension = THOR-50M tension divided by 2

Neither age nor sex met the significance standard for inclusion in the model ($p<0.1$). However, when all data (males and females) were included, models tended to perform poorly according to the Hosmer-Lemeshow goodness of fit test ($p<0.1$, Table 4.16). This prompted investigation of models that included only male specimens. When only male specimens were considered, the models using the tension datasets (T-1,T-2,T-3,T-4,T-5,T-6), and the tension, flexion and extension datasets (T-1,T-2,T-3,T-4,T-5,T-6,E-1,F-1) performed best, with high AUC values (0.96) and other acceptable goodness of fit statistics. Including compression data (datasets C-1 through C-5) in the development of the risk curve tended to shift the curve to the left in a seemingly unrealistic fashion, resulting in lower Nij values producing higher risks of injury. This may be due, in part, to the methods used in the experimental studies (particularly C-3, C-4, and C-5). Compression studies on whole spines can be confounded by bending moments developed through neck buckling that were unmeasured in the studies (e.g. Nightingale et al., 1997), but nonetheless contributed to overall failure. Given these uncertainties in the experimental data, along with the decreased model fit statistics for the risk curve, these studies are not included at this time. The available compression studies are still used to inform on the critical intercept in compression.

The resulting logistic regression takes the form:

$$p(AIS \geq 2/3) = \frac{1}{1+e^{(-\beta_0-\beta_1 x)}}$$

where:

β_0	=	Intercept
β_1	=	Independent parameter coefficient
x	=	Nij (calculated using upper load cell values)

Table 4.17. Model parameter estimates for Nij.

Model	β_0	β_1
T-1,T-2,T-3,T-4,T-5,T-6, E-1, F-1, AIS 3+, Males	-4.9372	4.5294
T-1,T-2,T-3,T-4,T-5,T-6, E-1, F-1, AIS 2+, Males	-4.3085	5.4079

Table 4.18. Resulting Nij injury assessment reference values.

Model	10%	25%	50%
T-1,T-2,T-3,T-4,T-5,T-6, E-1, F-1, AIS 3+, Males	0.60	0.85	1.09
T-1,T-2,T-3,T-4,T-5,T-6, E-1, F-1, AIS 2+, Males	0.39	0.59	0.80

The AIS 2+ and AIS 3+ risk functions and 95% confidence intervals are shown in Figure 4.9.

a)

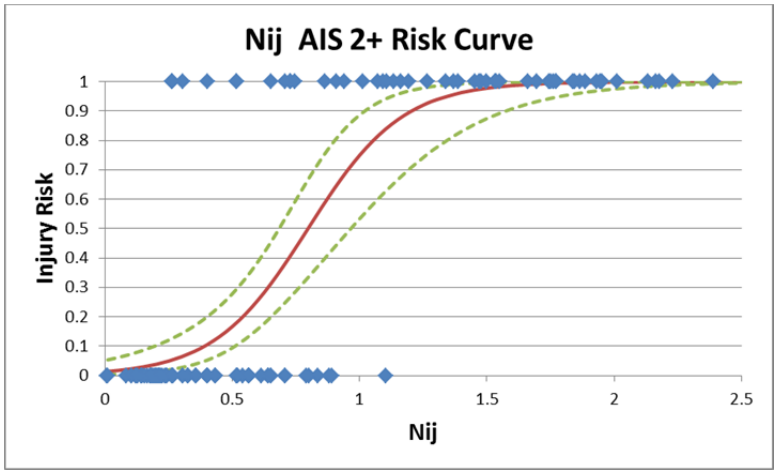

b)

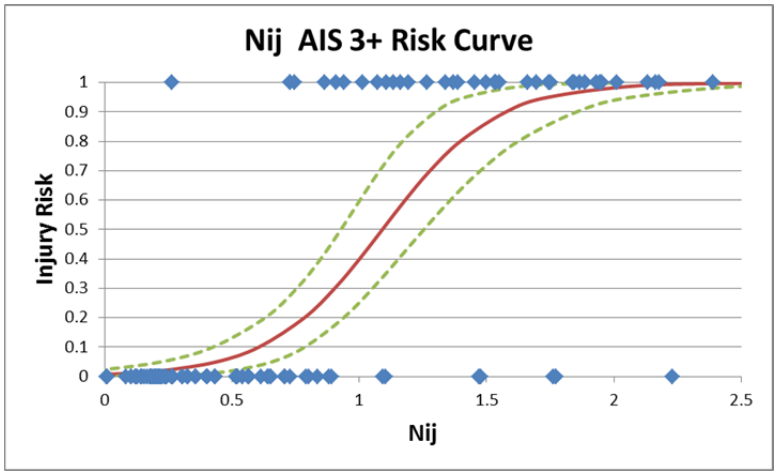

Figure 4.9. Nij risk curve using model (T-1,T-2,T-3,T-4,T-5,T-6, E-1, F-1, Males): a) AIS 2+; b) AIS 3+.

Once logistic regression was used to determine model goodness of fit, an additional form of the risk function was developed using left/right censored survival analysis. All failure data were considered to be left censored and all non-failure data were right-censored. The survival based risk function closely matched the logistic regression curve, but has the advantage of passing through zero at zero stimulus. The survival analysis risk function, which assumes a Weibull distribution, takes the form:

$$p(AIS \geq 3) = 1 - exp\left(exp\left(\frac{\ln(x) - \beta_0}{\alpha}\right)\right)$$

where:

β_0	=	Intercept
x	=	Nij (calculated from upper neck load cell values)
α	=	scale

Table 4.19. Model parameter estimates.

Model	β_0	α
T-1,T-2,T-3,T-4,T-5,T-6, E-1, F-1, AIS 3+, Males	0.2209	0.3644
T-1,T-2,T-3,T-4,T-5,T-6, E-1, F-1, AIS 2+, Males	-0.1147	0.3916

4.9 **Application of Risk Functions to THOR-50M**

Peak Neck Tension:

$$p(AIS \geq 3) = \frac{1}{1 + e^{\left(5.5763 - 0.00264\frac{F_T}{2}\right)}}$$

where:

F_T = Peak tension force measured by the z-axis of the THOR upper neck load cell (in N)

Simplified:

$$p(AIS \geq 3) = \frac{1}{1 + e^{(5.5763 - 0.00132F_T)}}$$

Nij:

$$p(AIS \geq 2) = \frac{1}{1 + e^{(4.3085 - 5.4079 N_{ij})}}$$

$$p(AIS \geq 3) = \frac{1}{1 + e^{(4.9372 - 4.5294 N_{ij})}}$$

$$N_{ij} = \left| \frac{F_z(t)}{F_{zc}} + \frac{M_y(t)}{M_{yc}} \right|_{max}$$

where:

$F_z(t)$ = Peak force measured by the z-axis of the THOR upper neck load cell (in N)

$M_y(t)$ = Peak moment measured by the y-axis of the THOR upper neck load cell (in Nm)

F_{zc} = Critical intercept for force:

$$F_{zc} = \begin{cases} 4200 \; for \; F_z(t) > 0 \\ -6400 \; for \; F_z(t) < 0 \end{cases}$$

M_{yc} = Critical intercept for moment:

$$M_{yc} = \begin{cases} 88.1 \; for \; M_y(t) > 0 \\ -117 \; for \; M_y(t) < 0 \end{cases}$$

4.10 **Fleet Test Data: THOR-50M**

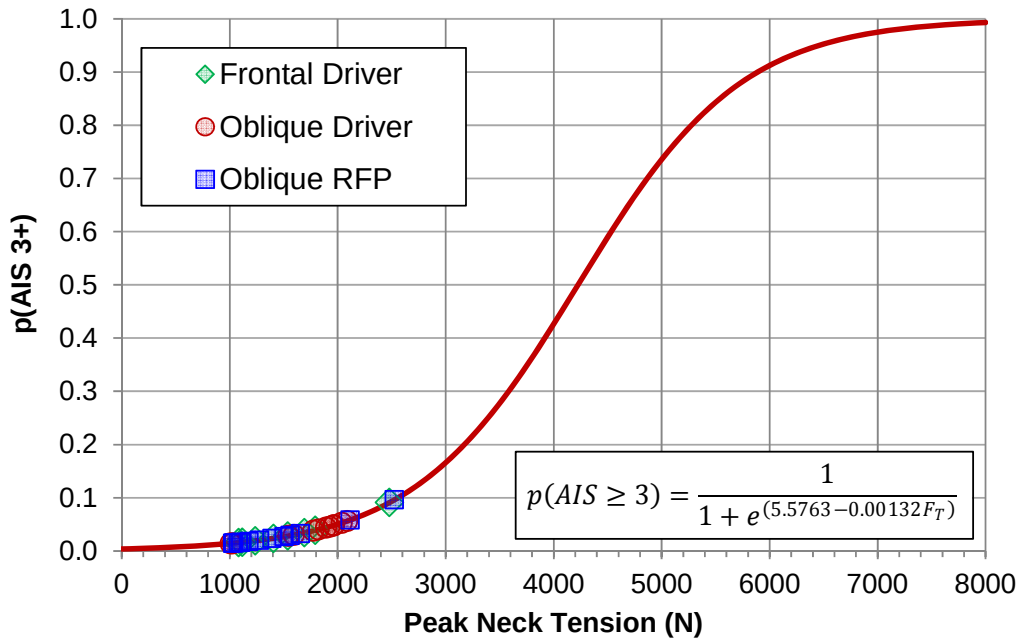

Figure 4.10. Probability of AIS 3+ neck injury predicted using peak neck tension measured from fleet test results for the driver in the frontal rigid barrier test mode and both the driver and right front passenger in the Oblique MDB test mode.

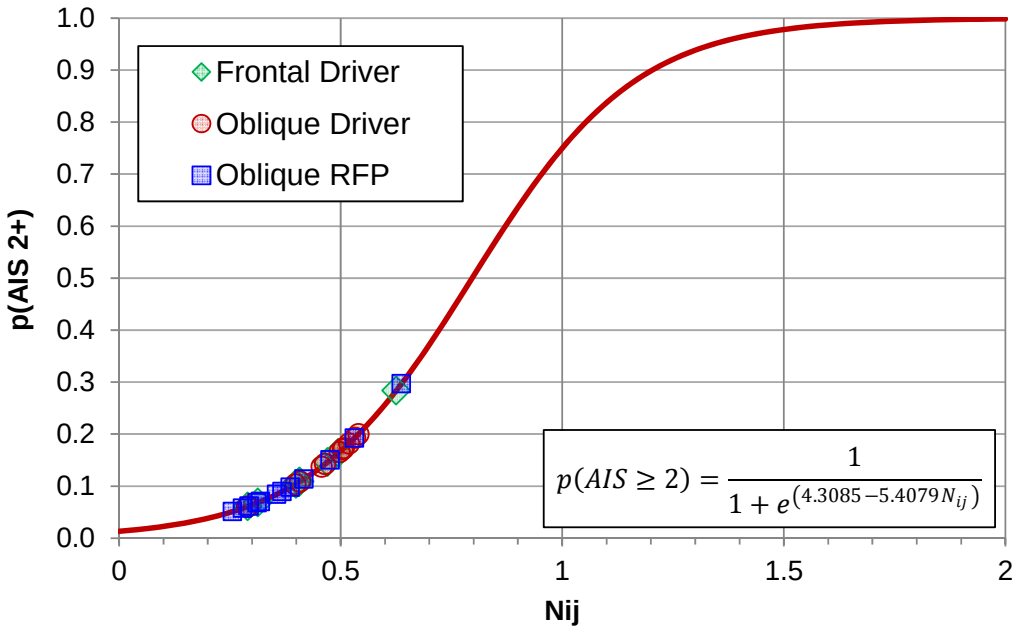

Figure 4.11. Probability of AIS 2+ neck injury predicted using Nij measured from fleet test results for the driver in the frontal rigid barrier test mode and both the driver and right front passenger in the Oblique MDB test mode.

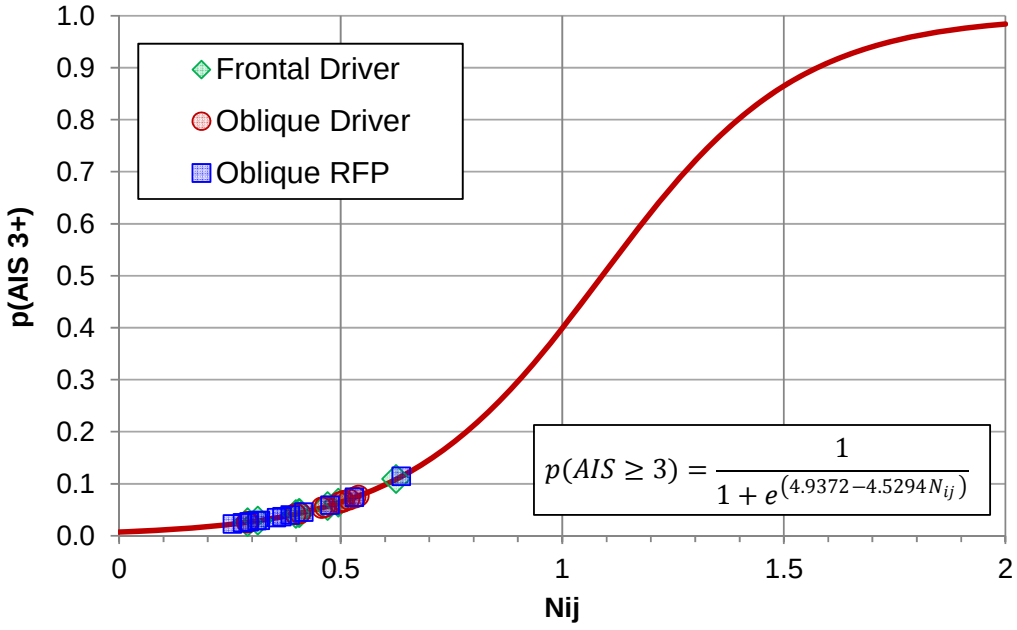

Figure 4.12. Probability of AIS 3+ neck injury predicted using Nij measured from fleet test results for the driver in the frontal rigid barrier test mode and both the driver and right front passenger in the Oblique MDB test mode.

4.11 **Limitations**

Age was not found to be a significant covariate in the risk function, even though age is known to affect spinal tolerance (Pintar et al. 1998). The intended age of application of the risk function (40 years old) is notably younger than the average age of the PMHS (57 years).

The risk functions above have been developed assuming relaxed musculature. Therefore, muscle tensing was not accounted for, as has been done in previous versions of Nij.

While a combined loading criterion may be desirable due to the many different mechanisms associated with real world injury, the traditional Nij formulation presented herein has limitations. For example, the Nij formulation is based on the assumption that the neck structure acts as an Euler-Bernoulli beam, with the principle of superposition being used to sum the stress due to the moment and the stress due to the axial force, for a composite total stress in the bone. In fact, the neck exhibits complex dynamic behavior (e.g. multiple mode buckling) that may not be accurately represented by beam theory. Further work is ongoing to validate combined loading formulations.

5 CHEST

5.1 Field and Historical Fleet Data

Similar to observations with brain injury, there appears to be an opposite trend in fleet data predicted injury risk from NCAP tests (Figure 5.1) and injury rates from field data (Figure 5.2). Injury risk was calculated using the risk function that is currently in use with the Hybrid III 50th in frontal NCAP testing (NHTSA, 2008).

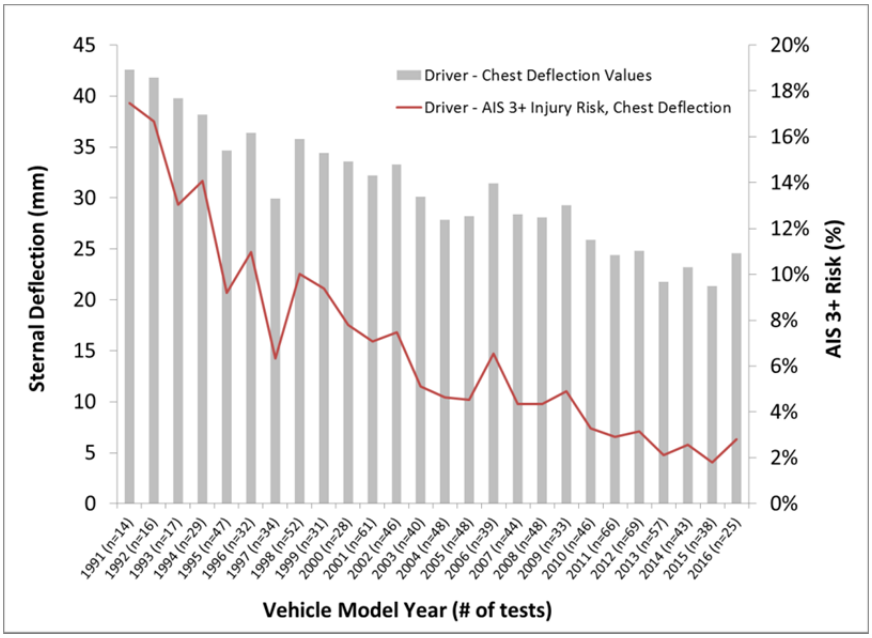

Figure 5.1. Hybrid III 50th Male NCAP driver chest deflections and predicted injury risk (AIS 3+) for tests from model year 1990 to 2016.

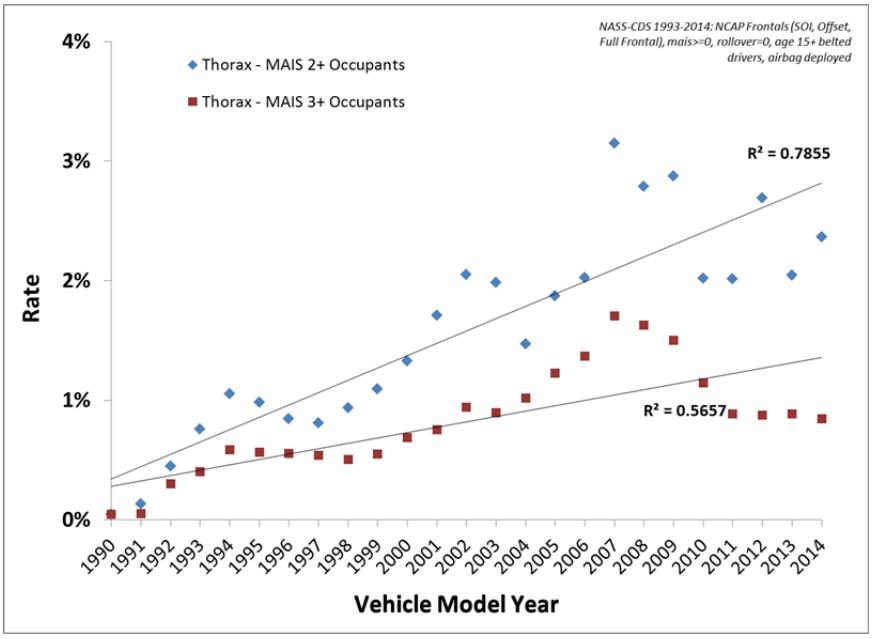

Figure 5.2. Thorax MAIS 2+ and 3+ rate versus model year (1990 to 2012) for belted and airbag restrained drivers in frontal crashes from NASS-CDS 1993 to 2014.

Figure 5.3 shows the regional mechanisms of injury assigned to thoracic injuries in 280 CIREN front-row belted occupants involved in frontal crashes. These mechanisms are inferred from the available data and may have been limited to available researcher/published biomechanical knowledge at the time. It is important to note that the mechanisms shown are regional mechanisms, not organ-specific mechanisms. That is, the chosen mechanism represents the type of loading/motion experienced by the entire thoracic region. Compression is the dominant mechanism for skeletal injuries, while the soft tissues are more frequently injured from a combination of compression and the rate of compression.

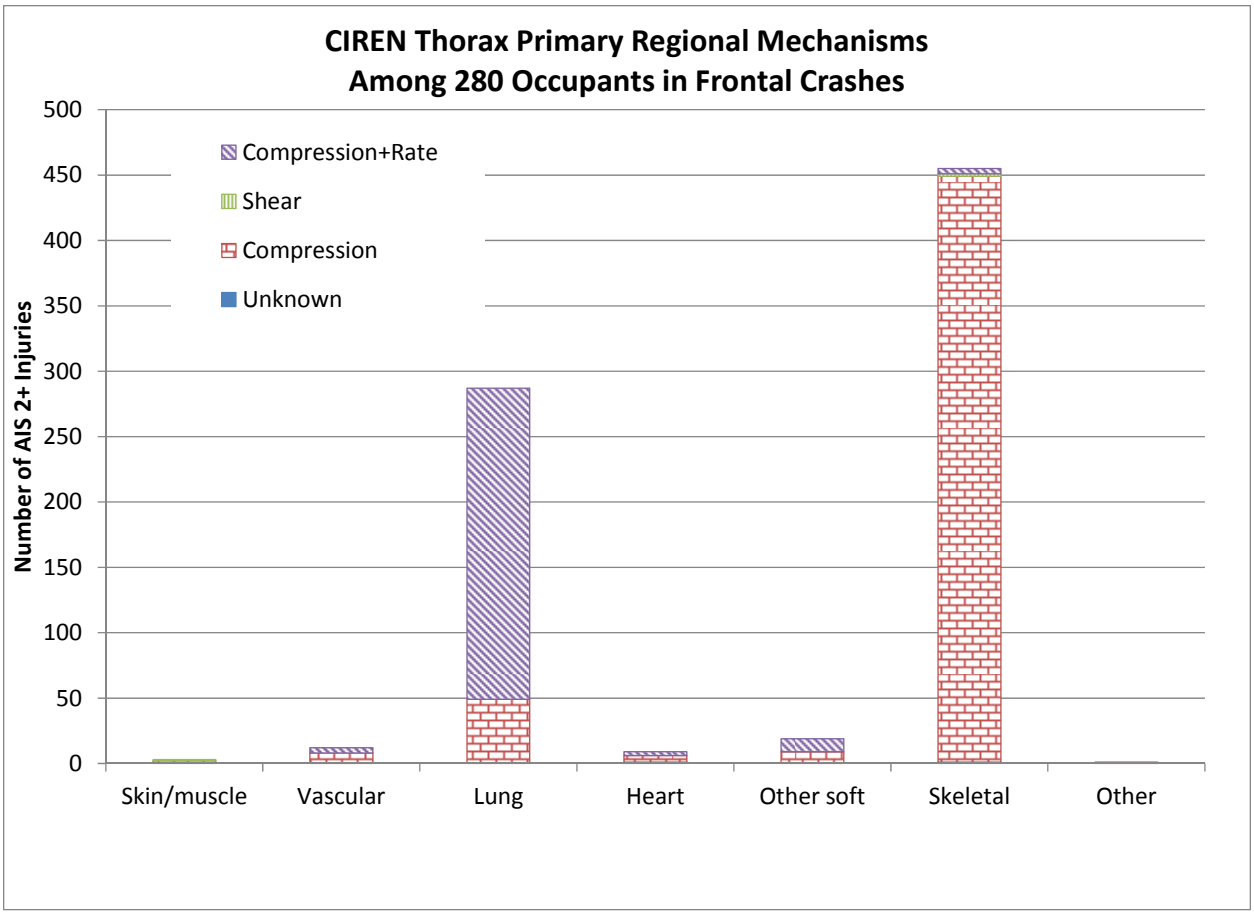

Figure 5.3. Recorded mechanisms of thoracic injuries for belted front row occupants involved in frontal crashes from the CIREN database.

5.2 Literature Review

Eppinger et al. (1999) presented a summary of historical research into the development of thoracic injury criteria, primarily focused on those applicable to the Hybrid III 50th ATD for use in Federal Motor Vehicle Safety Standards (FMVSS) No. 208. Based on the historical research, a set of thoracic injury risk predictors were selected and logistic regression models were fit to the results of 71 PMHS sled tests. The predictor variables investigated were thoracic spine resultant acceleration (*As*), normalized central chest deflection at the measurement location of the Hybrid III 50th ATD (*dc*), normalized deflection at any of five measurement locations on the chest (*dmax*), chest deflection velocity, and viscous criterion. Of these predictors, the best injury predictor was a linear combination of thoracic spine resultant acceleration and the normalized deflection at any of the five measurement locations on the chest. This predictor was defined as the combined thoracic injury criteria, or *CTI*. Injury risk functions were developed for *As* alone, *dc* alone (as measurement of *dmax* is not possible for the Hybrid III 50th), and *CTI*. These injury risk curves were not directly implemented to develop injury assessment reference values (IARVs) for FMVSS No. 208, as the *dc* limit was taken to be 63 mm and the *As* limit was taken to

be 60 gs to harmonize with the Canadian Motor Vehicle Safety Standards (CMVSS). The *CTI* was not used for regulatory purposes, but for analysis purposes only.

In the 2008 NCAP Final Decision Notice (NHTSA, 2008), it was noted that the injury risk function developed by Eppinger et al. (1999) did not account for age and was not adequately adjusted to reflect real-world chest injury risk. Instead, the chest injury risk function presented by Laituri et al. (2005), which was developed based on a larger set of published PMHS test data and included more diverse loading conditions, was used. To relate the PMHS-based injury risk function to the Hybrid III 50th ATD, a transfer function was developed by Laituri et al. (2005) using a subset of matched pair tests. The resulting chest injury risk function related the peak chest deflection as measured by the Hybrid III 50th sternum potentiometer along with the age of the subject to the risk of AIS 3+ thoracic injury, as defined as seven or more rib fractures. For AIS 1990 (1998 update) four fractured ribs or more constituted an AIS 3+ thoracic injury. Laituri et al. added three fractured ribs for the threshold of seven per reference to earlier studies that had found a difference in the number of fractured ribs between dead specimens (e.g. PMHS) and live subjects (Viano et al. 1977; Foret-Bruno et al. 1978). As implemented in Frontal NCAP, an age of 35 years was selected to represent the average age of the driving population.

Both the Eppinger et al. 1999 and Laituri et al. 2005 injury risk functions required corrections or assumptions to account for the limitation of the single-point measurement capability of the Hybrid III 50th ATD. NHTSA has previously identified instrumentation opportunities beyond a single-point chest deflection measurement system that may improve the assessment of thoracic loading in a vehicle environment with advanced restraint technology such as air bags and pretensioners (Yoganandan et al., 2009). Thoracic trauma imparted to restrained occupants does not always occur at the same location on the rib cage for all occupants in all frontal crashes (Morgan et al., 1994). Kuppa and Eppinger (1998) found that, in a dataset consisting of 71 human subjects in various restraint systems and crash severities, using the maximum deflection from multiple measurement locations on the chest resulted in improved injury prediction. As such, multi-point deflection instrumentation was prioritized in the development of the THOR ATD (Haffner, 2001).

Real-world data also demonstrate the need for a multipoint deflection measurement to better reflect actual fracture/injury patterns and better discriminate between vehicle performances. In a small sample of restrained occupants with rib fractures, Shimamura et al. (2003) found that rib fractures were more common in the lower ribs (6-12) compared with the upper ribs, suggesting that the deployed airbag shared and distributed the load to the upper chest but had less effect near the seat belt buckle where concentrated seat belt loads still occurred. Lee et al. (2015) used the CIREN database to examine the rib fracture patterns of 158 belt- and airbag-restrained front seat occupants and found that 63% of fractures occurred on the inboard (with respect to the vehicle) side of the chest. Notably, only 40% of the occupants sustained sternal fracture (indicative of central loading). Asymmetric fracture patterns (both upper/lower and left/right) suggest that peak deflections typically do not occur centrally and thus are unlikely to correspond to the location of the mid-sternal chest slider in the Hybrid III family of dummies.

5.3 **Design**

Throughout the development of the THOR-50M ATD, specific attention was given to the human-like response and injury prediction capability of the chest. The rib cage geometry is more realistic because the individual ribs are angled downward to better match the human rib orientation (Kent et al., 2003). Performance requirements were selected to ensure human-like behavior in response to central chest impacts, oblique chest impacts, and steering rim impacts to the rib cage and upper abdomen (NHTSA, 2005a). Better chest anthropometry means that the dummy's interaction with the restraint system (as the seat belt lies over the shoulder and across the chest, for example) is more representative of the interaction humans would experience. The THOR-50M ATD is capable of measuring three-dimensional deflections at four different locations on the rib cage. This instrumentation, coupled with its thoracic biofidelity, provides the THOR-50M ATD with the ability to predict thoracic injuries and to potentially drive realistic restraint system countermeasures.

5.4 **Instrumentation**

THOR-50M ATD was designed to measure thoracic deformation at multiple points to facilitate the prediction of injury risk. There are four Infrared Telescoping Rod for Assessment of Chest Compression (IR-TRACC) assemblies to measure the three-dimensional position time-history of four points on the anterior rib cage relative to the local spine segment of rib origination (Figure 5.4). The anterior attachment points are at the vertical level of the fourth and eighth anatomical ribs, and at the lateral level of the costochondral junction. The upper chest IR-TRACC attachment points are 40 millimeters from the sagittal centerline of the ATD, while the lower chest IR-TRACC attachment points are 80 millimeters from the sagittal centerline. The posterior attachment point of the upper thorax IR-TRACCs is on the Upper Thoracic Spinebox, which spans the anatomical landmarks of T4 through T8. The posterior attachment point of the lower thorax IR-TRACCs is on the Thoracic Spine Load Cell Flex Joint Adaptor Plate, which is at the anatomical level of L1. Between the upper and lower thorax IR-TRACC attachment points is a flexible joint known as the Upper Thoracic Spine Flex Joint, so the reference coordinate system for the upper and lower thorax 3D motion measurements can change dynamically during a loading event.

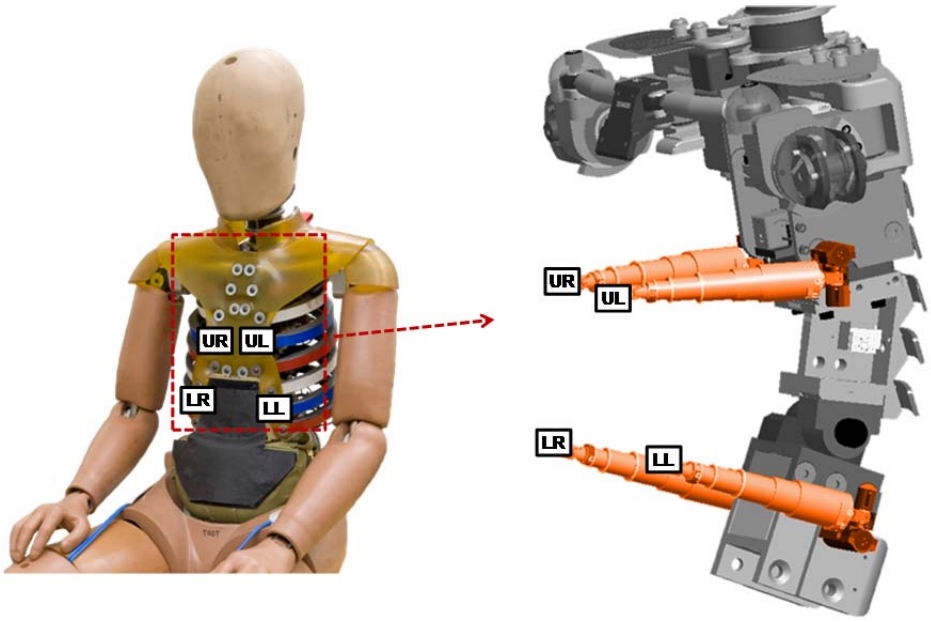

Figure 5.4. (Left) Location of the four measurement points on the thorax of the THOR. (Right) Attachment of the IR-TRACC assemblies to the spine.

THOR-50M was not designed to measure sternum deflection, in part due to the design of the sternum assembly which was developed to meet the biofidelity requirement in the low-speed blunt thoracic impact condition. The space occupied by the sternum assembly prevents installation of an IR-TRACC or similar measurement device to the anterior surface of the sternum. However, since the upper thorax IR-TRACC attachment points are at the vertical level of the anatomic mid-sternum landmark, sternum deflection can be approximated using the midpoint of the line between the two upper thorax IR-TRACC assemblies.

In addition to the IR-TRACC deflection measurement system, the THOR-50M can also be instrumented with a uniaxial sternum accelerometer, triaxial accelerometers installed along the spine at the level of T1, T6, and T12, and a five-axis (three forces, two moments) load cell installed between the lumbar spine pitch change mechanism and the lumbar spine flex joint at the approximate anatomical level of T12. Clavicle loads cells can also be installed, but are not included in the THOR-50M described in the September 2015 drawing package (NHTSA, 2015a). THOR-50M thoracic instrumentation is summarized in Table 5.1.

Table 5.1. THOR-50M ATD thoracic instrumentation.

Sensor	Measurement Description	Measurement Axes
Upper Left IR-TRACC assembly	3D position of left 4th rib WRT upper thoracic spine	XL, YL, ZL
Upper Right IR-TRACC assembly	3D position of right 4th rib WRT upper thoracic spine	XL, YL, ZL
Lower Left IR-TRACC assembly	3D position of left 8th rib WRT lower thoracic spine	XL, YL, ZL
Lower Right IR-TRACC assembly	3D position of right 8th rib WRT lower thoracic spine	XL, YL, ZL
Sternum accelerometer	Acceleration of sternum	XL
Spine accelerometer(s)	Acceleration of the spine at T1, T6, T12	XL, YL, ZL
Spine load cell	Force and moment at T12	Force: XL, YL, ZL; Moment: XL, YL

5.5 **Biofidelity**

Parent (2016) evaluated the biofidelity of the THOR-50M chest in two conditions: sternal impact and lower ribcage oblique impact. In the sternal impact condition, THOR-50M demonstrated excellent internal and external biofidelity, with Biofidelity Ranking System (BioRank) scores of 0.815 and 0.732, respectively. In the lower ribcage oblique impact condition, the THOR-50M demonstrated good internal and external biofidelity, with BioRank scores of 1.268 and 1.227, respectively. In all thoracic impact conditions, the THOR-50M was quantitatively more biofidelic than the H3-50M. Additionally, in four whole-body restraint frontal impact sled test conditions, the THOR-50M demonstrated good internal biofidelity, which is primarily a measure of the biofidelity of multi-point rib cage deflection.

5.6 **Data**

Several datasets were considered in the development of a thoracic injury criterion for the THOR ATD. First, the data presented in the development of the thoracic injury criterion for the Hybrid III ATD for use in Federal Motor Vehicle Safety Standards (FMVSS) No. 208 as presented by Eppinger et al. (1999) were reviewed. This set of 71 data points, of which 63 were considered after removing outliers, included post-mortem human surrogate (PMHS) sled tests at velocities of between 23 km/h and 59 km/h in various restraint configurations including belt-only (2-point and 3-point), airbag only, and belt and airbag conditions. In each test, chestbands were used to measure external chest deformation, which was presented at five different locations: left, center, and right at the vertical level of the 4th rib, and left and right at the vertical level of the 8th rib. The relationship between PMHS external deflection and the internal deflection measured by the Hybrid III ATD was accounted for in the development of the Combined Thoracic Injury (CTI) criterion by subtracting 8 millimeters from the deflection component of the deflection vs. acceleration regression line. It is not clear, however, if this 8-millimeter shift was accounted for in the development of the chest deflection risk function. Such a relationship would be necessary to apply the injury criteria developed by Eppinger et al. (1999) to THOR, as the relationship between the measured and calculated PMHS chestband deflection and the multi-point internal deflection measured by THOR is unknown.

One approach to address this limitation would be to conduct identical tests with THOR-50M ATD and relate the measured THOR internal deflection to the measured PMHS external deflection. However, since many of these tests were conducted in the early 1990s, obtaining identical test fixtures and

restraint systems would be difficult or impossible. Instead, a more recent matrix of PMHS tests was collected by the University of Virginia based on the availability of test fixtures and restraints, consisting of frontal impact sled tests in 12 different velocity or restraint conditions with a total of 42 PMHS observations. In each of these 12 test conditions, at least two THOR-50M tests were conducted (summarized in Crandall, 2013; individual test references presented in Table 5.2). Later, two additional matched pair test conditions were conducted using both PMHS and THOR-50M, one set with the occupant in a near-side oblique configuration (Crandall, 2015), the other with the occupant in a far-side oblique configuration (Crandall, 2014). A total of 14 test conditions were considered in this matched-pair study, with a total of 48 PMHS observations (Table 5.2). For tests sponsored by NHTSA, which include a majority of the PMHS tests and all of the THOR-50M tests, NHTSA Biomechanics Test Database test numbers are included in the table. A limitation to this test series is that the measurement of PMHS thoracic deformation was not consistent for all tests, as some used single chestbands, some used multiple chestbands, and others used the VICON system to measure skeletal deformation directly. Due to this limitation, the matched pair tests are used herein to relate PMHS outcome to THOR measurements in the same test condition.

Table 5.2. Source data for PMHS sled tests.

Occupant Position	Environment [Reference]	Restraint	Delta-V (km/h)	Age	Sex	Mass (kg)	Height (cm)	AIS 3+	PMHS BioDB	THOR BioDB
Front Driver	Gold Standard [Lopez-Valdes, 2010]	3-point standard belt	10	59	F	80	167	No		11125
				69	M	84	178	No		11126
				60	M	81	191	No		
Front Driver	Gold Standard [Lopez-Valdes, 2010]	3-point standard belt	40	59	F	80	167	Yes		11123
				69	M	84	178	Yes		11124
				60	M	81	191	Yes		
Front Passenger	1997 Ford Taurus [Forman, 2006a]	3-point force-limited belt plus airbag	48	57	M	70	174	No	8371	11129
				69	F	53	155	Yes	8372	11130
				72	F	59	156	Yes	8373	
				57	M	57	177	No	8374	
Front Passenger	1997 Ford Taurus [Kent, 2001]	Lap belt with airbag	48	40	M	47	150	Yes	8377	11131
				70	M	70	176	No	8378	11132
				46	M	74	175	No	8379	
Front Passenger	1997 Ford Taurus [Forman, 2006a]	3-point standard belt with airbag	48	55	M	85	176	Yes	8382	11127
				69	M	84	176	Yes	8383	11128
				59	F	79	161	Yes	8384	
Front Passenger	1997 Ford Taurus [Forman, 2006a]	3-point standard belt	29	49	M	58	178	No		11133
				44	M	77	172	No		11134
				39	M	79	184	No		
Front Passenger	1997 Ford Taurus [Forman, 2006b]	3-point standard belt	38	44	M	77	172	No		11135
										11136
Front Passenger	Gold Standard 1 [Shaw, 2009]	3-point standard belt	40	76	M	70	178	Yes	9546	11117
				47	M	68	177	Yes	9547	11118
				54	M	79	177	Yes		11119
				49	M	76	184	Yes		
				57	M	64	175	Yes		
				72	M	81	184	Yes	11014	
				40	M	88	179	Yes	11015	
				37	M	78	180	No	11016	
Front Passenger	Gold Standard 2 [Shaw, 2012]	3-point force-limited belt	30	59	M	68	178	No	11468	11120
				66	M	70	179	No	11469	11121
				67	M	68	177	Yes	11509	11122
				67	M	68	173	Yes	11510	
				74	M	70	183	No	11511	
Rear Passenger	2004 Ford Taurus [Forman, 2009]	3-point standard belt	48	51	M	55	175	Yes	9337	11143
				57	F	109	165	Yes	9338	11144
				57	M	59	179	Yes	9339	11145
Rear Passenger	2004 Ford Taurus [Forman, 2009]	3-point force-limited belt with pretensioner	48	67	M	71	175	Yes		11140
				69	M	60	171	No		11141
				72	M	73	175	Yes		11142
Rear Passenger	2004 Ford Taurus [Kent, 2011]	3-point inflatable force-limited belt with pretensioner	48	72	M	88	173	Yes		11137
				69	M	69	175	No		11138
				40	M	83	186	No		11139
Front Passenger	Gold Standard 3 (Near-side Oblique) [Crandall, 2015]	3-point force-limited belt	30	69	M	72	173	Yes	11518	11514
				66	M	76	172	Yes	11519	11515
				67	M	65	177	No	11520	11516
										11517
Front Passenger	Far-side Oblique [Crandall, 2014]	3-point force-limited belt with airbag	59.5	73	M	69	180	Yes	11500	11503
				83	M	85	178	Yes	11501	11504
				63	M	69	187	Yes	11502	11505
										11506

Given the approach of using matched pair tests to relate PMHS outcome to THOR measurements in the same test condition, the Eppinger et al. (1999) dataset was revisited to consider any test conditions that were similar enough to the test conditions presented in Table 5.2 to be included. Subjects were considered for inclusion if they were unembalmed, could be located in the NHTSA Biomechanics Database, were tested at a velocity within ±2 km/h of a matched THOR test, and were tested in the

same restraint condition as a matched THOR test. This winnowed the original 71 subjects down to just 5: three subjects in a lap belt with airbag condition at 48 km/h, and two subjects in a three-point belt plus airbag condition at 48 km/h (Table 5.3). It is hypothesized that the similarity in restraint is more important than the difference in occupant position (driver vs. right front passenger) and environment (1986 Ford Tempo vs. 1997 Ford Taurus).

Table 5.3. Source data for additional PMHS sled tests.

Occupant Position	Environment	Restraint	Delta-V (km/h)	Age	Sex	Mass (kg)	Height (cm)	AIS 3+	PMHS BioDB	THOR BioDB
Driver	1986 Ford Tempo	Lap belt with airbag	48.3	67	F	50		Yes	2857	11132
				64	M	70		Yes	2854	
				58	M	73		No	2856	
Driver	1986 Ford Tempo	3-point standard belt with airbag	48.3	67	F	57		Yes	2861	11127
				68	M	59		Yes	2878	

Additionally, impactor tests were considered for inclusion in the matched pair dataset, as THOR-50M response data are available for both blunt sternal impact and lower thorax oblique impact conditions. PMHS observations in blunt sternal impact tests at various speeds and masses are presented in Kroell et al. (1971 and 1974). Based on the analysis presented by Neathery et al. (1975), half of the 48 observations presented by Kroell were recommended for elimination based on differences in spine fixation, impactor travel restriction, post-test injury assessment technique, and instrument failure, as well as one subject that was “clearly an outlier.” Of the 24 remaining tests, 17 were considered herein based on similarity in impact velocity (4.3 m/s, 4.8 m/s, and 6.7 m/s) and impact mass (23 kg) to existing THOR-50M test conditions (Table 5.4). Also considered herein are 7 PMHS observations in a lower thorax oblique impact condition presented by Yoganandan et al. (1997).

Table 5.4. Source data for PMHS impactor tests.

Test Condition	Delta-V (km/h)	Age	Sex	Mass (kg)	Height (cm)	AIS 3+	PMHS BioDB	THOR BioDB
Blunt Thoracic Impact Nominal 23kg Impactor @ 6.7 m/s	26.7	81	M	76.2	168	Yes		
	24.8	80	M	53.1	165	Yes		
	24.2	78	M	65.8	176	Yes		
	24.2	19	M	71.2	196	No		
	24.2	29	M	56.7	180	No		
	24.2	72	M	74.8	188	Yes		
	25.9	52	M	74.8	183	Yes		
	26.4	46	M	94.8	178	No		
	24.9	72	M	63.0	163	Yes		
	22.7	60	F	59.0	160	Yes		
	26.1	67	F	62.6	163	Yes		
	26.4	76	F	57.6	156	Yes		
	27.8	58	F	61.2	163	Yes		
Blunt Thoracic Impact Nominal 23kg Impactor @ 4.8 m/s	17.5	61	M	54.4	183	No		
	18.2	64	M	64.0	181	Yes		
	18.8	75	M	77.1	174	Yes		
Blunt Thoracic Impact Nominal 23kg Impactor @ 4.3 m/s	15.6	66	M	79.4	180	Yes		
Lower Thorax Oblique Impact Nominal 23kg Impactor @ 4.3m/s	15.5	72	M	82	170	Yes	3085	
		81	M	63	175	Yes		
		84	M	68	168	No		
		86	M	56	170	No		
		62	M	61	174	Yes		
		70	M	91	169	Yes		
		68	M	83	178	Yes		

Different combinations of the datasets presented in Table 5.2, Table 5.3, and Table 5.4 are carried through the analysis and referenced throughout this report as follows:

Table 5.5. Description of dataset combinations evaluated throughout report.

Name	Description
SledOnly	only the observations in Table 5.2
SledExtended	combined observations in Table 5.2 and Table 5.3
Sled+Impactor	combined observations in Table 5.2, Table 5.3, and Table 5.4
SledNoOBL	only the observations from Table 5.2, but without either set of oblique observations
SledNoFSO	only the observations from Table 5.2, but without the Far-side Oblique (FSO) observations

5.7 Predictor Variable

Several variables were considered for use as the predictive parameter in a thoracic injury criterion. As the input dataset includes test data measured using the THOR-50M ATD, measurements from the sensors shown in Table 5.1 and metrics calculated from these sensors can be considered as independent parameters. While sternum and spine acceleration and spine force data are often collected during THOR crash tests, this study focused on deflection-based measurements as previous research has demonstrated a strong relationship between rib deflection and rib strain, which in turn relates to risk of fracture. Several calculations of deflection-based measurements were considered for application as the independent parameter in the THOR thoracic injury criterion (Table 5.6).

The PC Score metric, developed through a Principal Component Analysis (PCA) methodology by the University of Virginia, is described further in McMurry et al, 2016a and 2016b, which were provided as deliverables under Cooperative Agreement DTNH22-07-H-00247. The difference between these two reports is that the former uses the SledNoOBL dataset, while the latter uses the SledNoFSO dataset.

Table 5.6. Deflection metrics considered.

Deflection Metric	Description	Calculation
x-axis Deflection	Deflection of the anterior attachment point of the IR-TRACC assembly along the x-axis of the local spine coordinate system (LCS)	See *THOR Instrumentation Processing Manual*
Resultant Deflection	Vector resultant deflection of the anterior attachment point of the IR-TRACC assembly	$\max\left(\sqrt{X_{LCS}^2 + Y_{LCS}^2 + Z_{LCS}^2}\right)$
Change in Chord Length	Change in distance between the anterior and posterior IR-TRACC assembly attachment points	$\sqrt{r_0^2 + \delta^2} - \max\left(\sqrt{r^2 + \delta^2}\right)$
Peak ____ Deflection	The above three metrics can be calculated at each of the four quadrants; the peak deflection measurement calculates the maximum of a given metric across all four quadrants	$\max(UL, UR, LL, LR)$
PC Score	Result of Principal Component Analysis (PCA) described in UVA IRF report	See Appendix

To determine whether inclusion of all or multiple quadrants for each deflection metric should be included in a multivariate risk function formulation, a stepwise multiple logistic regression was carried out using both x-axis and Resultant deflection metrics. The initial model considered five parameters – the upper left, upper right, lower left, and lower right quadrant deflections, and an additional parameter representing the peak deflection of all four quadrants. For both deflection metrics, and for all datasets considered, adding any of the individual quadrant deflections in addition to the peak deflection did not result in a statistically-significant description of the remaining variance.

While change in chord length was originally considered because it was thought to better correlate with rib strain, it was found to be well-correlated with Peak x-axis Deflection. This is demonstrated for the SledOnly dataset in Figure 5.5, but held true for all combinations of datasets as well. Thus, chord length was eliminated from consideration as an independent variable for simplicity.

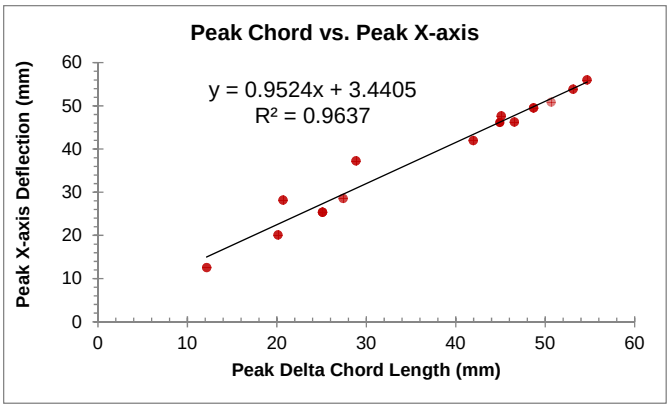

Figure 5.5. Relationship between change in chord length and peak x-axis deflection in the SledOnly dataset.

5.8 Covariates

A stepwise multiple logistic regression was carried out to assess the sensitivity of several covariates. If addition of a given variable as a covariate in a logistic regression along with the independent variable described above resulted in a statistically-significant ($p < 0.05$) description of variance in the fitted model, the covariate should be included in the injury risk function. Covariates considered were age, mass, stature, and sex, which were available for all subjects in all datasets. For all datasets considered, adding age as a covariate in addition to the Peak x-axis Deflection or Peak Resultant Deflection resulted in a statistically-significant description of the remaining variance. Mass, stature, and sex were not significant explanatory variables.

5.9 Dependent Variable

The dependent variable used in the development of a thoracic injury criterion was the presence of an Abbreviated Injury Scale (AIS) score of 3 or greater (AIS 3+). Based on the AIS 2005 Update 2008, an AIS 3 skeletal injury to the thorax is defined by fractures of three or more ribs without flail at any location of either or both sides of the ribcage including costal cartilage (AAAM, 2008). While soft tissue injuries can also result in AIS 3 or greater scores, these injuries are difficult or impossible to diagnose in PMHS, at least per the rules of 2005/2008 AIS (AAAM, 2008). For example, pulmonary contusions result from an inflammatory response and require living tissue for this to occur.

5.10 Injury Risk Function Formulation

Three sets of injury risk functions (nonparametric, logistic, and survival analysis) were formulated for each independent parameter (Peak x-axis Deflection, Peak Resultant Deflection), for each dataset (SledOnly, Sled+Impactor, SledExtended, SledNoFSO), and both with and without age as a covariate. Goodness-of-fit metrics described in Hasija et al. (2011) were calculated for the logistic and survival analysis risk curves, including the Receiver Operating Characteristic (ROC) Area Under Curve (AUC), maximum log likelihood, and Hosmer-Lemeshow Goodness-of-Fit test.

5.10.1 Nonparametric

Nonparametric survival functions were formulated using the SAS PROC LIFETEST procedure for both Peak x-axis Deflection (Figure 5.6) and Peak Resultant Deflection (Figure 5.7) metrics. Both metrics indicate only subtle differences between the SledOnly, SledExtended, and SledNOFSO datasets, but marked differences in the Sled+Impactor dataset.

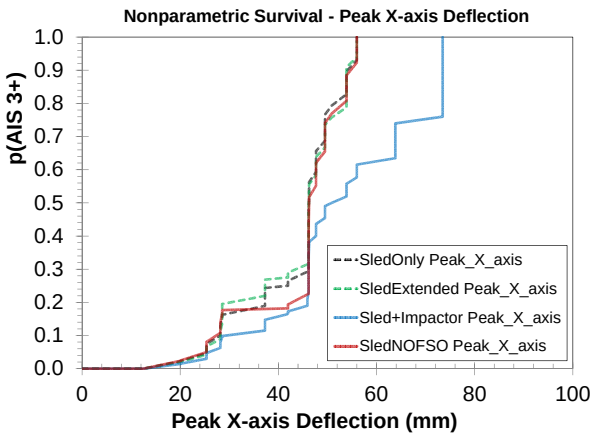

Figure 5.6. Nonparametric survival function for four datasets using peak x-axis deflection as a predictor.

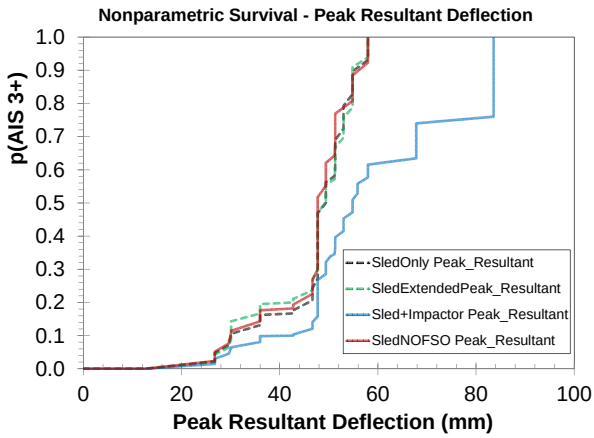

Figure 5.7. Nonparametric survival function for four datasets using peak resultant deflection as a predictor.

5.10.2 Logistic Regression

Logistic regression was carried out to develop risk functions for both predictors for all four datasets, both with and without age as a covariate using the SAS PROC LOGISTIC procedure. For each combination, the AUROC, maximum log likelihood, and Hosmer-Lemeshow Goodness-of-Fit test results are reported in Table 5.7. The logistic regression risk functions take one of two forms:

Without Age: $p(AIS \geq 3) = \frac{e^{(\beta_0+\beta_1 x)}}{1+e^{(\beta_0+\beta_1 x)}}$

With Age: $p(AIS \geq 3) = \frac{e^{(\beta_0+\beta_1 x+\beta_2 a)}}{1+e^{(\beta_0+\beta_1 x+\beta_2 a)}}$

where:

β_0	=	Intercept
β_1	=	Independent parameter coefficient
x	=	Independent parameter value
β_2	=	Age coefficient
a	=	Subject age, in years

Table 5.7. Fit statistics for logistic regression models.

Dataset	Predictor	Age as Covariate	N	-2 Log L	AUROC	Hosmer and Lemeshow Pr>ChiSq
Sled+Impactor	Peak X	Yes	72	76.124	0.801	0.0693
Sled+Impactor	Peak X	No	72	85.149	0.686	0.3540
SledExtended	Peak X	Yes	53	52.079	0.832	0.3280
SledExtended	Peak X	No	53	60.111	0.742	0.3553
SledNoFSO	Peak X	Yes	45	46.682	0.827	0.5285
SledNoFSO	Peak X	No	45	51.642	0.759	0.0563
SledOnly	Peak X	Yes	48	48.248	0.830	0.3388
SledOnly	Peak X	No	48	54.979	0.736	0.2850
Sled+Impactor	Peak Resultant	Yes	72	76.017	0.801	0.0863
Sled+Impactor	Peak Resultant	No	72	84.268	0.712	0.2705
SledExtended	Peak Resultant	Yes	53	50.264	0.856	0.6434
SledExtended	Peak Resultant	No	53	57.006	0.792	0.8068
SledNoFSO	Peak Resultant	Yes	45	45.459	0.832	0.7547
SledNoFSO	Peak Resultant	No	45	50.176	0.772	0.8166
SledOnly	Peak Resultant	Yes	48	45.889	0.849	0.6985
SledOnly	Peak Resultant	No	48	51.376	0.796	0.7434
SledNoOBL	Peak Resultant	Yes	42	41.599	0.845	0.5021
SledNoOBL	Peak Resultant	No	42	45.804	0.788	0.2906
SledNoFSO	PCA	Yes	45	45.642	0.839	0.6925
SledNoFSO	PCA	No	45	50.280	0.759	0.3577
SledNoOBL	PCA	Yes	42	41.856	0.848	0.3565
SledNoOBL	PCA	No	42	46.142	0.773	0.4626

Of the logistic regression models, the highest AUROCs occurred for the models using Peak Resultant Deflection as the predictor, with age as a covariate, and either the SledOnly or SledExtended datasets (Figure 5.8). Parameter estimates for these two models are shown in Table 5.8.

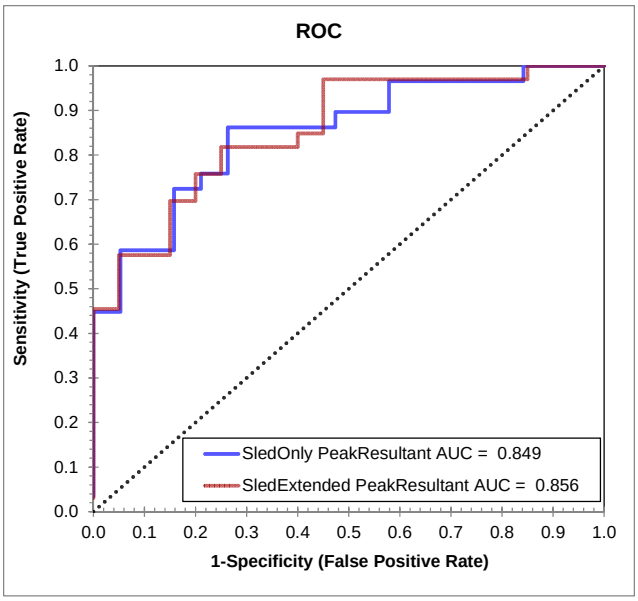

Figure 5.8. Receiver Operating Characteristic (ROC) for the logistic regression models with the highest AUC.

Table 5.8. Model parameter estimates.

Model	β_0	β_1	β_2
SledOnly, Peak Resultant	-8.8274	0.1168	0.0748
SledExtended, Peak Resultant	-8.9521	0.1122	0.0822

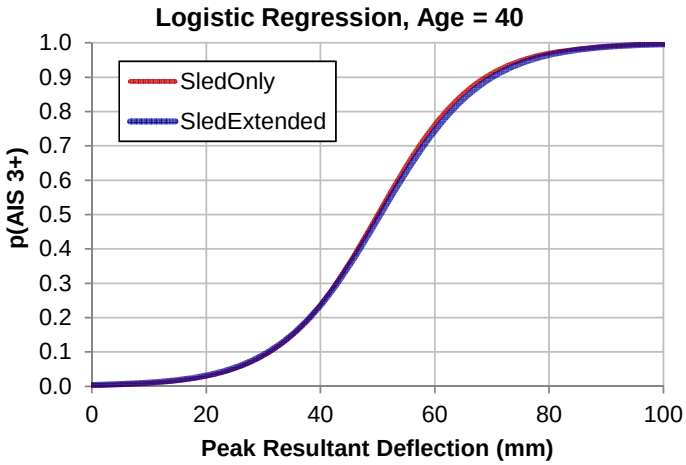

Figure 5.9. The difference between the logistic risk functions fit to the SledOnly and SledExtended datasets is negligible.

The risk functions and confidence intervals for the two models with the highest AUROC were calculated at three different values of the age covariate: 35 years old, the average age of a belted adult (15+ years) male driver between 162 cm and 182 cm in height in a frontal crash during case years 2000-2010; 45 years old, the average age of a belted adult (15+ years) male driver between 162 cm and 182 cm in height who sustained an AIS 3+ thoracic injury in a frontal crash during case years 2000-2010; and 61 years old, the average age of the PMHS subjects in the dataset (Figure 5.10).

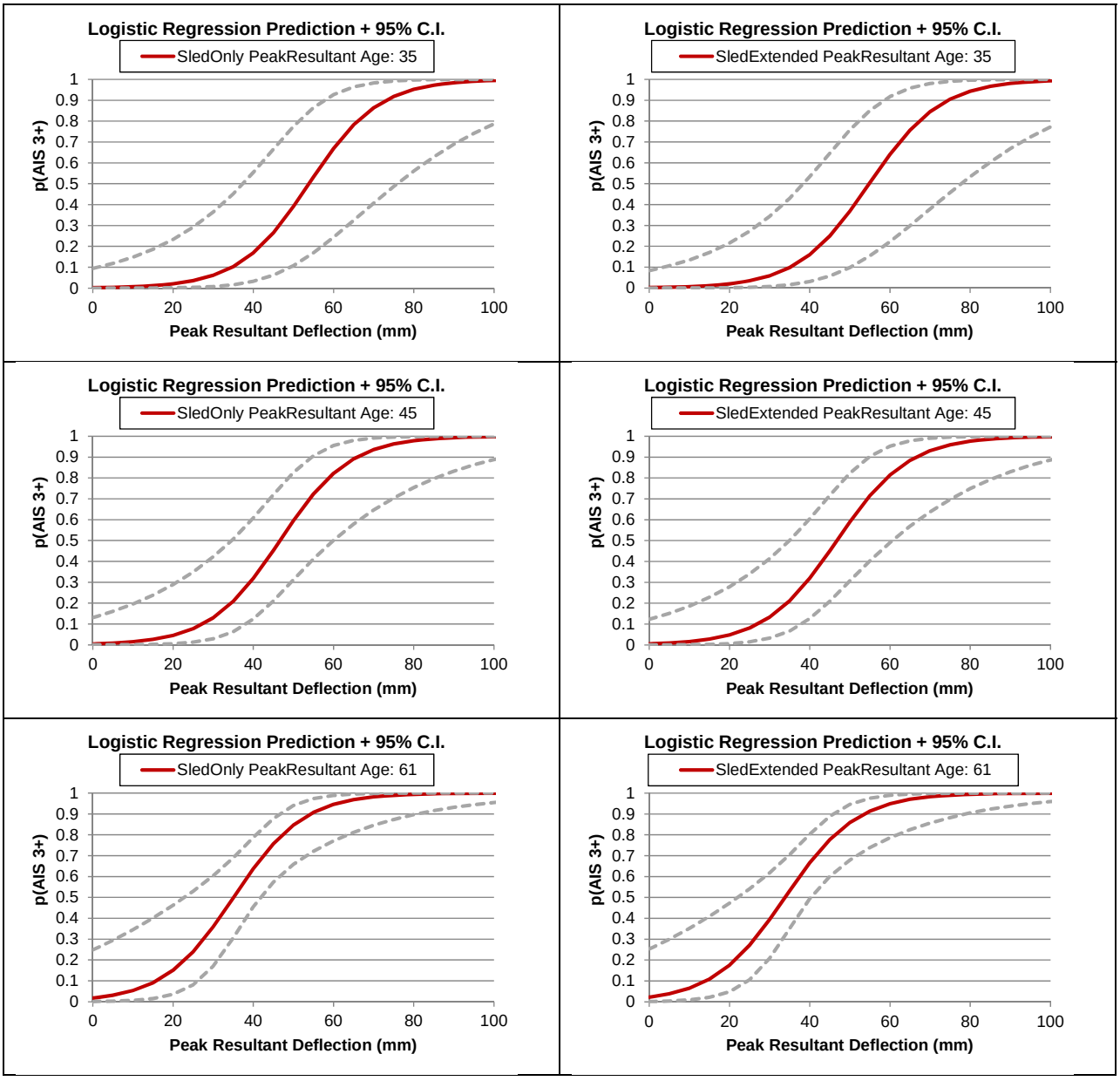

Figure 5.10. Risk function and confidence intervals for logistic models with highest AUROC, shown at different values of the age covariate.

5.10.3 Survival Analysis

Survival analysis was also carried out to develop risk functions for all four datasets using the SAS PROC RELIABILITY procedure. Models were developed for Peak Resultant Deflection, since this parameter provided a similar or better model fit than Peak x-axis Deflection for all logistic models except for the Sled+Impactor datasets, and for PCA for the applicable datasets. All survival models also included age as a covariate, as including age resulted in a better model fit for all logistic models. For each combination,

maximum log likelihood is reported in Table 5.9. The survival analysis risk function assumes a Weibull distribution takes the form:

$$p(AIS \geq 3) = 1 - e^{-\left(\frac{x}{e^{(\beta_0+\beta_1 a)}}\right)^{\alpha}}$$

where:

β_0	=	Intercept
x	=	Independent parameter value
β_1	=	Age coefficient
a	=	Subject age, in years
α	=	1/scale

Table 5.9. Parameter estimates and fit statistics for survival analysis models.

Dataset	Predictor	N	β_0	β_1	α	Maximum Log Likelihood
Sled+Impactor	Peak Resultant	72	5.1575	-0.0214	1.2314	-37.94896
SledExtended	Peak Resultant	53	4.8601	-0.0192	2.7187	-24.67252
SledOnly	Peak Resultant	48	4.7324	-0.0167	2.9521	-22.48054
SledNoFSO	Peak Resultant	45	4.7316	-0.0166	2.8768	-22.34810
SledNoOBL	Peak Resultant	42	4.6972	-0.0159	2.9266	-20.42483
SledNoFSO	PCA	45	2.8179	-0.0179	2.6404	-22.41762
SledNoOBL	PCA	42	2.8087	-0.0177	2.6427	-20.53101

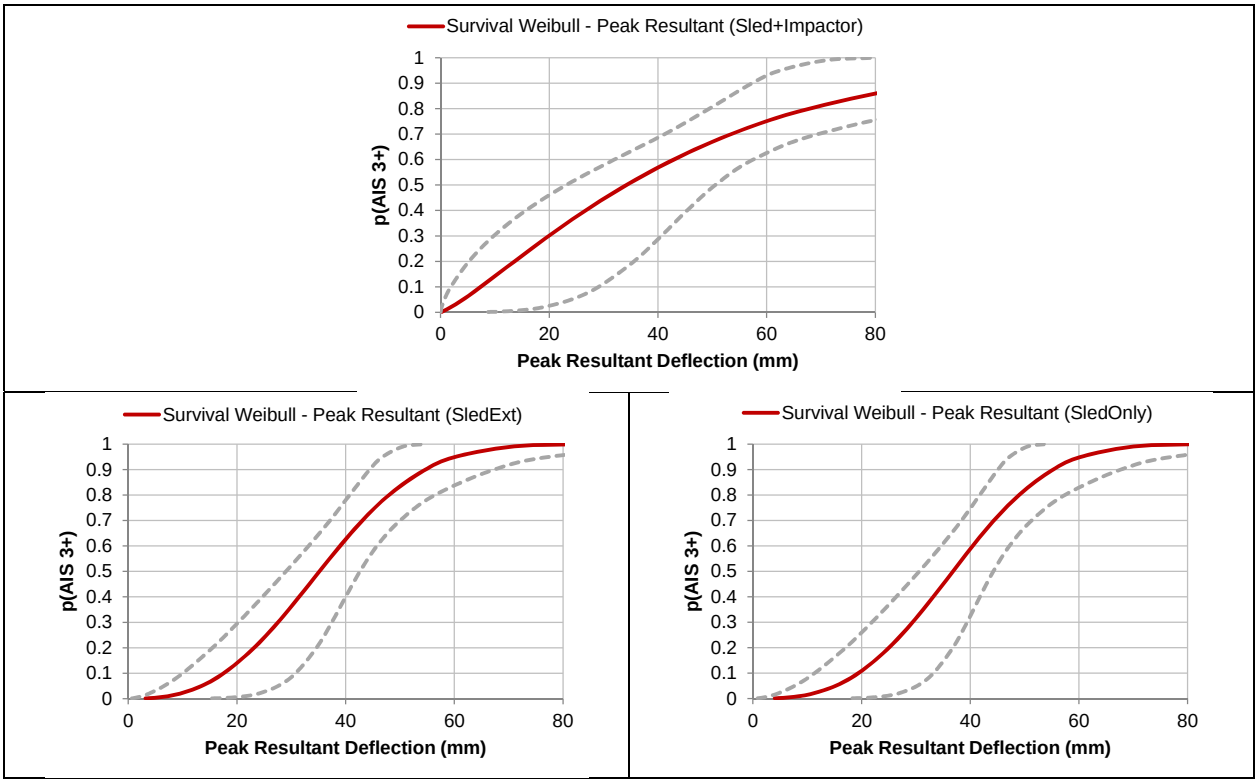

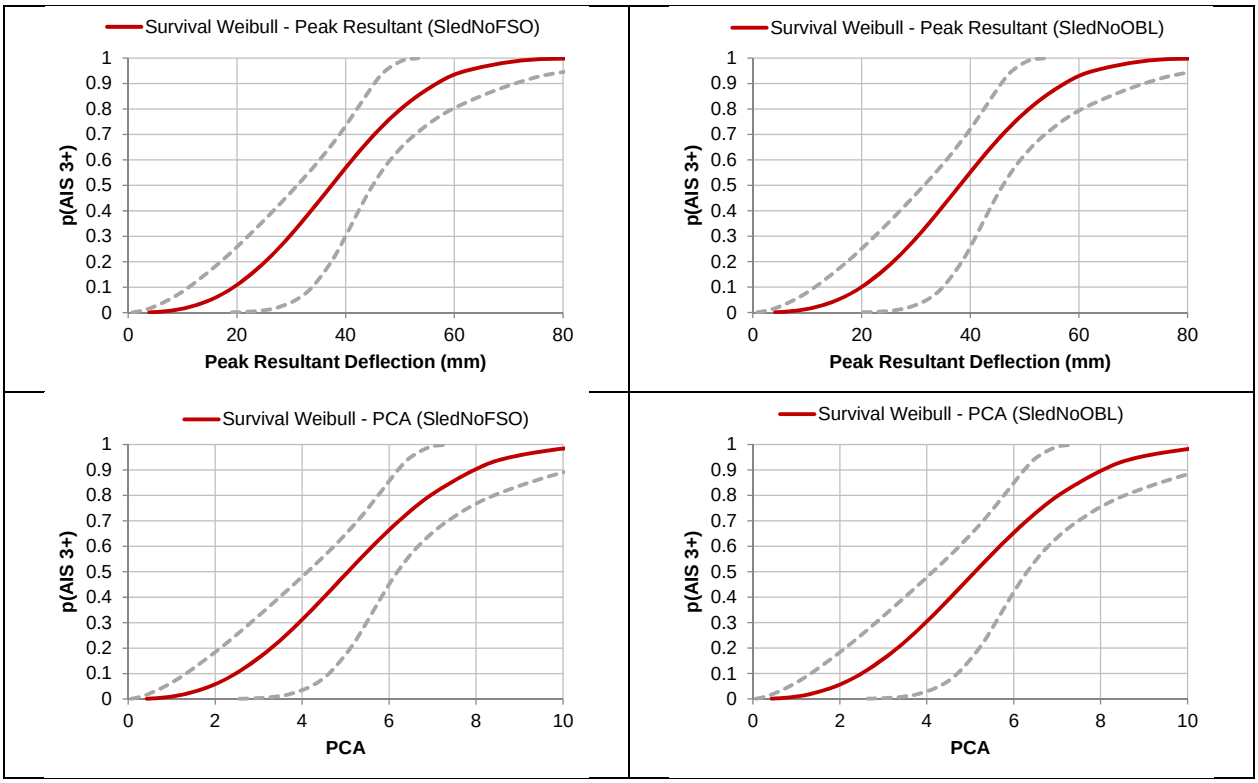

Figure 5.11. Survival Weibull estimates and 95% confidence intervals for models in Table 5.9.

Comparing models using PCA and Peak Resultant Deflection as predictors, half of the models demonstrated a better goodness of fit based on maximum log likelihood using either predictor. As both PCA and Peak Resultant Deflection appear to show similar predictive ability, Peak Resultant Deflection is preferred for its relative simplicity. Likewise, while there are some discernable differences between the logistic and Survival Weibull models (Figure 5.12), Survival Weibull model is preferred for its representation of zero risk at a zero stimulus value. Since the logistic model fit to the SledExtended dataset provides the highest AUROC, this dataset is used to fit the final model.

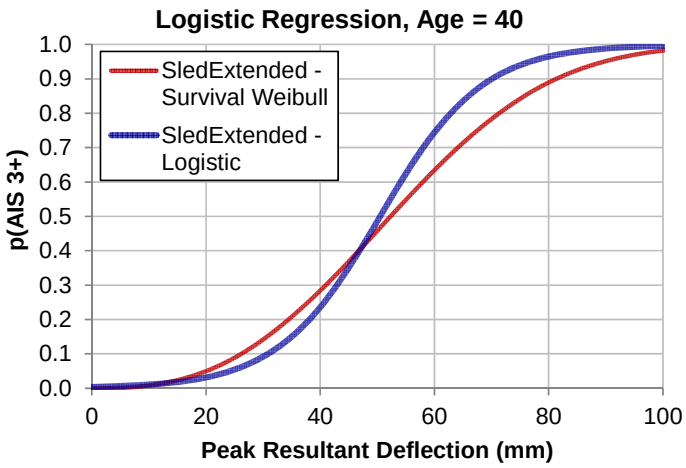

Figure 5.12. The difference between the Survival Weibull and logistic risk functions, both including age as a covariate, presented at an age of 40 years old.

The recommended risk function is:

$$p(AIS \geq 3) = 1 - e^{-\left(\frac{R_{max}}{e^{(4.8601 - 0.0192a)}}\right)^{2.7187}}$$

where:

R_{max}	=	Peak resultant deflection, in millimeters
a	=	Age, in years

Simplifying, assuming Age = 40 years (see Section 2.5):

$$p(AIS \geq 3) = 1 - e^{-\left(\frac{R_{max}}{59.865}\right)^{2.7187}}$$

5.11 **Fleet Test Data: THOR-50M**

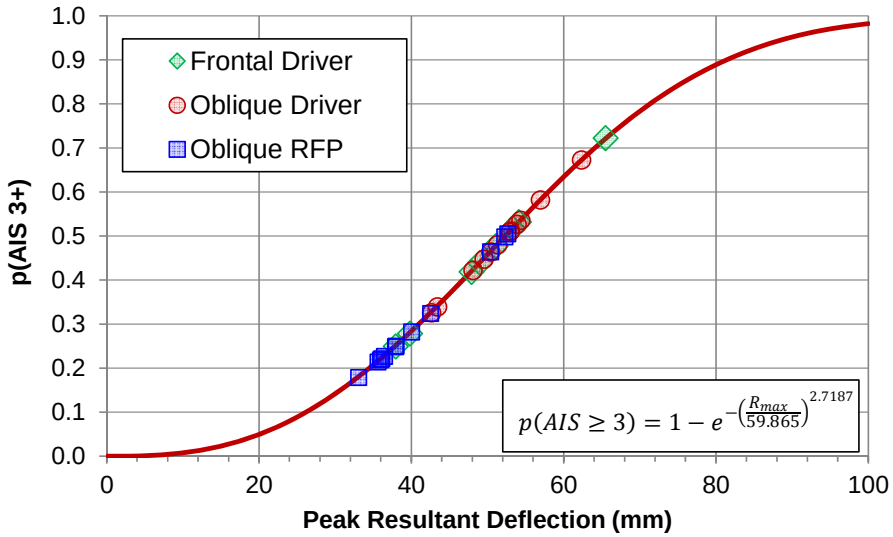

Figure 5.13. Distribution of fleet test results superimposed over Survival Analysis risk function.

5.12 **Limitations**

The assessment of injury to PMHS is more rigorous than possible on live subjects sustaining injury in car crashes. For example, the PMHS are often autopsied after the research test, and rib fractures are investigated at a level of detail that is not possible through physical external examination and reading of radiology from live subjects. Because of this, the number of rib fractures recorded from PMHS research tests may be an overestimate of the number of rib fractures that a live human would sustain in a similar loading condition. Eppinger et al. (1999) describes how the thoracic injury risk curves were shifted to account for this over-reporting, along with age differences between the PMHS dataset and the average driving population and the increased fragility of PMHS compared to live humans, by shifting the curve to the right along the independent axis such that the 50% risk level for PMHS became the 25% risk level for live humans. While the reasoning for the shift appears to be sound, sufficient information to describe the magnitude of the shift is not provided thus cannot be replicated herein.

To assess the sensitivity of the resulting risk function to the possible overestimation of rib fractures in PMHS, the formulation of the dependent variable was modified to represent a variable number of fractured ribs (NFR). Previous research has demonstrated that post mortem subjects may sustain 2 to 3 more fractured ribs (Viano et al., 1977), or 3 and 5 more rib fractures (Foret-Bruno et al., 1978), than live subjects. Therefore, formulations of the dependent variable were carried out at NFR ≥ 3, which is consistent with the dependent variable defined in Section 5.9; NFR ≥ 4, which would be consistent with the description of an AIS 3+ injury according to AIS 1998 (AAAM, 1998); NFR ≥ 5, to bridge the gap; NFR ≥ 6, to represent a number of fractured ribs measured in PMHS tests which, once adjusted to represent live subjects based on an adjustment by 3 fractured ribs (to be consistent with both referenced studies), would represent an AIS 3+ skeletal thoracic injury to a live subject according to AIS 2005 (2008 Update)

(AAAM, 2008); and NFR ≥ 7, similar to the NFR ≥ 6 but to represent an AIS 3+ injury to a live subject according to AIS 1998 (AAAM, 1998). The latter, NFR ≥ 7, would be consistent with the definition used by Laituri et al. (2005).

Survival Weibull Injury risk functions were fit using the SledExtended dataset and are presented at an age of 40 years (Figure 5.14, along with the corresponding equations in Table 5.10). Generally, as the number of fractured ribs in the dependent variable definition increases, the risk curve shifts to the right (e.g. higher value of peak resultant definition for the same level of risk), while the NFR ≥ 7 risk function demonstrates a different shape. The change in shape of the NFR ≥ 7 risk function likely occurs due to the change in a low-deflection data point (26.7 mm) from an injury observation to a non-injury observation. It can be see that the injury risk functions formulated for 3 and 4 rib fractures as the injury threshold are very comparable. Without the aforementioned correction for PMHS versus living specimens, these two curves represent the AIS 2005 (2008 update) and 1990 (1998 update) definitions for AIS 3+ injury, respectively.

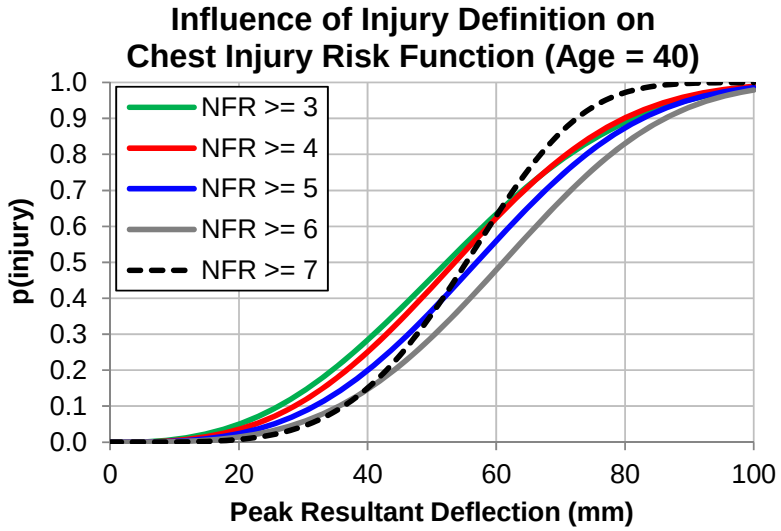

Figure 5.14. Sensitivity of the thoracic injury risk function to the number of fractured ribs selected in the dependent variable definition.

Table 5.10. Injury risk functions shown in Figure 5.14

Dependent Variable	Risk Function
NFR ≥ 3	$p(AIS \geq 3) = 1 - e^{-\left(\frac{R_{max}}{59.865}\right)^{2.7187}}$
NFR ≥ 4	$p(AIS \geq 3) = 1 - e^{-\left(\frac{R_{max}}{60.485}\right)^{3.0051}}$
NFR ≥ 5	$p(AIS \geq 3) = 1 - e^{-\left(\frac{R_{max}}{63.809}\right)^{3.2171}}$
NFR ≥ 6	$p(AIS \geq 3) = 1 - e^{-\left(\frac{R_{max}}{67.836}\right)^{3.4808}}$
NFR ≥ 7	$p(AIS \geq 3) = 1 - e^{-\left(\frac{R_{max}}{60.093}\right)^{4.4560}}$

The ability of PMHS to predict injuries other than rib fractures is also a limitation to the development of thoracic injury criteria. While rib fractures may be overestimated in PMHS research tests, soft tissue injuries such as pneumothorax and lung contusions may be underreported. This limitation arises from the need for clinical diagnosis for classification of these injuries based on the Abbreviated Injury Scale definition. For example, a major hemothorax injury is classified by more than 1000 cc of blood loss on at least one side (AAAM, 2008), which for a PMHS is not possible to measure due to the lack of blood flow. Likewise, other soft tissue injuries such as lung contusions are diagnosed through bruising in live humans, which would not occur in PMHS for the same reason.

6 ABDOMEN

6.1 Field and Historical Fleet Data

The current frontal crash test standards and consumer metric programs do not directly measure abdominal injury risk. As such, it is not possible to present any abdominal injury trends from crash testing.

Figure 6.1 shows the trend of AIS 3+ abdominal injury for belted drivers in frontal crashes. Different than observed in preceding sections, there appears to be no significant increasing or decreasing trend.

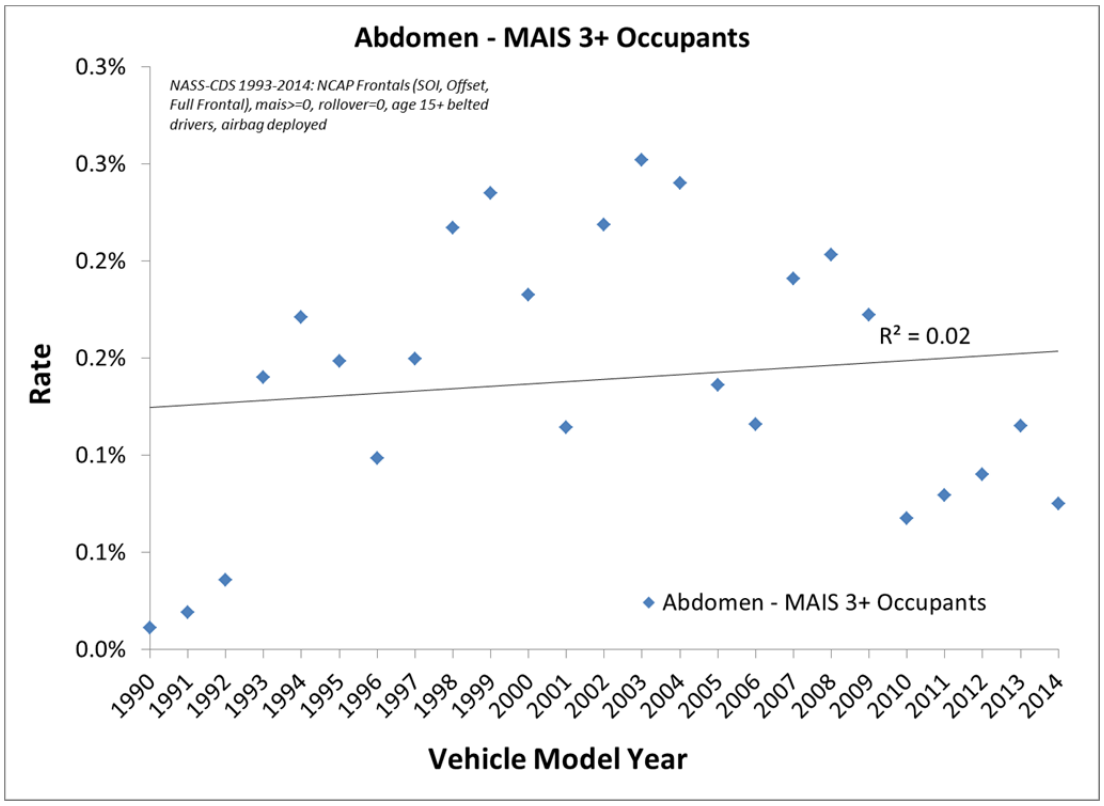

Figure 6.1. AIS 3+ abdominal injury trends by vehicle model year (1990 to 2014) from frontal crashes in NASS-CDS (1993 to 2014).

Table 1.1 and Table 1.2 (presented in Chapter 1) show unadjusted counts of MAIS 2+ and 3+ injured occupants by body regions associated with the THOR-50M as well as total injury counts for those body regions, respectively. Figure 1.2 presents the attributable cost associated with the respective body regions at the AIS 2+ level. For both belted and unbelted front row occupants involved in frontal crashes, the occurrence and attributable cost associated with abdomen injuries is lower than the majority of other body regions. Nonetheless, there remains a need for an abdomen-specific injury criterion to protect against abdominal injuries due to seat belt or steering wheel related compression or other sources of abdominal loading that may be present in different seating positions, restraint geometries, and/or crash types.

Figure 6.2 shows the regional mechanisms of injury assigned to abdominal injuries in 124 CIREN front-row belted occupants involved in frontal crashes. These mechanisms are inferred from the available data and may have been limited to available researcher/published biomechanical knowledge at the time. It is important to note that the mechanisms shown are regional mechanisms, not organ-specific mechanisms. That is, the chosen mechanism represents the type of loading/motion experienced by the entire abdominal region. Abdominal injuries, in general, were attributed to a combination of compression and rate of compression.

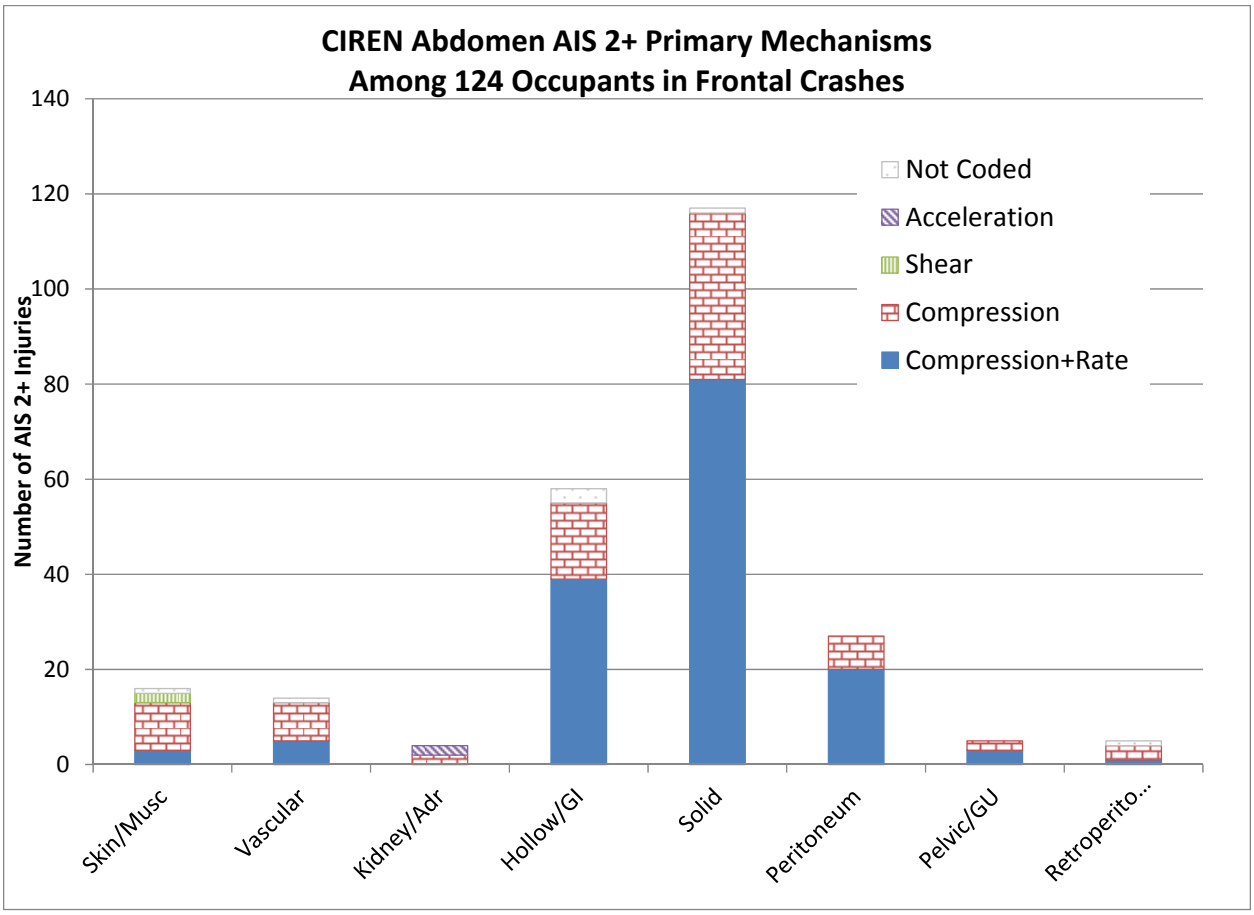

Figure 6.2. Recorded mechanisms of abdominal injuries for belted front row occupants involved in frontal crashes from the CIREN database.

6.2 Literature Review

The risk of abdominal injury in motor vehicle crashes is important to consider because the abdomen is a possible load path of the seat belt, primarily the lap belt portion between the buckle and the belt-to-vehicle anchor. While the intended function of the lap belt is to engage the bony pelvis at the anterior-superior iliac spine (ASIS), this does not always occur due to submarining brought about by occupant posture, initial position, anthropometry, and both vehicle and occupant motion during a crash. Intrusion of the lap belt into the abdomen can bring about compression of the abdominal organs, including the liver, spleen, and digestive system, which do not necessarily benefit from the protection of the rib cage.

Additionally, contact between the steering rim and the abdomen is a potential load path specific to the driver seating position, and has been shown to be the primary object associated with abdominal injuries for drivers.

Klinich et al. (2008) reviewed abdominal injury was over the time period of 1998 to 2004, which included vehicles no older than model year 1985. While less common than head, chest, and lower extremity injuries, an estimated 10,000 occupants sustain AIS 2+ abdomen injuries in frontal crashes each year. The liver and spleen are the most frequently injured organs for both drivers and right front passengers in frontal crashes. The odds of a belted driver sustaining an abdominal organ injury are substantially higher when the driver also sustains 2 or more rib fractures compared to 1 or no fractures (16, 30, and 12 times higher for the liver, spleen, and kidney respectively). This study was supplemented with a CIREN dataset, which included 526 cases involving AIS 2+ abdomen injury in vehicles from model year 1985 through 2005. As in the NASS dataset, the liver (50%) and spleen (29%) were the most frequently injured abdominal organs for drivers in frontal crashes.

A study of crash injury data from the United Kingdom's Co-operative Crash Injury Study (CCIS) from 1998 to 2010 showed that rear passengers have a substantially higher rate of AIS 2+ and AIS 3+ abdominal injury compared to front seat passengers and drivers (Frampton et al. 2012). Drivers and front seat passengers most frequently sustained injuries to solid organs (liver and spleen), while rear seat occupants most frequently sustained injuries to the hollow organs (jejunum-ileum, mesentery, and colon). Injury patterns were sensitive to rib fracture, as some organ injuries (kidney, liver, mesentery, pancreas, and spleen) were more likely when two or more rib fractures occurred, while others (colon, duodenum, jejunum-ileum, stomach) were more likely when zero or one rib fractures occurred.

6.3 **Design**

The abdomen of the THOR-50M consists of two components, the upper abdomen and the lower abdomen. The upper abdomen is the region on the dummy that represents the lower thoracic cavity, which fills the volume that exists between the lowest three ribs, above the lower abdomen and in front of the spine (Figure 6.3). The lower abdomen is defined as the region of the human body between the lower thoracic rib cage and the pelvic girdle.

The upper and lower abdomen components of THOR are represented by structural fabric bags containing foam inserts which define the compression stiffness. Both abdomen inserts are anchored posteriorly to the spine, while the upper abdomen insert is additionally anchored to the lower rib cage through three rib-to-bib attachment bolts on each side. When the lumbar spine pitch change joint is set to the "slouched" position, the abdomen inserts are in contact with one another; when in the "erect" and "neutral" positions, the gap between the abdominal inserts is filled with the lower abdomen neutral/erect position foam. This gap is also spanned by two steel stiffeners on each side that are installed into the torso jacket. The bottom surface of the lower abdomen insert is coincident with the pelvis, which includes bilateral mechanical representations of the anterior-superior iliac spine (ASIS).

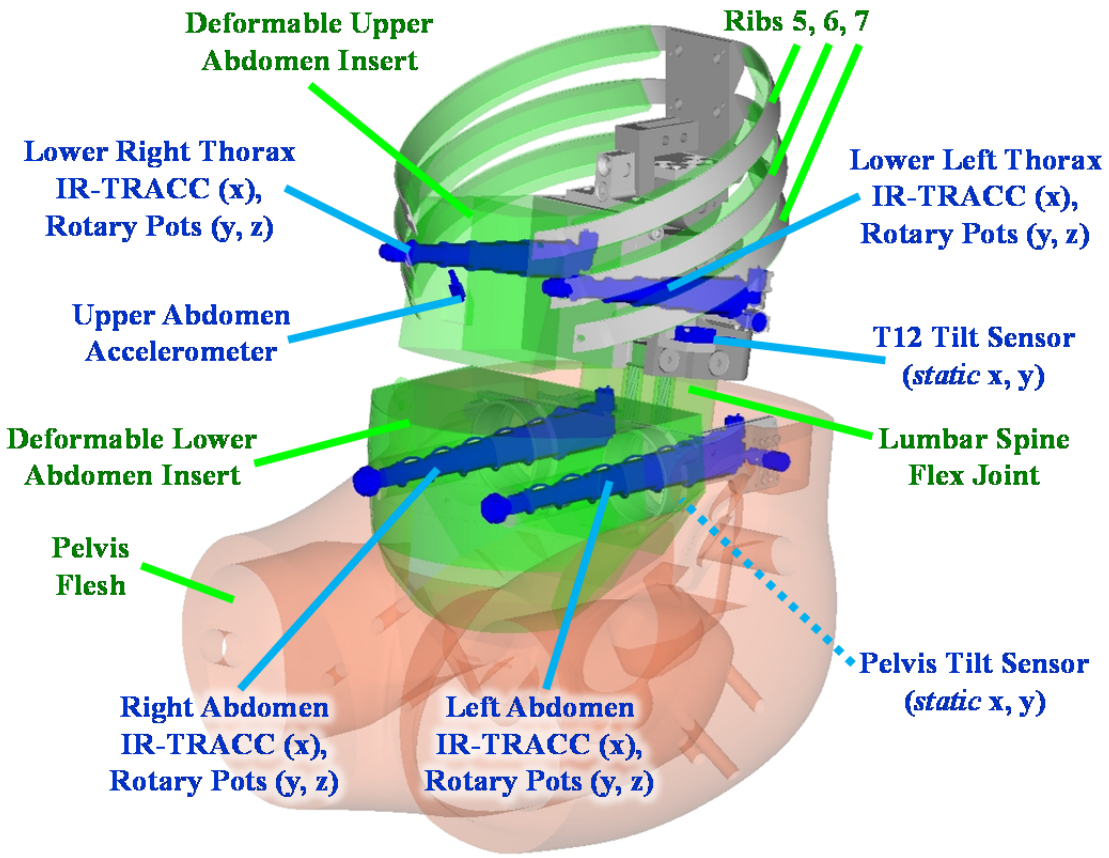

Figure 6.3. Design and instrumentation in the THOR-50M upper and lower abdomen.

6.4 Instrumentation

The upper abdomen is no longer instrumented, as the high-tension string potentiometer in the THOR-NT design resulted in permanent deformation of the foam inserts (Ridella and Parent, 2011) and often underestimated the upper abdominal deflection (Shaw et al., 2004). The upper abdomen deflection instrumentation would be at the same vertical level of the lower thorax IR-TRACC measurement locations, should a measure of upper abdomen deflection related to skeletal deformation of the lower rib cage be necessary (Figure 6.3).

The lower abdomen includes bilateral IR-TRACC three-dimensional displacement measurement devices located at the vertical center of the lower abdomen insert and laterally offset by roughly 65 millimeters. In the AMVO posture, the anterior attachment location of the IR-TRACC is nearly coincident with point 25, the maximum abdominal protrusion, in the x-z plane. The anterior attachment point is 24 millimeters inferior of the umbilicus (point 24) along the z-axis and in a similar location along the x-axis. The posterior attachment point is at the vertical level of the iliocristale (point 27).

The IR-TRACC assemblies include two rotational potentiometers attached to the base of the IR-TRACC tube. The IR-TRACC tube itself allows up to 120 millimeters of deflection, while the rotational potentiometers have a range of motion of roughly 10 degrees in each direction before contact occurs

between the IR-TRACC tube and the flared overload cone. Since the IR-TRACC units function on light emission and subsequent sensing, there is no pre-load applied to the foam abdomen insert.

6.5 **Biofidelity**

Parent (2016) presented an evaluation of THOR-50M biofidelity in three conditions: steering rim impact to the upper abdomen, rigid bar impact to the lower abdomen, and belt loading to the lower abdomen. Since the upper abdomen loading condition primarily stresses the lower rib cage, it is not relevant to the assessment of lower abdomen biofidelity. In the rigid bar impact condition, the THOR-50M demonstrated good internal biofidelity, but poor external biofidelity as the reaction force was greater than the associated PMHS response corridor. In the belt loading condition, the THOR-50M demonstrated excellent external biofidelity in comparison to the force-penetration biofidelity corridor, though the maximum deflection measured was lower than that of the mean PMHS response. At the abdomen body region level, the BioRank results for the THOR-50M demonstrate good internal and marginal external biofidelity.

6.6 **Data**

Kent et al. (2008) presented the results of 45 tests of porcine specimens subjected to compressive loading of the upper and lower abdomen in both a ramp-and-release (RR) and ramp-and-old (RH) loading condition (Table 6.1). From this data, several injury risk functions were developed and evaluated, and it was determined that maximum normalized abdominal penetration was the most appropriate predictor of injury resulting from abdomen belt loading. This study considered only the RR condition in the development of injury risk functions, as it was thought that the RH condition may have exacerbated the severity of the injuries during the hold phase of the event.

Table 6.1. Source data for PMHS tests.

ID	d_{max}	Condition	Site	MAIS
1.07	0.36	RR	Lower	3
1.08	0.37	RR	Upper	4
1.09	0.37	RR	Lower	0
1.10	0.55	RR	Lower	2
1.11	0.32	RR	Lower	0
1.12	0.32	RR	Lower	2
1.13	0.35	RR	Upper	2
1.15	0.40	RR	Lower	2
1.16	0.46	RR	Lower	3
1.17	0.23	RR	Lower	0
1.18	0.26	RR	Upper	2
1.20	0.43	RR	Upper	3
1.21	0.43	RR	Lower	3
1.22	0.39	RR	Lower	3
1.23	0.40	RR	Lower	2
1.24	0.40	RR	Upper	2
1.25	0.42	RR	Lower	4
1.26	0.40	RR	Upper	3
1.27	0.30	RR	Upper	1
1.28	0.42	RR	Lower	3
1.29	0.52	RR	Lower	3
1.30	0.23	RR	Upper	0
1.31	0.37	RR	Upper	3
1.32	0.36	RR	Lower	0
1.33	0.40	RR	Upper	3
1.34	0.45	RR	Upper	3
1.35	0.44	RR	Lower	3
1.36	0.27	RR	Upper	0
1.39	0.46	RR	Upper	3
1.41	0.43	RR	Lower	3
1.43	0.47	RR	Lower	2
1.44	0.56	RR	Lower	3
1.45	0.62	RR	Upper	4
1.01	0.45	RH	Lower	2
1.02	0.54	RH	Lower	4
1.03	0.48	RH	Lower	3
1.04	0.49	RH	Lower	3
1.05	0.50	RH	Upper	4
1.06	0.65	RH	Upper	4
1.37	0.31	RH	Lower	0
1.38	0.48	RH	Upper	3
1.40	0.52	RH	Lower	3
1.42	0.50	RH	Lower	3
1.46	0.64	RH	Upper	3
1.47	0.56	RH	Lower	3

6.7 **Injury Risk Function Formulation**

To first qualitatively evaluate the input dataset, nonparametric survival analysis was carried out. The dataset was divided by two strata: loading condition (RR vs. RH) and loading site (Upper vs. Lower). There was a notable qualitative increase in survival time of the RH group compared to the RR group (Figure 6.4). This is contrary to the assertion of Kent et al. (2008), as this suggests a higher injury risk in the RR group for a given peak normalized abdomen compression compared to the RH group. However, there are only two non-injured observations in the RH group, and there is no overlap between the non-injured and injured observations, so evaluation of the RH group independently is not advisable.

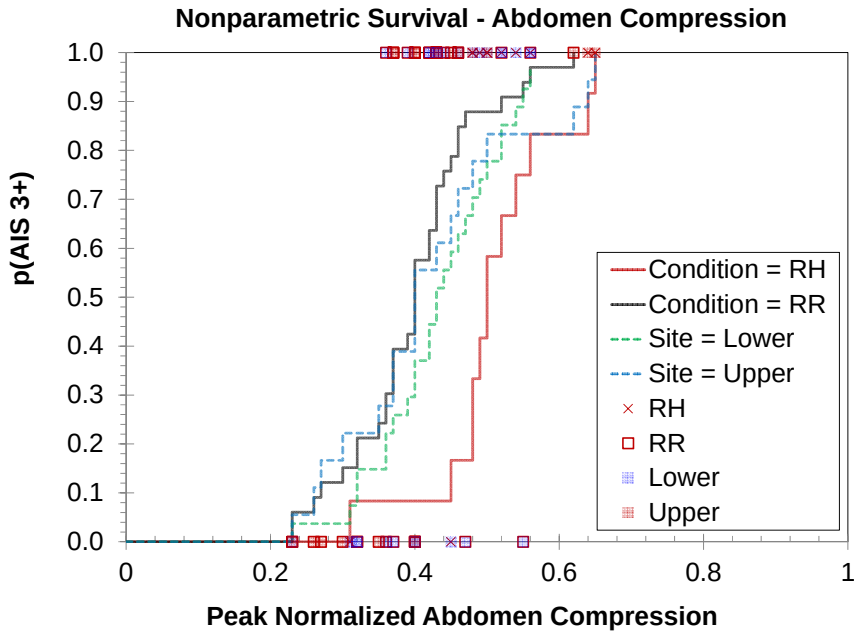

Figure 6.4. Nonparametric survival analysis of abdomen injury risk, stratified by condition and loading site.

Risk functions were developed through both logistic regression and survival analysis for the RR only and combined RR and RH groups. There was not a significant influence on the shape or magnitude of the risk functions using the RR dataset alone (as in Kent et al., 2008) or both the RR and RH datasets (Figure 6.5). A logistic regression risk function could not be fit to the RH only dataset, as there were no overlapping non-injury and injury data points. It is recommended to use the binary logistic injury risk function using the largest dataset available (RR+RH), as the dataset includes a combination of both injured and non-injured observations, there is sufficient overlap of these points in the transition region, and there is not a meaningful difference between the logistic and Survival Weibull risk functions.

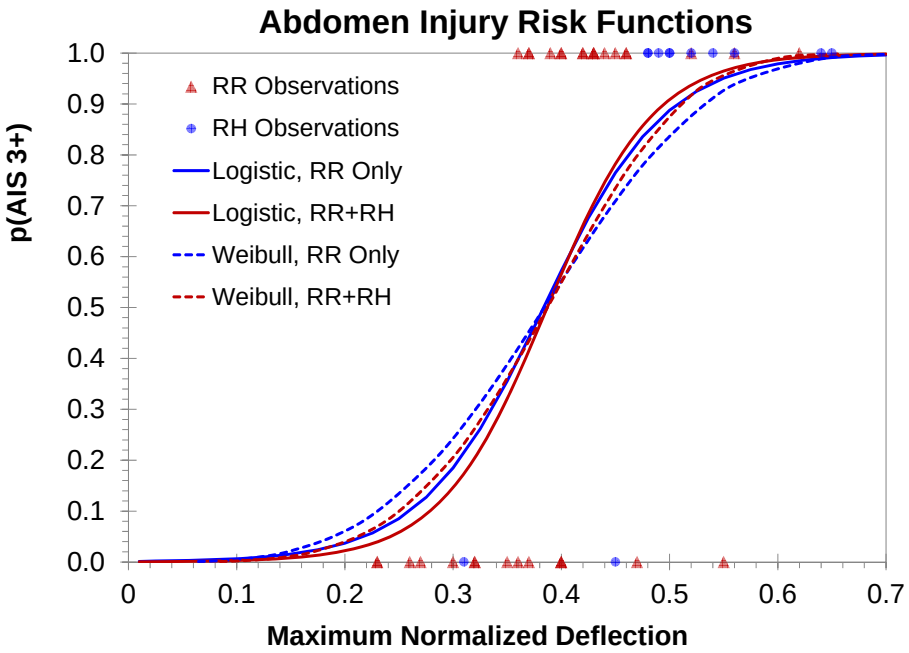

Figure 6.5. Comparison of injury risk functions formed using logistic regression and survival analysis, for both the RR only and the RR and RH groups combined.

The qualitative difference between the Upper and Lower loading site groups was comparatively small (Figure 6.4), which is consistent with the findings of Kent et al. (2008) who found no significant difference between the Upper and Lower groups. To investigate further, injury risk functions were fit using logistic regression to the Lower only, Upper only, and combined Upper and Lower observations (Figure 6.6). The logistic risk function for the Upper Only group is steeper than the Lower Only and Combined groups, as there is limited overlap in the non-injury and injury data for the Upper Only group. The Combined group, however, resulted in a similar risk curve to the Lower Only group, suggesting that the influence of the Upper Only group on the combined dataset is relatively small. Therefore, inclusion of data points from both the Upper and Lower loading site groups is recommended for this analysis.

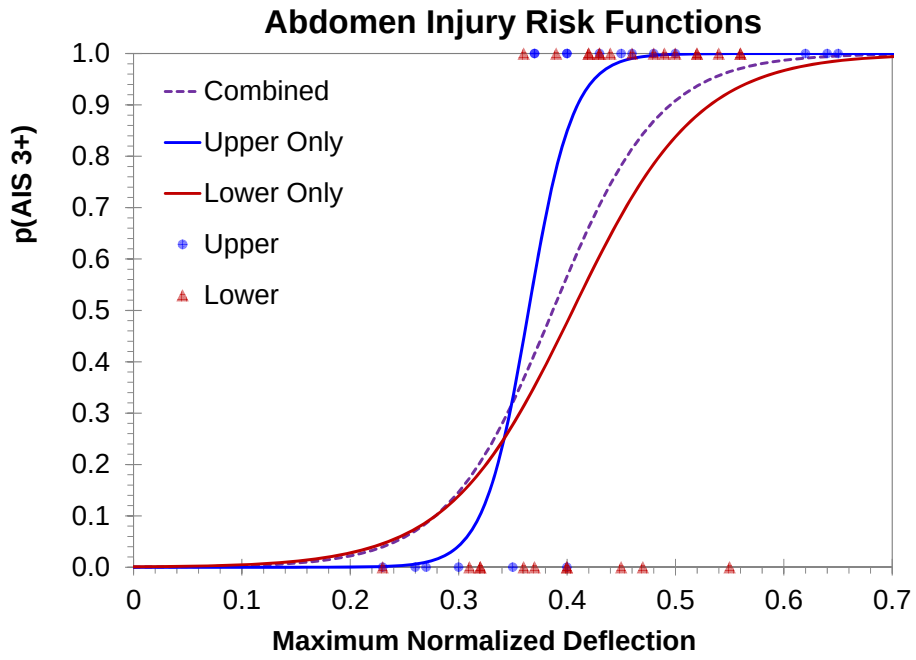

Figure 6.6. Comparison of injury risk functions formed using logistic regression for the Lower only, Upper only, and both Lower and Upper groups combined.

6.8 Application of Risk Function to THOR-50M

The THOR-50M ATD is equipped to measure the compression of the abdomen, thus the maximum normalized abdominal penetration can be measured nearly directly using the THOR instrumentation. One limitation is that while the IR-TRACC assemblies are mounted to the anterior aspect of the abdomen, there may be some compression of the torso jacket which is not captured in the IR-TRACC compression measurements. To calculate maximum normalized abdominal penetration, the peak of the left and right abdominal IR-TRACC x-axis deflections is divided by 229 millimeters, the abdominal depth of the THOR-50M ATD at the location of the IR-TRACC attachment points.

Recommended injury risk function:

$$p(AIS \geq 3) = \frac{1}{1 + e^{\left(7.849 - 20.287 \frac{\delta_{max}}{d_{THOR}}\right)}}$$

where:

δ_{max}	=	Peak of the left and right peak abdomen x-axis deflection
d_{THOR}	=	THOR abdomen depth at location of IR-TRACC attachment points [229 millimeters]

Simplified:

$$p(AIS \geq 3) = \frac{1}{1 + e^{(7.849 - 0.0886 \delta_{max})}}$$

6.9 **Fleet Test Data: THOR-50M**

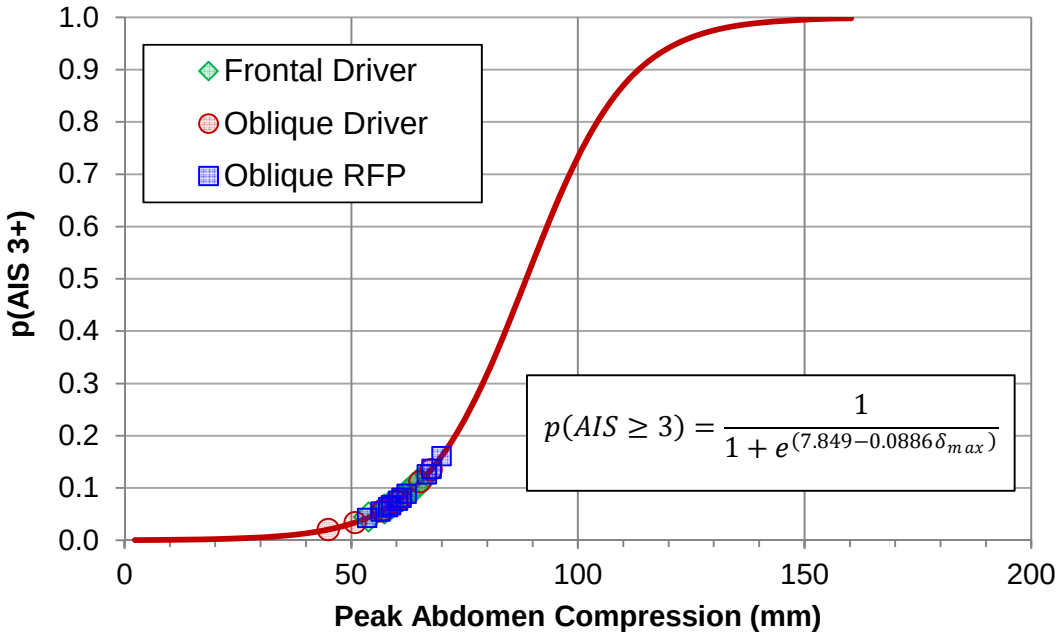

Figure 6.7. Peak abdomen compression from frontal rigid barrier and oblique moving deformable barrier tests using THOR-50M.

6.10 **Limitations**

There are a few caveats that limit the application of the abdomen injury risk function to the prediction of abdomen injury using the THOR-50M ATD. First, the injury risk function was developed using porcine specimens as human surrogates. The benefit of this approach is the ability to diagnose soft tissue injuries which would not be possible with PMHS, though the drawback is that the relationship between live porcine specimens and live humans is not known. Second, the injury criteria tests were conducted in a fixed-back configuration, which does not consider inertial loading due to acceleration or deceleration of the body as well as the internal organs of the abdomen which would occur in a belted frontal crash environment. Third, the relationship between PMHS response and THOR-50M response presents a limitation since in the abdomen belt loading condition, the THOR-50M demonstrated poor biofidelity. That said, the abdomen belt loading biofidelity evaluation was conducted in a free-back configuration, thus the biofidelity performance may not be the same in the fixed-back configuration of the injury criteria development tests. Finally, the biofidelity performance of the THOR-50M compared to a live human is also not directly known. These limitations should be taken into consideration in the application of the abdominal injury risk function to THOR-50M.

7 KNEE, THIGH AND HIP

7.1 Field and Historical Fleet Data

Table 7.1 shows the weighted (unweighted in parenthesis) counts for hip/pelvis and knee/femur AIS 2+ and AIS 3+ injuries for belted and airbag restrained drivers in frontal crashes for NASS-CDS case years 2000 to 2014. It can be seen that roughly two-thirds of hip/pelvis injuries occur in the absence of femur/knee 2+ or 3+ injuries.

Table 7.1 Hip/pelvis versus femur/knee injuries for belted, airbag restrained drivers in frontal crashes; NASS-CDS 2000-2014.

		Femur/Knee AIS 2+		Femur/Knee AIS 3+	
		0	1	0	1
Hip/Pelvis AIS 2+	0	5,135,672 (13,223)	69,043 (581)	5,186,096 (13,478)	18,620 (326)
	1	12,352 (166)	6,583 (114)	12,964 (185)	5,971 (95)
Hip/Pelvis AIS 3+	0	5,142,913 (13,323)	72,986 (639)	5,193,744 (13,586)	22,154 (376)
	1	5,111 (66)	2,640 (56)	5,315 (77)	2,436 (45)

Figure 7.1 shows the trend of AIS 3+ KTH injury for belted drivers in frontal crashes. There does not appear to be any significant increasing or decreasing trend with newer model years. In contrast, Figure 7.2 shows a decreasing trend of peak femur forces and associated injury risk (risk function from NHTSA, 2008) with newer model year vehicles as evaluated with the Hybrid III 50th male dummy in full frontal, 35-mph tests.

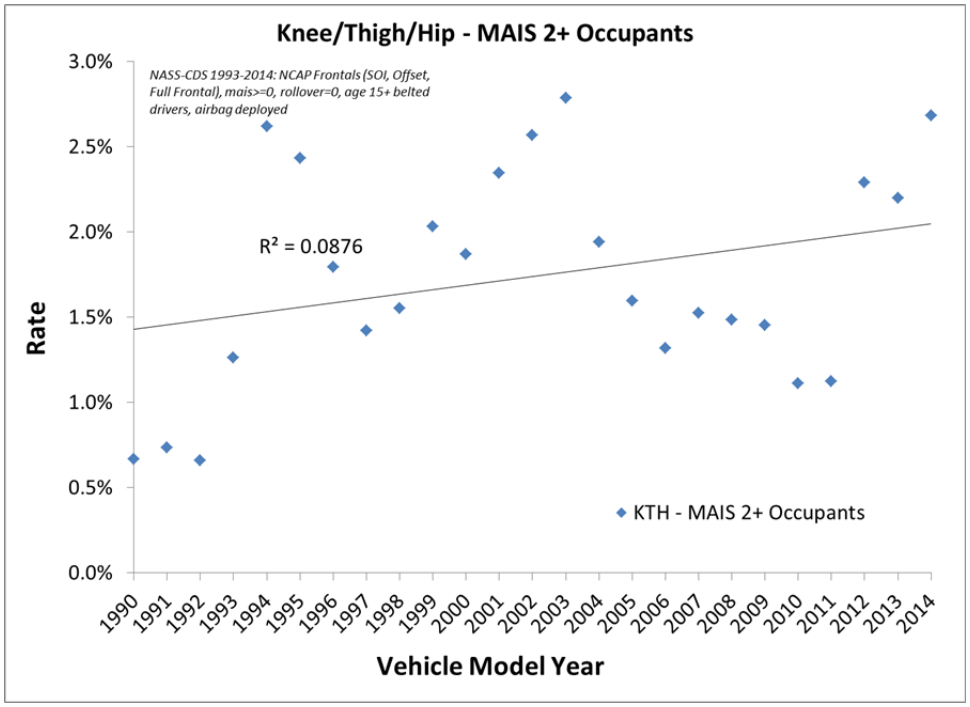

Figure 7.1. AIS 2+ knee/thigh/hip injury trends by vehicle model year (1990 to 2014) from frontal crashes in NASS-CDS (1993 to 2014).

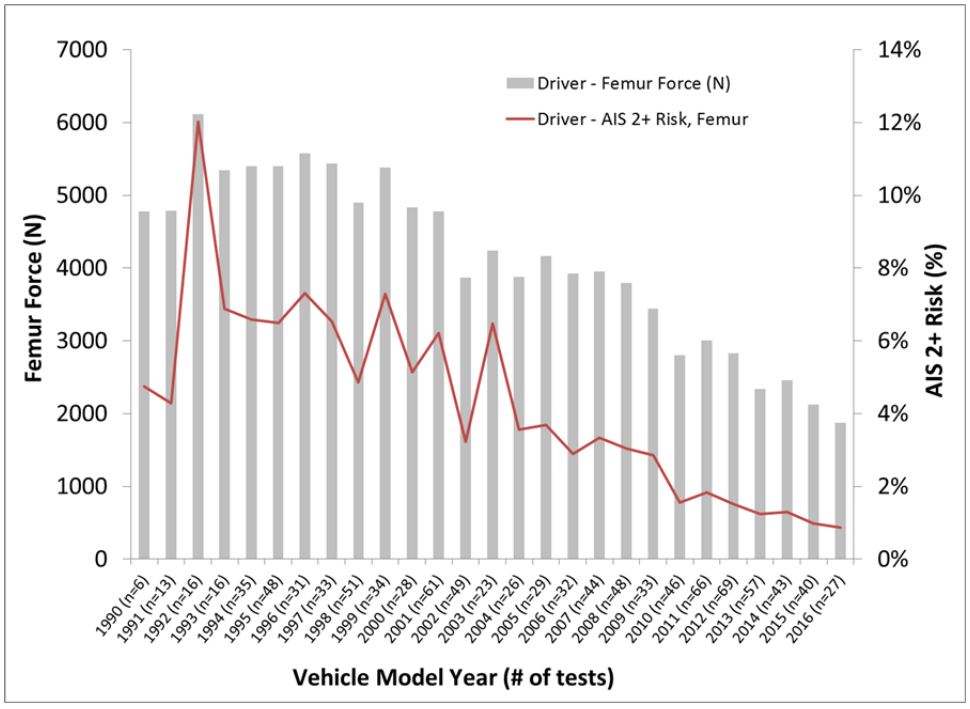

Figure 7.2. Hybrid III 50th male frontal NCAP average peak femur axial force and injury risk (AIS 2+) for model year 1990 to 2016

Figure 7.3 shows the regional mechanisms of injury assigned to knee, thigh, hip, and pelvis injuries in 165 CIREN front-row belted occupants involved in frontal crashes. These mechanisms are inferred from the available data and may have been limited to available researcher/published biomechanical knowledge at the time. It is important to note that the mechanisms shown are regional mechanisms, not organ-specific mechanisms. That is, the chosen mechanism represents the type of loading/motion experienced by the entire abdominal region. The overwhelming majority of injuries to the knee, thigh, and hip region are due to compression – in most cases directed along the length of the femur.

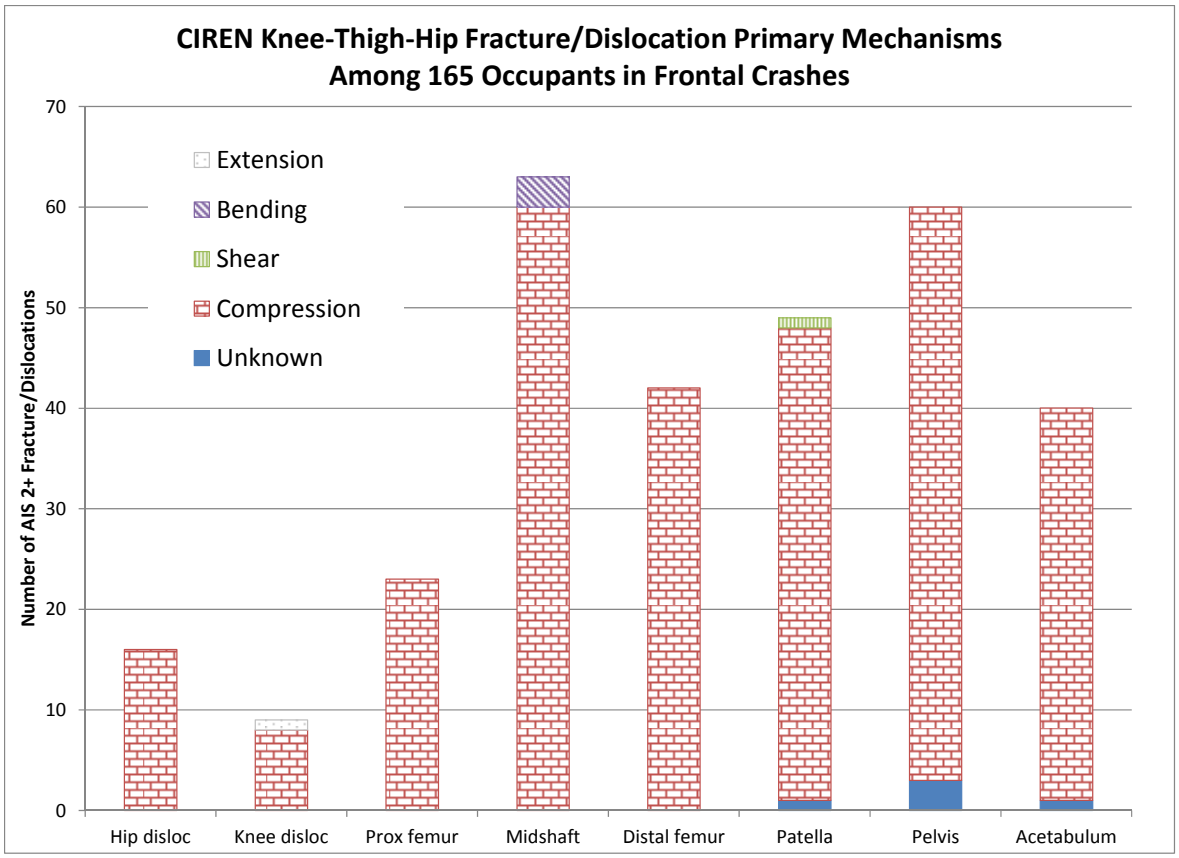

Figure 7.3. Recorded mechanisms of knee, thigh, hip, and pelvis injuries for belted front row occupants involved in frontal crashes from the CIREN database.

7.2 Literature Review

The importance of protection of the knee, thigh, and hip in motor vehicle crashes is highlighted by the research of Rudd et al. (2011), who showed that AIS 3+ KTH injuries were the most commonly-occurring injuries in small overlap and oblique frontal crashes.

In both FMVSS No. 208 and Frontal NCAP, the only KTH injury assessment carried out is an assessment of femur fracture risk based on peak compressive force. As applied in FMVSS No. 208, the IARV for femur compressive force measured by the Hybrid III 50th ATD is 10 kN (49 CFR 571.208.S6.5), while the femur force injury risk function presented by Eppinger et al. (1999) is used in the Frontal NCAP rating system (NHTSA, 2008).

Since the implementation of the injury criteria development study carried out by Eppinger et al. (1999), a large body of work has been conducted and published by the University of Michigan Transportation Research Institute (UMTRI) to understand KTH injury mechanisms and injury prediction in frontal crashes (Rupp et al. 2003, 2005, 2006, 2009a, 2009b). These studies are referenced heavily where appropriate throughout this section.

7.3 Design

The knee/thigh/hip (KTH) region of the THOR-50M is configured to mimic the structure and range of motion of the human. Starting from the knee, a revolute joint at the knee allows flexion and extension of the lower leg with respect to the upper leg. A sliding joint at the interface between the distal femur and the proximal tibia at the knee allows linear translation perpendicular to the tibia that represents both bending of the proximal tibia and extension of the posterior cruciate ligament (PCL). At approximately the mid-shaft of the femur, a translational joint allows compression along the axis of the femur using a guided plunger which compresses a rubber element. This joint was designed to meet the human response to femur compression defined by Rupp et al. (2003). The proximal femur is attached to the pelvis through a spherical joint at the acetabulum, which in turn is attached to the body of the pelvis through a load cell. The pelvis bone is functionally rigid and includes a human-like iliac wing representation, and the entire pelvis is covered with a single-piece flesh component. A diagram of the topology and instrumentation of the THOR-50M KTH is shown in Figure 7.4.

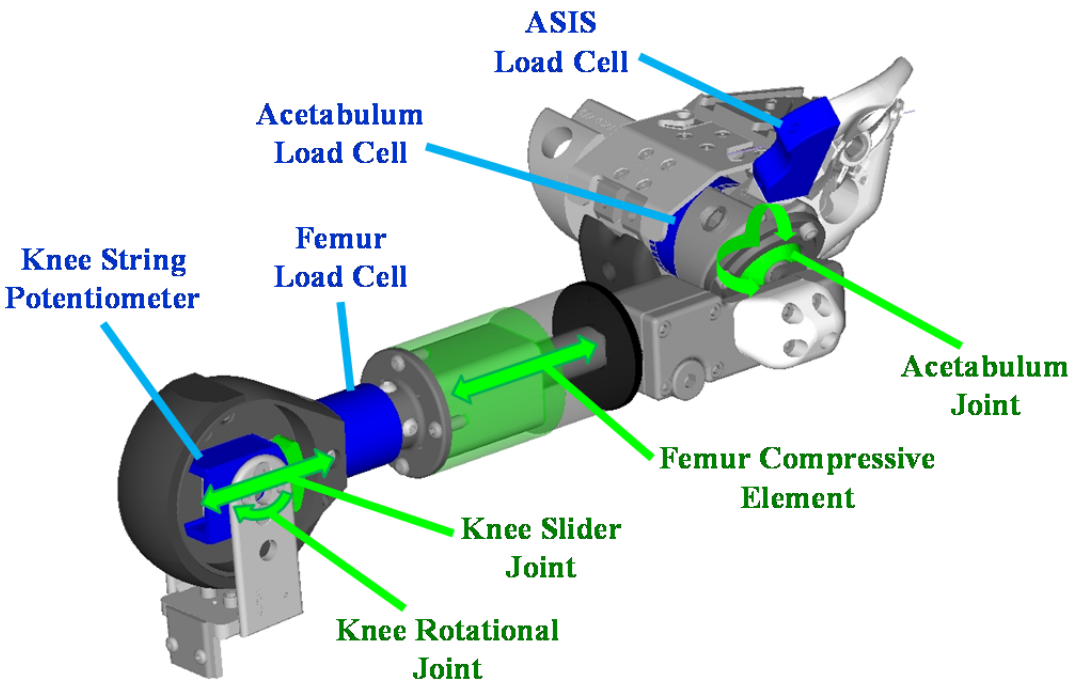

Figure 7.4. Joint and instrumentation configuration of THOR-50M KTH

7.4 Instrumentation

THOR-50M ATD KTH instrumentation is summarized in Table 7.2.

Table 7.2. THOR-50M ATD thoracic instrumentation.

Sensor	Measurement Description	Measurement Axes
Knee string potentiometer	Translation of proximal tibia with respect to distal femur along an axis perpendicular to tibia	Displacement: XL
Femur load cell	Force and moment between knee and femur	Force: XL, YL, ZL Moment: XL, YL, ZL
Acetabulum load cell	Force between the proximal femur and the pelvis	Force: XL, YL, ZL
ASIS load cell	Force and moment applied to the ASIS, typically through lap belt loading	Force: XL Moment: YL

7.5 Biofidelity

Biofidelity of the THOR-50M KTH was assessed in two conditions (Parent, 2016): femur compression and knee shear. In the femur compression condition, the THOR-50M demonstrated good internal and external biofidelity with BioRank scores of 1.400 and 1.100, respectively, while the Hybrid III 50th demonstrated poor internal and external biofidelity. In the knee shear condition, for which only external BioRank scores are available, the THOR BioRank score was outside of the acceptable biofidelity range (2.331), while the Hybrid III 50th demonstrated good biofidelity with BioRank score of 1.248.

7.6 Knee/Femur Injury

There are two injury mechanisms for which injury risk functions have been developed for the KTH: knee/femur injury and hip injury. Assessment of injury related to knee/femur loading is not unique to THOR-50M, as a femur injury risk function has been developed for human subjects by Kuppa et al. (2001) and is currently being applied in consumer information testing using the Hybrid III family of frontal impact ATDs (NHTSA, 2008). This injury risk function was developed through logistic regression of the results of whole PMHS reported by Morgan et al. (1989). The dataset contained 126 tests, of which 14 had no reported data for applied knee force. Since applied knee force is the primary variable of interest, these 14 specimens were excluded. Of the remaining 112 tests, 34 sustained AIS 2 or greater injury. Although the injuries were predominantly to the knee (e.g. patella) and distal femur (e.g. femoral condyles), 11 specimens (33%) had thigh injuries (e.g. femoral shaft, femoral neck) and three specimens (9%) sustained hip injury (one of which was isolated and two of which had associated knee/femur injuries). Given the breadth of injuries sustained, the risk function is assumed to apply to all knee/femur injuries. Rupp et al. (2009b) reanalyzed the same dataset using a Survival Weibull model in order to capture the censoring effects of the injury and non-injury data, though the difference between the resulting risk function and the risk function developed by Kuppa et al. (2001) was negligible (Figure 7.5) aside from the perceived benefit of the Survival Weibull model having exactly zero predicted risk at an applied force level of zero.

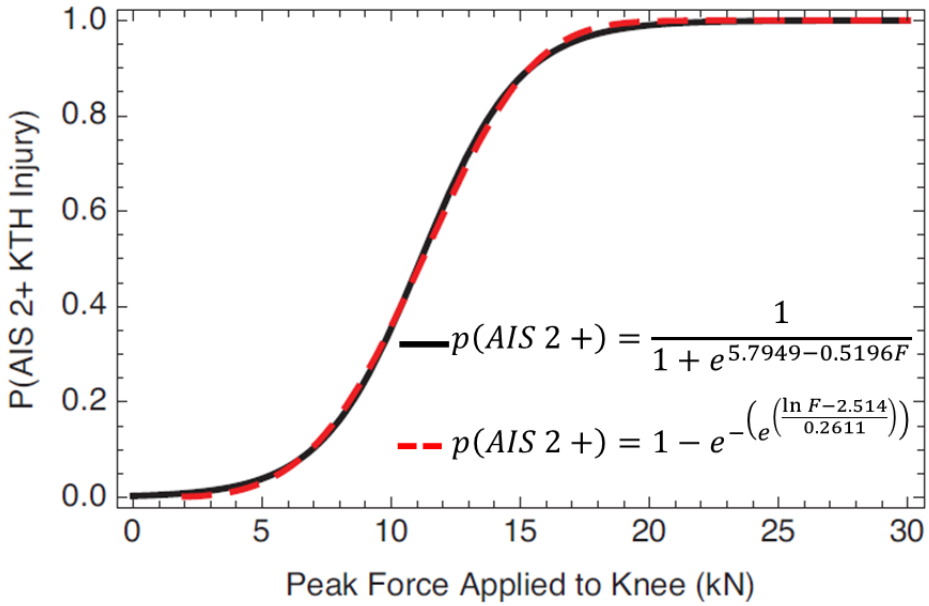

Figure 7.5. Comparison of logistic and Survival Weibull risk curves (modified from Rupp et al., 2009b).

While the risk curves presented in Figure 7.5 relate the peak force applied to the knee to the risk of knee and distal femur injury, the injury risk function has been applied for the Hybrid III (e.g. as applied in the New Car Assessment Program) using the peak force measured by the femur load cell (NHTSA, 2008). Several studies have demonstrated that the peak force measured in the femur is lower than the peak force applied to the knee for both PMHS and ATDs. Donnelly et al. (1987) conducted pendulum impacts to the unrestrained femur of whole subjects for both PMHS and the Hybrid III 50th male ATD. The PMHS tests from this study were included in the Morgan et al. (1989) and Kuppa et al. (2001) analyses. In the PMHS tests, an implanted load cell in the shaft of the femur measured force in a similar fashion to the Hybrid III femur load cell. It was found that in the PMHS tests, there was a strong correlation between the force measured at the implanted femur load cell and the force applied to the knee, with the femur load cell measuring 53% of the peak applied force. An even stronger correlation was found in the Hybrid III tests, but a higher ratio of the impact force was measured at the femur load cell (68%). A separate estimate of the relationship between Hybrid III measured femur load cell forces and applied force to the knee was developed by Rupp et al. (2009a) in a test apparatus developed to represent knee bolster impacts in frontal crash tests. In these tests, the peak force measured at the Hybrid III femur load cell was 77% of the applied force independent of knee bolster force-deflection characteristic.

Using the measured Hybrid III femur load cell peak force instead of the peak applied force as input to the injury risk function would result in a *lower* estimate of injury risk than intended. For instance, if the Hybrid III measured a 10 kN peak femur force, the estimated force applied to the knee of the Hybrid III would be either 13.0 kN, assuming the Rupp et al. (2009a) estimate of 77%, or 14.7 kN, assuming the Donnelly et al. (1987) estimate of 68%. Using the measured Hybrid III force directly in the Kuppa et al. (2001) injury risk function would predict a 35% risk of AIS 2+ injury, while using the estimated force applied to the knee as the input to the risk function as originally developed would result in a predicted injury risk of 70% to 85%.

Due to the improvements in biofidelity of the THOR-50M compared to the Hybrid III, it is assumed that the limitations of the application of the knee/femur injury risk function developed by Kuppa et al. (2001) are only alleviated when applied to THOR-50M compared to Hybrid III. However, since the construction of the THOR-50M knee is similar to that of the Hybrid III and is likely more coupled than the human knee, the force measured at the femur load cell is lower than the force applied to the knee. Therefore, correction for this difference between applied force at the knee and peak force measured at the load cell is recommended before calculation of injury risk.

Several approaches were investigated to determine the relationship of the peak applied force at the knee to the peak force measured at the femur load cell of the THOR-50M. One approach would be to assume the same relationship as the Hybrid III 50th percentile male ATD, for which the distal femur and knee structure is nearly identical. Another approach was to investigate pendulum impacts to the knee of the THOR-50M in a qualification test condition, as described below.

Seated knee impacts to the THOR-50M were conducted at several impact velocities and impact conditions using a 5-kilogram pendulum impactor. In an unrestrained back condition, the knee was impacted at six increasing velocities. The average of the ratios between peak load cell force and peak applied force computed at each velocity is 58%, and a linear fit to the data for each set results in ratio of slopes of 55% (Figure 7.6). However, the ratio of measured force to applied force appears to follow a higher-order polynomial or power relationship, with impacts at lower velocities being closer to an equal ratio. Tests were also conducted in a fixed-back condition at six impact velocities, and the resulting ratios of peak femur load cell force to peak applied force was consistently 55% (Figure 7.7), though this may be due to the smaller range of velocities in the fixed-back condition.

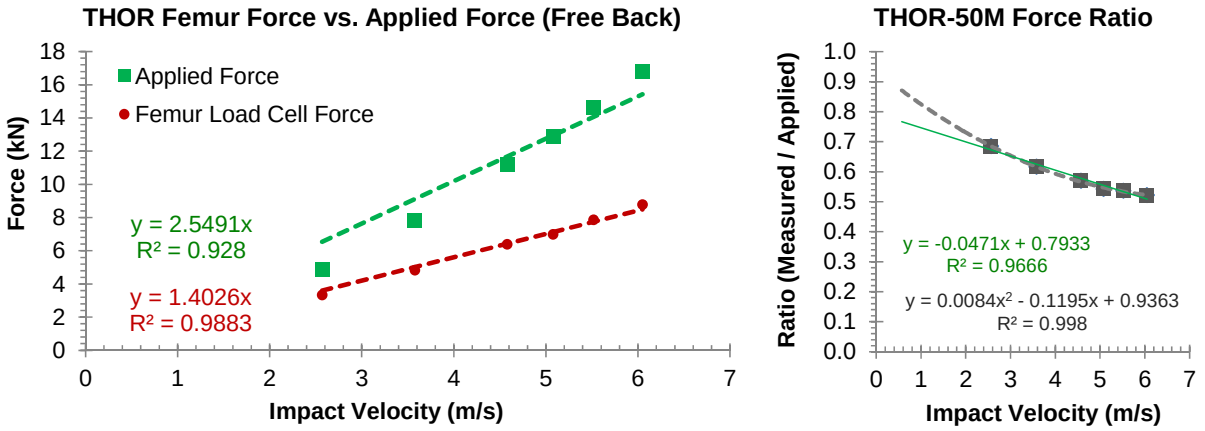

Figure 7.6. Relationship between force applied to the femur and force measured at the femur load cell for free-back tests with THOR-50M.

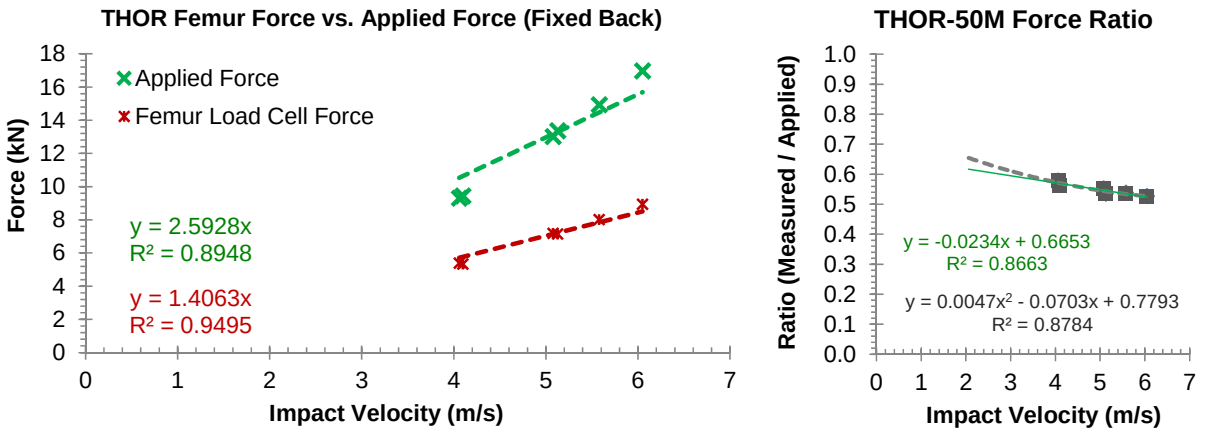

Figure 7.7. Relationship between force applied to the femur and force measured at the femur load cell for fixed-back tests with THOR-50M.

While these results suggest that the relationship of applied femur force to load cell force for THOR is more similar to the PMHS than Hybrid III, it is not clear how significant the difference in impact mass might be, as the tests reported by Donnelly et al. (1987) used a 23-kilogram impactor while the THOR tests reported above used a 5-kilogram impactor. It is also unclear how well either condition relates to the loading condition seen in a motor vehicle crash, where the femurs are restrained by the knee bolster and loaded inertially by the remaining effective mass of the body. In addition, because the relationship between applied force at the knee and measured force at the femur load cell in THOR-50M was shown above to be sensitive to impact velocity in pendulum testing (Figure 7.6 and Figure 7.7), selection of a single transfer function would not be straightforward because the impact velocity could not be measured during a crash test.

For the reasons described above, it is not recommended to use pendulum impacts to the knee of the THOR-50M in a qualification test condition to develop the correction factor for peak applied knee force to the peak measured femur force. Instead, the analysis presented by Rupp et al. (2009a) in testing of the Hybrid III under loading rates occurring in FMVSS No. 208 and US NCAP crash tests is recommended as the knee and distal femur of the THOR-50M and Hybrid III are structurally similar. Therefore, a correction factor accounting for the estimated 77% of the applied force at the knee measured by the femur load cell force is recommended for THOR-50M.

The recommended knee/femur risk function for the THOR-50M is:

$$p(AIS\ 2+) = \frac{1}{1 + e^{5.7949 - 0.5196 F_{LC} \times r_{KtoF}}}$$

where:

F_{LC} = Peak compressive force measured by the z-axis for the THOR femur load cell (in kN)

r_{KtoF} = Ratio of applied force at knee to measured force at femur load cell [1/0.77] (Rupp et al., 2009a)

Simplified:

$$p(AIS\ 2+) = \frac{1}{1 + e^{5.7949 - 0.6748 F_{LC}}}$$

7.7 Hip Injury

Contrary to knee/femur injury, the prediction of pelvis injury related to axial femur loading is a unique capability of THOR-50M due to its biofidelity and instrumentation. As such, further analysis is necessary to determine an appropriate injury risk function to predict injury to the pelvis in motor vehicle crashes.

7.8 Hip Injury: Data

Rupp et al. conducted compressive loading tests of 27 PMHS knee-thigh-hip complex specimens using a pneumatic ram (Rupp et al., 2009b). The iliac wing of the specimen was fixed and the knee was loaded along the axis of the femur through a molded knee interface. The target loading rate was 300 N/ms, which was argued to be representative of knee-bolster loading rates seen in unbelted crash tests (Rupp et al. 2003), though individual specimen loading rates varied from 62 N/ms to 566 N/ms. For the dataset presented in Rupp et al. (2009b), the specimens were positioned in a “neutral” posture consistent with standard driving posture as defined by Schneider at al. (1983). Additional tests were conducted with flexion and adduction applied and it was found that there was a statistically-significant decrease in tolerance with increase in both flexion and adduction compared to the standard driving posture (Rupp et al. 2003). For completeness, both the neutral posture dataset presented by Rupp et al. (2009b), referred to here as “Neutral” and including all specimens with flexion and adduction angles of 0°, and the complete set of tests documented in Rupp (2006), referred to here as “Complete,” are considered in this analysis. Subject anthropometry and associated fracture forces are shown in Table 7.3.

Table 7.3. Dataset considered in the development of a hip injury risk function (Rupp 2006).

Test ID	Fracture force (kN)	Gender	Age (yr)	Stature (cm)	Mass (kg)	Adduction (deg)	Flexion (deg)	NHTSA BioDB TSTNO
NB0105L	5.59	F	55	163	113	0	0	5240
NB0105R	5.37	F	55	163	113	0	0	5241
NB0106L	4.85	M	86	173	91	0	0	5419
NB0108L	7.57	M	79	180	82	0	0	5423
NB0108R	7.87	M	79	180	82	0	0	5424
NB0110L	6.6	M	60	178	125	0	0	5427
NB0112L	4.53	M	72	173	81	0	30	5861
NB0112R	6.67	M	72	173	81	0	0	5862
NB0114L	3.06	F	68	165	71	0	30	5864
NB0114R	4.65	F	68	165	71	0	0	5865
NB0216L	3.9	F	71	178	82	0	30	
NB0216R	5.59	F	71	178	82	0	0	
NB0217L	4.79	M	75	175	72	0	0	5924
NB0217R	2.91	M	75	175	72	0	30	5925
NB0218L	5.57	M	72	178	82	0	0	5926
NB0218R	5.35	M	72	178	82	-10	0	5927
NB0222L	8.85	M	41	176	91	0	0	6177
NB0222R	7.87	M	41	176	91	-10	0	6179
NB0224R	3.92	M	60	178	82	0	0	6189
NB0225L	5.65	F	86	168	68	0	0	6213
NB0225R	5.83	F	86	168	68	0	0	6215
NB0226L	6.6	M	62	183	91	0	0	6217
NB0228L	3.08	F	65	163	82	-10	0	6246
NB0228R	4.05	F	65	163	82	0	0	6248
NB0230L	4.71	M	45	185	75	-10	0	6493
NB0230R	6.09	M	45	185	75	0	0	6495
NB0231L	4.48	F	79	165	91	-10	0	6497
NB0231R	5.63	F	79	165	91	0	0	6499
NB0234L	8.17	M	74	175	100	0	0	6532
NB0234R	8.17	M	74	175	100	10	15	6534
NB0337L	5.09	M	58	175	62	10	15	6719
NB0337R	5.09	M	58	175	62	0	0	6722
NB0338LH	3.48	M	86	173	59	-10	0	6725
NB0338RH	4.59	M	86	173	59	0	0	6727
NB0340RH	7.54	M	63	183	66	0	0	
NB0341RH	6.89	M	79	165	68	0	0	6812
NB0342RH	6.26	M	83	189	93	0	0	6987
NB0343RH	9.79	M	79	191	109	0	0	6991
NB0345LH	5.75	M	82	173	75	10	0	6998
NB0345RH	5.11	M	82	173	75	0	0	7001
NB0447LH	7.69	F	49	157	59	10	0	7564
NB0447RH	6.14	F	49	157	59	0	0	7567
NB0448LH	6.1	M	76	178	80	10	0	7570
NB0448RH	6.13	M	76	178	80	0	0	7573
NB0450LH	6.03	M	73	178	86	0	0	7613
NB0450RH	6.12	M	73	178	86	10	0	7616

7.8.1 Hip Injury: Predictor Variable

The peak applied force (as tabulated in Table 7.3) was the only predictor variable considered for the development of the pelvis injury risk function. In line with the rationale presented in Rupp at al. (2009b), since each test resulted in some combination of hip fracture (fracture of the acetabulum, pubic rami, femoral head/neck, and/or hip dislocation) and there were no evident partial failures prior to the time

of peak applied force, it is assumed that the peak applied force is a known point of failure and considered to be uncensored.

7.8.2 Hip Injury: Covariates

To confirm the assumptions of Rupp et al. (2009b), who found only stature to be significant in the model fit to the Neutral dataset, parametric survival analysis (SAS PROC PHREG) using the stepwise variable selection method was carried out. The maximum significance level for entering the model was 0.25 and the maximum significance level for staying in the model was 0.10; several other significance levels were tested but provided the same outcome. As the gender categorical variable resulted in the highest χ^2 score, it was the first parameter added to the model; any other added parameters were subsequently removed. While this appears to contradict previous findings, it may result from the relationship between gender and stature; of the subjects in the considered dataset, the average male stature is 178 cm while the average female stature is 165 cm. To further investigate this discrepancy, both covariates are retained throughout model development.

Flexion and adduction angles were considered as covariates in the Complete model. Flexion was found to be a significant component of the model ($\chi^2 = 8.3948, p < 0.0038$), while adduction angle was not ($\chi^2 = 1.9038, p = 0.1677$). This finding is somewhat consistent with Rupp (2006), who showed that in matched pair tests that an adduction angle of 10 degrees resulted in a significant reduction in tolerance while an abduction angle did not.

Based on these findings, the covariates included in the remaining model development steps are flexion and either gender or stature.

7.8.3 Hip Injury: Dependent Variable

The dependent variable used in the development of a pelvis injury criterion was the presence of a hip fracture, as defined in Rupp at al. (2009b) as a fracture of the acetabulum, pubic rami, femoral head/neck, and/or hip dislocation. Depending on the severity of the fracture, the resulting injury can be coded as either AIS 2 or AIS 3 (Martin and Scarboro, 2011).

7.8.4 Hip Injury: Injury Risk Function Formulation

7.8.4.1 Nonparametric

A nonparametric survival function was formulated using the SAS PROC LIFETEST procedure. This survival function is shown in later comparisons to parametric survival models.

7.8.4.2 Logistic Regression

Logistic regression could not be carried out since there were no non-injury observations; all of the PMHS specimens included in this data sustained a hip fracture.

7.8.4.3 Survival Analysis

Survival analysis was also carried out to develop risk functions for all four datasets using the SAS PROC RELIABILITY procedure to estimate model parameters and confidence intervals. Models were developed

to predict failure based on uncensored peak applied force using gender, stature, both gender and stature, both flexion and gender, and both flexion and stature as covariates. Models developed for the Neutral dataset did not include flexion as a covariate, as this term would be negated by definition. Models were developed assuming several different probability distributions to determine the best fit to the data. Of these, the two best distributions were Weibull and Lognormal.

The Survival Weibull model takes the form:

$$p(Hip\ Fracture) = 1 - e^{-\left(\frac{F_{applied}}{e^{(\beta_0+\beta_1 c_1+\beta_2 c_2)}}\right)^{\alpha}}$$

where:

$F_{applied}$	=	Peak force applied to knee (in kN)
β_0	=	Intercept
β_1	=	1st covariate coefficient
c_1	=	1st covariate value
β_2	=	2nd covariate coefficient (if used)
c_2	=	2nd covariate value (if used)
α	=	1/scale

For each combination of covariates, model estimates and maximum log likelihood are reported in Table 7.4. The narrowest confidence intervals occurred in the models which include stature as a covariate, while the widest confidence intervals occurred for the models with gender and stature as covariates (Figure 7.8). Individual models presented at relevant covariate levels are shown for the model with gender as a covariate (Figure 7.9), stature as a covariate (Figure 7.10), and both gender and stature as covariates (Figure 7.11) for the Neutral dataset, as well as the models with gender and flexion (Figure 7.12) and stature and flexion (Figure 7.13) as covariates for the Complete dataset.

Table 7.4. Parameter estimates and fit statistics for survival analysis Weibull models.

Predictor	Covariate(s)*	Dataset	β_0	β_1	β_2	α	Maximum Log Likelihood
Peak applied force	Gender	Neutral	1.9639	-0.2563	N/A	5.4396	4.6034
Peak applied force	Stature	Neutral	-0.3564	0.0129	N/A	5.5685	5.5229
Peak applied force	Gender and stature	Neutral	0.3964	-0.1243	0.0087	5.8038	6.2372
Peak applied force	Gender	Complete	1.9036	-0.1988	N/A	4.3397	-3.6318
Peak applied force	Stature	Complete	0.3353	0.0087	N/A	4.2998	-4.0832
Peak applied force	Gender and stature	Complete	1.2439	-0.1381	0.0037	4.3646	-3.3961
Peak applied force	Gender and flexion	Complete	1.9371	-0.2094	-0.0124	4.5527	-0.5221
Peak applied force	Stature and flexion	Complete	0.3333	0.0089	-0.0118	4.4177	-1.4720

**Covariate units: gender represented by male = 0, female = 1; stature in cm; flexion in degrees from neutral posture*

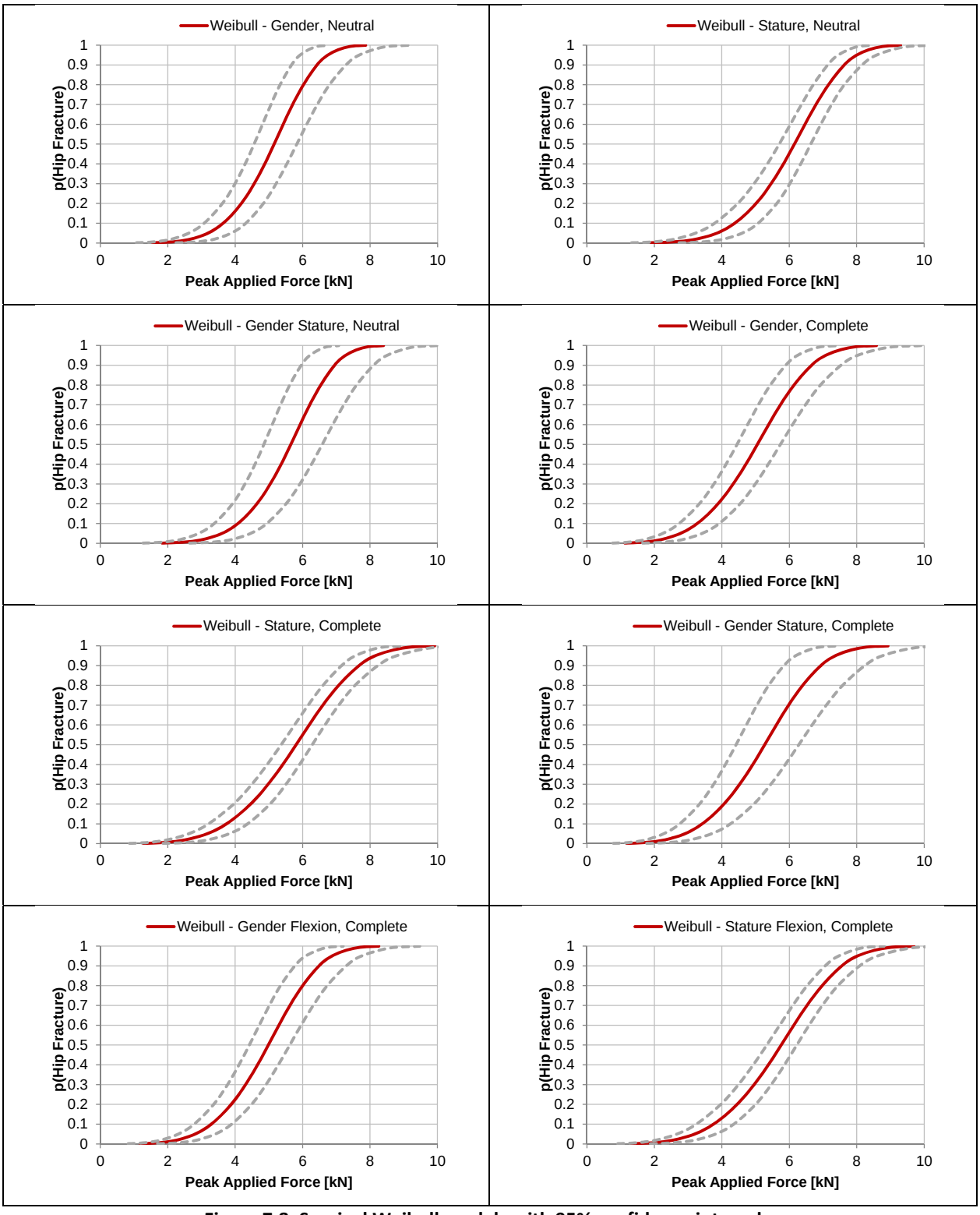

Figure 7.8. Survival Weibull models with 95% confidence intervals.

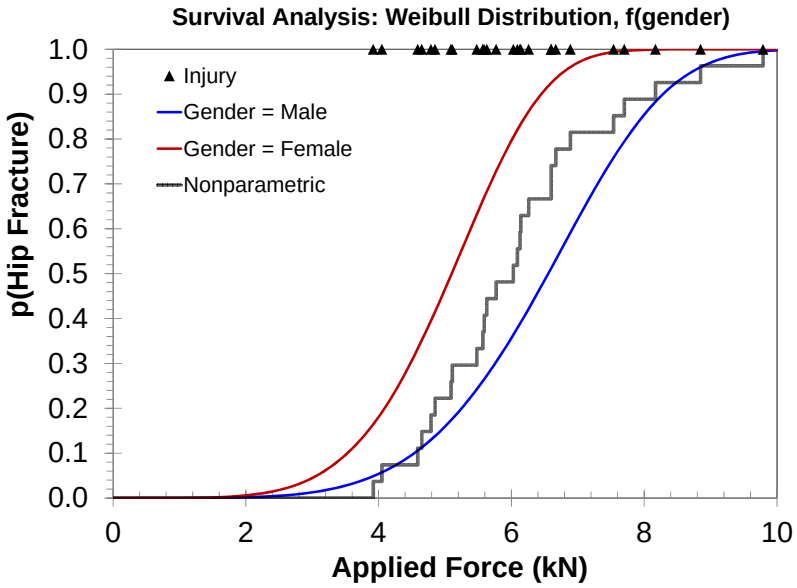

Figure 7.9. Survival Weibull injury risk function for applied force vs. hip fracture, with gender as a covariate.

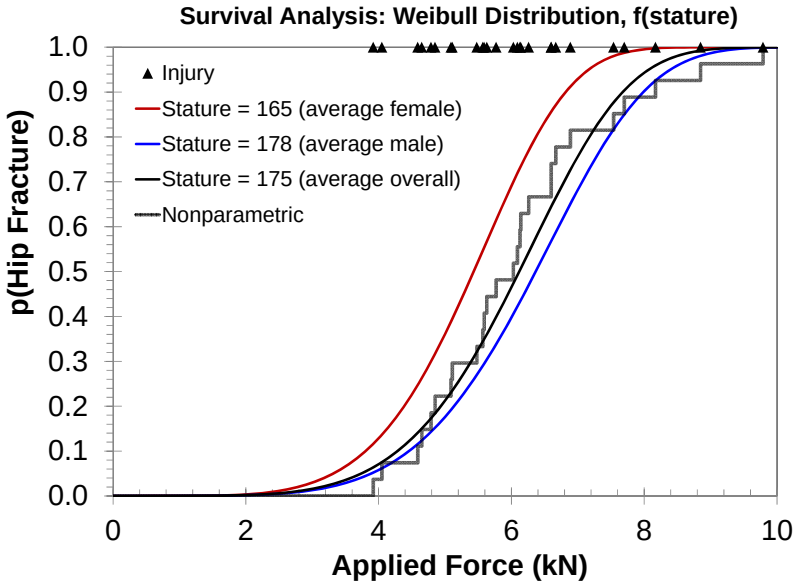

Figure 7.10. Survival Weibull injury risk function for applied force vs. hip fracture, with stature as a covariate.

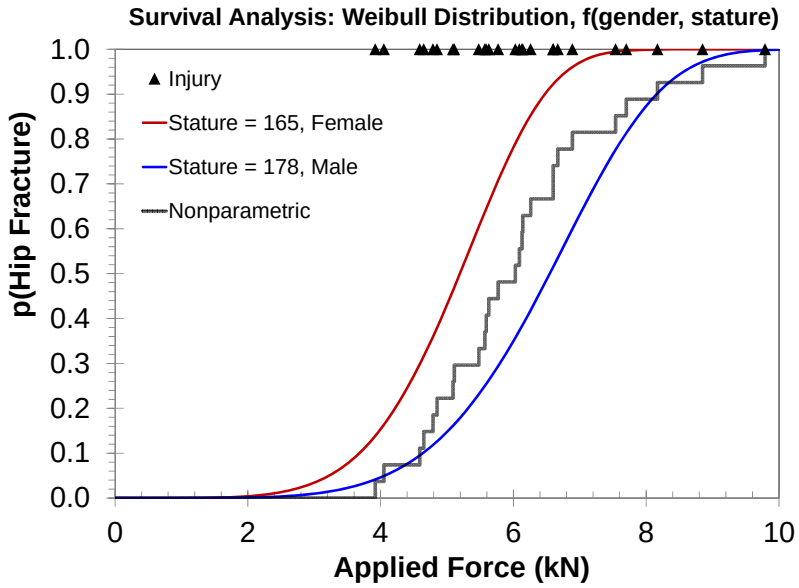

Figure 7.11. Survival Weibull injury risk function for applied force vs. hip fracture, with gender and stature as covariates.

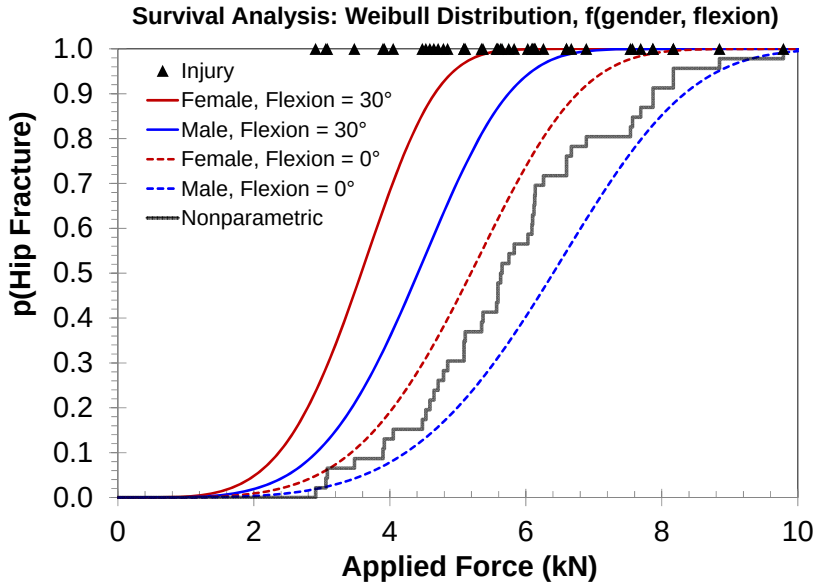

Figure 7.12. Survival Weibull injury risk function for applied force vs. hip fracture, with gender and hip flexion as covariates, presented for males and females and for neutral and 30° flexion covariate levels.

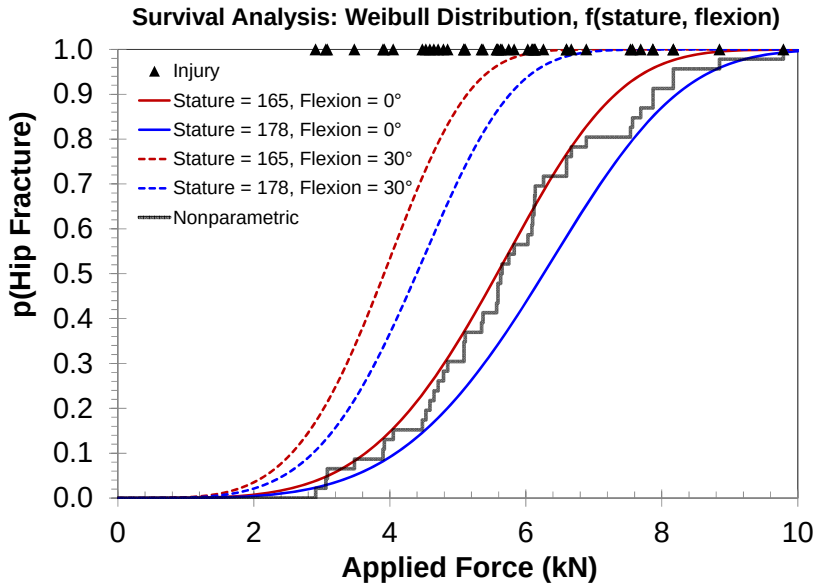

Figure 7.13. Survival Weibull injury risk function for applied force vs. hip fracture, with stature and hip flexion as covariates, presented for the average male and female statures in the dataset (178 cm and 165 cm, respectively) and for neutral and 30° flexion covariate levels.

The Survival Lognormal model takes the form:

$$p(Hip\ Fracture) = \Phi\left[\frac{\ln F_{applied} - \beta_0 + \beta_1 c_1 + \beta_2 c_2}{\sigma}\right]$$

where:

Φ	=	Cumulative normal distribution function
$F_{applied}$	=	Peak force applied to knee (in kN)
β_0	=	Intercept
β_1	=	1st covariate coefficient
c_1	=	1st covariate value
β_2	=	2nd covariate coefficient (if used)
c_2	=	2nd covariate value (if used)
σ	=	Standard deviation or scale

For each combination of covariates, model estimates and maximum log likelihood are reported in Table 7.5. As with the Weibull model, the narrowest confidence intervals occurred in the models with stature as a covariate, while the widest confidence intervals occurred for the model with both gender and stature as covariates (Figure 7.14). Individual models presented at relevant covariate levels are shown for the model with gender as a covariate (Figure 7.15), stature as a covariate (Figure 7.16), and both gender and stature as covariates (Figure 7.17) for the Neutral dataset, as well as the models with gender and flexion (Figure 7.18) and stature and flexion (Figure 7.19) as covariates for the Complete dataset.

Table 7.5. Parameter estimates and fit statistics for survival analysis Lognormal models.

Predictor	Covariate(s)*	Dataset	β_0	β_1	β_2	σ	Maximum Log Likelihood
Peak applied force	gender	Neutral	1.8349	-0.1576	N/A	0.2015	5.4913
Peak applied force	stature	Neutral	-0.2441	0.0117	N/A	0.1924	6.8726
Peak applied force	gender and stature	Neutral	-0.0650	-0.0243	0.0107	0.1923	6.8974
Peak applied force	gender	Complete	1.7733	-0.1848	N/A	0.2632	-3.8650
Peak applied force	stature	Complete	-0.2031	0.0110	N/A	0.2633	-3.8789
Peak applied force	gender and stature	Complete	0.6363	-0.1087	0.0064	0.2609	-3.4652
Peak applied force	gender and flexion	Complete	1.8109	-0.1651	-0.0133	0.2357	1.2082
Peak applied force	stature and flexion	Complete	-0.0755	0.0106	-0.0137	0.2339	1.5572

**Covariate units: gender represented by male = 0, female = 1; stature in cm; flexion in degrees from neutral posture*

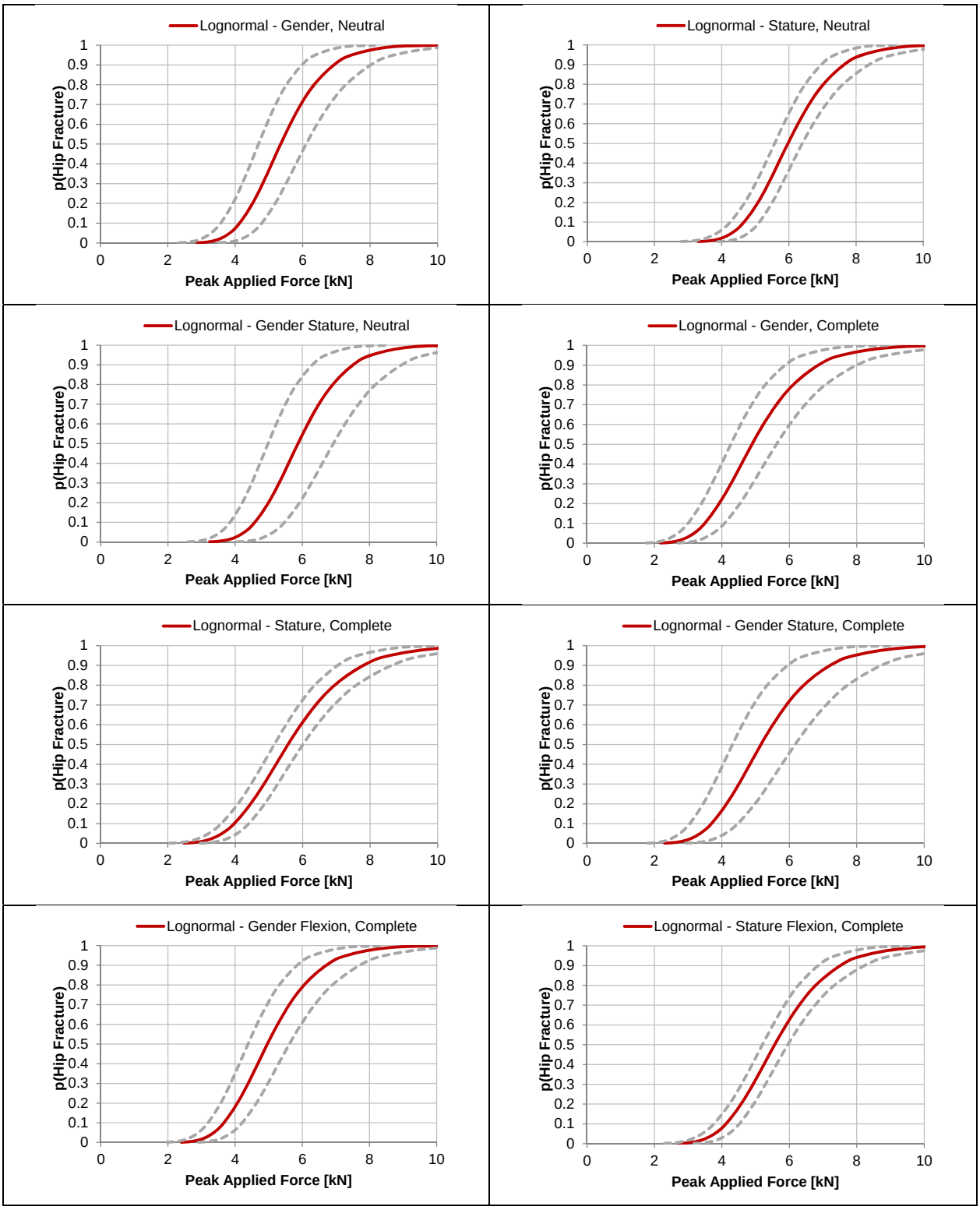

Figure 7.14. Survival Lognormal models with 95% confidence intervals.

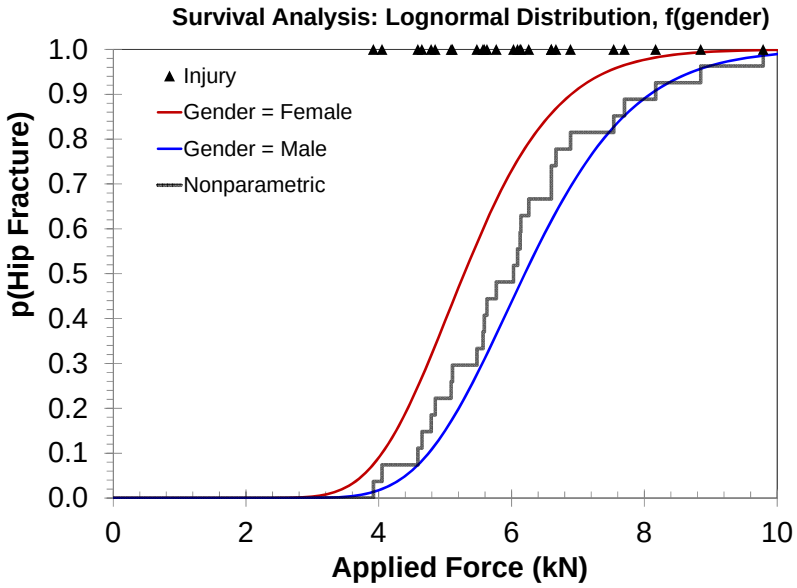

Figure 7.15. Survival Lognormal injury risk function for applied force vs. hip fracture, with gender as a covariate.

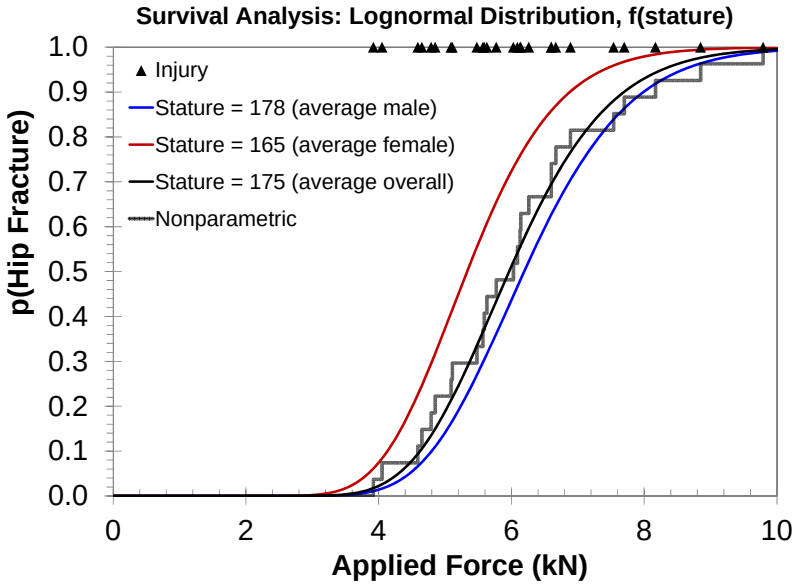

Figure 7.16. Survival Lognormal injury risk function for applied force vs. hip fracture, with stature as a covariate.

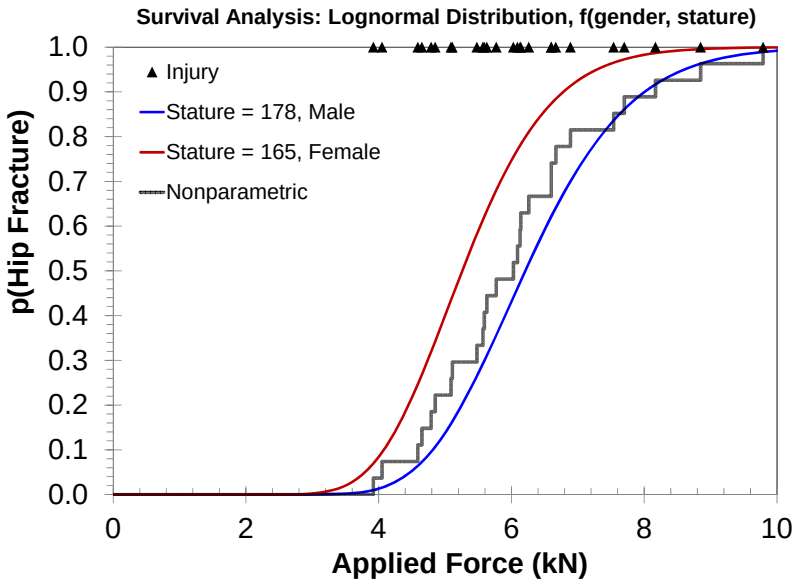

Figure 7.17. Survival Lognormal injury risk function for applied force vs. hip fracture, with gender and stature as covariates.

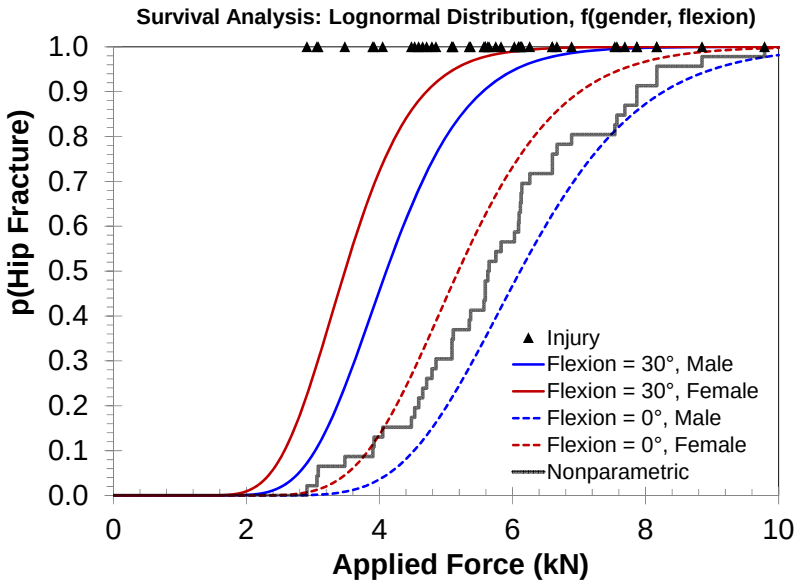

Figure 7.18. Survival Lognormal injury risk function for applied force vs. hip fracture, with gender and hip flexion as covariates, presented for males and females and for neutral and 30° flexion covariate levels.

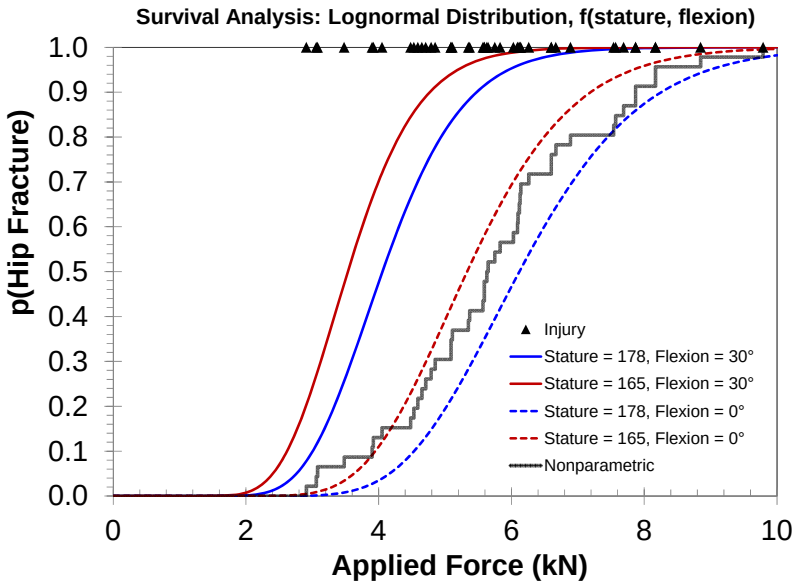

Figure 7.19. Survival Lognormal injury risk function for applied force vs. hip fracture, with stature and hip flexion as covariates, presented for the average male and female statures in the dataset (178 cm and 165 cm, respectively) and for neutral and 30° flexion covariate levels.

7.8.5 Hip Injury: Application to THOR-50M

Since the risk functions described above are based on the response of PMHS specimens, it is necessary to determine a relationship between PMHS response and THOR-50M response to apply the risk function to THOR-50M measurements in vehicle crash tests.

The predictor used to develop the PMHS risk function developed by Rupp et al. (2009b) and recreated here is peak applied force. In the tests used to develop this risk function, the pelvis was fixed and the force was applied to the knee using a pneumatic ram such that inertial effects were minimized and the reaction force at the hip was equal to the force applied at the knee. These forces were measured using load cells, one mounted along the axis of the ram and the other mounted on the hip mounting fixture with its local x-axis parallel to the ram, and as designed the measured forces at both the knee and the hip were similar (Figure 7.20). In tests where the hip posture was different than the neutral automotive seating posture, a bracket was installed between the hip mounting fixture and the hip load cell, so the local x-axis of the hip load cell remained parallel to the ram (Figure 7.21).

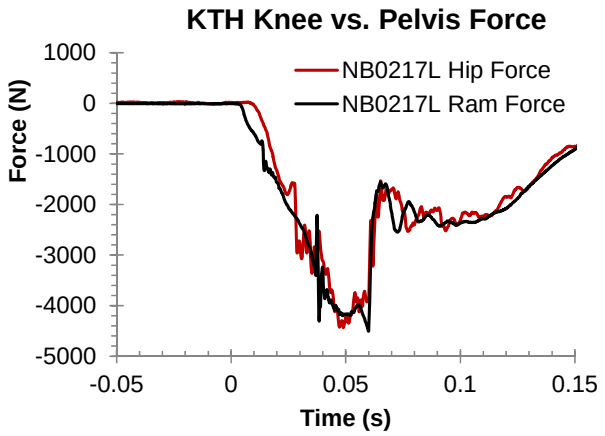

Figure 7.20. Applied force at the knee (ram force) and measured force at the hip (hip force) in test NB0217L (BioDB 5924). Test was conducted in neutral posture.

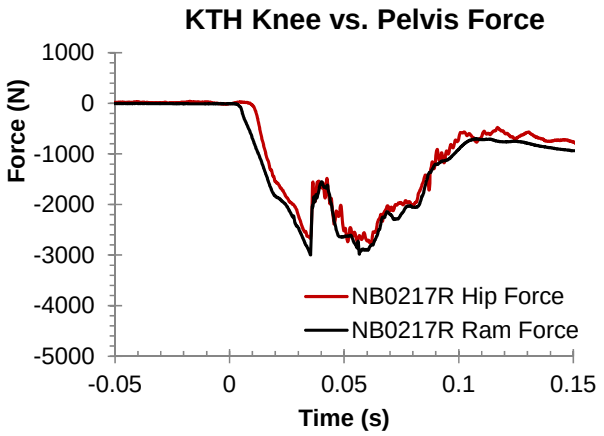

Figure 7.21. Applied force at the knee (ram force) and measured force at the hip in test NB0217R (BioDB 5925). Test was conducted in 30° flexion posture.

Since the THOR-50M femur was shown to be biofidelic in axial compression (Parent, 2016), it is assumed that the forces measured at the THOR-50M acetabulum would be equivalent to the forces applied to the PMHS specimens in the KTH injury criteria dataset. However, since the THOR-50M acetabulum measures forces along the x-, y-, and z-axes of the pelvis coordinate system, the nearest approximation of the force at the acetabulum as measured in the PMHS would be the resultant of these three forces.

While the THOR-50M demonstrated biofidelity in a laboratory test condition with direct loading along the shaft of the femur, additional correction is necessary to account for the differences in acetabulum forces measured in frontal motor vehicle crash test environment compared to those expected in human occupants. Martin at al. (2011) discussed the relationship between THOR-NT and PMHS regarding force transfer to the hip. In crash tests where there is a well-defined interaction between the femur/knee and the knee bolster, the peak resultant acetabulum force is roughly 50% of the peak axial femur force. Martin at al. (2011) also described a relationship between peak applied force and the peak force measured by the femur load cell of about 80%, presumably rounded from the Rupp et al. (2009a) estimate of 77%, which translates to the acetabulum load cell of THOR-NT measuring 40% of the peak applied force at the knee. For comparable loading to a PMHS, the percentage of peak force applied at the knee that is reacted at the hip is 55% (Rupp et al., 2009a). Combining these arguments, the ratio of the peak force applied to the knee of PMHS to that of the THOR-NT would be 55% / (80% x 50%), or roughly 1.3. In other words, the force measured at the hip of a PMHS would be 1.3 times higher than that measured by the THOR-NT in a comparable condition. This relationship is based on the assumption that the THOR-NT would produce the same force at the knee as a human occupant, which as noted by Martin et al. (2011) is more likely to be true with the modifications to the THOR implemented to in the Mod Kit (Ridella and Parent, 2011) improve KTH biofidelity.

The Mod Kit design updates (Ridella and Parent, 2011) have been incorporated into the THOR-50M design, which includes three changes to the knee-thigh-hip complex that could potentially require adjustments to the aforementioned assumptions made based on the THOR-NT design. First, the knee slider force-deflection characteristic was adjusted in an attempt to achieve a more biofidelic response in

knee shear. In the case of knee-to-knee-bolster impacts, the knee slider is not directly in the load path. While loading from the tibia can in turn load the femur load cell by way of the knee slider, the injury risk function was not developed with combined knee and tibia loading, thus contributions to the measured femur force through interactions of the tibia with the vehicle interior are not considered. Second, the femur compressive element was redesigned to achieve a more biofidelic response in femur axial compression. Third, the pelvis flesh was redesigned to reduce the coupling with the femur and allow a greater femur range of motion.

The construction of the knee of the THOR-50M is similar to that of the Hybrid III, in that the knee cap is effectively rigid and directly mounted to the femur load cell. Therefore, the relationship between applied force at the knee and measured force at the femur presented by Rupp et al. (2009a) is assumed to hold true for the THOR-50M as well. As discussed above, in low-mass pendulum impacts to the femur of the THOR-50M in both free-back and fixed-back conditions, the femur load cell measured roughly 55% of the peak applied force at the knee. However, it is not clear how representative this impact condition is to the knee loading condition seen in a motor vehicle crash, where the femurs are restrained by the knee bolster and loaded inertially by the remaining effective mass of the body. It is also evident that the ratio of impact force to measured femur force is sensitive to impact velocity (Figure 7.6), as lower velocities will result in a larger percentage of the impact force measured by the femur load cell. Given these limitations, and since the analysis carried out by Rupp et al. (2009a) considered loading rates similar to those occurring in FMVSS No. 208 and US NCAP crash tests with the Hybrid III, there is insufficient evidence to modify the 77% load transfer ratio of force measured at the femur to force applied to the knee.

Next, to investigate whether the assumption of femur-to-acetabulum force transfer from Martin et al. (2011) holds true for the THOR-50M design, femur and acetabulum forces were analyzed in both pendulum knee impacts (both free- and fixed-back) as well as several frontal rigid barrier crash tests. In both fixed-back (Figure 7.22) and free-back (Figure 7.23) pendulum impacts as described above, the ratio of peak femur load cell compressive force to peak acetabulum resultant force was on average 44% and the ratio of force-vs-velocity slopes was 43% for either condition. Again, such an evaluation is limited by the unknown representativeness of this impact condition to the knee loading condition seen in a motor vehicle crash.

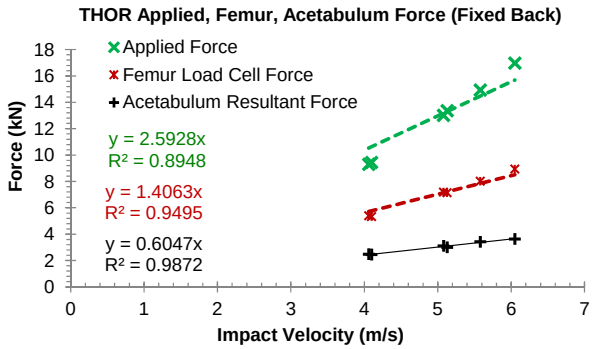

Figure 7.22. Force transmission in the THOR-50M femur in fixed-back pendulum impacts.

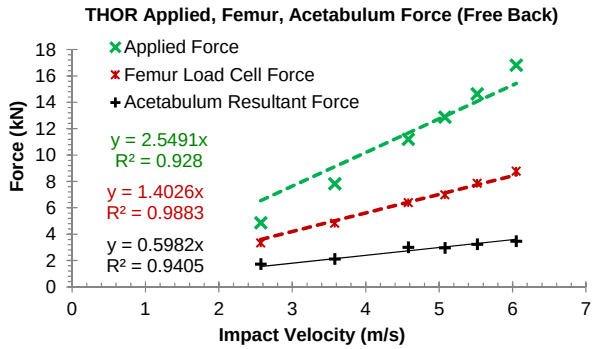

Figure 7.23. Force transmission in the THOR-50M femur in free-back pendulum impacts.

In an exemplar frontal rigid barrier crash test of a 2016 Nissan Rogue (VehDB TSTNO 9569) with a THOR-50M ATD in the driver's seat, at the time of peak left femur axial compressive force the resultant left acetabulum force measured 50% of the femur force (Figure 7.24). This is consistent with the idealized sled test presented by Martin et al (2011), which showed the same 50% relationship between peak resultant acetabulum force and peak femur compressive force using the THOR-NT ATD.

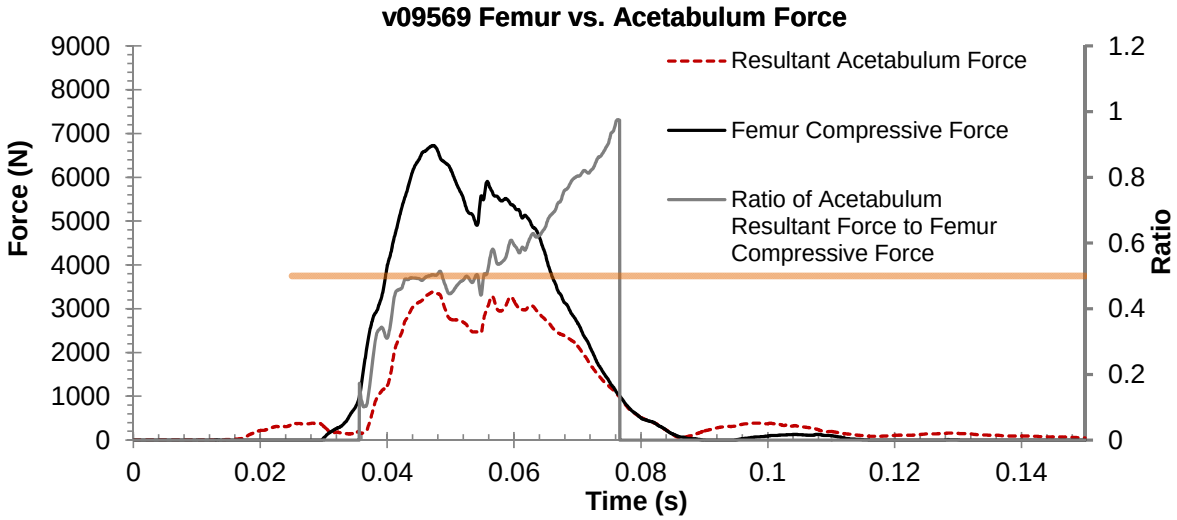

Figure 7.24. Comparison of left femur and acetabulum forces measured using THOR in the driver seat in a frontal rigid barrier test of a 2016 Nissan Rogue (VehDB TSTNO 9569).

Given the uncertainty of the representativeness of low-mass pendulum impacts to knee bolster impacts in motor vehicle crashes, and the similarity of at least one example of femur-to-acetabulum load transfer in a frontal rigid barrier crash test, there is not ample evidence to suggest an alternative to the proposed 77% transfer ratio of impact force to femur force or the 50% transfer ratio of femur force to acetabulum force. Thus, the transfer function to relate peak resultant acetabulum force measured on the THOR-50M to the acetabulum force used in development of the PMHS risk function is recommended as:

$$T_{hip} = \frac{r_{PMHS}}{r_{THOR}} = \frac{r_{PMHS}}{r_{KtoF} r_{FtoA}} = \frac{0.55}{0.77 \times 0.50} = 1.429$$

where:

T_{hip}	=	Ratio of estimated PMHS hip force to THOR measured peak acetabulum resultant force
r_{PMHS}	=	Ratio of applied force at knee to acetabulum force measured in PMHS (Rupp et al., 2009a)
r_{THOR}	=	Ratio of applied force at knee to acetabulum force measured in THOR
r_{KtoF}	=	Ratio of applied force at knee to measured force at femur load cell (Rupp et al., 2009a)
r_{FtoA}	=	Ratio of measured force at femur to measured resultant force at acetabulum (Martin et al., 2011)

As the injury risk function is sensitive to flexion angle, and the THOR ATD is not equipped to record dynamic flexion angle, estimation of a flexion angle is important for proper application of the hip fracture risk function. In several papers, the hip fracture risk function was presented by assuming a posture of 30 degrees of flexion and 15 degrees of abduction from the hip angles in the standard automotive seating posture, which was argued to be the approximate posture at the time of peak knee force in front-impact sled tests with airbag deployment (Rupp 2006, Rupp et al. 2009b). However, this assumption is based on tests of unbelted occupants with airbag deployment; a more conservative estimate of hip flexion angle in three-point belted occupant environments (as shown in Figure 7.25 for both THOR-50M and PMHS) is 15 degrees. While this results in a shift of the risk curve to the left, it is not as aggressive of a shift as would a 30 degree flexion angle. Further, injuries occurring at larger flexion angles may be less severe; for example, one of the lowest failure forces in the expanded dataset was a subject in the 30 degrees flexion condition. This subject sustained a hip dislocation at a peak applied force of 3.06 kN. In the matched pair test on the opposite aspect of the same PMHS, a peak applied force of 4.65 kN resulted in a fracture of the femoral neck.

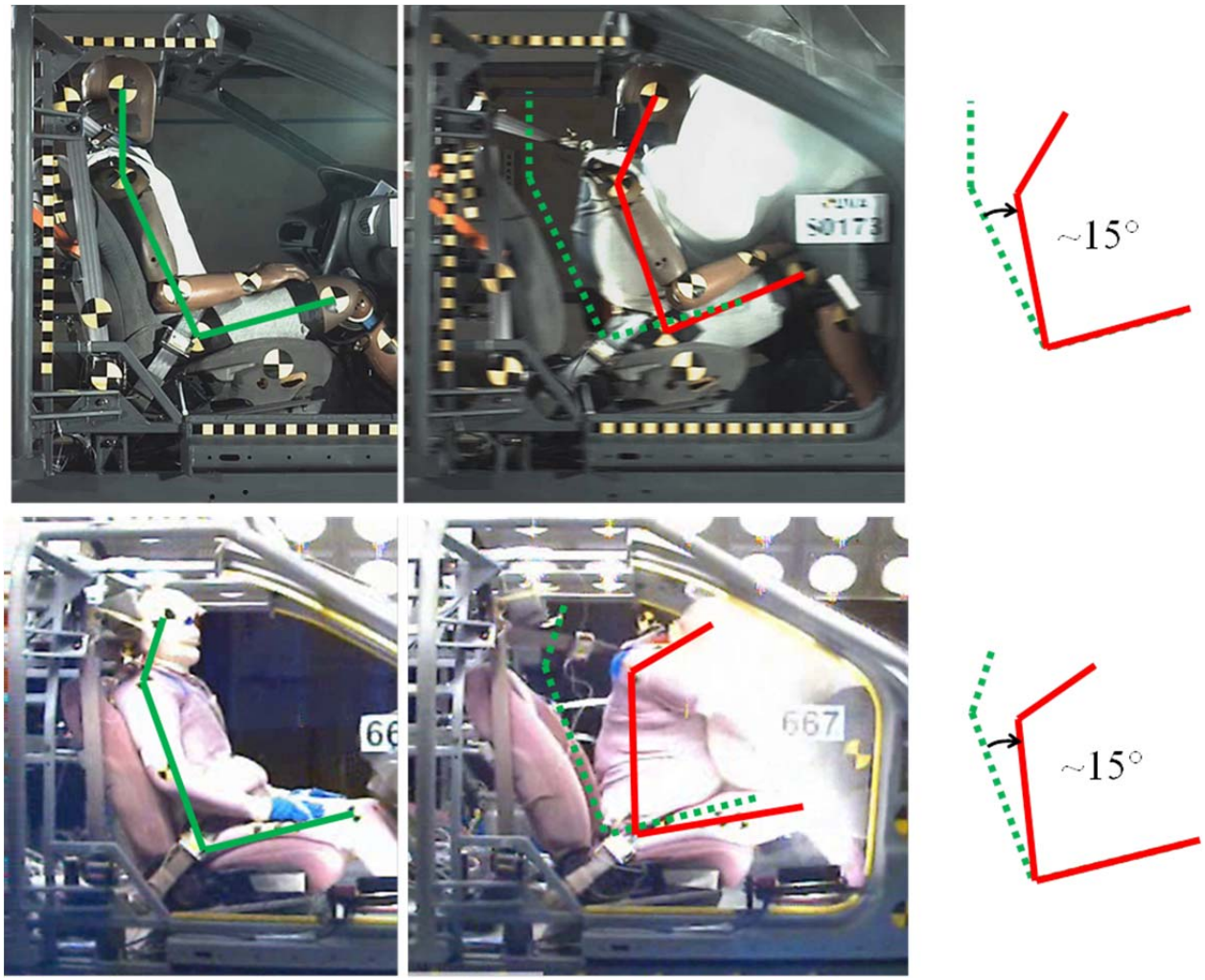

Figure 7.25. Hip flexion angles at time of peak femur load in a frontal sled test condition with three-point belts and airbags. THOR-50M ATD shown at top (BioDB TSTNO 11127) and example PMHS shown at bottom (BioDB TSTNO 8384).

As adduction angle was not found to be significant in the model, estimation of the adduction angle is not necessary to apply the risk function to THOR.

In summary, given the discussed limitations, the recommended risk function for application to THOR-50M to predict hip injuries is described below:

$$p(Hip\ Fracture) = \Phi\left[\frac{\ln T_{hip}F_{AR} + 0.0755 - 0.0106s + 0.0137f}{0.2339}\right]$$

where:

Φ	=	Cumulative normal distribution function
T_{hip}	=	Ratio of estimated PMHS hip force to THOR measured peak acetabulum resultant force [1.429]
F_{AR}	=	Peak resultant acetabulum force (in kN)
s	=	Stature (in cm) [nominal 178 cm]
f	=	Flexion angle from neutral automotive posture (in deg) [nominal 15 deg]

Simplified:

$$p(Hip\ Fracture) = \Phi\left[\frac{\ln 1.429F_{AR} - 1.6058}{0.2339}\right]$$

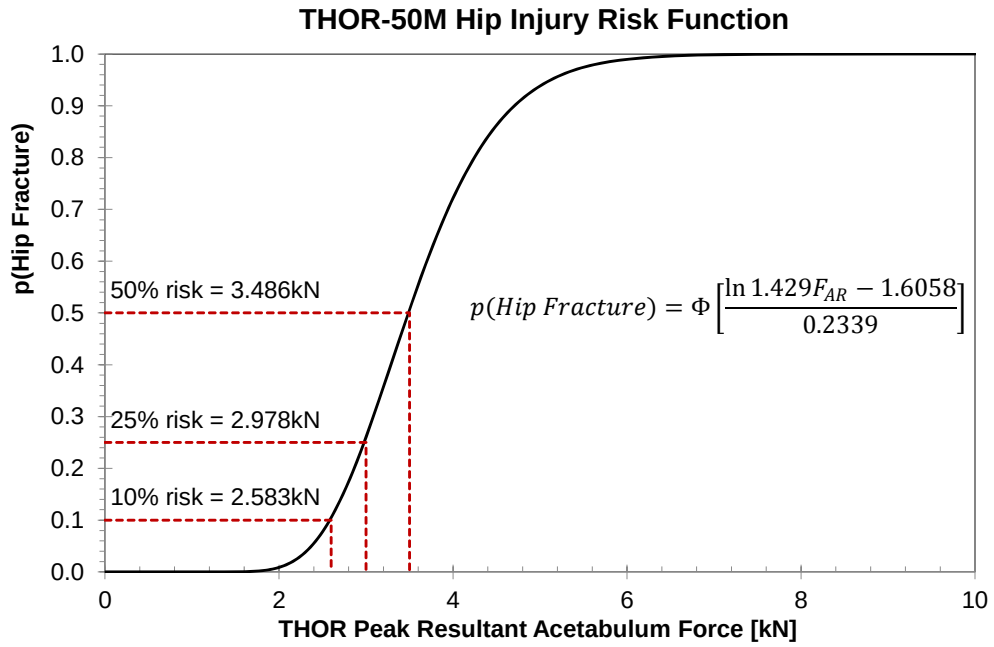

Figure 7.26. Recommended injury risk function for hip fracture with respect to measured peak resultant acetabulum force, including peak measurements for 10%, 25%, and 50% risk of hip fracture.

7.8.6 Hip Injury: Comparison to Literature

The injury risk function developed by Rupp et al. (2009b) is similar to the Survival Lognormal risk function using stature as a covariate. However, Rupp applied an additional correction factor to account for the fact that increases in hip angle, in both flexion and adduction, reduce the human tolerance for hip fracture (Rupp et al., 2003). This correction factor was appended to the risk function as a mean shift of 1% for each degree of hip abduction and -1% for each degree of hip flexion. This risk function has been presented differently in various publications; the intended application is believed to be:

$$p(Hip\ Fracture) = \Phi\left[\frac{\ln F_{applied} - (0.2141 - 0.0114s)\left(1 - \frac{f-a}{100}\right)}{0.1991}\right]$$

where:

Φ	=	Cumulative normal distribution function
$F_{applied}$	=	Peak force applied to knee (in kN)
s	=	Stature (in cm)
f	=	Hip flexion angle (in degrees)
a	=	Hip abduction angle (in degrees)

The recommended risk function above is very similar to the Rupp et al. (2009b) risk function as evaluated with the recommended covariate values of 178 cm stature, 30° flexion, and 15° abduction (Figure 7.27). However, if evaluated at 15° of flexion and 15° of abduction, the Rupp risk function predicts a lower risk of hip fracture for a given applied force. Not shown is the risk function evaluated at 15° flexion and 0° abduction, which would result in the same risk curve as the 30° flexion/15° abduction condition.

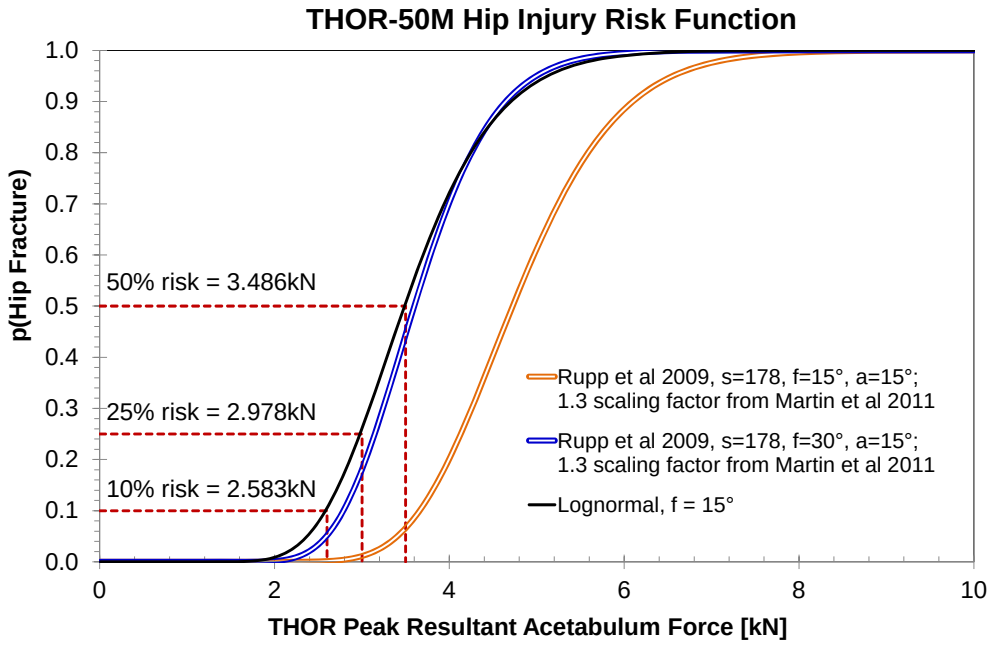

Figure 7.27. Hip fracture risk function compared to Rupp et al. (2009b), evaluated at flexion angles of 15° and 30°.

7.9 Fleet Test Data: THOR-50M

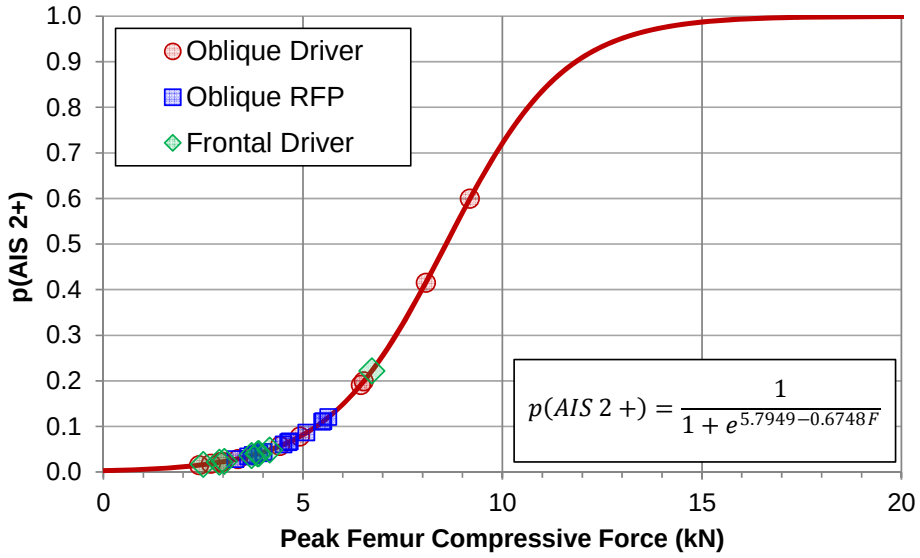

Figure 7.28. Peak femur compressive forces from frontal rigid barrier and oblique moving deformable barrier tests using THOR-50M.

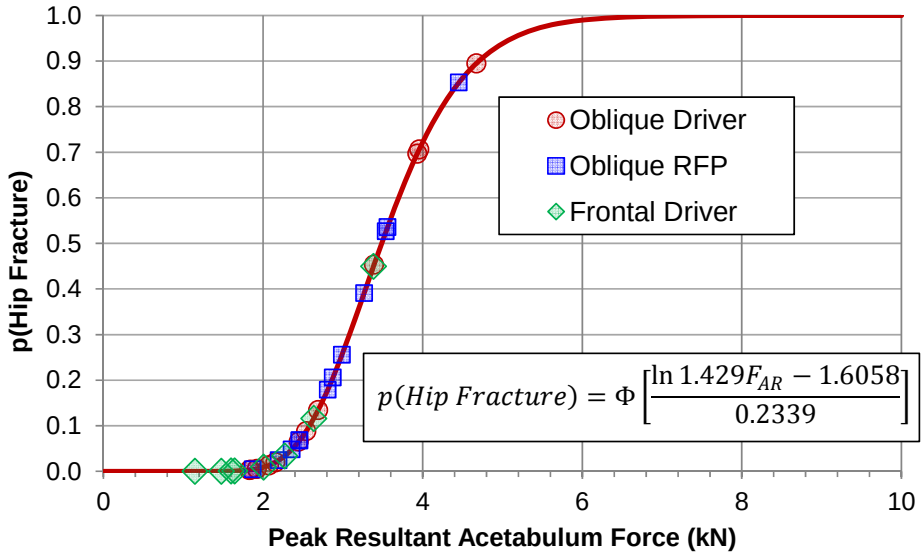

Figure 7.29. Peak acetabulum forces from frontal rigid barrier and oblique moving deformable barrier tests using THOR-50M.

7.10 **Limitations**

The relationship between applied force at the knee and the measurement of peak force at both the femur load cell and the acetabulum load cell has not been specifically validated for the THOR-50M ATD. As has been shown above, this relationship may be dependent on loading scenario, so a simple transfer function does not encapsulate all possible loading rates, stiffnesses, and geometries.

The relationship between applied force at the knee of PMHS and the THOR-50M ATD is not explicitly known. While the femur is quantitatively biofidelic in axial compression, the mass distribution and inertial properties of the knee-thigh-hip complex may differ from that of a PMHS or a live human.

The relationship between PMHS response and live human response is unknown.

8 LOWER EXTREMITY

8.1 Field Data and Historical Fleet Data

Below-knee injuries (leg, foot, and ankle) have been identified as a frequent and costly result of frontal crashes in numerous studies (Rudd et al. 2009; Dischinger, et al. 1994; Morgan, et al. 1991; Pattimore, et al. 1991; Dischinger et al. 2004). Injuries to the leg, foot, and ankle continue to make up a substantial proportion of reported AIS 2+ injuries in frontal crashes, and represent the highest-risk body region for AIS 2+ in frontal crashes regardless of severity (Table 1.1). Considering attributable costs (Figure 1.2), the relative importance of the lower extremity is evident despite being comprised mostly of AIS 2 severity injuries (Table 1.2).

Below-knee injuries in NASS-CDS frontal crashes were separated into sub-regions including the proximal tibia, tibia shaft, distal tibia, fibula, hindfoot, ankle malleoli, midfoot, and forefoot based on individual AIS codes (Figure 8.1). This breakdown demonstrates that the leg, including the tibia and fibula components, sustains the majority of the moderate to severe injuries in frontal crashes. The hindfoot category is made up of the talus, calcaneus, ankle (tibiotalar) joint, and subtalar (talocalcaneal) joint, and is separated from the malleolus injuries due to potential differences in causation.

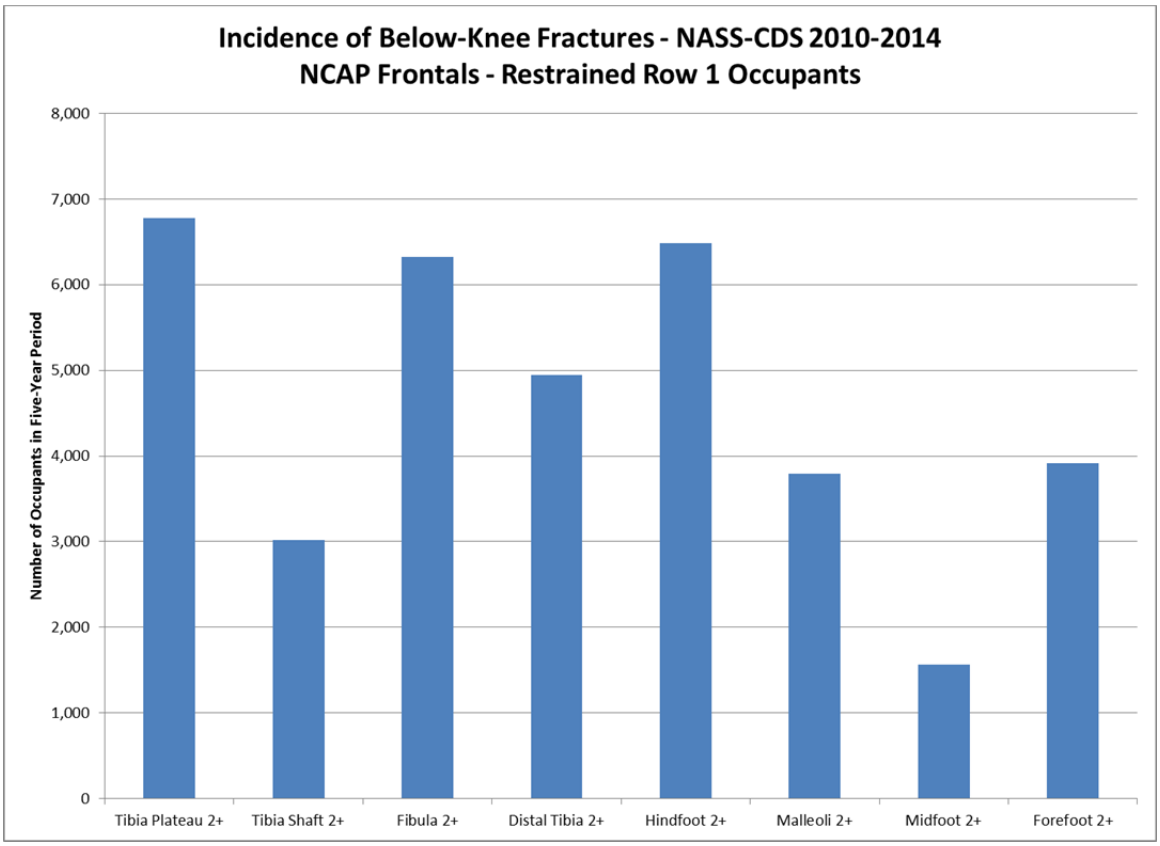

Figure 8.1. Incidence of AIS 2+ fractures and dislocations by below-knee sub-region for NASS-CDS restrained row 1 outboard frontal crash occupants from 2010-2014 data years. Counts represent total weighted numbers of AIS 2+ fractures and dislocations.

A review of frontal crashes with belted first-row occupants from the CIREN database resulted in 770 below-knee AIS 2+ fractures and dislocations among 216 occupants using the same query parameters as for the data in Figure 8.1. Many AIS 2 and all AIS 3+ injuries are assigned primary, and sometimes secondary, regional injury mechanisms in CIREN. Application of the injury breakdown into sub-regions noted above demonstrates the role various injury mechanisms play in producing AIS 2+ fractures and dislocations to the below-knee structures (Figure 8.2). Compression of the leg and hindfoot components is responsible for the large majority of the injuries for which CIREN codes injury mechanisms. Joint rotation is noted as the primary mechanism for some of the ankle injuries (distributed among the fibula, distal tibia, hindfoot, and malleolus groups), but these structures are generally also loaded in compression in frontal crashes. Of the injuries for which a regional injury mechanism is not coded, most of those occur in the foot where compression and twisting due to contact with the toepan or pedals are the most likely mechanisms. Fibula injuries not assigned a mechanism are likely similar to the tibia shaft in causation. Taken in combination with Figure 8.1, the findings in Figure 8.2 suggest that a focus on compression of the tibia and hindfoot would address most of the below-knee injuries, and may also address some midfoot and forefoot injuries.

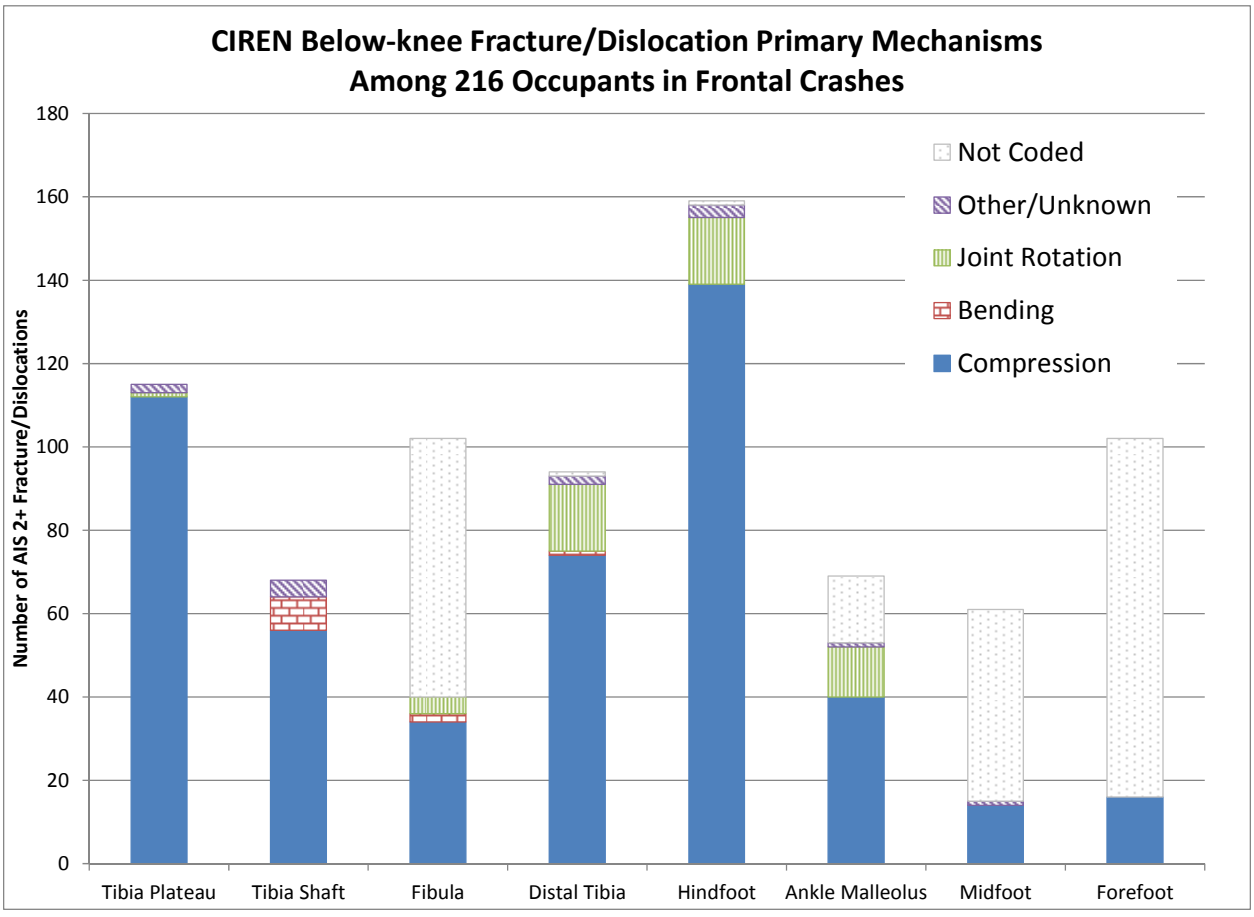

Figure 8.2. Primary regional injury mechanisms for the below-knee sub-regions identified in 216 restrained first row CIREN case occupants involved in frontal crashes.

Vehicle model year-based trends for AIS 2+ tibia/fibula and foot/ankle injuries for belted drivers in frontal crashes are shown in Figure 8.3 and Figure 8.4, respectively. The trend for Hybrid III 50th male Tibia Index and peak tibia force values in 35-mph full frontal tests can be seen in Figure 8.5 and Figure 8.6.

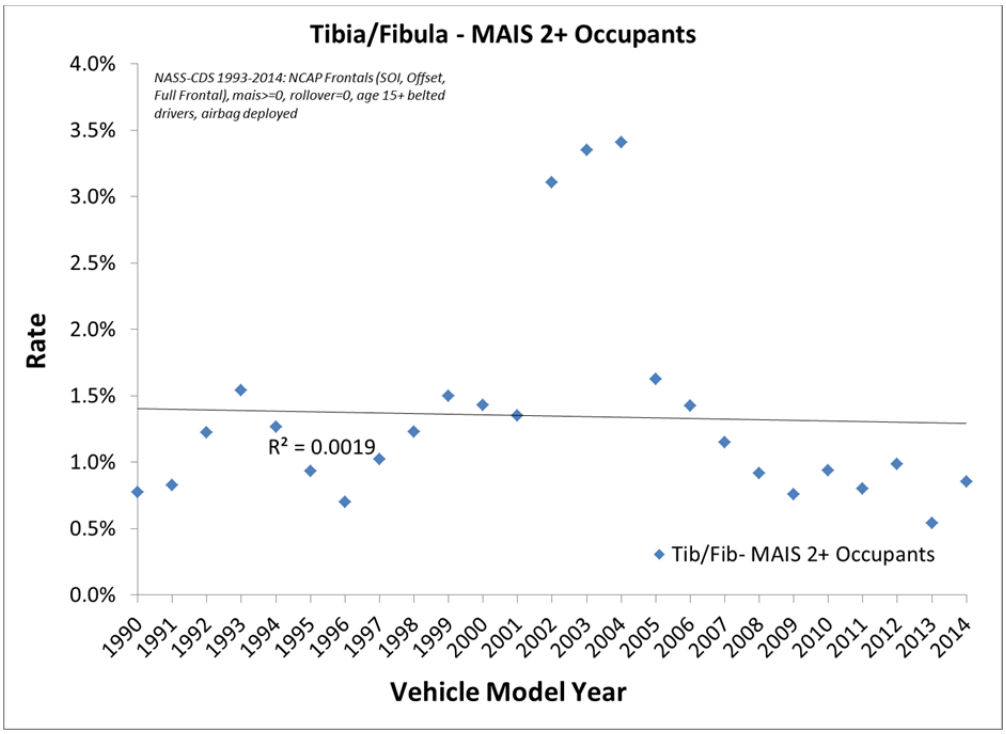

Figure 8.3. AIS 2+ tibia/fibula injury trends by vehicle model year (1990 to 2014) from frontal crashes in NASS-CDS (1993 to 2014).

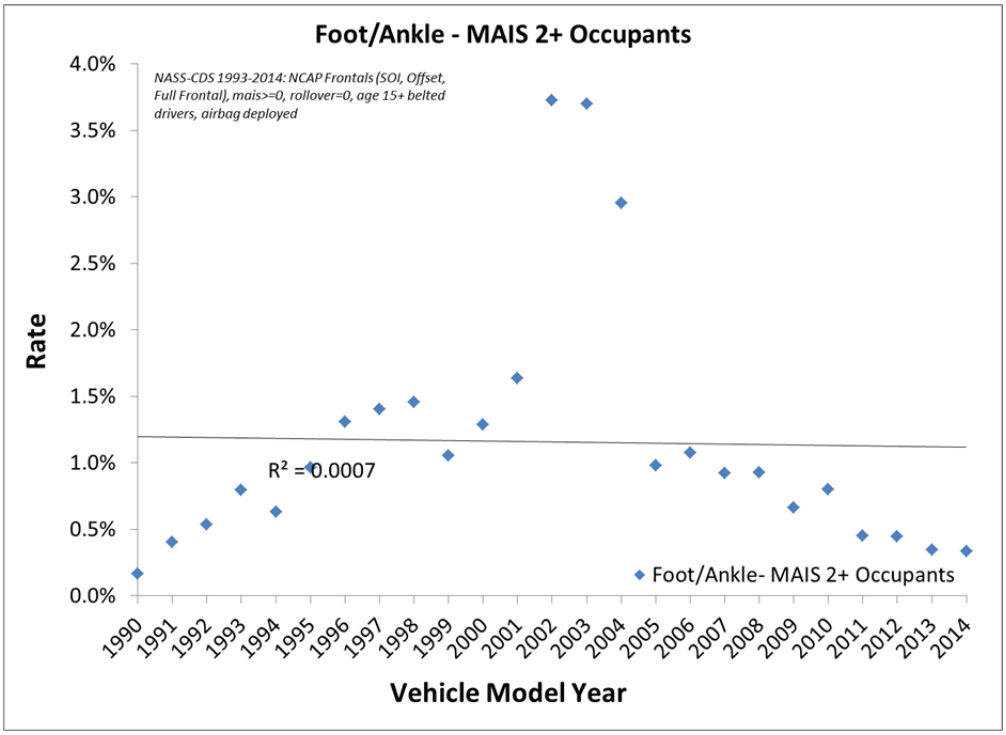

Figure 8.4. AIS 2+ foot/ankle injury trends by vehicle model year (1990 to 2014) from frontal crashes in NASS-CDS (1993 to 2014).

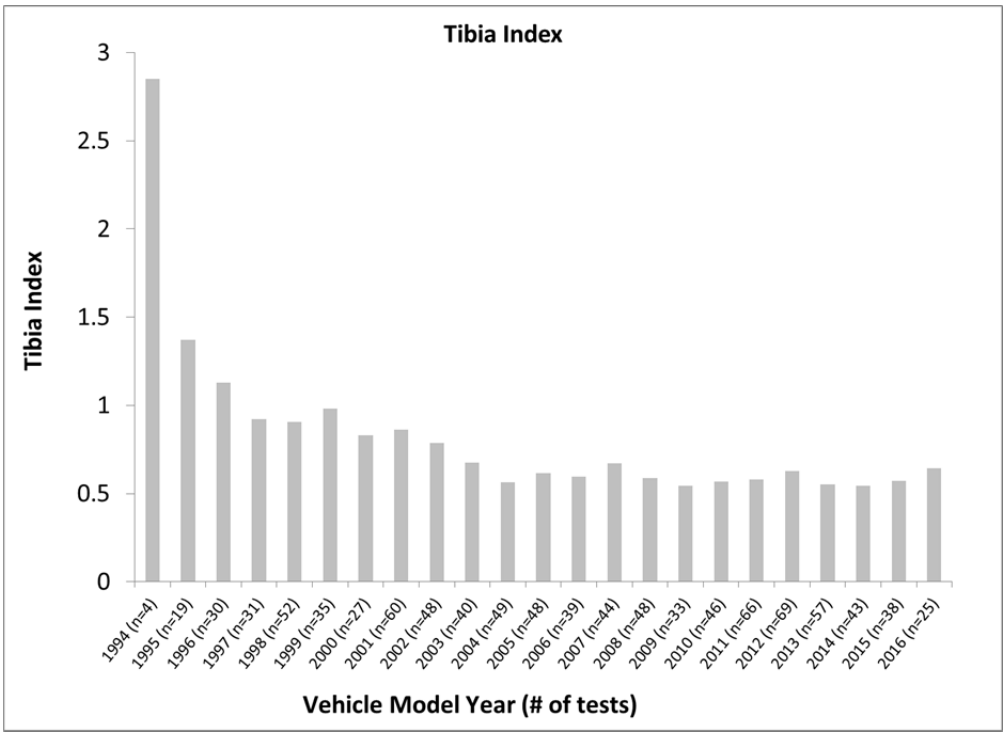

Figure 8.5. Hybrid III 50th male frontal NCAP average peak Tibia Index for model year 1990 to 2016.

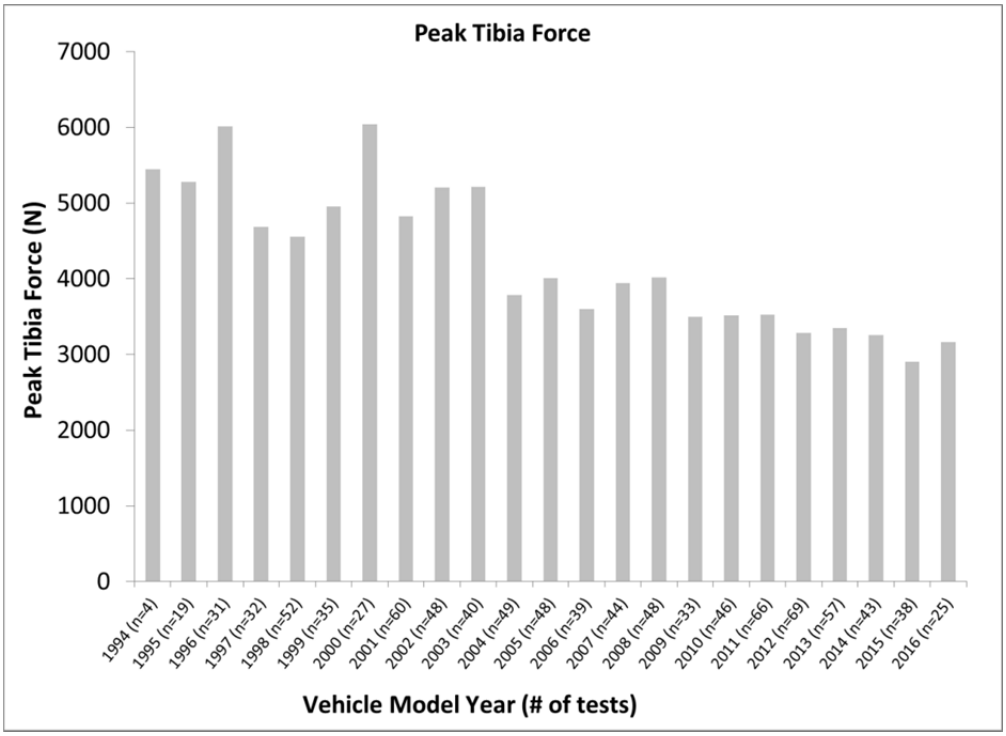

Figure 8.6. Hybrid III 50th male frontal NCAP average peak tibia force for model year 1990 to 2016.

8.2 Design

The mechanical design of the THOR-50M lower extremity provides several advances over previous lower extremity designs. A compliant section in the tibia shaft, similar to the THOR-50M compliant femur section, provides more biofidelic force transmission from the heel to the knee complex. The spring damper Achilles tendon system aids in producing the desired ankle motion and torque characteristics. The ankle design provides correct range of motion, joint axes placement, and biofidelic torque vs. angle response for the two primary axes (dorsi/plantar-flexion and inversion/eversion), with soft stop elements defining the stiffness at the extremes of motion. The molded shoe design, which was added to the docketed THOR-50M drawing package in the 2016 drawing package update (NHTSA, 2016b), integrates the foot and shoe into a single part.

8.3 Instrumentation

The lower extremity includes sensors to measure injury parameters (Figure 8.7). Five-channel upper and lower tibia load cells are incorporated into the design to provide force and moment data of the tibia shaft. A uniaxial compression load cell implemented into the Achilles tendon housing provides a direct measurement of the contribution of the Achilles to the overall ankle joint torque. Three rotary potentiometers measure the rotation of the individual ankle joints, thereby providing complete kinematic data. Finally, two uniaxial accelerometers on the tibia and a tri-pack accelerometer assembly on the foot plate allow the transformation of the measured tibia moment to the calculated ankle moment.

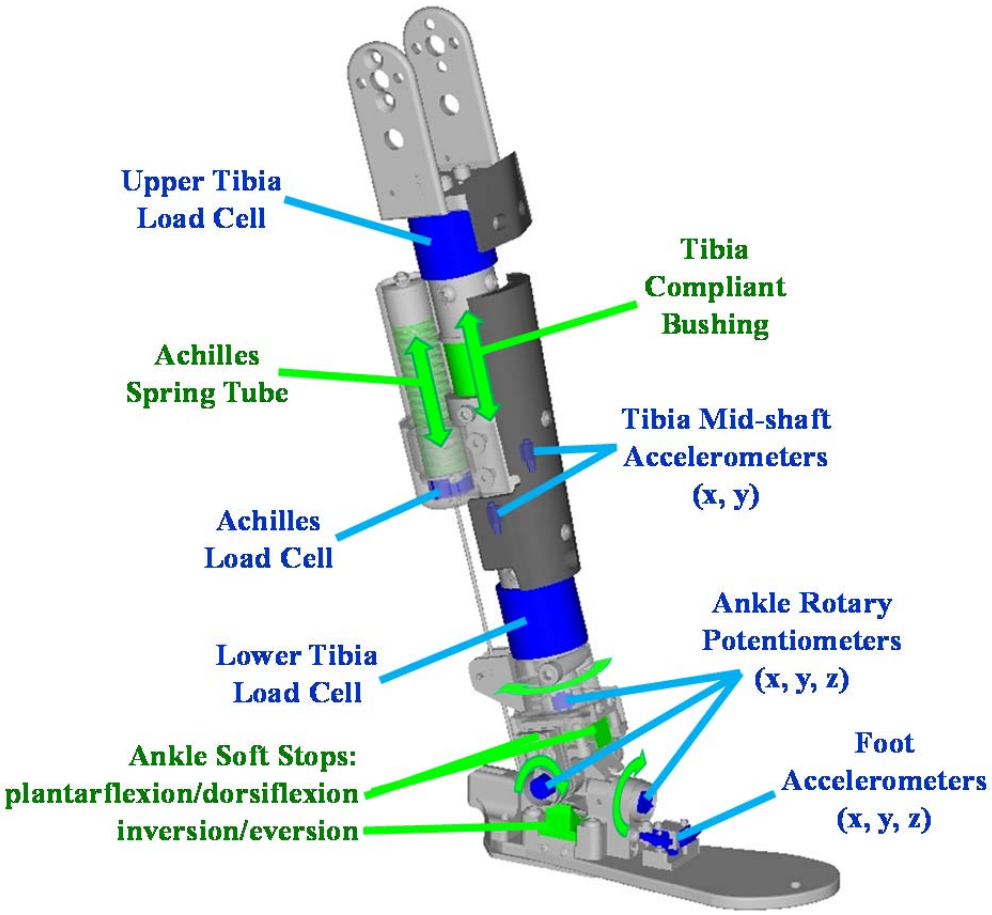

Figure 8.7. THOR-50M lower extremity instrumentation.

8.4 Biofidelity

Parent (2016) evaluated the biofidelity of the THOR-50M leg in three primary conditions: Dynamic Heel Impact, Dynamic Axial Compression, and Dynamic Dorsiflexion. In the Dynamic Heel Impact condition, both the THOR-50M and H3-50M demonstrated either excellent or good biofidelity. For Dynamic Axial Compression and Dynamic Dorsiflexion, THOR-50M also demonstrated either excellent or good biofidelity (the H3-50M was not tested in either of these two conditions).

8.5 Upper Tibia Axial Force

8.5.1 Data

Tibial plateau fractures are one of the most prevalent lower extremity injuries in frontal crashes (Figure 8.1). These injuries are typically produced by axial loading through the foot and leg, when the knee is entrapped (e.g. by the knee bolster), and intrusion of the toepan can intensify the magnitude of the loading. The risk curve proposed by Kuppa et al. (2001) used data from Banglmeier et al. (1999), in

which twelve pairs of human tibiofemoral joints were impacted in the superior direction along the axis of the tibia with the joint flexed to 90°. Newer data considered included Funk et al. (2000), in which axial impacts were applied to the plantar aspect of the foot. In that test series, foot/ankle fractures were produced in 15 tests and tibial plateau fractures were produced in 5 tests, and the average tibial plateau failure load was in agreement with previous studies (Funk et al., 2000). Given the small numbers of tibial plateau fractures produced in the newer dataset, the original Banglmeier (1999) dataset is retained for injury risk function development (Table 8.1, APPENDIX G). Although the relative strength of the foot/ankle complex is less than the tibial plateau, inertial loading and interactions with the knee bolster can contribute to higher loading in the upper tibia. Therefore NHTSA believes it is important to retain upper tibia axial force as a separate injury criterion given the frequency identified in real-world crashes (Figure 8.1).

Table 8.1. Descriptive statistics for upper tibia axial dataset.

n, injured	Mean Failure Force (kN)	Failure Force Range (Min-Max)	n, non-injured	Maximum Non-injury Force (kN)	Non-injury Force Range (Min-Max)
14	**7.7 ± 2.0**	**3.8 to 11.5**	**16**	**6.1 ± 1.6**	**3.7 to 9.4**

8.5.2 Injury Risk Function Formulation

Logistic regression was performed on the available data from Banglmeier et al. (1999), using axial load as the predictor variable. Stepwise multiple regression was carried out to assess the sensitivity of occupant-based covariates. Covariates considered were age and mass. For this dataset, mass was a significant covariate, while age was not. The dependent variable considered was the presence of an AIS 2 or greater (2+) injury.

Both logistic and survival injury risk functions were formulated. Goodness-of-fit metrics described in Hasija et al 2011 were calculated for the logistic and survival analysis risk curves, including the Receiver Operating Characteristic (ROC) Area Under Curve (AUC), maximum log likelihood, and Hosmer-Lemeshow Goodness-of-Fit test. These are reported in Table 8.3. The resulting form of the logistic regression function is the same as proposed by Kuppa et al. (2001). The logistic regression takes the form:

$$p(AIS \geq 2) = \frac{1}{1+e^{(-\beta_0-\beta_1 x-\beta_2 a)}}$$

where:

β_0	=	Intercept
β_1	=	Independent parameter coefficient
x	=	Upper Tibia Axial Force (kN)
β_2	=	Mass coefficient
a	=	Subject mass, in kg

Table 8.2. Model parameter estimates.

Model	β_0	β_1	β_2
Upper Tibia Axial Force	-0.5204	0.8189	-0.0686

The risk function and 95% confidence intervals were calculated assuming a standard mass of 75 kg.

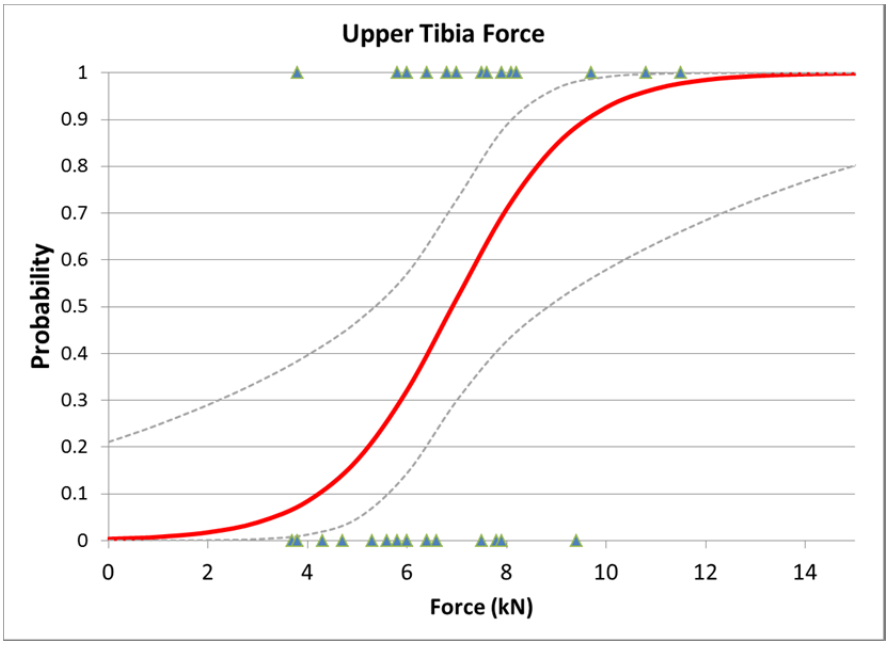

Figure 8.8. Logistic regression of upper tibia axial force data, including mean injury risk function and 95% confidence intervals, assuming mass of 75 kg.

Table 8.3. Significance and goodness of fit statistics for upper tibia force logistic regression with mass as a covariate.

Wald Pr>ChiSq	AUROC	Hosmer-Lemeshow Chi-Square	Hosmer-Lemeshow Pr>ChiSq
0.03	0.83	5.9	0.55

Logistic regression can clearly differentiate between well-correlated and non-correlated datasets, but has the drawback of resulting in a risk function that has a non-zero risk at zero stimulus level. Thus, a combined approach of logistic regression and left/right censored survival analysis is a good approach for creating injury risk curves (Hasija et al., 2011). For this case, once logistic regression was used to determine model goodness of fit, the final form of the risk function was developed using left/right censored survival analysis. The survival-based risk function closely matches the logistic regression curve

(Figure 8.9), but has the advantage of passing through zero at zero stimulus. The survival analysis risk function assumes a Weibull distribution and takes the form:

$$p\,(AIS \geq 2) = 1 - \exp\left(-\exp\left(\frac{lnx - \beta_0 - \beta_1 a}{\alpha}\right)\right)$$

where:

β_0	=	Intercept
x	=	Upper Tibia Axial Force (kN)
β_1	=	Mass coefficient
a	=	Subject mass, in kg
α	=	scale

Table 8.4. Model parameter estimates.

Model	β_0	β_1	α
Upper Tibia Axial Force	1.1929	0.0110	0.2513

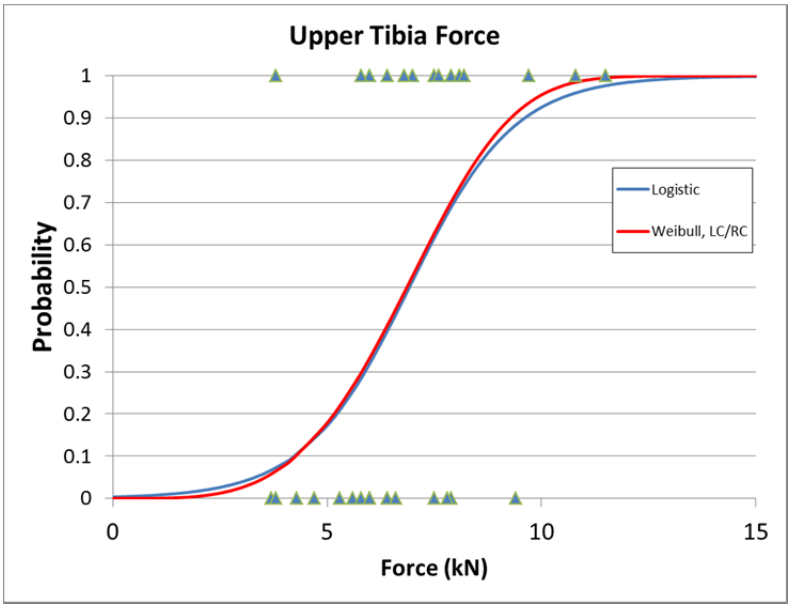

Figure 8.9. Logistic regression and left/right censored (LC/RC) survival Weibull distribution of upper tibia axial force data, assuming mass of 75 kg.

8.6 **Lower Tibia Axial Force**

8.6.1 Data

Distal tibia and hindfoot fractures are common lower extremity injuries sustained in frontal crashes (Figure 8.1). These injuries are most commonly produced by axial loading through the foot and leg (Figure 8.2). Several studies are available wherein axial load was applied to the plantar aspect of the foot (Table 8.5). These studies were evaluated to determine whether they could be combined for risk function development. The risk curve proposed by Kuppa, 2001 used a combined dataset from studies by Yoganandan et al. (1996), Begeman et al. (1996) and Roberts et al. (1993). However, Roberts et al. (1993) reported only footplate forces, and because peak footplate forces are typically much higher than peak tibial loads, it is inappropriate to combine these datasets. Yoganandan et al. (2015) evaluated these five studies, and combined only Yoganandan et al. (1996), Begeman et al. (1996) and Kitagawa et al. (1998) to develop new injury risk curves. Roberts et al. (1993) was excluded because only footplate force was recorded and Funk et al. (2002) was excluded because mean fracture forces were statistically different from the others. However, there were many small female subjects included in the Funk et al. (2002) study, which had the effect of lowering the overall mean fracture force. When either only male subjects or only "average height" (165-185 cm) subjects are considered, the mean fracture forces in the Funk study are not significantly different from the rest. As such, NHTSA deems it beneficial to include this data into a combined dataset (studies A, B, D and E, Table 8.5, APPENDIX G), accounting for age or gender as a covariate in the model (study C remains excluded due to the absence of recorded tibia forces). As demonstrated previously (Funk et al., 2002; Yoganandan et al., 2015), age is also a significant covariate in the model. The benefit to using the combined dataset is that it increases overall sample size and includes an appropriate number of non-injury data (compared with, for example, using the Funk et al., 2002 study alone). Although different boundary conditions and load cell locations exist in the combined dataset, the similarity of the injury-producing forces supports the approach combining these data. In addition, the THOR dummy, and humans in real world crashes, is expected to experience both free and fixed boundary conditions of the leg. Thus, this injury risk function will apply to both scenarios. Because many midfoot and forefoot fractures are also caused by loading to the plantar surface of the foot, this criterion will likely also address those injuries as well.

Table 8.5. Summary of biomechanical studies in which axial load was applied to the plantar aspect of the foot.

	Study	Boundary condition	Load-cell location	n, injured	n, non-injured	Specimen data available
A	Yoganandan et al. 1996	Free	Proximal end of tibia	13	13	Age, Sex, Height, Weight
B	Begeman et al. 1996	Fixed	Mid-tibia	5	12	Age, Sex, Weight
C	Roberts et al. 1993	Fixed	Foot plate	9	0	Age, Sex, Height, Weight
D	Kitagawa et al. 1998	Fixed	Proximal tibia	15	1	Age, Sex
E	Funk et al. 2002	Fixed	Implanted in tibial diaphysis	30	4	Age, Sex, Height, Weight

Table 8.6. Descriptive statistics for lower tibia axial dataset.

Study	All specimens		Male specimens only		
	Mean Failure Force (kN)	**Failure Force Range (Min-Max)**	**Mean Failure Force (kN)**	**Failure Force Range (Min-Max)**	**n, males**
A	7.8 ± 2.4	4.3 to 11.5	8.4 ± 2.1	5.5 to 11.5	11
B	7.8 ± 0.9	6.9 to 8.7	7.0	7.0	1
D	7.6 ± 0.9	5.7 to 9.1	8.0 ± 0.9	7.1 to 8.8	4
E	5.7 ± 2.2	2.6 to 10.8	7.0 ± 2.1	4.5 to 10.8	17
Combined	6.8 ± 2.2	2.6 to 11.5	7.7 ± 2.0	4.5 to 11.5	

8.6.2 Injury Risk Function Formulation

Axial force is the commonly reported predictor variable. The dependent variable considered was the presence of an AIS 2 or greater (2+) injury. Stepwise multiple regression was carried out to assess the sensitivity of occupant-based covariates. Covariates considered were age, sex and height. For this dataset, age and sex were significant covariates, while height was not. Using logistic regression, model significance and goodness of fit were evaluated for four variations of covariates, to determine which model best fit the data. The model with age and sex performed best (AUROC>0.8).

Table 8.7. Model statistics for lower tibia force logistic regression.

Model Covariates	Studies used	Wald Pr>ChiSq	AUROC	Hosmer-Lemeshow Chi-Square	Hosmer-Lemeshow Pr>ChiSq
None	A,B,D,E	0.0044	0.677	11.2	0.19
Age	A,B,D,E	0.0005	0.765	7.1	0.53
Age+Sex	A,B,D,E	0.001	0.803	6.2	0.62
Sex	A,B,D,E	0.001	0.751	12.75	0.12

The logistic regression takes the form:

$$p(AIS \geq 2) = \frac{1}{1+e^{(-\beta_0-\beta_1 x-\beta_2 a-\beta_3 b)}}$$

where:

β_0	=	Intercept
β_1	=	Independent parameter coefficient
x	=	Lower Tibia Axial Force (kN)
β_2	=	Age coefficient
a	=	Subject age, in years
β_3	=	Sex coefficient
b	=	Subject sex (Male = 1, Female = 0)

Table 8.8. Model parameter estimates.

Model	β_0	β_1	β_2	β_3
Age+Sex	-5.3542	0.48	0.0668	-1.2299

For calculation of 95% confidence intervals, a baseline age of 40 years and sex equal to 1 (male) were assumed.

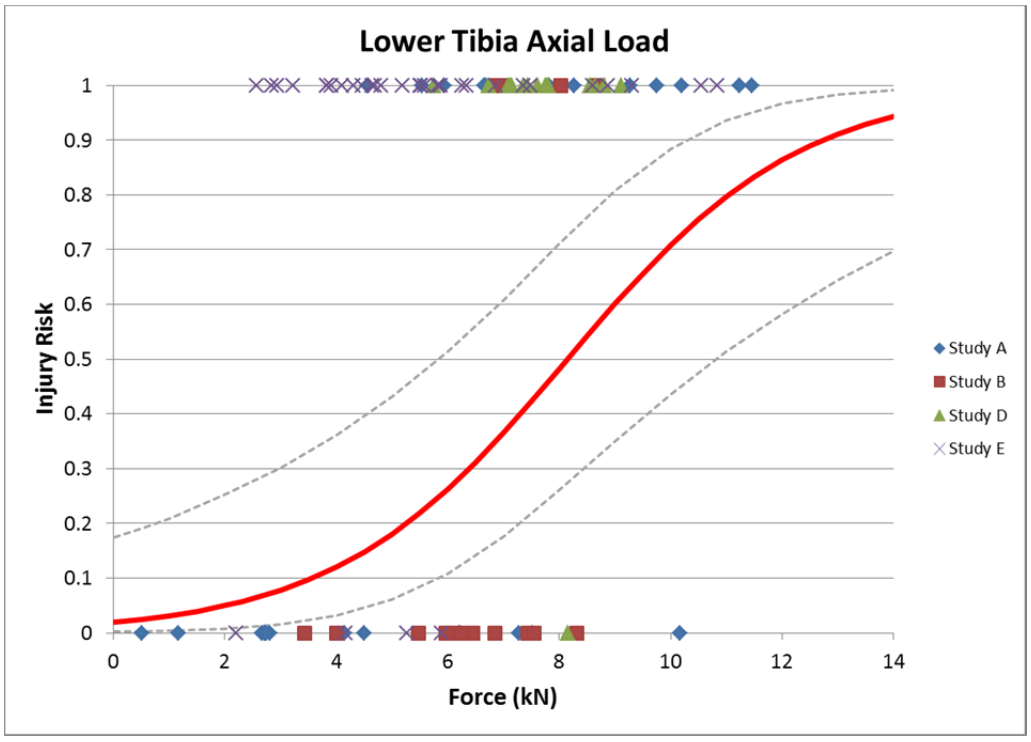

Figure 8.10. Logistic regression of lower tibia axial force data (mean injury risk function and 95% confidence intervals, assuming age of 40 years and male sex).

8.7 **Tibia Bending**

8.7.1 Data

Compressive axial loading was shown to be the most common mechanism overall for below-knee injuries in Figure 8.2 based on the coded primary mechanism in CIREN cases. The mid-shaft region of the tibia is known to have a higher tolerance to axial loading than the epiphyseal regions, but field data studies suggest bending is a more common mechanism of fracture for the tibia diaphysis (Ivarsson et al. 2008). Tibia and fibula shaft fractures, while mostly attributed to compressive axial loading, also occur in frontal crashes as a result of applied bending from eccentric loads to the foot, ankle rotations, and leg interaction with the knee bolster and surrounding components. In addition to the externally-applied bending, the total bending moment in the mid-shaft is augmented by induced bending due to axial loading given the human tibia's curvature.

The Tibia Index (TI) was developed as an injury criterion for combined bending and axial compressive loads in the mid-shaft of the tibia (Mertz et al., 1993). It was based on classical beam theory, and accounted for the interaction of stresses from bending and axial load. The Revised Tibia Index (RTI) was proposed by Kuppa et al. (2001), which incorporated updated critical values for both force and moment. The risk curve for RTI was based on three-point bending moment data from Nyquist et al. (1985) and Schreiber et al. (1998). Funk et al. (2004) noted that the adjusted critical force value presented by Kuppa et al. (2001) was inappropriate since it was based on the structural strength of the entire leg instead of representing the force equivalent of the ultimate stress, as is the foundation of the Tibia Index. For a number of reasons described subsequently, NHTSA is not planning to use TI or RTI for THOR at this time.

a) Because of curvature in the human tibia, applied axial loading induces bending moments in the shaft of the tibia that vary along its length depending on the eccentricity. Funk et al. (2004) showed that the RTI formulation does not appropriately account for these induced bending moments, thus calling into question the utility of RTI as an injury criterion. Furthermore, the THOR leg is straight and does not experience induced bending from axial load. While a human-like induced bending could be calculated based on the applied axial load, variations in the load path due to the centers of pressure at the knee and ankle joints of a human result in potential variation that cannot be adequately accounted for.
b) Prior studies have found that the anteroposterior and mediolateral bending strength of the tibia shaft are similar (Nyquist et al. 1985). This finding supports using a resultant moment in calculating a moment-based stress distribution, but induced moments from axial loading in the human tibia would act to shift the location of the maximum stresses warranting the need to account for the direction of eccentricity as well as moment components. The Tibia Index and Revised Tibia Index are calculated with the resultant moment, which does not lead to an accurate representation of the maximum stress in the tibia shaft cross-section. The induced moment may add to or subtract from the externally-applied moment, and using the resultant in the combined approach takes away from the intent of the formulation.

c) Although TI and RTI are intended to be a combined loading criterion, the proposed risk curve was not developed with any combined loading data, instead using three-point bending moment-only data from Nyquist et al. (1985) and Schreiber et al. (1998). Although some newer combined loading data is available (Untariou et al. 2008), such data is limited.

d) Data from 86 THOR vehicle tests demonstrates that RTI and resultant moment are highly correlated, whereas RTI is not correlated well with axial load, indicating that moment is primarily driving the RTI calculation (Figure 8.11).

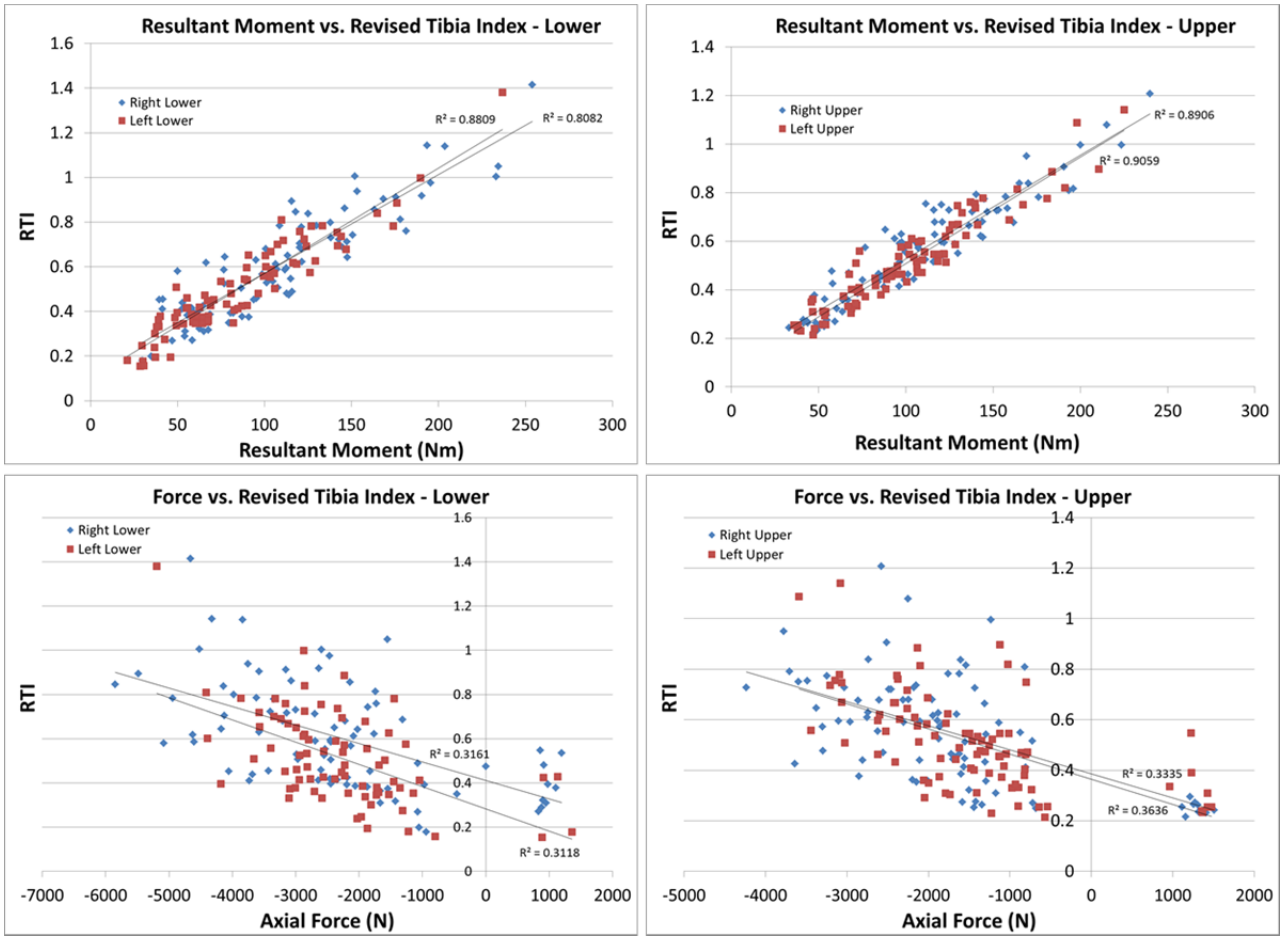

Figure 8.11. Tibia Force and Moment vs. RTI.

Resultant moment will be the measure of interest applicable to mid-shaft tibia fractures. While the most common fracture site is at the distal third, this criterion shall apply to the entire shaft and will be calculated for the upper and lower load cell locations. In the THOR leg, the upper and lower tibia resultant moments are generally similar in magnitude in the fleet tests, and do not show any clear trends in the contributions from the x-axis or y-axis components.

The data available in the literature are all failure tests. The three studies are Nyquist et al. (1985), Schreiber et al. (1998), and Untaroiu et al. (2008) (Table 8.9, APPENDIX G). Schreiber conducted quasi-static and dynamic tests, but only dynamic results were used. Nyquist only conducted bending tests,

while Schreiber and Untaroiu conducted tests with superimposed axial load. Specimen mass is available in the Nyquist and Schreiber studies, but not in Untaroiu, thus non-scaled results were used to formulate the risk function. An equivalent of the applied (external) moment was used in the formulation. Untaroiu calculated the total moment, inclusive of the applied moment and induced moment, and this value was taken to represent the external moment that is equivalent to a test without induced moments from axial load. Since the equivalent applied moment due to the externally-applied axial load in the Schreiber tests was not known, only the tests without superimposed axial load were used in the formulation of the risk function.

Table 8.9. Summary statistics from bending moment studies.

Study	n	Average raw moment	Average scaled moment
Nyquist et al. (1985)	21	308	346
Schreiber et al. (1998) without axial load	12	408	458
Schreiber et al. (1998) with 4448N axial load	9	311	382
Untaroiu et al. (2008) with varying axial load: Applied moment	20	152	n/a
Total moment		258	n/a

8.7.2 Injury Risk Function Formulation

Because only failure data were available, logistic regression-based analyses were not possible. Thus, risk functions are developed using survival analysis. The survival analysis risk function assumes a Weibull distribution and takes the form:

$$p\,(AIS \geq 2) = 1 - \exp\left(-\exp\left(\frac{lnx - \beta_0}{\alpha}\right)\right)$$

where:

β_0 = Intercept

x = Resultant Moment (Nm)

α = scale

Table 8.10. Model parameter estimates.

Model	β_0	α
Resultant Moment	5.8492	0.2965

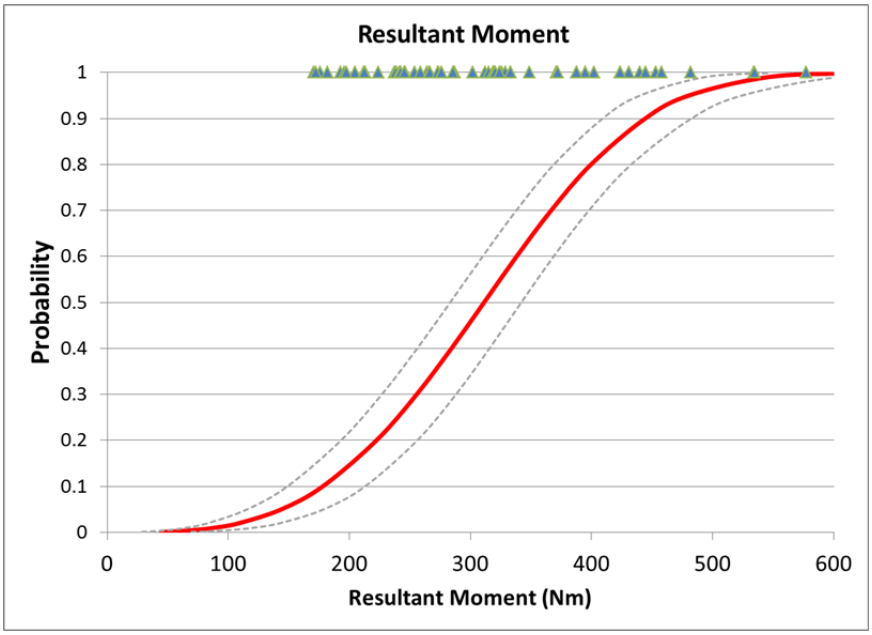

Figure 8.12. AIS 2+ tibia bending injury risk curve based on Survival-Weibull analysis.

8.8 Ankle Dorsiflexion

Ankle malleolar fractures, while mostly attributed to compressive axial loading in the CIREN dataset (Figure 8.2), can also be produced by rotation of the ankle, i.e. dorsiflexion. Available data in dorsiflexion includes a study by Portier et al. (1997) and a newer study by Rudd et al. (2004). The risk curve developed by Kuppa et al. (2001) was based on data from Portier et al. (1997). Rudd combined both datasets to create survival-based injury risk curves based separately on moment and angle.

To evaluate risk function development in dorsiflexion, stepwise multiple regression was carried out to assess model fit using different combinations of datasets and predictor variables. Both ankle moment and angle were evaluated as predictor variables. The dependent variable considered was the presence of an AIS 2 or greater (2+) injury. Logistic regression on the original Portier et al. (1997) demonstrated poor goodness-of fit statistics (Table 8.11) and extremely wide 95% confidence intervals (Figure 8.13). In addition, the combined dataset also did not appear to be well correlated based on moment or angle, and therefore logistic regression did not yield sufficiently robust results (Table 8.11, Figure 8.13). Further work is necessary to understand the experimental data, examine confounding factors, and/or conduct additional tests. Thus, NHTSA determined that criteria for ankle dorsiflexion should not be included in a rating scheme at this time.

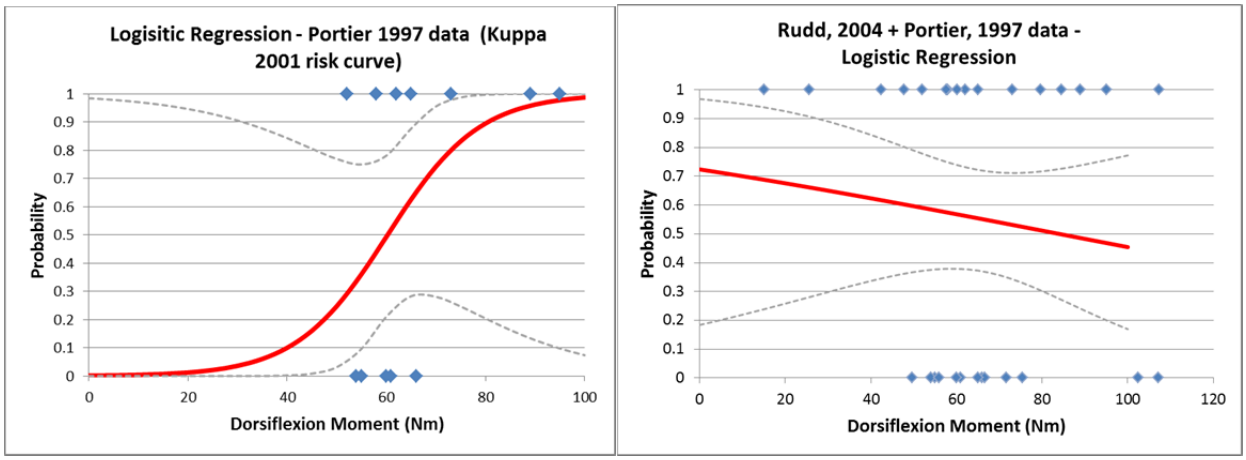

Figure 8.13. Logistic regressions on Portier et al. (1997) data alone and Portier and Rudd combined data demonstrates poor correlation. Dorsiflexion angle (not shown) also had poor correlation.

Table 8.11. Significance and goodness of fit statistics for logistic regression on combined dorsiflexion data.

Studies used	Predictor variable	Wald Pr>ChiSq	AUROC	Hosmer-Lemeshow Chi Square	Hosmer-Lemeshow Pr>ChiSq
Portier	Moment	0.22	0.71	10.5	0.40
Portier and Rudd	Moment	0.52	0.55	9.9	0.27
Portier and Rudd	Angle	0.09	0.73	7.1	0.53

While the lack of correlation in the available dorsiflexion data does not support development of a separate risk function at this time, results from field data analysis demonstrate that a focus on compression of the tibia and hindfoot will address most of the below-knee injuries, including malleolar fractures (Figure 8.2). In addition, ankle dorsiflexion will rarely, if ever, occur in the absence of applied axial load. Thus, it is expected that there will be benefit for these injuries even by rating only on tibia loads and moments.

8.9 Ankle Inversion/Eversion

Ankle malleolar fractures, while mostly attributed to compressive axial loading in the CIREN dataset (Figure 8.2), also occur in frontal crashes as a result of rotation of the ankle, i.e. inversion/eversion. Several studies have examined inversion and eversion (Table 8.12). These studies were evaluated to determine whether they could be combined for risk function development. The risk curve published by Kuppa et al. (2001) was developed using only the mean and standard deviation from a set of quasi-static data conducted by Parenteau et al. (1998), rather than the original data from that paper. Dynamic inversion/eversion data comes from Begeman et al. (1993) and Funk et al. (2002). Injury risk curves were developed by Funk et al. (2002) using survival analysis, with covariates of applied Achilles load, sex, and rotation direction (inversion vs. eversion) and neglecting the contribution of the few non-injury data

points. The human ankle becomes much stiffer with axial load (either applied or via superimposed Achilles loading), while THOR doesn't demonstrate this behavior. Thus, it is unclear whether these risk curves can be directly applied to THOR. In addition, the Funk analysis used only the injury data and did not include the available non-injury data.

As previously described, it was desired to follow a consistent process by which to differentiate between non-correlated and well-correlated datasets when considering the development of injury risk functions. Thus, to evaluate risk function development in inversion/eversion, stepwise multiple regression was carried out to assess model fit using different combinations of datasets and covariates (e.g. occupant sex and rotation direction). Both ankle moment and angle were evaluated as predictor variables. The dependent variable considered was the presence of an AIS 2 or greater (2+) severity injury. Results demonstrated that the combined dataset was not well correlated based on moment or angle (with or without covariates of rotation direction and specimen sex), and therefore logistic regression did not yield sufficiently robust results (Wald Pr > 0.05; AUROC < 0.8, Table 8.14).

Table 8.12. Studies on inversion/eversion of foot/ankle.

	Study	Condition	Rotation	n, injured	n, non-injured	Notes
A	Begeman et al. 1993	Dynamic	Inversion	6	3	
			Eversion	7	2	
B	Petit et al. 1996	Quasi-static	Inversion	5	0	Individual subject responses not reported
			Eversion	5	0	
C	Parenteau et al. 1998	Quasi-static	Inversion	8	0	
			Eversion	8	0	
D	Jaffredo et al. 2000	Dynamic	Inversion	0	6	Individual subject responses not reported
			Eversion	0	6	
E	Funk et al. 2002	Dynamic	Inversion	6	0	No applied Achilles load
			Eversion	7	0	
			Inversion	8	3	Applied Achilles load
			Eversion	10	2	

Table 8.13. Average failure and non-failure moments and angles in inversion and eversion.

	Study	Rotation	Mean Failure Moment (N-m)	Non-injury moment range (N-m)	Mean Failure Angle (deg)	Mean Non-injury Angle (deg)
A	Begeman et al. 1993	Inversion	33 ± 7	14 to 70	61 ± 6	51 ± 16
		Eversion	41 ± 14	25 to 120	59 ± 6	45 ± 11
B	Petit et al. 1996	Inversion	40 ± 46	-	34 ± 8	-
		Eversion	35 ± 9	-	32 ± 7	-
C	Parenteau et al. 1998	Inversion	34 ± 15	-	34 ± 8	-
		Eversion	48 ± 12	-	32 ± 7	-
D	Jaffredo et al. 2000	Inversion	-	13 to 40	-	19 ± 5
		Eversion	-	24 to 71	-	13 ± 1
E	Funk et al. 2002 (no Achilles load)	Inversion	24 ± 6	-	34 ± 10	-
		Eversion	42 ± 15	-	30 ± 8	-
	Funk et al. 2002 (Achilles load)	Inversion	72 ± 26	40 to 115	40 ± 12	33 ± 20
		Eversion	141 ± 65	46 to 76	41 ± 9	30 ± 23

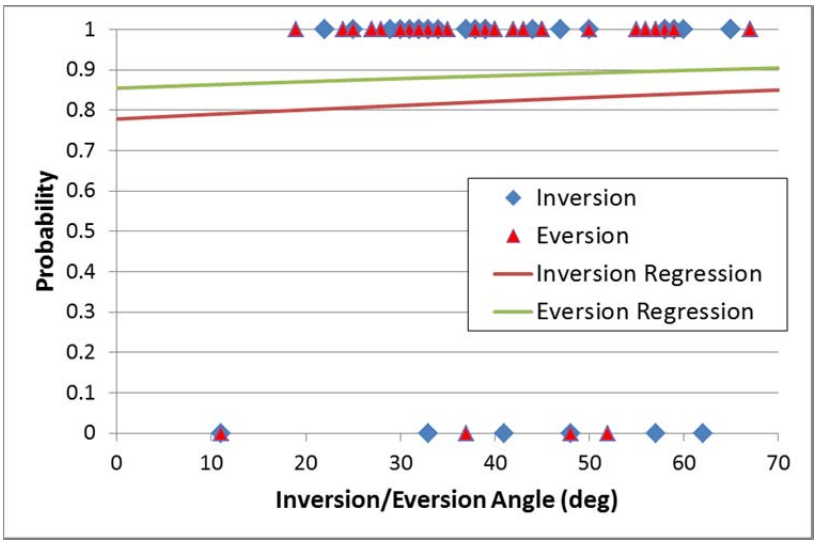

Figure 8.14. Insufficient non-injury data are available in inversion/eversion. In addition, data are not well correlated based on angle (or moment, not shown), as demonstrated by logistic regression.

Table 8.14. Significance and goodness of fit statistics for logistic regression on combined xversion data with covariate of rotation direction (inversion or eversion). Adding sex as a covariate did not improve model fit.

Studies Used	Predictor variable	Wald Pr>ChiSq	AUROC	Hosmer-Lemeshow Chi Square	Hosmer-Lemeshow Pr>ChiSq
A,C,E	Moment	0.74	0.69	5.1	0.75
A,E	Angle	0.74	0.55	8.3	0.31

While the lack of correlation in the available inversion/eversion data does not support development of a separate risk function at this time, results from field data analysis demonstrate that a focus on compression of the tibia and hindfoot will address most below-knee injuries, including malleolar fractures (Figure 8.1, Figure 8.2). In addition, like dorsiflexion, ankle inversion/eversion will rarely, if ever, occur in the absence of applied axial load. Thus, it is expected that there will be benefit for these injuries even by rating only on tibia loads and moments.

8.10 **Application of Risk Functions to THOR-50M**

Upper Tibia Force

$$p(AIS \geq 2) = \frac{1}{1 + e^{(0.5204 - 0.8189F + 0.0686m)}}$$

where:

F = Peak compressive force measured by the Z-axis for the THOR upper tibia load cell (in kN)

m = Subject mass (in kg)

Simplified, assuming a 78 kilogram occupant:

$$p(AIS \geq 2) = \frac{1}{1 + e^{(5.8712 - 0.8189F)}}$$

Lower Tibia Force

$$p(AIS \geq 2) = \frac{1}{1 + e^{(5.3542 - 0.48F - 0.0668a + 1.2299♂)}}$$

where:

F = Peak compressive force measured by the z-axis for the THOR lower tibia load cell (in kN)

a = Subject age (in years)

♂ = Subject sex (Male = 1, Female = 0)

Simplified, assuming a 40-year-old Male:

$$p(AIS \geq 2) = \frac{1}{1 + e^{(3.9121 - 0.48F)}}$$

Tibia Bending Moment

$$p(tibia\ fracture) = 1 - e^{-e^{\left(\frac{lnM_{res} - 5.8492}{0.2965}\right)}}$$

where:

M_{res} = Peak resultant moment = $\left|\sqrt{M_x(t)^2 + M_y(t)^2}\right|_{max}$

M_x, M_y = Moments measured at the x- and y-axes of the THOR upper or lower tibia load cell (in Nm)

8.11 **Fleet Test Data: THOR-50M**

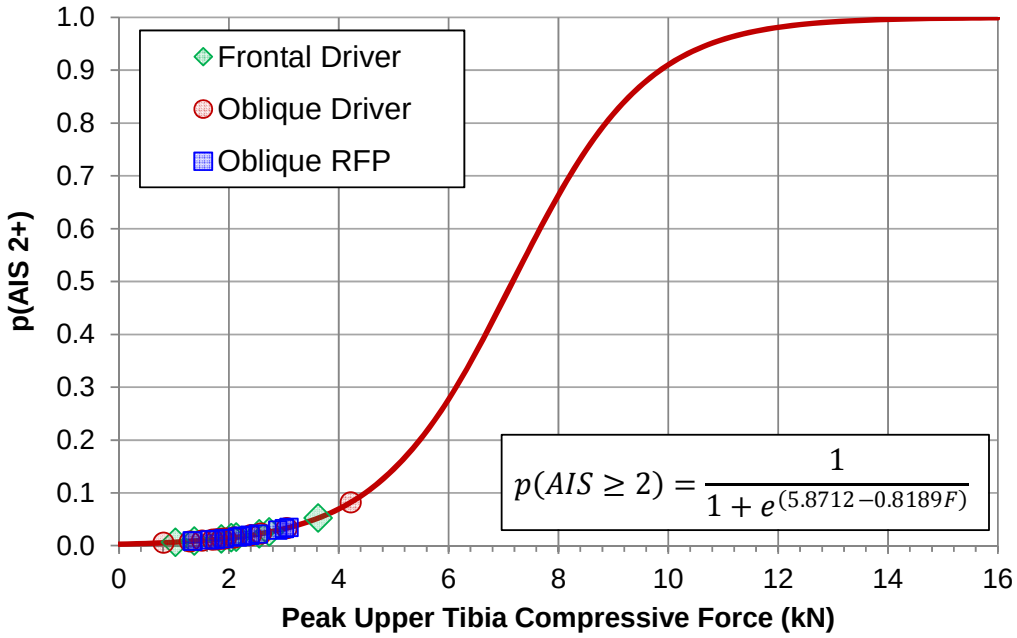

Figure 8.15. Probability of AIS 2+ lower leg injury predicted using peak upper tibia compressive force measured from fleet test results for the driver in the frontal rigid barrier test mode and both the driver and right front passenger in the Oblique MDB test mode.

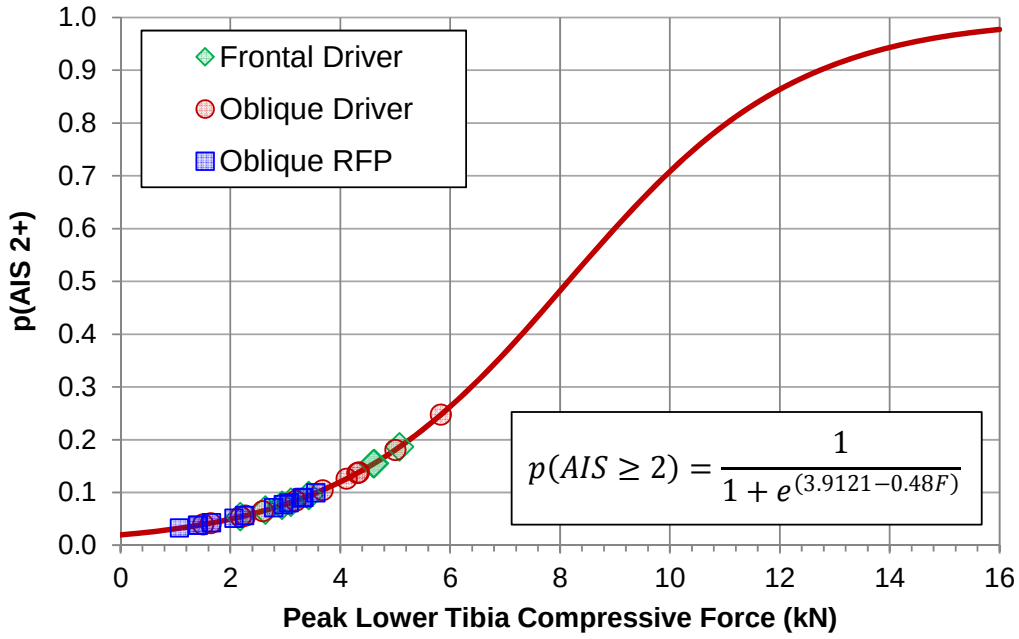

Figure 8.16. Probability of AIS 2+ lower leg injury predicted using peak lower tibia compressive force measured from fleet test results for the driver in the frontal rigid barrier test mode and both the driver and right front passenger in the Oblique MDB test mode.

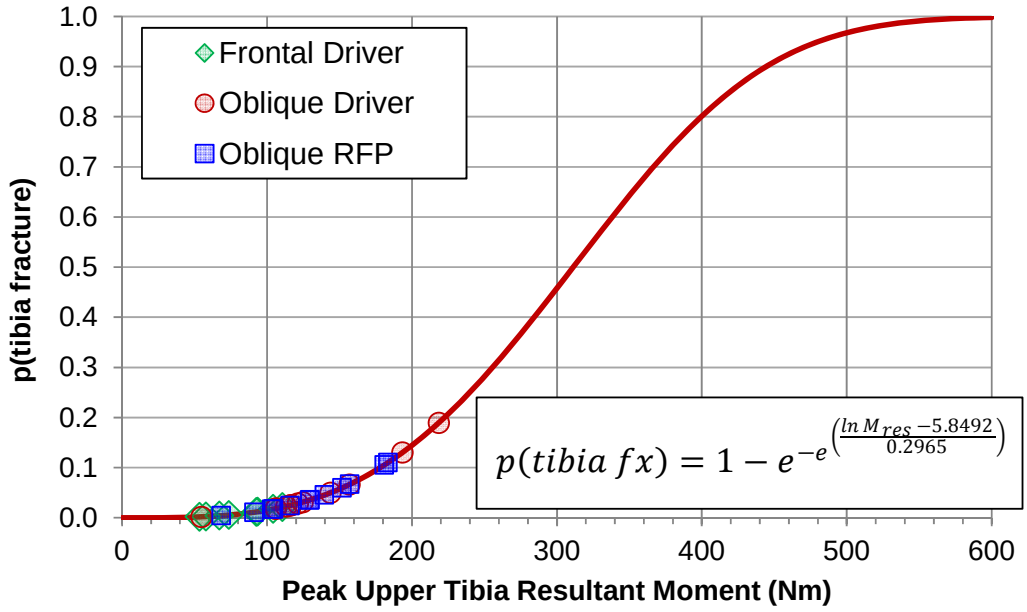

Figure 8.17. Probability of tibia fracture predicted using peak upper tibia resultant moment measured from fleet test results for the driver in the frontal rigid barrier test mode and both the driver and right front passenger in the Oblique MDB test mode.

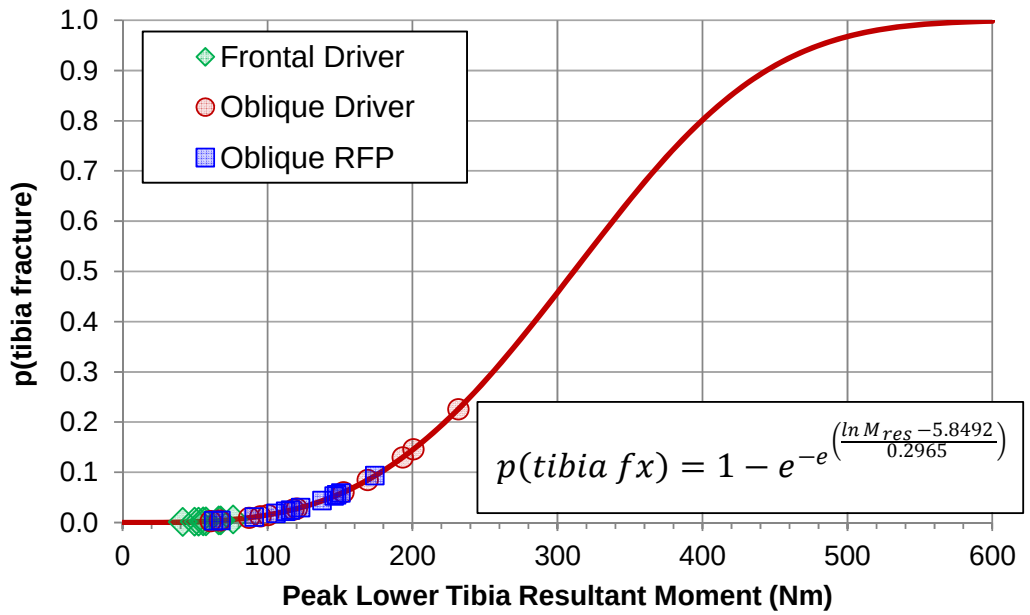

Figure 8.18. Probability of tibia fracture predicted using peak lower tibia resultant moment measured from fleet test results for the driver in the frontal rigid barrier test mode and both the driver and right front passenger in the Oblique MDB test mode.

8.12 **Limitations**

Matched pair tests have not been conducted. Therefore the risk functions presented here assume that THOR-50M responds exactly like a human cadaver. This is a reasonable assumption given THOR-50M's good to excellent biofidelity (Parent, 2016).

Age is included as a significant covariate in the lower tibia axial force risk function, but not in the risk functions for upper tibia axial force or tibia bending moment. The intended age of application of the risk function (40 years old) is notably younger than the average age of the PMHS (73 and 65 years, for upper tibia force and bending moment respectively) used to develop these risk functions.

9 COMPARING FLEET AND FIELD ESTIMATED INJURY RISK

9.1 **Introduction**

Many studies have attempted to compare the predicted risk of injury as estimated using test dummies and injury criteria in standardized crash tests (Laituri et al., 2009; Prasad et al., 2010; Prasad et al., 2014; Mueller et al., 2015) versus the risk of injury from real-world crash data (i.e. field data). While those studies described "risk" of injury-based point estimates derived from field data and compared them to estimates derived from crash or fleet test data with ATDs, they did not always describe the limitations of the field and/or fleet data (e.g. acknowledge or account for all occupant / crash parameters that affect injury risk) or they did not attempt to describe the error associated with their point or mean estimates of injury risk.

Like the prior studies, the aim of this study was to compare the risk or rates of injury in the real-world crashes versus the predicted risk of injury given frontal crash tests with the THOR-50M and the associated injury measures and risk functions presented earlier in this report.

9.2 **Methods**

To compare the risk of injury predicted by THOR-50M in crash tests versus the risk of injury in field data it is necessary to describe the severity of the crash test and then attempt to select field cases with equivalent severity.

9.2.1 Crash Tests

For both the left oblique and full frontal conditions, the fleet vehicles chosen for comparison to the field data are vehicles that performed 'Acceptable' or better overall in the Insurance Institute for Highway Safety's small overlap impact (SOI) test condition (IIHS, 2016). The vehicles also had to be equipped with a FMVSS No. 226 compliant side curtain airbag. Both of these prerequisites were intent on evaluating vehicles in the left oblique condition that represent the current state of the art for frontal crash safety. The table with full frontal and oblique driver tests that were used in this analysis can be found in APPENDIX D.

9.2.1.1 Left Oblique

NHTSA has performed over two-dozen left oblique crash tests. The original aim of the test procedure (Saunders et al. 2011, 2012) was to produce a peak delta V (or change in velocity) of 56 kph (35 mph) when testing an average size (approximately 1,500 kg) passenger car. The test involves a moving deformable barrier (MDB) striking a stationary vehicle. The overlap between the target vehicle and the MDB is 35% and the angle is 15 degrees. The resulting peak delta V that has been observed in NHTSA left oblique crash tests has ranged from 46 to 67 kph while the estimated principal direction of force (PDOF) has ranged from 336° to 343°. The damage extent, per SAE J224 (SAE, 1980), has ranged from 3-6 in these tests.

9.2.1.2 Full Frontal

NHTSA's 0-degree, full overlap rigid barrier test of 56 kph (35 mph) results in a delta V of approximately 64 kph (40 mph) including rebound velocity. Generally, the damage, per SAE J224, is an extent of 3 for full frontal NCAP tests.

9.2.2 Treatment of NASS-CDS Sample

As mentioned earlier, the aim is to compare field and fleet injury rates/risks and confidence intervals for crash populations of similar severity. In doing so, it is necessary that we restrict the NASS-CDS sample to crash/restraint system/occupant characteristics (delta V, belt use, crash type, occupant type/age, airbag deployment status) that are similar to the characteristics of the full frontal and oblique crash tests with a belted, airbag restrained THOR-50M.

NASS-CDS is considered a panel survey given that it samples the same data from the same sample or primary sampling units (PSUs) over multiple periods (years). Since the same PSUs are included over multiple case years, the annual estimates can be considered to be positively correlated. In using consecutive years of NASS-CDS data, the dataset needs to be correlated to estimate variance for a pooled, multi-year sample. For the purpose of this analysis, the last 15 years of NASS-CDS (2000 to 2014) are being studied. All of those years with the exception of 2002 to 2007 were limited to the same 24 Primary Sampling Units (PSUs). To maintain a correlated sample, data must be summed from the same 24 PSUs for all years in the sample. Case years 2002 to 2007 had three extra PSUs (42, 47 and 50). These three "extra" PSUs are removed to maintain a correlated sample from 2000 to 2014. PSUs 42, 47, and 50 were in the same stratum as PSUs 9 and 45. The sample weights for PSU 9 (adjusted weight equals 19.66987/7.67598 times the ratwgt) and 45 (adjusted weight equals 41.43575/16.16911 times the ratwgt) are adjusted to account for the removal of PSUs 42, 47 and 50. The resulting adjusted weight sample of data from 24 PSUs is the correlated sample used here forward.

Another requirement in maintaining a correlated sample is that we consider the type of data sampled in each year. For NASS-CDS 2000 to 2008, occupant injury and crash data was collected on all vehicles, regardless of vehicle age. Starting in 2009, occupant injury data was only collected and recorded for vehicles that were 10-years-old or newer. For 2009 to 2014 this means that roughly 40% of passenger cars/light trucks/vans did not have injury data recorded. To maintain a correlated sample of injury and non-injury data over the 15 years of NASS-CDS included, all years, including 2000 to 2008, were restricted to analysis of data for vehicles that were 10-years-old or newer in the respect sample years. This results in a range of vehicle model years from 1990 to 2015. While conventional wisdom would have one assume that the newer vehicle would be safer (have a lower injury risk for a given crash type) and that including older vehicles in the sample would present higher injury risk or rates than newer vehicles, the brain (Figure 3.1) and chest injury (Figure 5.2) trends shown earlier in this report suggest that newer vehicles actually have a higher risk of injury for some body regions. Additionally, in looking at the 2000-2014 sample (belted drivers in frontal crashes) with the vehicle model year restriction, there is no significant trend (increase or decrease) in the risk of MAIS 2+ or MAIS 3+ injuries (Figure 9.1). While the relative size of the targeted sample domain as a percent of the total sample does not change significantly year to year (more on this soon), including more case years allows for a larger raw count sample of cases to be included in the weighted analysis.

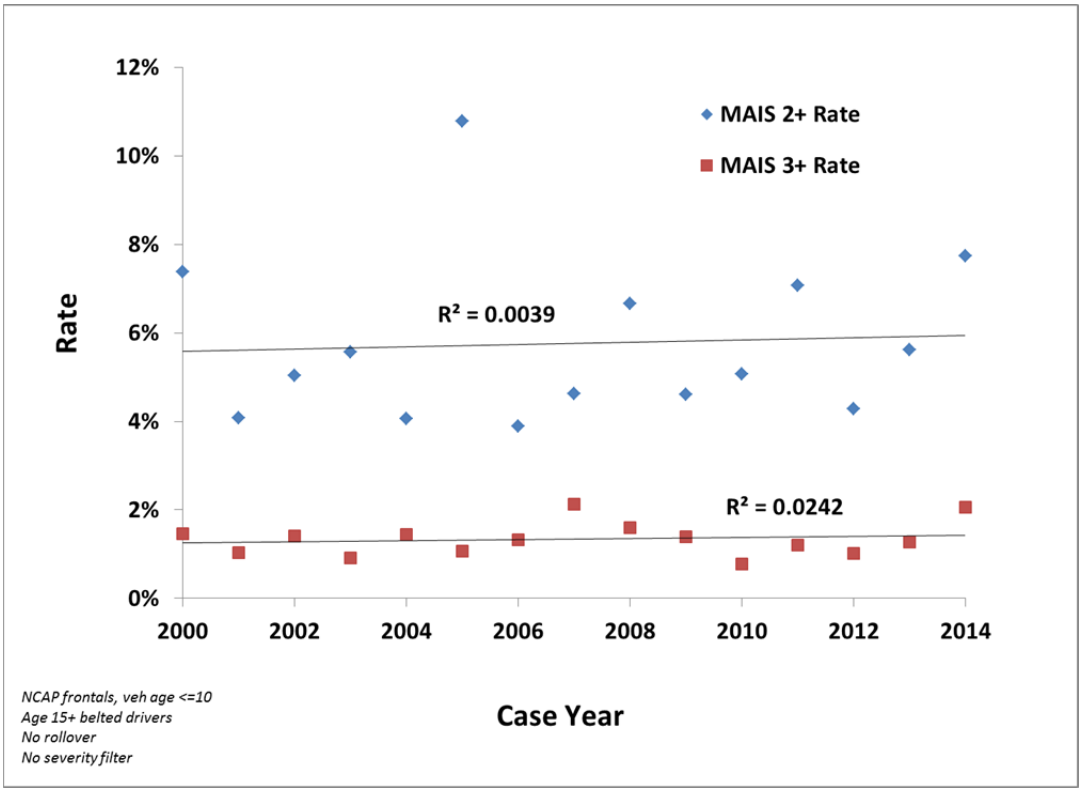

Figure 9.1. MAIS 2+ and 3+ rates for belted drivers in frontal crashes, NASS-CDS 2000 to 2014.

9.2.3 Crash / Occupant / Vehicle Parameters

NASS-CDS records numerous parameters that describe the crash type (type of object contacted, area and type of damage, principal direction of force), severity (damage extent, delta V, intrusion), occupant type (age, gender, height, weight, seat position, seat track position) and restraint system (belt usage, airbag deployment). The current analysis balances relative domain size concerns (i.e. sample size; details below) and the desire to "match" the full frontal and oblique condition through the selection of crash, occupant and restraint system parameters.

9.2.4 Injury Data

The occupant injury in NASS-CDS is queried for AIS 2+, 3+ and/or 4+ injury severities per AIS 1995/1998 (AAAM, 1998). While AIS 2005/2008 is the latest version (AAAM, 2008), NHTSA did not begin using it until 2010. Prior years used AIS 1995/1998 and 2010 through 2014 has both sets of AIS codes.

For comparing field and fleet data, it is necessary to group the field injury data to match with the intended target population for the corresponding THOR-50M injury measure. Table 9.1 summarizes how the respective injury data and THOR-50M injury measures are being paired for the analysis.

Table 9.1. AIS body regions / injury severity and paired THOR-50M injury measures.

AIS Body Region / Injury - Severity	THOR-50M Injury Measure
Skull or Facial Fracture - 2+	HIC_{15}
Skull or Facial Fracture - 3+	HIC_{15}
Brain - 3+	BrIC
Brain - 4+	BrIC
Neck - 2+	Nij
Neck - 3+	Nij, Tension (N)
Thorax - 3+	Resultant Chest Deflection (mm)
Abdomen - 3+	Resultant Abdomen Deflection (mm)
Hip/Pelvis - 2+	Resultant Acetabulum Force (N)
Thigh - 2+	Femur Axial Force (N)
Knee - 2+	Femur Axial Force (N)
Proximal Tibia - 2+	Upper Tibia Axial Force (N)
Tibia, Fibula Shaft - 2+	Upper and Lower Resultant Moment (Nm)
Distal Tibia - 2+	Lower Tibia Axial Force (N)

9.2.5 Sample Domain

The size of the target sample relative to the full NASS-CDS sample was considered a constraint in this study. Purcell and Kish (1979) described four classes of relative domain sizes (P_d). Equation (9.1) simply describes what the relative domain size is.

$$\boldsymbol{P_d} = \frac{\boldsymbol{N_d}}{\boldsymbol{N}} \qquad (9.1)$$

where N_d is the domain of interest and N is the size of the full sample domain.

For example, N_d is the domain represented by belted drivers in NCAP Frontal crashes over a given delta V range in NASS-CDS case years 2000-2014 for vehicle ages of less than or equal to 10 years. In this case, N is the total size of the weighted sample for NASS-CDS 2000-2014.

Purcell and Kish (1979) described four classes of P_d.

- Class 1 - Major Domain: $P_d > 1/10$ (or 10%)
- Class 2 - Minor Domain: $1/10 \leq P_d \leq 1/100$ (or 10% to 1%)
- Class 3 - Mini Domain: $1/100 \leq P_d \leq 1/1{,}000$ (or 1% to 0.1%)
- Class 4 - Rare Type Domain: $1/1{,}000 \leq P_d \leq 1/10{,}000$ (or 0.1% to 0.01%)

Purcell and Kish cautioned related to the use of class 3 and class 4 domain sizes. For class 3 they noted that "standard methods of survey estimation break down." For class 4 or Rare Type, they stated that

"for truly rare items (class 4), sample surveys are usually useless; separate and distinct methods are required."

For the purposes of the current study, the aim will be to narrow the target population from frontal crashes down to no smaller than a class 3 domain relative to the full NASS-CDS domain. While aiming for a larger (e.g. class 2) relative domain size would be desirable, the reason why this is not achievable will be discussed shortly.

9.2.6 Point Estimates and Confidence Intervals

Mean injury risk, standard deviation and 95% confidence intervals are calculated for the respective combinations of fleet data. The upper and lower limit at the 95% confidence level is calculated using equation 9.2, where 1.96, the Z-score at 95% confidence interval, is multiplied by the standard error of the mean (standard deviation (σ) divided by the square root of the sample size (n)). The resulting product is added and subtracted from the sample mean to establish the upper and lower confidence limits, respectively. It is this mean and the upper and lower 95% confidence limits that can be compared to field data estimates. If the confidence interval of the fleet and field data overlaps, then we cannot reject the hypothesis that the two rates are the same.

$$\mathbf{95\%\ Confidence\ Limits} = \mathbf{Sample\ Mean} \pm \mathbf{1.96} * \frac{\sigma}{\sqrt{n}} \qquad (9.2)$$

For field data estimates, the correlated sample with adjusted weights is used with the PROC SURVEYFREQ procedure in SAS 9.3 (SAS Institute, Inc.) to produce a point estimate for the rate of injury in the NASS-CDS sample as well as the upper and lower 95% confidence intervals.

9.3 **Results**

9.3.1 Parameter Selection

The previously stated aim was to look at the point estimate and associated 95% confidence interval for injury risk in crashes of similar severity to those that are represented in the frontal oblique and full frontal test conditions. Below are the final selected parameters that were used.

- **Delta V**: 40 < delta V ≤75 kph
- **Damage Extent**: 3-6
- **Type of Crash**: SOI, Offset, Full frontal w/ PDOF of 320-40
- **Seatbelt Use**: Yes
- **Airbag Deployment**: Yes
- **Seat Position**: Driver
- **Rollover**: No
- **Occupant Ejection**: No
- **Vehicle Age**: ≤ 10 years old to allow for target domain to go from 2000-2014

- **Case Years**: 2000-2014
- **Object Contacted**: Vehicle or large fixed object (medium/large pole, large tree, building, bridge, concrete barrier, building, wall, ditch/culvert)

Given the range of delta Vs seen in crash tests, the delta V range was restricted to crashes with delta V greater than 40 kph, but less than or equal to 75 mph. At the low end, this is less severe than the 46-kph minimum delta V observed in oblique testing. This was reduced to allow for inclusion of more cases (i.e. higher relative domain size). Additionally, given observed crash extent severities of 3-6, the field data was also restricted to crashes with 3-6 extents. Restricting only to extent and not delta V results in the average crash being much less severe than our standardized test (Table 9.2).

Table 9.2 shows the mean delta V values for frontal crashes by damage extent. It can be seen that the average delta V is much higher for MAIS 3+ injury cases than when all cases are included. Further, it can be seen in Table 9.3 how much influence filtering crash severity has on the estimated risk of injury when looking at the final selected crash parameters versus severity filtering only by extent versus no severity filter.

Table 9.2. Delta V (DV) versus damage extent for all cases versus MAIS 3+ cases (NASS-CDS 2010-14, frontal crashes, belted drivers).

Damage Extent	MAIS 3+ DV (kph)	All MAIS DV (kph)
1	19.4	17.7
2	32.8	24.1
3	41.9	26.7
4	52.1	26.9
5	61.6	24.7
6	46.7	19.2
7	37.2	21.4
8	49.6	20.3
9	32.6	19.9

Attempts were made to look at specific crash types (small overlap left and right, left and right oblique, left and right offset, full frontal) as individual domains, but the domain sizes were always class 4. Therefore, all frontal crashes were grouped together in a single domain with PDOF ranging from 320 to 40 degrees. Given that the majority of field cases are drivers and the fact that we have matched tests in both full frontal and left oblique with THOR-50M, the target population was limited to age 15 and older, belted drivers. Additionally, since all of our fleet tests at these severities result in airbag deployment, the cases were restricted to those with airbag deployment. Crashes were restricted to vehicle to vehicle crashes and crashes with large fixed objects such as large trees/poles and concrete barriers/walls/buildings, covering almost 90% of frontal crashes that met the other restrictions of target crash population.

Vehicle age was also restricted to vehicles that were 10-years old or newer in their given sample year. This was done largely due to the fact that 2009-2014 NASS-CDS data only collected injury data on newer vehicles, while in earlier NASS-CDS case years injury data was collected for all sampled vehicles. Given this restriction and the requirement to have a correlated sample, 2000 to 2008 NASS-CDS data analysis was also limited to vehicles that were 10-years old and newer.

The relative domain size aim of being class 3 or higher can be achieved by looking at one year of NASS-CDS data. However, the raw count sample size can be very small if restricting to a single year. Similarly, restricting to case years 2010-2014 also presents a relatively small sample of crashes. When looking at only 2010-2014 and restricting to the parameters listed above the raw count sample is limited to only 154 cases (18,742 weighted) with 85 that are MAIS 2+ and 42 that are MAIS 3+. In contrast, when including case years 2000 to 2009 the raw count sample goes up to 669 (83,799 weighted) with 386 MAIS 2+ and 240 MAIS 3+ cases, respectively. Thus, as previously described in the methods section, case years 2000 to 2014 were used.

As noted earlier, while class 3 or higher was the aim, it would be desirable to have a class 2 or higher relative domain size. For belted drivers in 320 to 40-degree PDOF full frontal, offset or small overlap frontal crashes to have a domain size of 2, the delta V restriction has to be removed. With the delta V restriction removed (second dataset in Table 9.3), Pd equals 1.19%. This puts the relative domain size for that sample just over the border from class 3 to class 2. However, as discussed earlier, these crashes on average are less severe than NHTSA's full frontal and left oblique crash conditions when restricting to only damage extent as the severity filter.

Table 9.3. Frontal crash severity groupings vs. injury risk estimates.

Injury Risk: All Injuries by Body Region, Age 15+, Belted NCAP Frontal Drivers (2000-2014)[1]												
	1. 40-75 KPH and Extent 3-6[2]				2. Extent 3-6[3]				3. All[4]			
Injury	Point Estimate	Std Error	CI Lower	CI Upper	Point Estimate	Std Error	CI Lower	CI Upper	Point Estimate	Std Error	CI Lower	CI Upper
MAIS 2+	53.5%	6.5%	39.3%	67.8%	18.3%	2.5%	12.9%	23.7%	5.5%	0.7%	4.0%	7.0%
MAIS 3+	29.5%	3.5%	21.7%	37.2%	7.7%	0.8%	6.0%	9.4%	1.4%	0.2%	1.0%	1.8%
All Head and Face - 2+	9.5%	2.7%	3.7%	15.4%	3.8%	0.4%	2.9%	4.8%	1.1%	0.1%	0.8%	1.3%
All Head and Face - 3+	5.5%	2.6%	0.0%	11.3%	1.2%	0.3%	0.5%	1.8%	0.2%	0.0%	0.2%	0.3%
Skull or Facial Fracture - 2+	1.6%	0.6%	0.4%	2.9%	0.6%	0.1%	0.5%	0.7%	0.2%	0.0%	0.1%	0.2%
Skull or Facial Fracture - 3+	0.4%	0.2%	0.0%	0.9%	0.2%	0.0%	0.1%	0.3%	0.0%	0.0%	0.0%	0.1%
Brain - 2+	8.5%	2.5%	3.0%	14.0%	3.5%	0.4%	2.6%	4.5%	1.0%	0.1%	0.8%	1.2%
Brain - 3+	5.3%	2.6%	0.0%	10.9%	1.1%	0.3%	0.4%	1.7%	0.2%	0.0%	0.1%	0.2%
Brain - 4+	2.7%	1.0%	0.4%	4.9%	0.6%	0.1%	0.3%	0.9%	0.1%	0.0%	0.1%	0.1%
Neck - 2+	2.4%	0.5%	1.4%	3.5%	0.7%	0.1%	0.5%	0.9%	0.2%	0.1%	0.1%	0.4%
Neck - 3+	0.7%	0.3%	0.0%	1.4%	0.2%	0.1%	0.1%	0.3%	0.1%	0.0%	0.0%	0.1%
Thorax - 2+	15.2%	1.8%	11.3%	19.2%	4.2%	0.5%	3.1%	5.3%	1.1%	0.2%	0.7%	1.5%
Thorax - 3+	12.5%	1.6%	8.9%	16.0%	3.2%	0.5%	2.1%	4.3%	0.6%	0.1%	0.4%	0.8%
Thorax (skeletal) - 2+	12.4%	1.7%	8.8%	16.0%	3.1%	0.6%	1.9%	4.4%	0.9%	0.2%	0.5%	1.3%
Thorax (skeletal) - 3+	8.2%	1.9%	4.1%	12.3%	1.9%	0.6%	0.7%	3.1%	0.3%	0.1%	0.1%	0.5%
Abdomen - 2+	3.8%	1.2%	1.2%	6.4%	1.5%	0.2%	1.0%	2.0%	0.3%	0.0%	0.2%	0.4%
Abdomen - 3+	1.8%	1.0%	0.0%	4.1%	0.7%	0.2%	0.3%	1.1%	0.1%	0.0%	0.0%	0.2%
Lower Extremities - 2+	33.4%	4.5%	23.5%	43.3%	9.5%	0.9%	7.5%	11.5%	2.6%	0.6%	1.3%	3.9%
Lower Extremities - 3+	13.0%	1.6%	9.5%	16.5%	3.5%	0.4%	2.7%	4.3%	0.5%	0.1%	0.4%	0.6%
Knee, Thigh or Hip - 2+	14.9%	3.5%	7.4%	22.5%	4.7%	0.5%	3.5%	5.8%	0.9%	0.1%	0.7%	1.1%
Knee, Thigh or Hip - 3+	8.5%	1.4%	5.5%	11.6%	2.1%	0.2%	1.6%	2.6%	0.3%	0.0%	0.2%	0.4%
Hip/Pelvis - 2+	5.3%	2.2%	0.6%	10.0%	1.4%	0.3%	0.6%	2.1%	0.2%	0.0%	0.1%	0.3%
Hip/Pelvis - 3+	1.8%	1.1%	0.0%	4.1%	0.5%	0.2%	0.2%	0.9%	0.1%	0.0%	0.0%	0.1%
Thigh - 2+	8.1%	1.8%	4.0%	12.1%	1.9%	0.3%	1.3%	2.4%	0.3%	0.0%	0.2%	0.3%
Knee - 2+	4.4%	1.5%	1.1%	7.8%	2.2%	0.4%	1.4%	3.0%	0.6%	0.1%	0.3%	0.8%
Leg, Foot or Ankle - 2+	24.6%	4.2%	15.4%	33.8%	6.3%	0.6%	4.9%	7.7%	1.9%	0.7%	0.4%	3.3%
Leg, Foot or Ankle - 3+	6.1%	1.1%	3.8%	8.4%	1.8%	0.3%	1.2%	2.5%	0.3%	0.0%	0.2%	0.3%
Tibia / Fibula ALL - 2+	16.8%	3.7%	8.7%	25.0%	4.4%	0.6%	3.1%	5.8%	0.9%	0.1%	0.7%	1.2%
Tibia / Fibula ALL - 3+	6.1%	1.1%	3.8%	8.4%	1.8%	0.3%	1.2%	2.5%	0.3%	0.0%	0.2%	0.3%
Proximal Tibia - 2+	2.6%	0.8%	0.8%	4.5%	0.9%	0.2%	0.3%	1.4%	0.1%	0.0%	0.0%	0.2%
Proximal Tibia - 3+	1.2%	0.5%	0.1%	2.2%	0.4%	0.1%	0.2%	0.5%	0.1%	0.0%	0.0%	0.1%
Tibia, Fibula Shaft - 2+	9.4%	1.7%	5.8%	13.0%	2.3%	0.3%	1.6%	3.0%	0.4%	0.0%	0.3%	0.5%
Tibia, Fibula Shaft - 3+	3.4%	1.1%	1.0%	5.8%	0.9%	0.2%	0.5%	1.2%	0.1%	0.0%	0.1%	0.2%
Distal Tibia - 2+	9.7%	3.9%	1.2%	18.2%	2.4%	0.4%	1.5%	3.4%	0.5%	0.1%	0.3%	0.8%
Distal Tibia - 3+	2.3%	0.9%	0.3%	4.2%	0.7%	0.3%	0.1%	1.3%	0.1%	0.0%	0.0%	0.1%
Foot/Ankle - 2+	17.2%	3.9%	8.7%	25.7%	4.0%	0.4%	3.1%	5.0%	1.4%	0.7%	0.0%	3.0%

1. NASS-CDS - Full frontal, offset, SOI; PDOFs of 320 to 40 deg; no center narrow and no unknown PDOF cases

2. Vehicle to vehicle/large fixed object (large tree, medium/large pole, concrete barrier/wall/building/bridge/ditch/culvert); rollover=0; bagdeply=1; vehage<=10; no ejection (P_d=0.14%)

3. No Delta V restrictions (P_d=1.19%)

4. No Delta V or Damage Extent Restrictions (P_d=13.30%)

9.3.2 Fleet Data Injury Values

Table 9.4 and Table 9.5 show the injury value summary for the full frontal and left oblique driver tests with the THOR-50M, respectively. The full frontal tests are from eight vehicles while the left oblique test is from 14 (APPENDIX D).

Table 9.4. Full Frontal Fleet Injury Value Summary, THOR-50M Driver (n=8).

				95% CI			
Injury Measure	**Avg**	**SD**	**CI/2**	**Lwr**	**Upr**	**Min**	**Max**
HIC_{15}	306	76	52	254	359	229	448
BrIC	0.68	0.11	0.08	0.60	0.76	0.53	0.85
Nij	0.43	0.11	0.07	0.35	0.50	0.29	0.63
Neck Tension (N)	1544	458	317	1227	1861	1083	2481
Chest Deflection (mm)	49.9	8.6	5.99	43.9	55.9	38.0	65.5
Abdomen Deflection (mm)	61.2	4.1	2.82	58.3	64.0	53.9	65.0
Acetabulum Peak F (N)	2020	725	502	1518	2523	1148	3384
Femur Peak F (N)	3851	1297	899	2952	4750	2502	6727
Tibia Upr Peak F (N)	2171	813	563	1608	2735	1034	3627
Tibia Lower Peak F (N)	3571	1061	735	2836	4306	2176	5076
Tibia Moment Peak (Nm)	82	21	15	67	97	56	111

Table 9.5. Left Oblique Fleet Injury Value Summary, THOR-50M Driver (n=14).

				95% CI			
Injury Measure	**Avg**	**SD**	**CI/2**	**Lwr**	**Upr**	**Min**	**Max**
HIC_{15}	222	66	35	187	256	103	310
BrIC	0.87	0.25	0.13	0.74	1.01	0.58	1.28
Nij	0.48	0.11	0.06	0.42	0.53	0.29	0.64
Neck Tension (N)	1811	409	214	1597	2025	1009	2392
Chest Deflection (mm)	52.1	5.5	2.9	49.3	55.0	42.7	62.3
Abdoment Deflection (mm)	60.7	4.9	2.6	58.1	63.3	52.3	67.7
Acetabulum Peak F (N)	2838	897	470	2368	3308	1828	4673
Femur Peak F (N)	4950	2106	1103	3846	6053	2401	9184
Tibia Upper Peak F (N)	2067	838	439	1628	2506	812	4218
Tibia Lower Peak F (N)	3309	1319	691	2618	4000	1504	5832
Tibia Moment Peak (Nm)	134	36	19	115	153	91	204

9.3.3 Injury Risk Point Estimates and Confidence Intervals

Table 9.6 and Table 9.7 show the injury risk summary for the full frontal and left oblique driver tests with the THOR-50M, respectively. The full frontal tests are from eight vehicles while the left oblique test is from 14 (see APPENDIX D for the make, model and model year of vehicles tested along with the NHTSA test number).

Table 9.6 – Fleet injury risk summary for full frontal tests with THOR-50M seated in driver's seat (n=8).

				95% CI			
Injury Measure - Severity	Mean	SD	CI/2	Lwr	Upr	Min	Max
HIC_{15} - 2+	7.5%	4.1%	2.9%	4.6%	10.3%	3.5%	15.6%
HIC_{15} - 3+	1.2%	1.1%	0.7%	0.45%	1.9%	0.3%	3.4%
BrIC - 3+	13.0%	12.4%	8.6%	4.4%	21.6%	0.1%	34.3%
BrIC - 4+	9.5%	9.2%	6.4%	3.1%	15.8%	0.0%	25.5%
Nij - 2+	13.0%	7.1%	4.9%	8.1%	17.9%	6.1%	28.3%
Nij - 3+	5.2%	2.6%	1.8%	3.3%	7.0%	2.6%	10.8%
Neck Tension - 3+	3.3%	2.5%	1.7%	1.6%	5.0%	1.6%	9.1%
Chest - 3+	45.6%	14.9%	10.3%	35.3%	55.9%	25.2%	72.1%
Abdomen - 3+	8.4%	2.5%	1.7%	6.7%	10.1%	4.4%	11.0%
Acetabulum Force - 2+	7.6%	15.6%	10.8%	0.0%	18.4%	0.0%	44.9%
Femur Force - 2+	5.6%	6.8%	4.7%	0.9%	10.3%	1.6%	22.2%
KTH Peak - 2+	9.4%	14.7%	10.2%	0.0%	19.6%	1.6%	44.9%
Tibia Force Upper - 2+	2.4%	1.8%	1.2%	1.2%	3.6%	0.8%	6.3%
Tibia Force Lower - 2+	7.0%	1.8%	1.3%	5.7%	8.3%	4.3%	10.2%
Tibia Moment - 2+	1.0%	0.7%	0.5%	0.5%	1.5%	0.2%	2.1%
Tib/Fib Peak - 2+	7.0%	1.8%	1.3%	5.7%	8.3%	4.3%	10.2%

Table 9.7 – Fleet injury risk summary for left oblique tests with THOR-50M seated in driver's seat (n=14).

				95% CI			
Injury Measure - Threshold	Avg	SD	CI/2	Lwr	Upr	Min	Max
HIC_{15} - 2+	3.7%	2.5%	1.3%	2.4%	5.0%	0.3%	7.4%
HIC_{15} - 3+	0.4%	0.4%	0.2%	0.2%	0.6%	0.0%	1.0%
BrIC - 3+	37.0%	32.3%	16.9%	20.1%	53.9%	2.0%	85.2%
BrIC - 4+	29.9%	27.6%	14.4%	15.4%	44.3%	1.4%	73.8%
Nij - 2+	16.4%	7.2%	3.8%	12.6%	20.1%	6.0%	30.4%
Nij - 3+	6.4%	2.7%	1.4%	5.0%	7.8%	2.6%	11.7%
Neck Tension - 3+	4.4%	2.0%	1.0%	3.4%	5.4%	1.4%	8.2%
Chest - 3+	49.6%	9.6%	5.0%	44.6%	54.7%	32.9%	67.3%
Abdomen - 3+	7.1%	4.1%	2.2%	5.0%	9.3%	0.0%	13.5%
Acetabulum Force - 2+	26.7%	30.9%	16.2%	10.5%	42.8%	0.3%	89.5%
Femur Force - 2+	13.9%	17.2%	9.0%	4.9%	22.9%	1.5%	59.9%
KTH Peak - 2+	27.7%	30.0%	15.7%	11.9%	43.4%	1.8%	89.5%
Tibia Force Upper - 2+	2.4%	2.3%	1.2%	1.2%	3.6%	0.7%	9.9%
Tibia Force Lower - 2+	7.7%	4.4%	2.3%	5.4%	10.0%	3.6%	18.1%
Tibia Moment - 2+	5.0%	4.5%	2.3%	2.6%	7.3%	1.1%	15.3%
Lower Leg Peak - 2+	8.4%	5.3%	2.8%	5.6%	11.2%	1.1%	18.1%

Table 9.8 shows the field data estimates and confidence interval for the 40-75 kph severity crashes as described earlier. Figure 9.2 and Figure 9.3 show the tabulated results in a bar chart format with bracketed 95% confidence intervals for frontal versus field and oblique versus field, respectively. For both full frontal and oblique, it can be seen that that roughly half of the field and fleet confidence intervals are overlapping. Again, this means that we cannot reject the hypothesis that the two rates are

the same when the 95% confidence intervals are overlapping. In some cases the field and fleet confidence intervals are not overlapping. In the full frontal condition, the fleet predicted risk with THOR-50M is "higher" than the field in some cases (HIC_{15} 2+, Nij 2+, Nij 3+, Neck Tension 3+, Chest Deflection 3+, Abdomen Deflection 3+) while other fleet confidence intervals are "lower" than the field (Tibia Moment 2+, Tibia/Fibula Peak Risk 2+).

In contrast to the full frontal fleet data, the HIC_{15} 2+, Tibia/Fibula shaft and Tibia/Fibula combined confidence intervals in oblique overlap the field data-based confidence intervals. BrIC 3+, BrIC 4+ and acetabulum 2+ can be added to the list of metrics that are higher in the fleet than in the field.

Table 9.8 - Field data estimates for frontal crashes, NASS-CDS 2000-2014.

	Point		95% CI	
Injury - Severity	Estimate	CI/2	Lwr	Upr
Skull or Facial Fracture - 2+	1.6%	1.3%	0.4%	2.9%
Skull or Facial Fracture - 3+	0.4%	0.5%	0.0%	0.9%
Brain - 3+	5.3%	5.7%	0.0%	10.9%
Brain - 4+	2.7%	2.3%	0.4%	4.9%
Neck - 2+	2.4%	1.0%	1.4%	3.5%
Neck - 3+	0.7%	0.7%	0.0%	1.4%
Thorax - 3+	12.5%	3.6%	8.9%	16.0%
Abdomen - 3+	1.8%	2.3%	0.0%	4.1%
Hip/Pelvis - 2+	5.3%	4.7%	0.6%	10.0%
Thigh - 2+	8.1%	4.0%	4.0%	12.1%
Knee - 2+	4.4%	3.3%	1.1%	7.8%
Knee, Thigh or Hip - 2+	14.9%	7.5%	7.4%	22.5%
Proximal Tibia - 2+	2.6%	1.8%	0.8%	4.5%
Distal Tibia - 2+	9.7%	8.5%	1.2%	18.2%
Tibia, Fibula Shaft - 2+	9.4%	3.6%	5.8%	13.0%
Tibia / Fibula ALL - 2+	16.8%	8.1%	8.7%	25.0%

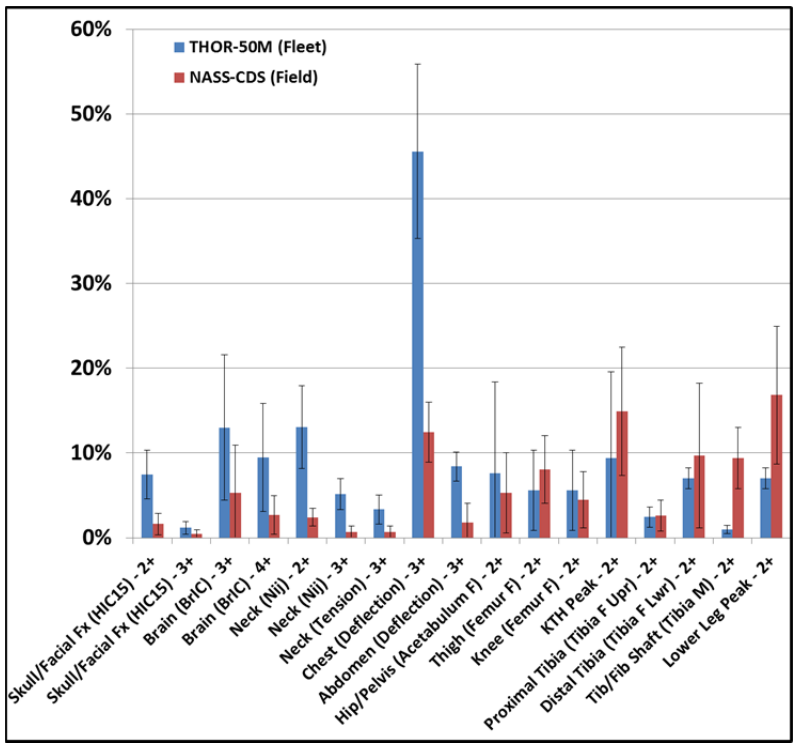

Figure 9.2. Full frontal fleet predicted injury risk with a driver seated THOR-50M versus field estimates and associated 95% confidence intervals.

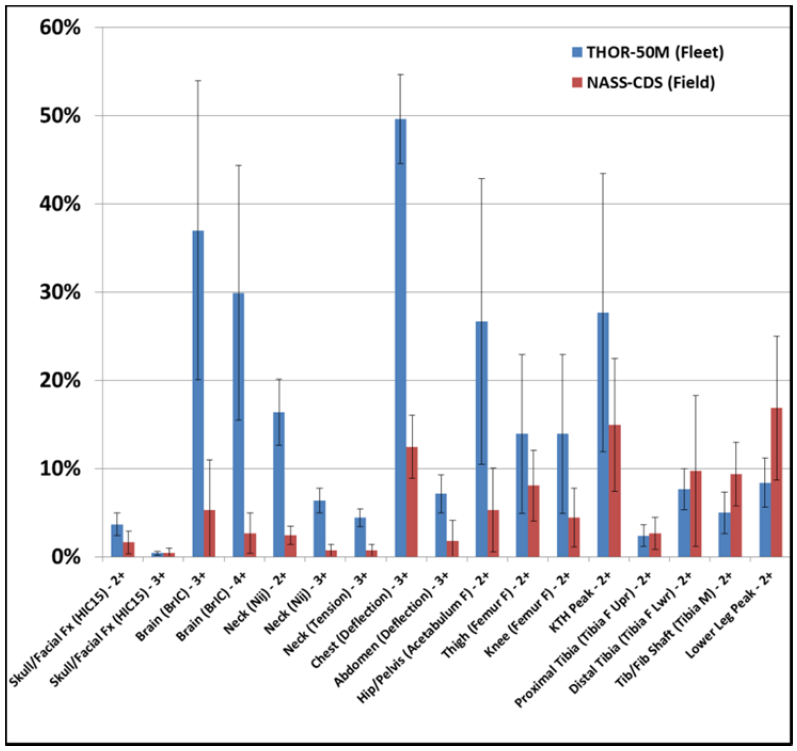

Figure 9.3. Oblique fleet predicted injury risk with a driver seated THOR-50M versus field estimates and associated 95% confidence intervals.

Collinear and frontal conditions can be separated into two separate domains for purposes of comparison. Though, as noted earlier this results in class 4 ("rare type") relative domain sizes (P_d < 0.1%). Regardless of whether oblique and collinear crashes are separate or together, the oblique fleet data for chest and BrIC does not overlap the field data. However, it can be seen that the risk of brain injuries (point estimate of 6.5% vs. 3.7%) is higher in oblique than collinear or zero degree frontal crashes. Point estimates for KTH measures are also higher in oblique than collinear frontal field cases. Though, as is the case with all measures in Table 9.9, the confidence intervals between oblique and collinear overlap. Thus, we cannot reject the hypothesis that the point estimates are the same.

Table 9.9. Comparison of oblique vs. collinear point estimates and confidence intervals.

Injury Risk: All Injuries by Body Region, Age 15+, Belted NCAP Frontal Drivers (2000-2014)[1]						
	Oblique Cases[2]			Collinear Cases[3]		
Injury	Point Estimate	CI Lower	CI Upper	Point Estimate	CI Lower	CI Upper
MAIS 2+	53.3%	36.2%	70.5%	53.7%	39.7%	67.7%
MAIS 3+	28.8%	18.5%	39.0%	30.4%	23.2%	37.6%
Skull or Facial Fracture - 2+	2.3%	0.6%	3.9%	0.8%	0.0%	1.7%
Skull or Facial Fracture - 3+	0.6%	0.0%	1.5%	0.1%	0.0%	0.38%
Brain - 3+	6.5%	0.0%	13.5%	3.7%	0.0%	7.7%
Brain - 4+	2.9%	0.0%	6.0%	2.3%	0.1%	4.5%
Neck - 2+	3.5%	1.8%	5.3%	0.9%	0.0%	1.9%
Neck - 3+	0.6%	0.0%	1.4%	0.8%	0.0%	1.7%
Thorax - 2+	9.5%	4.2%	14.7%	22.7%	17.9%	27.6%
Thorax - 3+	7.2%	3.3%	11.1%	19.4%	13.3%	25.4%
Abdomen - 3+	1.6%	0.0%	3.6%	2.1%	0.0%	5.0%
Knee, Thigh or Hip - 2+	17.5%	8.9%	26.1%	11.6%	4.1%	19.1%
Hip/Pelvis - 2+	7.5%	0.7%	14.3%	2.4%	0.0%	5.1%
Thigh - 2+	9.3%	4.4%	14.2%	6.5%	2.9%	10.0%
Knee - 2+	4.7%	1.5%	7.9%	4.1%	0.0%	8.4%
Tibia / Fibula ALL - 2+	16.8%	11.9%	21.8%	16.8%	1.5%	32.2%
Proximal Tibia - 2+	3.8%	0.5%	7.1%	1.1%	0.0%	2.4%
Tibia, Fibula Shaft - 2+	12.7%	8.3%	17.0%	5.1%	0.0	8.6%
Distal Tibia - 2+	6.6%	3.6%	9.7%	13.7%	0.0%	30.0%

1. NASS-CDS - Full frontal, offset, SOI; PDOFs of 320 to 40 deg; no center narrow and no unknown PDOF cases; vehicle to vehicle/large fixed object (large tree, medium/large pole, concrete barrier/wall/building/bridge/ditch/culvert); rollover=0; bagdeply=1; vehage<=10; no ejection; 40-75 kph; extent 3-6

2. Oblique cases - PDOFs include 320 to 350 and 10-40 (P_d =0.079%)

3. Collinear cases - PDOF = 0 (P_d =0.060%)

Figure 9.4 shows mean injury risk and 95% confidence interval for THOR-50M in full frontal and left oblique tests. In this case, the comparison is limited to the eight vehicles that were tested in both conditions. Similar to the field data, BrIC (brain) is higher in oblique than full frontal as are KTH measures. In contrast to the field, chest injury risk is higher in left oblique than in the full frontal

condition. However, it should be noted that the confidence intervals overlap for all injury risks other than for BrIC.

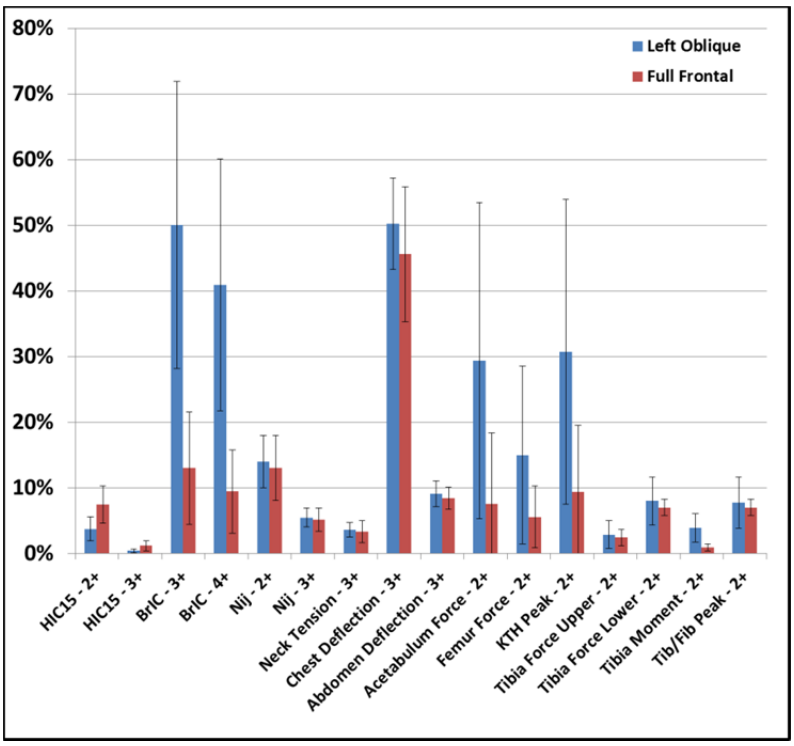

Figure 9.4. THOR-50M injury risk: Left oblique vs. full frontal mean and 95% confidence intervals (n=8).

The design of experiments described in APPENDIX C demonstrates the sensitivity of BrIC to different crash and restraint parameters. Of note, it can be seen in Figure C.8 and Figure C.10 as well as Figure C.11 the positive correlation between BrIC and change in PDOF (i.e. getting further away from zero degrees). For example, it can be seen in Figure C.10 that the range of BrIC at 0-degrees across the various parameters is from under 0.5 to roughly 0.8 while at a PDOF of 340 (20 degrees in the figure, same as the PDOF in NHTSA's oblique crash test condition) BrIC ranges from just under 0.5 to over 1.5. These DOE-based ranges compare well with the ranges seen in fleet testing with full frontal BrIC values ranging from 0.53 to 0.85 (Table 9.4) and in oblique where BrIC ranged from 0.58 to 1.28 (Table 9.5).

It would be desirable to be able to estimate the risk of injury in crash severities and orientations that match NHTSA's oblique test (~340-degree PDOF). However, the PDOF of 340 degrees represents roughly 10% of the total cases when looking at the three groupings of frontal crashes described in Table 9.3 (see Figure H.2 in the APPENDIX H). Looking only at 340 degree PDOF cases for the severity range selected results in a very small sample based on very few raw count cases.

9.4 Discussion and Limitations

In attempting to be no smaller than a class 3 or "mini" domain, we could not separate out full frontal and left obliques and maintain severity (delta V, damage extent), restraint status and vehicle age

restrictions. While this gives an overall picture of field injury in frontal crashes, it limits our ability to directly compare NHTSA's oblique and full-frontal collinear crash test results versus the field.

There are also numerous occupant, crash and vehicle factors parameters (i.e. independent variables) that are not adjusted for due to sample size issues or due to unknown and/or unavailable data. Many of these factors may be positively correlated (such as increased age) or negatively correlated (such as pre-impact braking or bracing) with the respective rates of injury that are estimated in the field data.

Age, gender, seat track position, height, and weight are examples of NASS-CDS coded variables that were not restricted (See APPENDIX H). Other factors such as the occupant's pre-impact position, pre-impact braking, pre-impact bracing/muscle tone, performance of restraints (such as fit, deployment timing) cannot be accounted for. In particular, pre-impact braking has been shown to be associated with a reduced risk of injury in frontal crashes versus no braking (Craig et al., 2011). Studies have demonstrated the potential for reduced chest displacement and thus chest injury risk with increased levels of bracing or muscle activation (Bose and Crandall, 2008; Iwamoto et al. 2011)

Given the fact that many sensitive parameters are either unknown or left unfiltered and given the small sample size when attempting to limit to crash severities comparable to the NHTSA test conditions, the results of the field data point estimates (Table 9.8, Table 9.9) may not accurately represent the actual risk of injury for an occupant of similar anthropometry, seated similarly to the THOR-50M in mid-seat track position in crashes resulting in the delta V and PDOF observed in NHTSA's left oblique and full frontal crash test conditions. Additionally, it is possible that our fleet testing (limited to 8 full frontals and 14 left obliques) may not represent the average vehicle in the current new vehicle fleet or the average vehicle in the field data sample. Of note, the models of vehicles represented in APPENDIX D and used for full frontal and oblique fleet comparisons to the field represent roughly 8% and 12% of total vehicle sales, respectively.

While it is desirable to make definitive comparisons and conclusions when contrasting field data- and fleet testing-based injury risks, the limitations described above make these comparisons subject to many limitations. In utilizing field data of similar crash severity (delta V, damage extent), restraint system status (belted, airbag deployment) and occupant types (adult drivers) similar to those in fleet tests, while removing rollover and ejection cases left very small sample sizes, the resulting sample size is small (raw and weighted). Couple this with the limitation described above regarding crash, vehicle, restraint system and occupant variables that could not be accounted for and the limited size of the fleet test sample, and the resulting comparisons of confidence intervals (overlapping or not) need to be used with caution.

Limitations aside, the fleet, field and human body modeling based analyses all show a higher risk or brain injury in oblique crash conditions than in 0-degree or collinear conditions. Similarly, field and fleet data also both suggest a higher risk for knee/thigh/hip injuries in oblique crashes versus collinear crashes. Additionally, lower extremity field and fleet data compared well for both full frontal and oblique where the majority of confidence intervals were overlapping. For both full frontal and oblique, the predicted thoracic injury risk was higher for in fleet testing than predicted by the field. As discussed

in earlier in the report, the current THOR-50M are cadaver-based risk functions with no adjustment for living versus post-mortem subjects or clinical versus experimental rib fracture detection. In the current NCAP (NCAP, 2008) the risk function that was applied set the AIS 3+ 1995/1998 based limit at seven fractured ribs instead of four as is described in AIS (AAAM, 1998). If NHTSA entertained changing the chest injury risk function as has previously be done, it would bring the mean risk and associated confidence interval closer to the estimate from the field data. However, the reduction in risk for a given deflection when considering a risk function based on 6 or 7 fractured ribs (Figure 5.14) would not reduce the risk to the level where fleet and field confidence intervals for chest injury risk overlap.

10 REFERENCES

Alquié, A., 1865. Étude Clinique et Expérimentale de la Commotion Traumatique ou ébranlement de L'encéphale. *Gazette Medical de Paris*, 20, 226–230; 254–256; 314–319; 382–385; 396–398; 463–466; 500–504.

Association for Advancement of Automatic Medicine, 1998. Abbreviated Injury Scale 1990, Update 1998. AAAM, Des Plaines, IL.

Association for Advancement of Automatic Medicine, 2008. Abbreviated Injury Scale 2005, Update 2008. AAAM, Barrington, IL.

Banglmaier, R.F., Dvoracek-Driksna, D., Oniang'o, T.E. and Haut, R.C., 1999. Axial compressive load response of the 90 flexed human tibiofemoral joint. In: *Proceedings of the 43rd Stapp Car Crash Conference* (No. 99SC08), 127-139.

Begeman, P., Balakrishnan, P., Levine, R. and King, A., 1993. Dynamic human ankle response to inversion and eversion. In: *Proceedings of the 37th Stapp Car Crash Conference* (No. 933115).

Begeman P.C., Aekbote K., 1996. Axial load strength and some ligament properties of the ankle joint. In: *6th Injury Prevention Through Biomechanics Symposium*. Detroit, MI: Wayne State University, 125–135.

Blincoe, L. J., Miller, T. R., Zaloshnja, E., and Lawrence, B. A., 2015. The economic and societal impact of motor vehicle crashes, 2010. (Report No. DOT HS 812 013) Washington, DC: National Highway Traffic Safety Administration.

Bose, D., Crandall, J. R., 2008. Influence of active muscle contribution on the injury response of restrained car occupants. *Ann Adv Automot Med* 52, pp. 61-72.

Carter, J.W., Ku, G.S., Nuckley, D.J. and Ching, R.P., 2002. Tolerance of the cervical spine to eccentric axial compression. In: *Proceedings of the 46th Stapp Car Crash Conference* (No. 2002-22-0022).

Chancey, V.C., Nightingale, R.W., Van Ee, C.A., Knaub, K.E. and Myers, B.S., 2003. Improved estimation of human neck tensile tolerance: reducing the range of reported tolerance using anthropometrically correct muscles and optimized physiologic initial conditions. *Stapp Car Crash Journal*, 47, 135-153.

Craig, M.J., Scarboro, M. and Ridella, S.A., 2011. Predicting occupant outcomes with EDR data. In: *Proceedings of the 22nd International Technical Conference on the Enhanced Safety of Vehicles,* (No. 11-0326).

Crandall, J., 2013. Injury criteria development: THOR Metric SD-3 shoulder advanced frontal crash test dummy. NHTSA Biomechanics Database (Report b11117-1).

Crandall, J., 2014. ATD thoracic response test development, 20 degree far side oblique frontal, front passenger position, Tests UVAS0243-245. NHTSA Biomechanics Database (Report b11500-1).

Crandall, J., 2015. ATD thoracic response test development, Gold standard buck condition 3: Force limited belt, 30 km/h 30 degree oblique frontal, Tests UVAS0313-315. NHTSA Biomechanics Database (Report b11518-1).

Dibb, A., Nightingale, R., Chauncey, V., Fronheiser, L., Tran, L., Ottaviano, D., and Myers B., 2006. Comparative structural neck responses of the THOR-NT, Hybrid III, and human in combined tension-bending and pure bending. *Stapp Car Crash Journal*, 50, 567-581.

Dibb, A.T., Nightingale, R.W., Luck, J.F., Chancey, V.C., Fronheiser, L.E. and Myers, B.S., 2009. Tension and combined tension-extension structural response and tolerance properties of the human male ligamentous cervical spine. *Journal of Biomechanical Engineering*, 131(8), pp 081008-1.

Dibb, A.T., 2011. Pediatric head and neck dynamic response: A computational study [PhD thesis]. Durham, NC: Duke University.

Dischinger, P.C., Burgess, A.R., Cushing, B.M., O'Quinn, T.D., Schmidhauser, C.B., Ho, S.M., Juliano, P.J. and Bents, F.D., 1994. Lower extremity trauma in vehicular front-seat occupants: patients admitted to a level 1 trauma center. *Society of Automotive Engineers* (No. 940710).

Dischinger, P.C., Read, K.M., Kufera, J.A., Kerns, T.J., Burch, C.A., Jawed, N., Ho, S.M. and Burgess, A.R., 2004. Consequences and costs of lower extremity injuries. In: *Proceedings of Association for the Advancement of Automotive Medicine Annual Conference*, 48, 339-353.

Donnelly, B.R., Roberts, D.P., 1987. Comparison of cadaver and Hybrid III dummy response to axial impacts of the femur. In: *Proceedings of the 31st Stapp Car Crash Conference* (No. 872204), 105-116.

Eigen, A.M., Martin, P.G., 2005. Identification of real world injury patterns in aid of dummy development. In: *Proceedings of the 19th International Technical Conference on the Enhanced Safety of Vehicles Conference* (No. 05-0219).

Elhagediab, A., Rouhana, S., 1998. Patterns of abdominal injury in frontal automotive crashes. In: *Proceedings of the 16th International Technical Conference on the Enhanced Safety of Vehicles* (No. 98-S1-W-26).

Eppinger, R., Sun, E., Bandak, F., Haffner, M., Khaewpong, N., Maltese, M., Kuppa, S., Nguyen, T., Takhounts, E., Tannous, R., Zhang, A., Saul, R., 1999. Development of improved injury criteria for the assessment of advanced automotive restraint systems–II. Washington, DC: National Highway Traffic Safety Administration.

Foret-Bruno, J., Hartemann, F., Thomas, C., Fayon, A., Tarrière, C., Got, C., Patel, A., 1978. Correlation between thoracic lesions and force values measured at the shoulder of 92 belted occupants involved in real accidents. In: *Proceedings of the 22nd Stapp Car Crash Conference* (No. 780892), 271-292.

Forman, J., Lessley, D., Kent, R., Bostrom, O., Pipkorn, B., 2006a. Whole-body kinematic and dynamic response of restrained PMHS in frontal sled tests. *Stapp Car Crash Journal*, 50, 299-336.

Forman, J., Lessley, D., Shaw, C.G., Evans, J., Kent, R., Rouhana, S.W., Prasad, P., 2006b. Thoracic response of belted PMHS, the Hybrid III, and the THOR-NT mid-sized male surrogates in low speed, frontal crashes. *Stapp Car Crash Journal*, 50, 191-215.

Forman, J., Lopez-Valdes, F., Lessley, D., Kindig, M., Kent, R., Ridella, S., Bostrom, O., 2009. Rear seat occupant safety: an investigation of a progressive force-limiting, pretensioning 3-point belt system using adult PMHS in frontal sled tests. *Stapp Car Crash Journal*, 53, 49-74.

Frampton, R., Lenard, J., Compigne, S., 2012. An in-depth study of abdominal injuries sustained by car occupants in frontal crashes. In: *Annals of Advances in Automotive Medicine 56th Annual Conference*, 56, 137-149.

Funk, J.R., Tourret, L.J. and Crandall, J.R., 2000. Experimentally produced tibial plateau fractures. In: *Proceedings of the 2000 International Conference on the Biomechanics of Impact*, 171-182.

Funk, J.R., Crandall, J.R., Tourret, L.J., MacMahon, C.B., Bass, C.R., Patrie, J.T., Khaewpong, N. and Eppinger, R.H., 2002. The axial injury tolerance of the human foot/ankle complex and the effect of Achilles tension. *Journal of Biomechanical Engineering*, 124(6), 750-757.

Funk, J.R., Srinivasan, S.C., Crandall, J.R., Khaewpong, N., Eppinger, R.H., Jaffredo, A.S., Potier, P. and Petit, P.Y., 2002. The effects of axial preload and dorsiflexion on the tolerance of the ankle/subtalar joint to dynamic inversion and eversion. *Stapp Car Crash Journal*, 46, 245-265.

Funk, J.R., Rudd, R.W., Kerrigan, J.R. and Crandall, J.R., 2004. The effect of tibial curvature and fibular loading on the tibia index. *Traffic Injury Prevention*, 5(2), 164-172.

Gabler, L.F., Crandall, J.R, Panzer, M.B., 2016. Investigating brain injury tolerance in the sagittal plane using a finite element model of the human head. *International Journal of Automotive Engineering*, 7(1), 37-43.

Gennarelli, T.A., Ommaya, A.K. , Thibault, L.E., 1971. Comparison of linear and rotational accelerations in experimental cerebral concussion. In: *Proceedings of the 15th Stapp Car Crash Conference*, 797-803.

Gennarelli, T.A., Thibault, L.E., and Ommaya, A.K., 1972. Pathophysiologic responses to rotational and translational accelerations of the head. *Stapp Car Crash Journal,* 16, 296-308.

Gennarelli, T.A., 1985. The state of the art of head injury biomechanics. In: *Proceedings of the American Association for the Advancement of Automotive Medicine*, 29, 447-463.

Glaister, D.H., 1975. Human tolerance to impact acceleration, *Injury*, 9, 191-198.

Goggio, A.F., 1941. The mechanism of contre-coup injury. *Journal of Neurology and Psychiatry*, 4(1), 11-22.

Goldsmith, W. and Monson, K.L., 2005. The state of head injury biomechanics: past, present, and future, Part 2: Physical experimentation. *Critical Reviews Biomedical Engineering,* 33(2), 105–207.

Hardy, W., Schneider, L., Rouhana, S., 2001. Abdominal impact response to rigid-bar, seatbelt, and airbag loading. *Stapp Car Crash Journal*, 45, 1-32.

Haffner, M., Rangarajan, N., Artis, M., Beach, D., Eppinger, R., Shams, T., 2001. Foundations and elements of the NHTSA THOR Alpha ATD design. In: *Proceedings of the 17th International Technical Conference on the Enhanced Safety of Vehicles* (No. 458).

Hasija, V., Takhounts, E.G. and Ridella, S.A., 2011. Evaluation of statistical methods for generating injury risk curves. In: *Proceedings of the 22nd International Technical Conference on the Enhanced Safety of Vehicles* (No. 11-0331).

Hertz, E., 1993. A note on the head injury criterion (HIC) as a predictor of the risk of skull fracture. In: *Proceedings of the 37th Association for the Advancement of Automotive Medicine Annual Conference*, 303-311.

Hess, R.L., Weber, K., Melvin, J.W., 1980. Review of literature and regulation relating to head impact, tolerance and injury criteria. (Report no. UM-HSRI-80-52-I) Ann Arbor, MI: University of Michigan Transportation Research Institute.

Holbourn, A.H.S., 1943. Mechanics of head injuries. *The Lancet*, 242, 438–441.

Hosmer, D. W., Jr. and Lemeshow, S., 2000. *Applied logistic regression.* 2nd ed. New York: John Wiley & Sons.

Insurance Institute for Highway Safety, 2016. Small overlap frontal crashworthiness evaluation test protocol (Version IV). http://www.iihs.org/Ratings/Protocols/current/small_overlap_test_protocol.pdf

Ivarsson, B.J., Manaswi, A., Genovese, D., Crandall, J.R., Hurwitz, S.R., Burke, C. and Fakhry, S., 2008. Site, type, and local mechanism of tibial shaft fracture in drivers in frontal automobile crashes. *Forensic Science International*, 175(2), 186-192.

Iwamoto, M., Nakahira, Y., Sugiyama, T., 2011. Investigation of pre-impact bracing effects for injury outcome using and active human FE model with 3D geometry of muscles. In: *Proceedings of the 22nd International Conference on the Enhanced Safety of Vehicles*, Washington, DC.

Jaffredo, A., Potier, P., Robin, S., Le Coz, J.Y. and Lassau, J.P., 2000. Cadaver lower limb dynamic response in inversion-eversion. In: *Proceedings of the 2000 International IRCOBI Conference on the Biomechanics of Impact*, 183-194.

Kent, R.W., Crandall, J.R., Bolton, J., Prasad, P., Nusholtz, G., Mertz, H., 2001. The influence of superficial soft tissues and restraint condition on thoracic skeletal injury prediction. *Stapp Car Crash Journal*, 45, 183-204.

Kent, R., Shaw, C.G., Lessley, D.J., Crandall, J.R. and Svensson, M.Y, 2003. Comparison of belted Hybrid III, THOR, and cadaver thoracic responses in oblique frontal and full frontal sled tests. In: *Proceedings of Society of Automotive Engineers 2003 World Congress and Exhibition* (No. 2003-01-0160).

Kent, R., Stacey, S., Kindig, M., Forman, J., Woods, W., Rouhana, S., Higuchi, K., Tanji, H., St. Lawrence, S., Arbogast, K., 2006. Biomechanical response of the pediatric abdomen, Part 1: Development of an experimental model and quantification of structural response to dynamic belt loading. *Stapp Car Crash Journal*, 50, 1-26.

Kent, R., Stacey, S., Kindig, M., Woods, W., Evans, J., Rouhana, S., Higuchi, K., Tanji, H., St. Lawrence, S., Arbogast, K., 2008. Biomechanical response of the pediatric abdomen, Part 2: Injuries and their correlation with engineering parameters. *Stapp Car Crash Journal*, 52, 135-166.

Kent, R.W., Lopez-Valdes, F.J., Dennis, N.J., Lessley, D., Forman, J., Higuchi, K., Tanji, H., Ato, T., Kameyoshi, H., Arbogast, K., 2011. Assessment of a three-point restraint system with a pre-tensioned lap belt and an inflatable, force-limited shoulder belt. *Stapp Car Crash Journal*, 55, 141-159.

Keon, T., 2016. Alternative approaches to occupant response evaluation in frontal impact crash testing. *SAE International Journal of Transportation Safety* (No. 2016-01-1540), 4, 202-217.

Kitagawa, Y., Ichikawa, H., King, A.I. and Levine, R.S., 1998. A severe ankle and foot injury in frontal crashes and its mechanism. In: *Proceedings of the 42nd Stapp Car Crash Conference* (No. 983145).

Klinich, K., Saul, R., Auguste, G., Backaitis, S., and Kleinberger, M. 1996. Techniques for developing child dummy protection reference values. National Highway Traffic Safety Administration Report.

Klinich, K., Flannagan, C., Nicholson, K., Schneider, L., Rupp, J., 2009. Abdominal injury in motor-vehicle crashes. (Report No. UMTRI-2009-40) Ann Arbor, MI: University of Michigan Transportation Research Institute.

Kroell, C., Schneider, D., and Nahum, A., 1971. Impact tolerance and response of the human thorax. *Society of Automotive Engineers* (No. 710851).

Kroell, C., Schneider, D., and Nahum, A., 1974. Impact tolerance and response of the human thorax II. *Society of Automotive Engineers* (No. 741187).

Kuppa, S., Eppinger, R., 1998. Development of an improved thoracic injury criterion. In: *Proceedings of the 42nd Stapp Car Crash Conference* (No. 983153).

Kuppa, S., Haffner, M., Eppinger, R., and Saunders, J., 2001. Lower extremity response and trauma assessment using the THOR-Lx/HIIIr and the Denton leg in frontal offset vehicle crashes. *In: Proceedings of the 17th International Technical Conference for the Enhanced Safety of Vehicles* (No. 456).

Kuppa, S., Wang, J., Haffner, M., Eppinger, R., 2001. Lower extremity injuries and associated injury criteria. *In: Proceedings of the 17th International Technical Conference for the Enhanced Safety of Vehicles* (No. 457).

Laituri, T., Prasad, P., Sullivan, K., Frankstein, M., Thomas, R., 2005. Derivation and evaluation of a provisional, age dependent AIS 3+ thoracic risk curve for belted adults in frontal impacts. In: *Proceedings of Society of Automotive Engineers World Congress and Exhibition* (No. 2005-01-0297).

Laituri, T.R., Henry, S., Kachnowski, B., Sullivan, K., 2009. Initial assessment of the next-generation USA frontal NCAP: fidelity of various risk curves for estimated field injury rates of belted drivers. In: *Proceedings of Society of Automotive Engineers World Congress and Exhibition* (No. 2009-01-0386).

Lebarbé, M., Donnelly, B.R., Petit, P., Moorhouse, K., 2015. A frontal response specification for assessing the biofidelity of an anthropometric test dummy: Part 1 - Upper body. In: *Proceedings of International Conference on the Biomechanics of Impact Conference*, 467-485.

Lee, E.L., Craig, M. and Scarboro, M., 2015. Real-world rib fracture patterns in frontal crashes in different restraint conditions. *Traffic Injury Prevention*,16(S2), S115-S123.

Lopez-Valdes, F.J., Lau, A., Lamp, J., Riley, P., Lessley, D.J., Damon, A., Kindig, M., Kent, R.W., Balasubramanian, S., Seacrist, T., Maltese, M.R., Arbogast, K.B., Higuchi, K., Tanji, H., 2010. Analysis of spinal motion and loads during frontal impacts. Comparison between PMHS and ATD. In: *Annals of Advances in Automotive Medicine 54th Annual Conference*, 54, 61-78.

Maiman, D.J., Sances Jr, A., Myklebust, J.B., Larson, S.J., Houterman, C., Chilbert, M. and El-Ghatit, A.Z., 1983. Compression injuries of the cervical spine: a biomechanical analysis. *Neurosurgery*, 13(3), 254-260.

Margulies, S.S. and Thibault, L.E., 1992. A proposed tolerance criterion for future axonal injury in man. *Journal of Biomechanics,* 25(8), 917-923.

Martin, P. G., Scarboro, M., 2011. THOR-NT: Hip injury potential in narrow overlap and oblique frontal crashes. In: *Proceedings of the 22nd International Technical Conference on the Enhanced Safety of Vehicles* (No. 11-0234).

McLean, A.J. and Anderson, R.W.G., 1997. Biomechanics of closed head injury. Chapter 2. In: Reilly, P., Bullock, R. (Eds) *Head injury*. London: Chapman & Hall, 25–37.

McMurry, T., Poplin, G., Forman, J., Ash, J., Shaw, C.G., Crandall, J., "Provisional THOR Chest Injury Risk Function," NHTSA Biomechanics Database (Report b11117-2), 2016a.

McMurry, T., Poplin, G., Forman, J., Ash, J., Shaw, C.G., Crandall, J., "Provisional THOR Chest Injury Risk Function with Frontal and Oblique Sled Tests," NHTSA Biomechanics Database (Report b11514-2), 2016b.

Meaney, D.F., Morrison, B., Bass, C.D., 2014. The mechanics of traumatic brain injury: a review of what we know and what we need to know for reducing its societal burden. *Journal of Biomechanical Engineering,* 136(2), pp 021008.

Melvin J.W., Lighthall J.W., Ueno K., 1993. Brain injury biomechanics. In: Nahum, A.M., Melvin, J.W. (Eds) *Accidental Injury*. New York: Springer-Verlag, 269–290.

Mertz, H.J., Patrick, L.M., 1971. Strength and response of the human neck. *Society of Automotive Engineers* (No. 710855).

Mertz, H.J., Hodgson, V.R., Thomas, L.M., and Nyquist, G.W., 1987. An assessment of compressive neck loads under injury-producing conditions. *Physician and Sports Medicine,* 6(11), 95-106.

Mertz, H.J., Weber, D.A., 1982. Interpretations of the impact responses of a 3-year-old child dummy relative to child injury potential. *Society of Automotive Engineers* (No. 826048).

Mertz, H.J., 1993. Anthropometric test devices. Chapter 4. In: Nahum, A.W., Melvin, J.W. (Eds) *Accidental Injury*. New York: Springer-Verlag.

Mertz, H.J., Prasad, P., 2000. Improved neck injury risk curves for tension and extension moment measurements of crash dummies. In: *Proceedings of the 44th Stapp Car Crash Conference* (No. 2000-01-SC05), 59-76.

Morgan, R., Eppinger, R.H., Marcus, J., 1989. Human cadaver patella-femur-pelvis injury due to dynamic frontal impact to the patella. In: *Proceedings of the 12th International Conference on Experimental Safety Vehicles*.

Morgan, R.M., Eppinger, R.H. and Hennessey, B.C., 1991. Ankle joint injury mechanism for adults in frontal automotive impact. In: *Proceedings of the 35th Stapp Car Crash Conference* (No. 912902).

Morgan, R.M., Eppinger, R.H., Haffner, M.P., Yoganandan, N., Pintar, F.A., Sances, A., Crandall, J.R., Pilkey, W.D., Klopp, G.S., Kallieris, D., Miltner, E., Mattern, R., Kuppa, S.M., and Sharpless, C.L., 1994. Thoracic trauma assessment formulations for restrained drivers in simulated frontal impacts. In: *Proceedings of the 38th Stapp Car Crash Conference* (No. 942206), 15-34.

Mueller, B., MacAllister, A., Nolan, J., Zuby, D., 2015. Comparison of HIC and BrIC head injury risk in IIHS frontal crash tests to real-world head injuries. In: *Proceedings of the 24th International Technical Conference on the Enhanced Safety of Vehicles* (No. 15-0272).

Nahum, A., Smith, R., Ward, C., 1977. Intracranial pressure dynamics during head impact. In: *Proceedings of the 21st Stapp Car Crash Conference* (No. 770922), 337–366.

National Highway Traffic Safety Administration, 2000. Final Economic Assessment: FMVSS No. 208 Advanced Air Bags. www.regulations.gov, NHTSA-2000-7013-0006.

National Highway Traffic Safety Administration, 2005. Biomechanical response requirements of the THOR NHTSA advanced frontal dummy, Revision 2005.1. (Report No: GESAC-05-03), Washington, DC: U.S. Department of Transportation [http://www.nhtsa.gov/DOT/NHTSA/NVS/Biomechanics%20&%20Trauma/THOR-NT%20Advanced%20Crash%20Test%20Dummy/thorbio05_1.pdf]

National Highway Traffic Safety Administration, 2008. Consumer Information; New Car Assessment Program; Final Decision Notice. 73 Federal Register 134, pp 40016-40050.

National Highway Traffic Safety Administration, 2015a. THOR-50M Drawing Package, September 2015 Draft. Docket ID NHTSA-2015-0119-0005.

National Highway Traffic Safety Administration, 2015b. THOR 50th Percentile Male Qualification Procedures Manual DRAFT 2015-10-16. Docket ID NHTSA-2015-0119-0016.

National Highway Traffic Safety Administration, 2016a. NCAP. Docket ID NHTSA-2015-0119-0001.

National Highway Traffic Safety Administration, 2016b. THOR-50M Drawing Package. Docket ID NHTSA-2015-0119.

Neathery, R., Kroell, C., Mertz, H., 1975. Prediction of thoracic injury from dummy responses. *Society of Automotive Engineers* (No. 751151).

Nightingale, R.W., McElhaney, J.H., Camacho, D.L., Kleinberger, M., Winkelstein, B.A. and Myers, B.S., 1997. The dynamic responses of the cervical spine: buckling, end conditions, and tolerance in compressive impacts. In: *Proceedings of the 41st Stapp Car Crash Conference* (No. 973344).

Nightingale, R.W., Chancey, V.C., Ottaviano, D., Luck, J.F., Tran, L., Prange, M. and Myers, B.S., 2007. Flexion and extension structural properties and strengths for male cervical spine segments. *Journal of Biomechanics*, 40(3), 535-542.

Nuckley, D.J., Hertsted, S.M., Eck, M.P. and Ching, R.P., 2005. Effect of displacement rate on the tensile mechanics of pediatric cervical functional spinal units. *Journal of biomechanics*, 38(11), 2266-2275.

Nusholtz, G.S., Lux, P., Kaiker, P.S., Janicki, M.A., 1984. Head impact response - skull deformation and angular accelerations. In: *Proceedings of the 28th Stapp Car Crash Conference* (No. 841657), 41-74.

Nusholtz, G.S., Kaiker, P.S., Lehman, R.J., 1988. Steering system abdominal impact trauma. (Report No. UMTRI-88-19) Ann Arbor, MI: University of Michigan Transportation Research Institute.

Nusholtz, G.S., Kaiker, P.S., 1994. Abdominal response to steering wheel loading. In: *Proceedings of the International Technical Conference on the Enhanced Safety of Vehicles* (No. 94-S1-O-05).

Nyquist, G.W., Cheng, R., El-Bohy, A.A. and King, A.I., 1985. Tibia bending: strength and response. *Society of Automotive Engineers* (No. 851728).

Nyquist, G.W., Begeman, P., King, A.I, and Mertz, H.J., 1980. Correlation of field injuries and GM hybrid III dummy responses for lap-shoulder belt restraint. *Journal of Biomechanical Engineering,* 102(2), 103-109.

Ommaya, A.K., 1984. Biomechanics of head injury: Experimental aspects. In: Nahum, A., Melvin J.W. (Eds) *The Biomechanics of Trauma*. East Norwalk, CT: Appleton-Century-Crofts, 245-269.

Panjabi, M.M., Oda, T., Crisco III, J.J., Oxland, T.R., Katz, L., and Nolte, L.P. 1991. Experimental study of atlas injuries I: Biomechanical analysis of their mechanisms and fracture patterns. *Spine,* 16, S460-S465.

Parent, D., Craig, M., Ridella, S., McFadden, J., 2013. Thoracic biofidelity assessment of the THOR Mod Kit ATD. In: *Proceedings of the 23rd International Technical Conference on the Enhanced Safety of Vehicles* (No. 13-0327).

Parent, D., 2016. THOR-50M Biofidelity Report. National Highway Traffic Safety Administration, Docket ID 2015-0119.

Parenteau, C.S., Viano, D.C. and Petit, P.Y., 1998. Biomechanical properties of human cadaveric ankle-subtalar joints in quasi-static loading. *Journal of Biomechanical Engineering*, 120(1), 105-111.

Pattimore, D., Ward, E., Thomas, P. and Bradford, M., 1991. The nature and cause of lower limb injuries in car crashes. In: *Proceedings of the 35th Stapp Car Crash Conference* (No. 912901).

Petit, P., Portier, L., Foret-Bruno, J.Y., Trosseille, X., Parenteau, C.S., Tarriere, C. and Lassau, J., 1997. Quasistatic characterization of the human foot-ankle joints in a simulated tensed state and updated accidentological data. In: *Proceedings of the International Research Council on the Biomechanics of Injury Conference,* 25, 363-376.

Pintar, F.A., Yoganandan, N., Voo, L., Cusick, J.F., Maiman, D.J. and Sances, A., 1995. Dynamic characteristics of the human cervical spine. In: *Proceedings of the 39th Stapp Car Crash Conference* (No. 952722).

Pintar, F.A., Yoganandan, N. and Voo, L., 1998. Effect of age and loading rate on human cervical spine injury threshold. *Spine*, 23(18), 1957-1962.

Pintar, F.A., Yoganandan, N. and Baisden, J., 2005. Characterizing occipital condyle loads under high-speed head rotation. *Stapp Car Crash Journal*, 49, 33-47.

Portier, L., Petit, P., Domont, A., Trosseille, X., Le Coz, J.Y., Tarrière, C. and Lassau, J.P., 1997. Dynamic biomechanical dorsiflexion responses and tolerances of the ankle joint complex. In: *Proceedings of the 41st Stapp Car Crash Conference* (No. 973330).

Prasad, P. and Daniel, R.P., 1984. A biomechanical analysis of head, neck, and torso injuries to child surrogates due to sudden torso acceleration. In: *Proceedings of the 28th Stapp Car Crash Conference* (No. 841656).

Prasad, P., Mertz, H.J., 1985. The position of the United States delegation to the ISO Working Group 6 on the use of HIC in the automotive environment. In: *Society of Automotive Engineers Government/Industry Meeting and Exposition* (No. 851246).

Prasad, P., Mertz, H.J., Dalmotas, D.J., Augenstein, J.S., Digges, K., 2010. Evaluation of the field relevance of several injury risk functions. In: *Proceedings of the 54th Stapp Car Crash Conference* (No. 2010-22-0004).

Prasad, P., Dalmotos, D., German, A., 2014. The field relevance of NHTSA's oblique research moving deformable barrier tests. In: *Proceedings of the 58th Stapp Car Crash Conference* (No. 2014-22-0007).

Purcell, N., Kish, L., 1979. Estimation for small domains. *Biometrics*, 35(2), 365-84.

Pudenz, R.H. and Shelden, C.H., 1946. The lucite calvarium; a method for direct observation of the brain; cranial trauma and brain movement. *Journal of Neurosurgery*, 3(6), 487-505.

Reichert, R., Park, C., Morgan, R.M., 2014. Development of integrated vehicle-occupant model for crashworthiness safety analysis. (Report No. DOT HS 812 087) Washington DC: National Highway Traffic Safety Administration.

Ridella, S., Parent, D., 2011. Modifications to improve the durability, usability, and biofidelity of the THOR-NT dummy. In: *Proceedings of the 22nd International Technical Conference on the Enhanced Safety of Vehicles* (No. 11-0312).

Robbins, D.H., 1983. Development of anthropometrically based design specifications for an advanced adult anthropomorphic dummy family; Volume 2-Anthropometric specifications for mid-Sized male dummy. (Report No. DOT-HS-806-716) Washington, DC: National Highway Traffic Safety Administration.

Roberts, D., Donnelly, B., Severin, C., Medige, J., 1993. Injury Mechanisms and Tolerance of the Human Ankle Joint. Atlanta, GA: Centers for Disease Control.

Rudd, R., Crandall, J., Millington, S., Hurwitz, S. and Heglund, N., 2004. Injury tolerance and response of the ankle joint in dynamic dorsiflexion. *Stapp Car Crash Journal*, 48, 1-26.

Rudd, R.W., 2009. Updated analysis of lower extremity injury risk in frontal crashes in the United States. In: *Proceedings of the 21st International Technical Conference on the Enhanced Safety of Vehicles* (No. 09-0556).

Rudd, R., Scarboro, M., Saunders, J., 2011. Injury analysis of real-world small overlap and oblique frontal crashes. In: *Proceedings of the 22nd International Technical Conference on the Enhanced Safety of Vehicles* (No. 11-0384).

Rupp, J.D., Reed M.P., Jeffreys, T.J., Schneider, L.W., 2003. Effects of hip posture on the frontal impact tolerance of the human hip joint. *Stapp Car Crash Journal,* 47, 21-33.

Rupp, J.D., Reed, M.P., Madura, N.H., Miller, C.S., Kuppa, S.M., Schneider, L.W., 2005. Comparison of the inertial response of the THOR-NT, Hybrid III, and unembalmed cadaver to simulated knee-to-knee-bolster impacts. In: *Proceedings of the 19th International Technical Conference on the Enhanced Safety of Vehicles* (No. 05-0086).

Rupp, J.D., 2006. Biomechanics of hip fractures in frontal motor vehicle crashes [Ph.D. Dissertation]. Ann Arbor, MI: University of Michigan.

Rupp, J.D., Reed, M.P., Miller, C.S., Madura, N.H, Klinich, K.D., Schneider, L.W., Kuppa, S.M., 2009a. Development of new criteria for assessing the risk of knee-thigh-hip injury in frontal impacts using Hybrid III femur force measurements. In: *Proceedings of the 21st International Technical Conference on the Enhanced Safety of Vehicles* (No. 09-0306).

Rupp, J.D., Flannagan, C.A., Kuppa, S.M., 2009b. Development of new injury risk curves for the knee/distal femur and the hip for use in frontal impact testing. (Report No. UMTRI-2009-08) Ann Arbor, MI: University of Michigan Transportation Research Institute.

Saunders, J., Craig, M., Suway, J., 2011. NHTSA's test procedure evaluations for small overlap/oblique crashes. In: *Proceedings of the 22nd International Technical Conference on the Enhanced Safety of Vehicles* (No. 11-0343).

Saunders, J., Parent, D. P., Craig, M. J., 2012. Moving deformable barrier test procedure for evaluating small overlap/oblique crashes. *SAE International Journal of Commercial Vehicles,* 5, 172-195.

Saunders, J., Parent, D., Ames, E., 2015. NHTSA oblique crash test results: vehicle performance and occupant injury risk assessment in vehicles with small overlap countermeasures. In: *Proceedings of the 24th International Technical Conference for the Enhanced Safety of Vehicles* (No. 15-0108).

Schneider, L.W., Robbins, D.H., Pflüg, M.A., Snyder, R.G., 1983. Development of anthropometrically based design specifications for an advanced adult anthropomorphic dummy family, Volume 1. (Report No. DOT-HS-806-715) Washington, DC: National Highway Traffic Safety Administration.

Schreiber, P., Crandall, J., Hurwitz, S. and Nusholtz, G.S., 1998. Static and dynamic bending strength of the leg. *International Journal of Crashworthiness*, 3(3), 295-308.

Shaw, N.A., 2002. The neurophysiology of concussion. *Progress in Neurobiology,* 67(4), 281-344.

Shaw, G., Lessley, D., Bolton, J., Crandall, J., 2004. Assessment of the THOR and Hybrid III crash dummies: steering wheel rim impacts to the upper abdomen. *Society of Automotive Engineers* (No. 2004-01-0310).

Shaw, C.G., Parent, D., Purtsezov, S., Lessley, D., Crandall, J.R., Kent, R.W., Guillemot, H., Ridella, S., Takhounts, E., Martin, P., 2009. Impact response of restrained PMHS in frontal sled tests: skeletal deformation patterns under seat belt loading. *Stapp Car Crash Journal*, 53, 1-48.

Shaw, C.G., Lessley, D., Ash, J., Crandall, J., 2012. Development of an alternative frontal impact condition to assess thoracic response using the THOR Mod Kit dummy. In: *Proceedings of Society of Automotive Engineers of Japan* (No. 20125216).

Shimamura, M., Ohhashi, H., Yamazaki, M., 2003. The effects of occupant age on patterns of rib fractures to belt-restrained drivers and front passengers in frontal crashes in Japan. *Stapp Car Crash Journal,* 47, 349-365.

Society of Automotive Engineers, 1980. Collision Deformation Classification, Surface Vehicle Standard J224.

Takhounts, E., Eppinger, R., Campbell, J., Tannous, R., Power, Erik., and Shook, L., 2003. On the development of the SIMon finite element head model. *Stapp Car Crash Journal,* 47, 107-33.

Takhounts, E., Ridella, R., Hasija, V., Tannous, R., Campbell, J., Malone, D., Danelson, K., Stitzel, J., Rowson, S., and Duma, S., 2008. Investigation of traumatic brain injuries using the next generation of Simulated Injury Monitor (SIMon) finite element head model. *Stapp Car Crash Journal,* 52, 1-31.

Takhounts, E.G., Craig, M., Moorhouse, K., McFadden, J., Hasija, V., 2013. Development of Brain Injury Criteria (BrIC). *Stapp Car Crash Journal*, 57, 243-66.

Takhounts, E., 2015. Computational modeling and injury criteria for motor-vehicle crashes. In: *Proceedings of the 59th Stapp Car Crash Conference*, invited lecture. http://www.nhtsa.gov/DOT/NHTSA/NVS/Biomechanics%20&%20Trauma/Stapp_2015.pdf

Thunnissen, J., Wismans, J., Ewing, C.L. and Thomas, D.J., 1995. Human volunteer head-neck response in frontal flexion: a new analysis. In: *Proceedings of the 39th Stapp Car Crash Conference* (No. 952721).

Viano, D., Kroell, C., Warner, C., 1997. Comparative thoracic impact response of living and sacrificed porcine siblings. In: *Proceedings of the 21st Stapp Car Crash Conference* (No. 770930).

Von Gierke, H., 1964. Transient acceleration, vibration and noise problems in space flight. In: Schaefer K.E. (ed.) *Bioastronautics*. New York: Macmillan, 27-75.

Wang, M.C., Pintar, F., Yoganandan, N. and Maiman, D.J., 2009. The continued burden of spine fractures after motor vehicle crashes. *Journal of Neurosurgery: Spine*, 10(2), 86-92.

Wismans, J., Philippens, M., Van Oorschot, E., Kallieris, D. and Mattern, R., 1987. Comparison of human volunteer and cadaver head-neck response in frontal flexion. In: *Proceedings of the 31st Stapp Car Crash Conference* (No. 872194).

Untaroiu, C.D., Ivarsson, J., Genovese, D.R., Bose, D. and Crandall, J.R., 2008. Biomechanical injury response of leg subjected to combined axial compressive and bending loading. *Biomedical Sciences Instrumentation*, 44, 141-146.

Yliniemi, E.M., Pellettiere, J.A., Doczy, E.J., Nuckley, D.J., Perry, C.E. and Ching, R.P., 2009. Dynamic tensile failure mechanics of the musculoskeletal neck using a cadaver model. *Journal of Biomechanical Engineering*, 131(5), pp 051001.

Yoganandan, N., Pintar, F.A., Boynton, M., Begeman, P., Prasad, P., Kuppa, S.M., Morgan, R.M. and Eppinger, R.H., 1996. Dynamic axial tolerance of the human foot-ankle complex. In: *Proceedings of the 40th Stapp Car Crash Conference* (No. 962426).

Yoganandan, N., Pintar, F., Kumaresan, S., Haffner, M., Kuppa, S., 1997. Impact biomechanics of the human thorax-abdomen complex. *International Journal of Crashworthiness*, 2(2), 219-228.

Yoganandan, N., Pintar, F., Rinaldi, J., 2009. Evaluation of the RibEye deflection measurement system in the 50th percentile Hybrid III dummy. (Report No. DOT HS 811 102) Washington DC: National Highway Traffic Safety Administration.

Yoganandan, N., Arun, M.W., Pintar, F.A. and Banerjee, A., 2015. Lower leg injury reference values and risk curves from survival analysis for male and female dummies: meta-analysis of postmortem human subject tests. *Traffic Injury Prevention*, 16(S1), S100-S107.

APPENDIX A. Vehicle Test Data – BrIC Correlation Studies

TEST-OCCLOC	DATABASE	TEST-OCCLOC	DATABASE	TEST-OCCLOC	DATABASE
4303-01	NHTSA	5301-02	NHTSA	7292-01	NHTSA
4242-01	NHTSA	5567-01	NHTSA	7293-01	NHTSA
4205-02	NHTSA	5594-02	NHTSA	7366-01	NHTSA
4273-01	NHTSA	5595-01	NHTSA	7368-01	NHTSA
4198-01	NHTSA	5595-02	NHTSA	7371-01	NHTSA
3897-01	NHTSA	5609-01	NHTSA	7429-01	NHTSA
4266-02	NHTSA	5613-01	NHTSA	7433-01	NHTSA
4247-01	NHTSA	5711-01	NHTSA	7434-01	NHTSA
3916-01	NHTSA	5715-01	NHTSA	7428-01	NHTSA
4264-02	NHTSA	6370-01	NHTSA	7431-01	NHTSA
3901-02	NHTSA	7966-01	NHTSA	7427-01	NHTSA
4250-01	NHTSA	7977-01	NHTSA	7432-01	NHTSA
4251-01	NHTSA	7978-01	NHTSA	7430-01	NHTSA
4215-02	NHTSA	7989-01	NHTSA	7426-01	NHTSA
4237-02	NHTSA	8000-01	NHTSA	7458-01	NHTSA
4080-01	NHTSA	8024-01	NHTSA	7441-01	NHTSA
4090-01	NHTSA	8035-01	NHTSA	7457-01	NHTSA
4264-01	NHTSA	8045-01	NHTSA	7444-01	NHTSA
4090-02	NHTSA	8048-01	NHTSA	7456-01	NHTSA
4223-02	NHTSA	8055-01	NHTSA	7467-01	NHTSA
4267-02	NHTSA	8064-01	NHTSA	7468-01	NHTSA
4215-01	NHTSA	8068-01	NHTSA	7476-01	NHTSA
4242-02	NHTSA	8071-01	NHTSA	7967-01	NHTSA
4259-01	NHTSA	8077-01	NHTSA	7984-01	NHTSA
3987-01	NHTSA	8080-01	NHTSA	7990-01	NHTSA
4255-02	NHTSA	8081-01	NHTSA	7998-01	NHTSA
4235-01	NHTSA	8091-01	NHTSA	8033-01	NHTSA
4235-02	NHTSA	8106-01	NHTSA	8047-01	NHTSA
4265-02	NHTSA	8153-01	NHTSA	8053-01	NHTSA
4249-02	NHTSA	8151-01	NHTSA	8054-01	NHTSA
4240-01	NHTSA	8156-01	NHTSA	8069-01	NHTSA
4237-01	NHTSA	6830-01	NHTSA	8072-01	NHTSA
4259-02	NHTSA	6831-01	NHTSA	8078-01	NHTSA
4198-02	NHTSA	6852-01	NHTSA	8079-01	NHTSA
3915-02	NHTSA	6855-01	NHTSA	8082-01	NHTSA
3901-01	NHTSA	6872-01	NHTSA	8092-01	NHTSA
4241-01	NHTSA	6873-01	NHTSA	8102-01	NHTSA
4252-01	NHTSA	6937-01	NHTSA	8108-01	NHTSA

TEST-OCCLOC	DATABASE	TEST-OCCLOC	DATABASE	TEST-OCCLOC	DATABASE
3952-02	NHTSA	7144-01	NHTSA	8149-01	NHTSA
5287-01	NHTSA	7145-01	NHTSA	8157-01	NHTSA
9089-01	NHTSA	5461-01	NHTSA	7145-04	NHTSA
3800-01	NHTSA	5472-01	NHTSA	7431-04	NHTSA
4551-01	NHTSA	7977-02	NHTSA	7467-04	NHTSA
3875-01	NHTSA	7989-02	NHTSA	7468-04	NHTSA
3899-01	NHTSA	8024-02	NHTSA	7476-04	NHTSA
3818-01	NHTSA	8035-02	NHTSA	8069-04	NHTSA
4547-01	NHTSA	8045-02	NHTSA	8078-04	NHTSA
4380-01	NHTSA	8055-02	NHTSA	8092-04	NHTSA
3845-01	NHTSA	8064-02	NHTSA	7955-01	NHTSA
4497-01	NHTSA	8068-02	NHTSA	7979-01	NHTSA
4547-04	NHTSA	8080-02	NHTSA	7988-01	NHTSA
3898-01	NHTSA	8081-02	NHTSA	7997-01	NHTSA
4551-04	NHTSA	8091-02	NHTSA	8052-01	NHTSA
3799-04	NHTSA	8104-02	NHTSA	9089-04	NHTSA
4380-04	NHTSA	8106-02	NHTSA	7773-01	NHTSA
3820-01	NHTSA	8153-02	NHTSA	7851-01	NHTSA
4456-04	NHTSA	8156-02	NHTSA	7852-01	NHTSA
3819-04	NHTSA	5713-03	NHTSA	7861-01	NHTSA
4456-01	NHTSA	5714-03	NHTSA	7862-01	NHTSA
3799-01	NHTSA	5715-03	NHTSA	7867-01	NHTSA
4378-01	NHTSA	6852-04	NHTSA	8084-01	NHTSA
4292-01	NHTSA	6855-04	NHTSA	8084-02	NHTSA
4498-01	NHTSA	6865-04	NHTSA	8085-01	NHTSA
3803-04	NHTSA	6925-04	NHTSA	8085-02	NHTSA
3802-01	NHTSA	6937-04	NHTSA	8086-01	NHTSA
4292-04	NHTSA	7366-04	NHTSA	8086-02	NHTSA
3803-01	NHTSA	7368-04	NHTSA	8087-01	NHTSA
4482-01	NHTSA	7428-04	NHTSA	8087-02	NHTSA
3800-04	NHTSA	7441-04	NHTSA	8088-01	NHTSA
4471-01	NHTSA	7457-04	NHTSA	8088-02	NHTSA
4313-01	NHTSA	7427-04	NHTSA	8089-01	NHTSA
3819-01	NHTSA	7432-04	NHTSA	8089-02	NHTSA
4859-01	NHTSA	7444-04	NHTSA	8096-01	NHTSA
5296-01	NHTSA	7426-04	NHTSA	8096-02	NHTSA
5317-01	NHTSA	7456-04	NHTSA	8097-01	NHTSA
5405-01	NHTSA	7429-04	NHTSA	8097-02	NHTSA
5406-01	NHTSA	7434-04	NHTSA	8099-01	NHTSA
5407-01	NHTSA	7433-04	NHTSA	8099-02	NHTSA

TEST-OCCLOC	DATABASE	TEST-OCCLOC	DATABASE	TEST-OCCLOC	DATABASE
5408-01	NHTSA	6872-04	NHTSA	8381-01	NHTSA
5416-01	NHTSA	7144-04	NHTSA	8381-02	NHTSA
8475-01	NHTSA	9126-01	NHTSA	9482-02	NHTSA
8476-01	NHTSA	9126-02	NHTSA	9483-01	NHTSA
8477-01	NHTSA	9127-01	NHTSA	9483-02	NHTSA
8478-01	NHTSA	9127-02	NHTSA	9499-01	NHTSA
8478-02	NHTSA	9206-01	NHTSA	9499-02	NHTSA
8488-01	NHTSA	9207-01	NHTSA	9500-01	NHTSA
8488-02	NHTSA	9208-01	NHTSA	9500-02	NHTSA
8510-01	NHTSA	9209-01	NHTSA	9501-01	NHTSA
8512-01	NHTSA	9210-01	NHTSA	9501-02	NHTSA
8591-01	NHTSA	9211-01	NHTSA	9566-01	NHTSA
8787-01	NHTSA	9212-01	NHTSA	9567-01	NHTSA
8787-02	NHTSA	9213-01	NHTSA	9568-01	NHTSA
8788-01	NHTSA	9214-01	NHTSA	9569-01	NHTSA
8788-02	NHTSA	9216-01	NHTSA	9570-01	NHTSA
8789-01	NHTSA	9217-01	NHTSA	9571-01	NHTSA
8789-02	NHTSA	9218-01	NHTSA	9572-01	NHTSA
8875-01	NHTSA	9219-01	NHTSA	9572-02	NHTSA
8875-02	NHTSA	9220-01	NHTSA	9573-01	NHTSA
8881-01	NHTSA	9221-01	NHTSA	9573-02	NHTSA
8881-02	NHTSA	9222-01	NHTSA	9574-01	NHTSA
8882-01	NHTSA	9332-01	NHTSA	9574-02	NHTSA
8882-02	NHTSA	9333-01	NHTSA	9585-01	NHTSA
8998-01	NHTSA	9334-01	NHTSA	9585-02	NHTSA
8998-02	NHTSA	9335-01	NHTSA	9586-01	NHTSA
8999-01	NHTSA	9336-01	NHTSA	9586-02	NHTSA
8999-02	NHTSA	9337-01	NHTSA	9587-01	NHTSA
9042-01	NHTSA	9354-01	NHTSA	9587-02	NHTSA
9042-02	NHTSA	9354-02	NHTSA	9699-01	NHTSA
9043-01	NHTSA	9476-01	NHTSA	9699-02	NHTSA
9110-01	NHTSA	9476-02	NHTSA	9725-01	NHTSA
9110-02	NHTSA	9477-01	NHTSA	9725-02	NHTSA
9121-02	NHTSA	9477-02	NHTSA	9726-01	NHTSA
9122-01	NHTSA	9478-01	NHTSA	9727-01	NHTSA
9122-02	NHTSA	9478-02	NHTSA	9727-02	NHTSA
9123-01	NHTSA	9479-01	NHTSA	9802-01	NHTSA
9123-02	NHTSA	9479-02	NHTSA	9802-02	NHTSA
9124-01	NHTSA	9480-02	NHTSA	9804-01	NHTSA
9124-02	NHTSA	9481-01	NHTSA	9804-02	NHTSA

TEST-OCCLOC	DATABASE	TEST-OCCLOC	DATABASE	TEST-OCCLOC	DATABASE
9125-01	NHTSA	9481-02	NHTSA	CEN1324-01	IIHS
9125-02	NHTSA	9482-01	NHTSA	CEN1326-01	IIHS
9806-01	NHTSA	9151-01	NHTSA	CEN1327-01	IIHS
9807-01	NHTSA	9151-02	NHTSA	CEN1328-01	IIHS
9807-02	NHTSA	9152-01	NHTSA	CEN1335-01	IIHS
9202-04	NHTSA	9152-02	NHTSA	CEN1336-01	IIHS
9204-04	NHTSA	9154-01	NHTSA	CEN1337-01	IIHS
9332-02	NHTSA	9154-02	NHTSA	CEN1338-01	IIHS
9333-02	NHTSA	9155-01	NHTSA	CEN1339-01	IIHS
9334-02	NHTSA	9155-02	NHTSA	CEN1341-01	IIHS
9335-02	NHTSA	9223-01	NHTSA	CEN1344-01	IIHS
9336-02	NHTSA	9223-02	NHTSA	CEN1345-01	IIHS
9337-02	NHTSA	9805-01	NHTSA	CEN1346-01	IIHS
9566-02	NHTSA	9805-02	NHTSA	CEN1347-01	IIHS
9567-02	NHTSA	CEN1219-01	IIHS	CEN1348-01	IIHS
9568-02	NHTSA	CEN1220-01	IIHS	CEN1349-01	IIHS
9569-02	NHTSA	CEN1221-01	IIHS	CEF1206-01	IIHS
9570-02	NHTSA	CEN1223-01	IIHS	CEF1207-01	IIHS
9571-02	NHTSA	CEN1224-01	IIHS	CEF1208-01	IIHS
9135-02	NHTSA	CEN1225-01	IIHS	CEF1301-01	IIHS
9137-01	NHTSA	CEN1227-01	IIHS	CEF1302-01	IIHS
9137-02	NHTSA	CEN1228-01	IIHS	CEF1303-01	IIHS
9138-01	NHTSA	CEN1229-01	IIHS	CEF1304-01	IIHS
9138-02	NHTSA	CEN1230-01	IIHS	CEF1305-01	IIHS
9139-01	NHTSA	CEN1231-01	IIHS	CEF1306-01	IIHS
9139-02	NHTSA	CEN1233-01	IIHS	CEF1307-01	IIHS
9140-01	NHTSA	CEN1234-01	IIHS	CEF1308-01	IIHS
9140-02	NHTSA	CEN1235-01	IIHS	CES1308-01	IIHS
9142-01	NHTSA	CEN1236-01	IIHS	CES1309-01	IIHS
9143-01	NHTSA	CEN1301-01	IIHS	CES1310-01	IIHS
9144-01	NHTSA	CEN1302-01	IIHS	CES1308-04	IIHS
9144-02	NHTSA	CEN1303-01	IIHS	CES1309-04	IIHS
9145-01	NHTSA	CEN1304-01	IIHS	CES1310-04	IIHS
9146-01	NHTSA	CEN1307-01	IIHS	CEN1330-01	IIHS
9146-02	NHTSA	CEN1309-01	IIHS	CEN1333-01	IIHS
9147-02	NHTSA	CEN1313-01	IIHS		
9148-01	NHTSA	CEN1314-01	IIHS		
9148-02	NHTSA	CEN1321-01	IIHS		
9150-01	NHTSA	CEN1322-01	IIHS		
9150-02	NHTSA	CEN1323-01	IIHS		

APPENDIX B. Algorithm for Computing Time Duration of Angular Velocity Pulse

A sample pulse is shown in Figure B.1 to explain the algorithm:

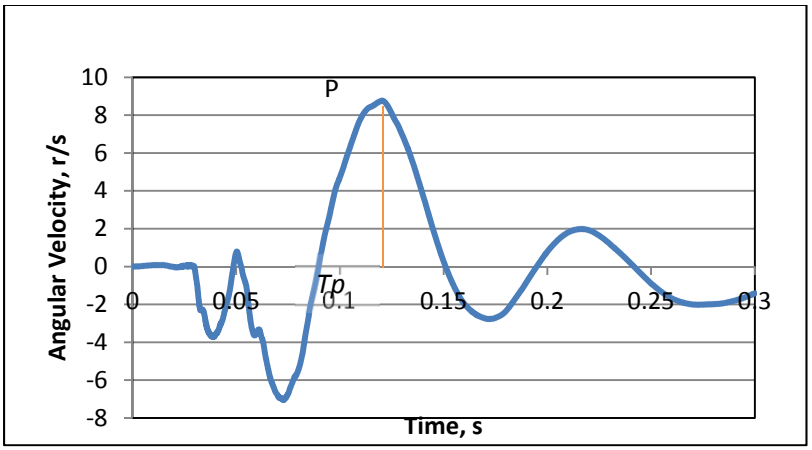

Figure B.1. Peak of the pulse (P) and time of peak (Tp) for an example angular velocity time-history.

1. Time step is determined (dt)
2. The peak of the pulse (P) is computed along with the time of peak (Tp)
3. The area around the peak is then incrementally calculated by moving the time counter (i) on either side as:
    a. Compute area under the curve A_i from $Tp - i \times dt$ to $Tp + i \times dt$.
    b. If the peak is too close to the either end of the time spectrum then the counter movement is not symmetrical around the peak i.e.
        i. if peak is close to time zero then,
            1. compute area from $Tp - i \times dt$ to $Tp + i \times dt$ till $t = 0$ is reached
            2. then compute area from 0 to $Tp + i \times dt$
        ii. if peak is close to $end\ time$ then,
            1. compute area from $Tp - i \times dt$ to $Tp + i \times dt$ till $t = end$ is reached
            2. then compute area from $Tp - i \times dt$ to $end\ time$
4. Counter is stopped when the first maximum in area is found in the first 100ms. $DeltaT$ is computed at this point ,which corresponds to the time of angular velocity pulse
    1. $DeltaT = (Tp + i \times dt) - (Tp - i \times dt)$
5. P and $DeltaT$ are used in the BrIC formulation.

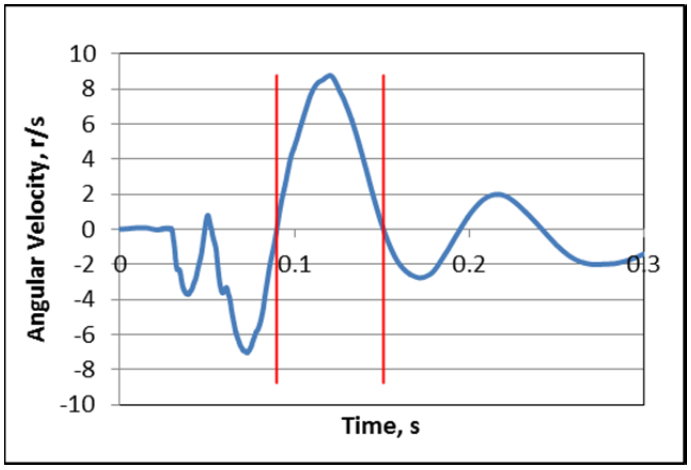

Figure B.2. DeltaT for an example angular velocity time-history.

APPENDIX C. BrIC Design of Experiments and Optimization

DESIGN OF EXPERIMENTS

Design of experiments (DOE) is frequently used to investigate the effect of various parameters on the outcome variable. To conduct DOE study and investigate the effect of various parameters on BrIC, a full finite element (FE) model of a Toyota Yaris (developed by the George Washington University) was modified and simplified in the manner shown below (Figure C.1).

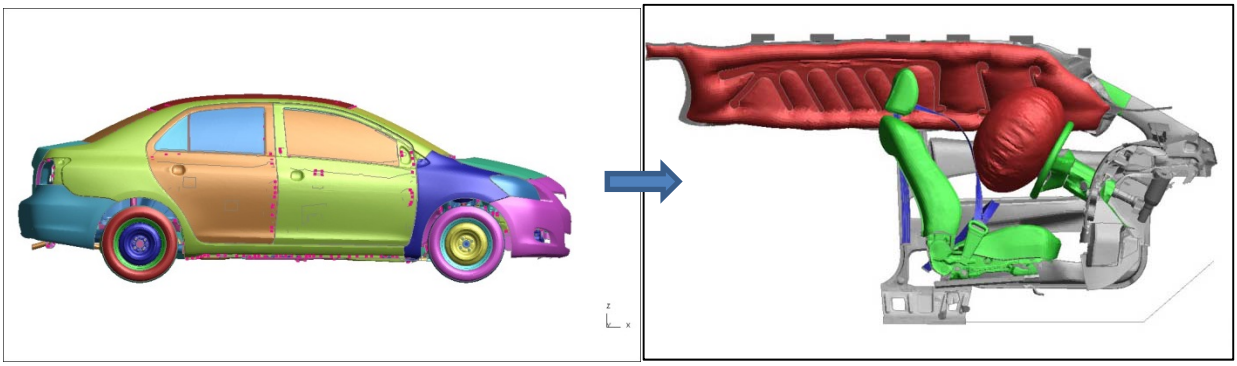

Figure C.1. Full FE model of Toyota Yaris (left) with simplified interior and restraint system components (right).

Following are the simplifications made in the model for DOE study:

- Roof rails, door, B-pillar on the driver side and floor were deformable in the full FE model, but were made rigid so that no intrusion is considered in this analysis
- Knee bolster, A-pillar were kept deformable
- Driver seat was kept deformable and the Simplified 50th percentile male GHBMC model was used and positioned in the seat using pre-simulation
- Steering column assembly was kept deformable including the steering wheel; steering wheel stiffness was increased to represent steering wheel deformation of the majority of mid-size sedans (this stiffness in the original model was too low causing excessive deformations of the steering wheel when compared to those of the majority of the cars)
- The distance to the side door was increased to represent a mid-sized sedan
- A 50-liter frontal airbag was used
- The side curtain airbag was obtained from TRW and used in this analysis
- The belt system with retractor, pre-tensioner and load limiter was used; the belt is fitted to the Simplified GHBMC model using Primer 12.0 software package (Oasys Ltd., Solihull, UK)
- The seat was positioned to represent mid-track position of a mid-sized sedan

Several DOE studies were conducted using metamodeling techniques, which allowed for construction of surrogate design models for the purpose of design exploration, such as variable screening. Surrogate design models help save time when compared to running direct simulations. LS-Opt software package (LSTC Inc., Livermore) was used in this analysis, which provided the capability of using five standard types of metamodeling techniques, namely polynomial response surfaces, Neural Networks, Radial Basis Function (RBF) Networks, Kriging and Support Vector Regression. At the core, these techniques differ in

the regression methods employed to construct the surrogate models. The polynomial response surface method and the RBF use linear regression, while neural networks use nonlinear regression methods.

Of the metamodeling techniques tested, the Feed Forward Neural Network (FFNN) method provided the best accuracy for the response parameters and is thus used in all DOE studies presented here (example of the fit is given in Figure C.2).

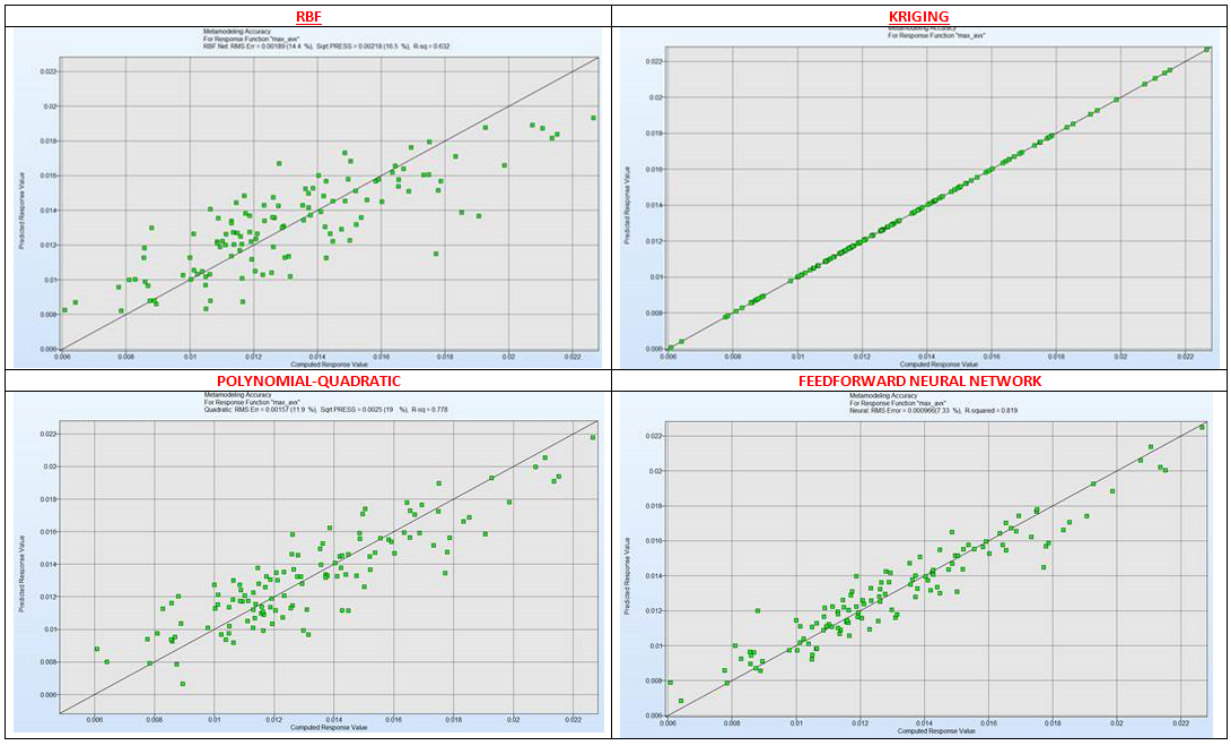

Figure C.2. Fit of various metamodels. Note that Kriging by definition gives a perfect fit and shows zero prediction errors. This prevents the use of standard model selection criteria (such as R^2). Since the metamodel fit using Kriging method is difficult to assess, the next best method (FFNN) was used.

Space-filling sampling scheme guarantees an optimal coverage of the design space and was used in these studies (Figure C.3).

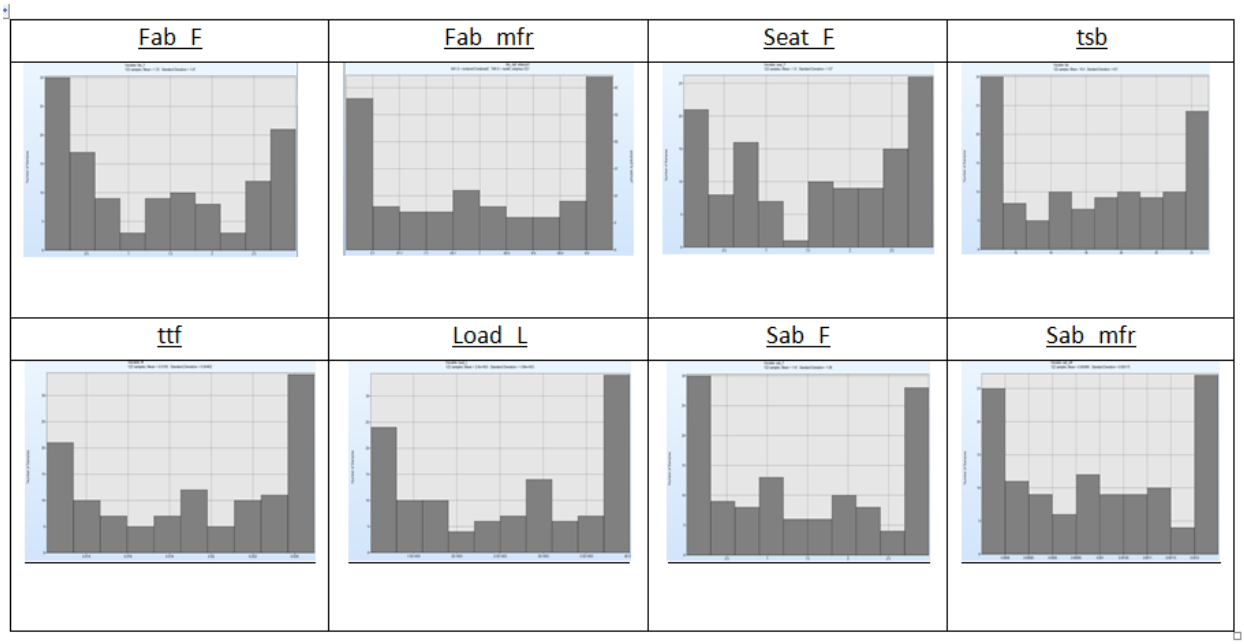

Figure C.3. Space filling sampling method demonstrates sampling for each varied parameter. For example, the full factorial DOE for nine parameters (Table C.1) and 10 values per parameter would require approximately 1,000,000,000 simulations, which will take (at 2.5 hours per simulation) approximately 285,288 years to be completed (instead of approximately one week).

The nominal crash pulse used for these analyses was taken from NHTSA Research and Development test 8484 (the setup is shown in Figure C.4).

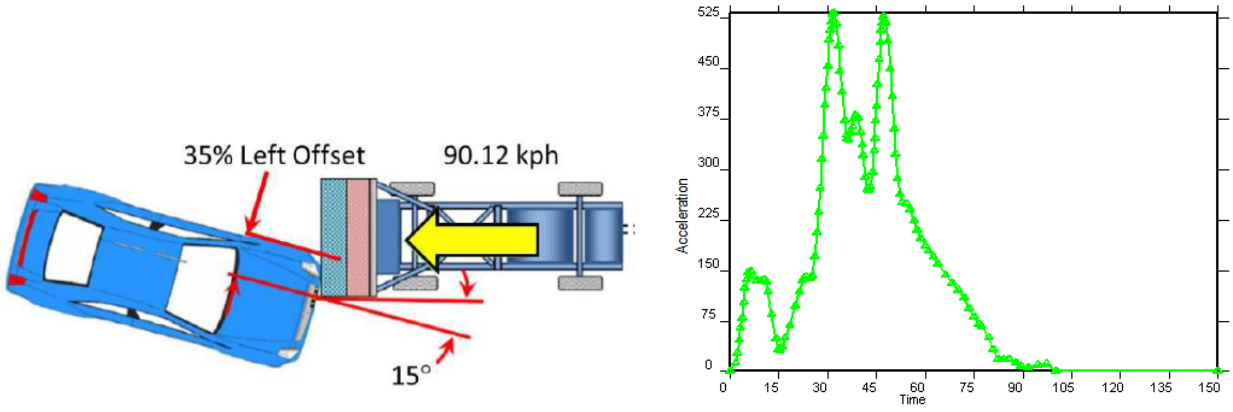

Figure C.4. Test setup for test number 8484 and the corresponding crash pulse that was used in all studies (frontal and oblique impacts). Note that the crash pulse was taken from the oblique test and is more severe than that of a typical NCAP crash pulse.

The simplified human FE model, used in these studies, complements the Global Human Body Models Consortium (GHBMC) detailed 50th percentile male occupant (M50-O) by providing kinematic and kinetic data with a significantly reduced run time using the same body habitus. The simplified occupant model (M50-OS) was developed using the same source geometry as the M50-O. Though some meshed components were preserved, the total element count was reduced by remeshing, homogenizing, or in

some cases omitting structures that are explicitly contained in the M50-O. Bones are included as rigid bodies, with the exception of the ribs, which are deformable but were remeshed to a coarser element density than the M50-O. Material models for all deformable components were drawn from the biomechanics literature. Kinematic joints were implemented at major articulations (shoulder, elbow, wrist, hip, knee, and ankle) with moment vs. angle relationships from the literature. The M50-OS simplified model has 354,000 elements; in contrast, the M50-O detailed model has 2.2 million elements. The model can be repositioned without requiring simulation. The M50-OS model ran a 150ms event on 40 processors in 2.5 hours compared to 25 hours for M50-O detailed model. M50-OS model (Figure C.5) exhibited a significant reduction in run time and thus was used for DOE and optimization studies.

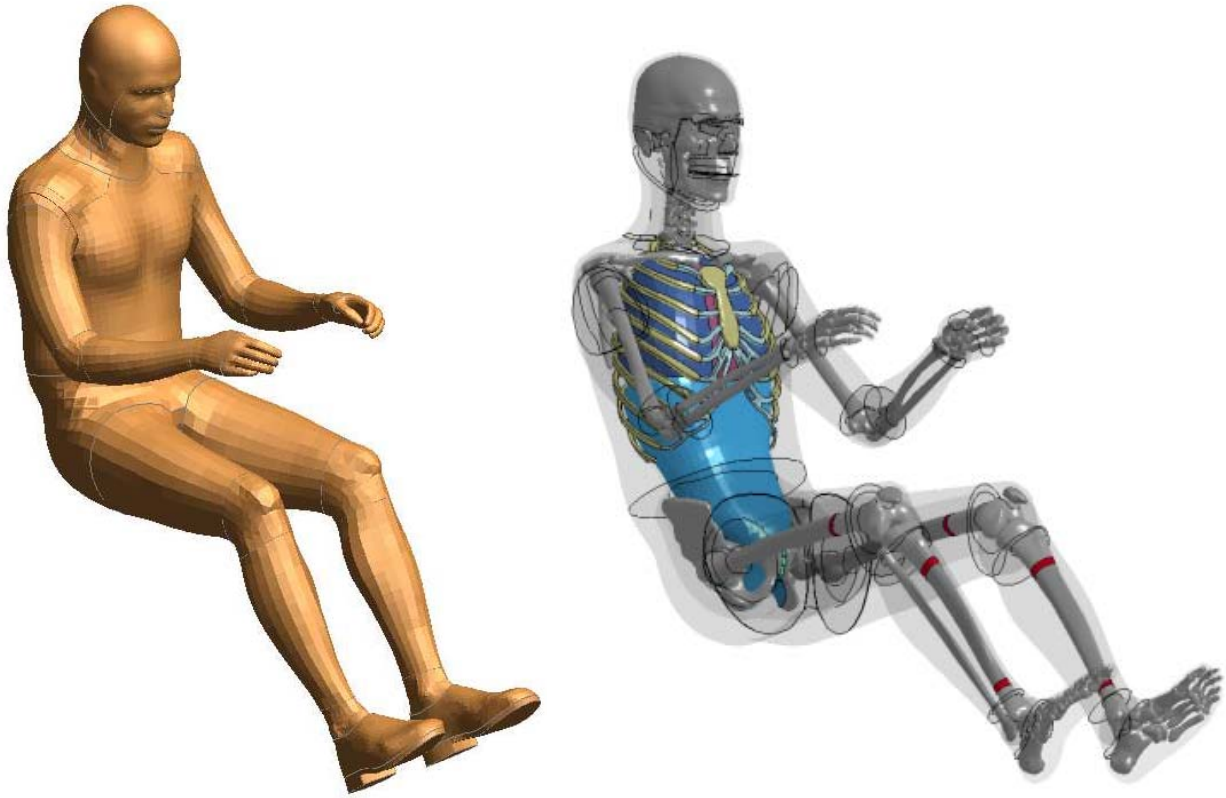

Figure C.5. Simplified GHBMC human 50th percentile male occupant model (M50-OS) was used in all DOE and optimization studies.

DOE Study #1 (include Delta-V and PDOF)

First DOE study included changes in delta-V and the principal direction of force (PDOF) in the analysis. The range of Delta-V was obtained by scaling the magnitude of the pulse shown in Figure C.4 while keeping the time unchanged. Table C.1 lists all the parameters varied in the DOE study #1, including their nominal values and the range.

Table C.1. Parameters varied in the DOE study #1.

Parameters	Nominal	Range
Crash Pulse, cpulse	0.94 (35mph)	0.65 (25mph) – 1.25 (47mph)
PDOF	0^{o}	0^{o} - 30^{o}
Front Airbag Friction, fab_F	0.5	0 – 3
Frontal Airbag Mass Flow Rate, fab_mfr	1	0.75 – 1.25
Load Limiter , load_L	3000 N	1000- 4000
Side Airbag Friction, sab_F	0.3	0 - 3
Frontal Airbag (firing) Time, ttf	18 ms	12- 25
Side Airbag (firing) Time, tsb	18 ms	12 - 25
Side Airbag Mass Flow Rate, sab_mfr	1	0.75 – 1.25

Figure C.6 demonstrates the setup and results for the nominal values of parameters given in Table C.1 and

Table C.2 relists the nominal values and the value of BrIC.

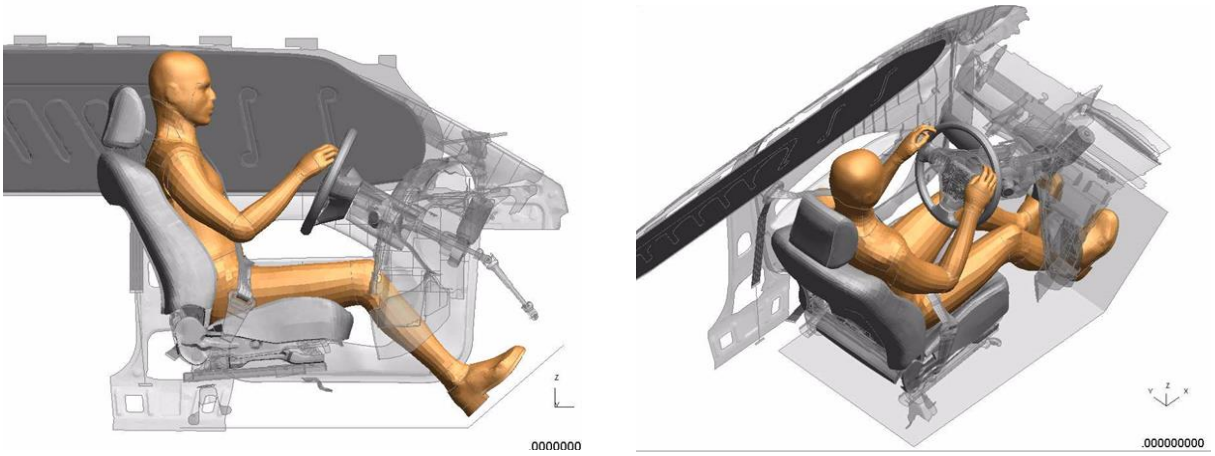

(a) (b)

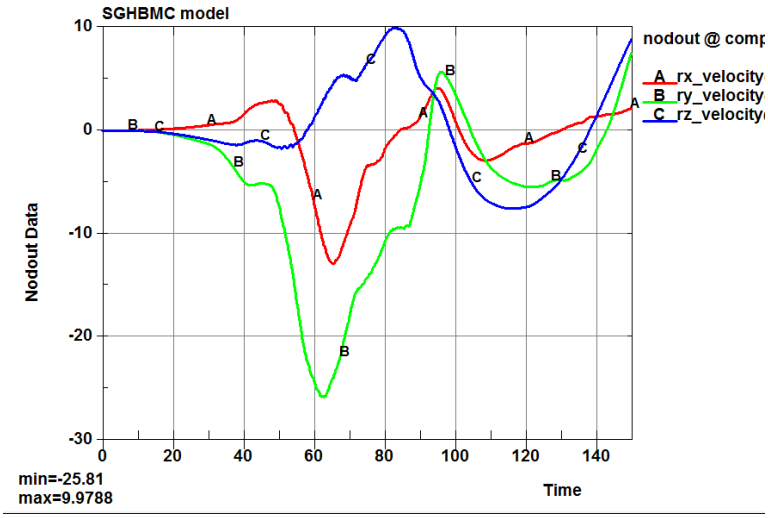

(c)

Figure C.6. Initial position setup for the run with nominal values given in

Table C.2; right view (a), top oblique view (b), and the FE model output for the head angular velocity components time histories (c).

Table C.2. Results of the run with the nominal parameters.

Crash Pulse	Fab_F	Fab_MFR	Load_L	Sab_F	ttf	tsb	Sab_mfr	BrIC
35 mph	0.5	1.0	3000	0.3	18	18	1.0	**0.55**

The value of BrIC for the nominal run (somewhat representing NCAP tests with more aggressive pulse) was 0.55, representing rather low risk of brain injury.

Figure C.7 demonstrates the metamodel-based global sensitivity of BrIC for various parameters when varied within the ranges given in Table C.1.

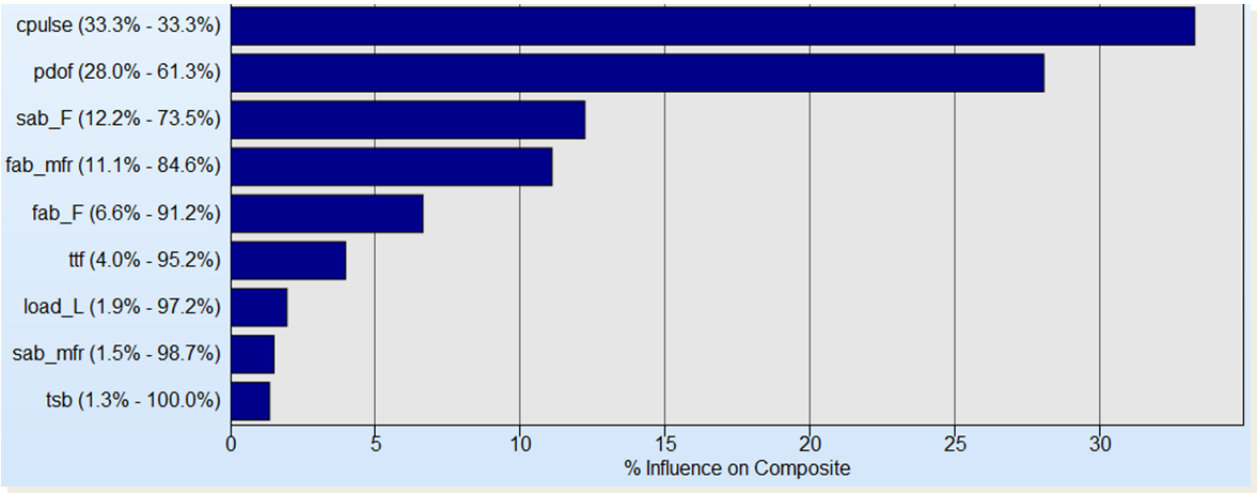

Figure C.7. Influence of all parameters listed in Table C.1 on BrIC.

It is clear that the most influential parameter affecting BrIC is delta-V (cpulse) changing BrIC by a third (33.3%) within the given range. The next most influential parameter affecting BrIC is PDOF (28.0% influence). Cumulatively delta-V and PDOF affect the values of BrIC by 61.3%. Figure C.8 gives a more detailed look of the influence of delta-V and PDOF on the values of BrIC when other parameters are constrained to their nominal values, demonstrating that with the increased PDOF the influence of Delta-V on the values of BrIC increases. For example, for a 20^0 oblique test, the value of BrIC will change from approximately 0.55 at Delta-V of 25 mph to 1.2 at Delta-V of 47 mph (in Figure C.8 the Delta-V of 35 mph corresponds to the value of cpulse of 0.00094). The relationship between Delta-V and BrIC is almost linear for any PDOF.

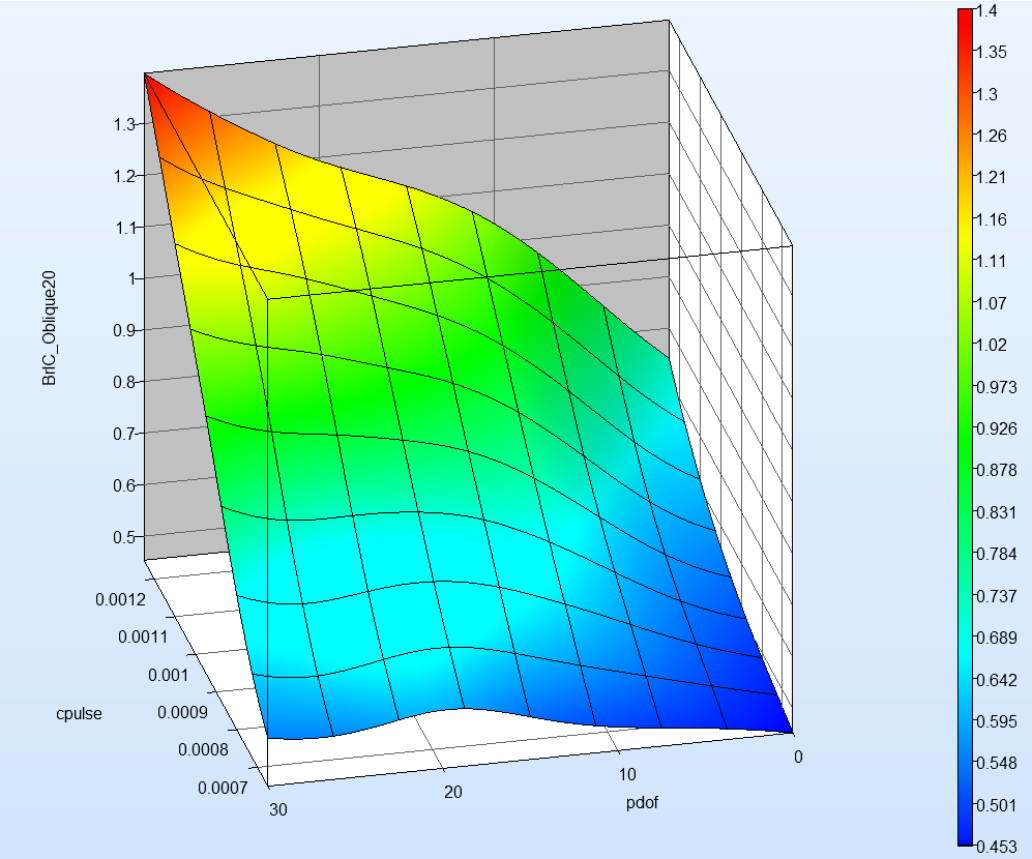

Figure C.8. Relationship between BrIC and Delta-V and PDOF demonstrating strong relationship between all three parameters, and especially that between BrIC and Delta-V.

Without the use of metamodels, however, when a limited number of tests is used to investigate relationships between various parameters, misleading conclusions about their complex inter-relationships may be reached. For example, Figure C.9 demonstrates a scatter plot of BrIC versus delta-V for each run in this DOE study, in which the relationship between the two parameters may appear rather weak especially when the range of other parameters is rather large (representing various vehicles) and when a limited range Delta-Vs is considered. This is the situation where the use of metamodels is very helpful (contrast the scattered plot in Figure C.9 with the actual relationship between the parameters given in Figure C.8).

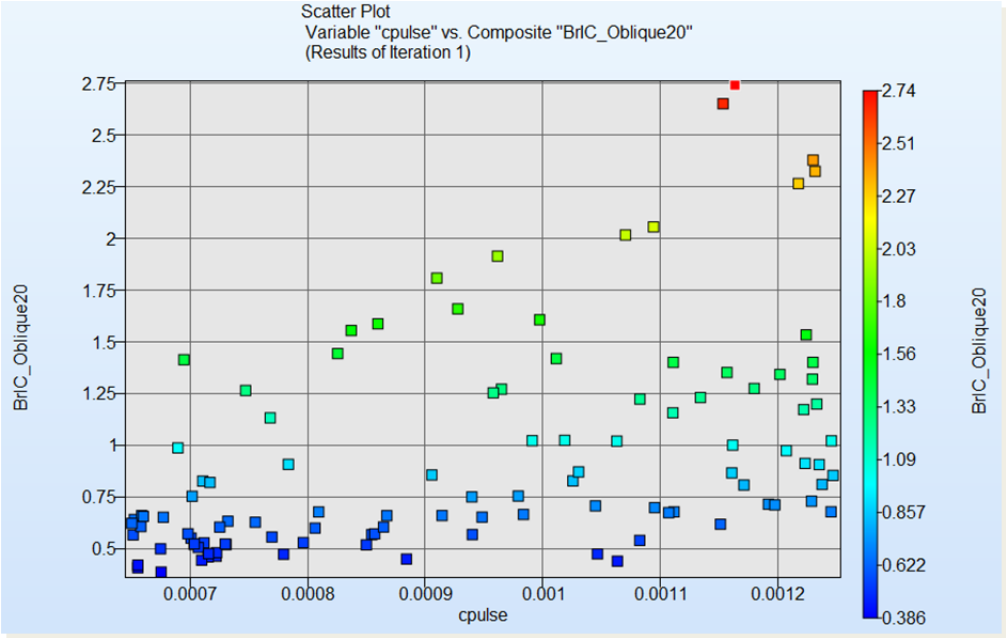

Figure C.9. BrIC versus Delta-V demonstrating a rather large scatter when all other parameters are varied.

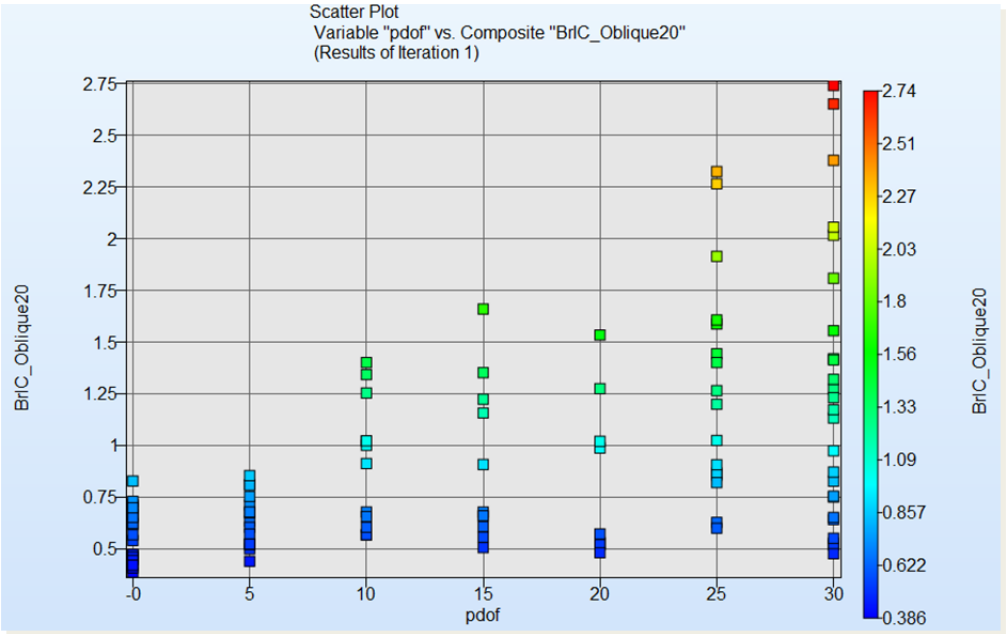

Figure C.10. BrIC versus PDOF demonstrating an increasing range of values of BrIC with increased PDOF.

Figure C.10 shows the relationship between BrIC and PDOF. With increased PDOF angle the range of values of BrIC is increasing. However, it can also be observed that there exists a set of parameters reducing the values of BrIC to under 0.6 for almost all angles of PDOF.

Figure C.11 completes the description of the DOE study #1 with the simulation based correlation matrix demonstrating that the relationships between BrIC and Delta-V (cpulse) and PDOF are also the strongest

(higher correlation coefficients) and positive (increasing Delta-V and PDOF causes BrIC to increase). Note the correlation coefficient is higher for PDOF than for Delta-V in the simulation based correlation matrix, while the percent influence is higher for the Delta-V (Figure C.9). This is because Figure C.9 is based on the metamodel results, while the correlations matrix is based on the actual limited number of runs.

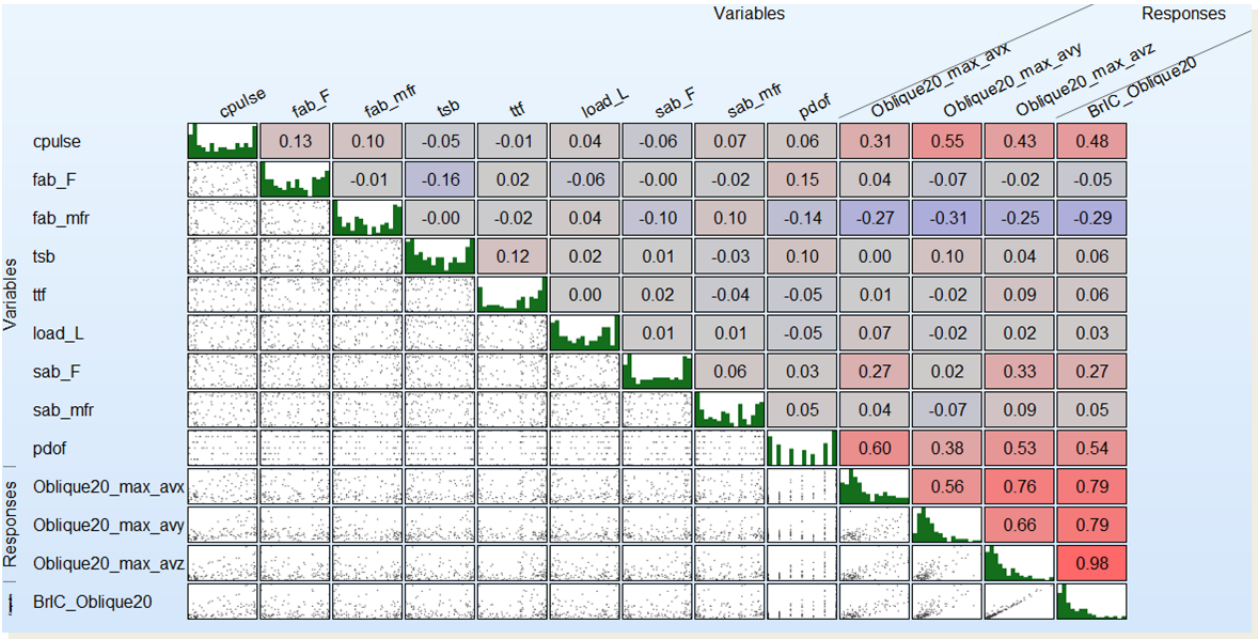

Figure C.11. Correlation matrix for the DOE study #1 showing correlation coefficients between all the variables and responses of the study.

Following are the conclusions from the DOE study #1:

- Out of nine parameters varied in this study (see
- Table C.2 for the list of parameters, their nominal values and the varied range), Delta-V influences BrIC the most, followed by PDOF
- Increasing PDOF increases the range of values of BrIC, yet it is possible to find a set of parameters with values of BrIC less than 0.6
- When investigating relationships between various parameters, such as BrIC and Delta-V, metamodels are more useful than just a scatter plot of the two parameters because various other parameters (for example, when looking at the fleet tests of various vehicles with various sets of restraint parameters) contaminate the relationship (contrast Figures C.8 and C.9) leading to erroneous conclusions about the "true" relationship
- Correlation between the values of BrIC and Delta-V and PDOF is the strongest (higher correlation coefficients) and positive (with increased Delta-V and PDOF the values of BrIC also increase)

Now that the importance of Delta-V and PDOF has been established, the next DOE study will investigate influence of other parameters on BrIC with fixed Delta-V at 35 mph and three values of PDOFs (0^0 representing frontal impact, -20^0 representing near side driver oblique impact, and $+20^0$ representing far side driver oblique impact).

DOE Study #2 (Fixed Delta-V and PDOF)

Table C.3 lists the eight parameters investigated in the DOE study #2 (instead of nine in DOE study #1). Here Delta-V and PDOF were removed and Seat Friction added to see if, for example, having leather or fabric seat makes the difference in BrIC response.

Table C.3. Parameters varied in the DOE study #2.

Parameters	Nominal	Range
Frontal Airbag Friction, fab_F	0.5	0 – 3
Frontal Airbag Mass Flow Rate, fab_mfr	1	0.75 – 1.25
Seat Friction, seat_F	0.5	0 - 3
Load Limiter , load_L	3000 N	1000- 4000
Side Airbag Friction, sab_F	0.3	0 - 3
Frontal Airbag (firing) Time, ttf	18 ms	12- 25
Side Airbag (firing) Time, tsb	18 ms	12 - 25
Side Airbag Mass Flow Rate, sab_mfr	1	0.75 – 1.25

The simulation setup and results for the nominal values of parameters for frontal impact (0^0 PDOF) are identical to those given in Figure C.6 and

Table C.2, where BrIC was equal to 0.55. The time histories of the head angular velocities for the near side driver impact (-20^0 PDOF) with the nominal values of parameters are shown in Figure C.12, giving BrIC of 0.58 (

Table C.4).

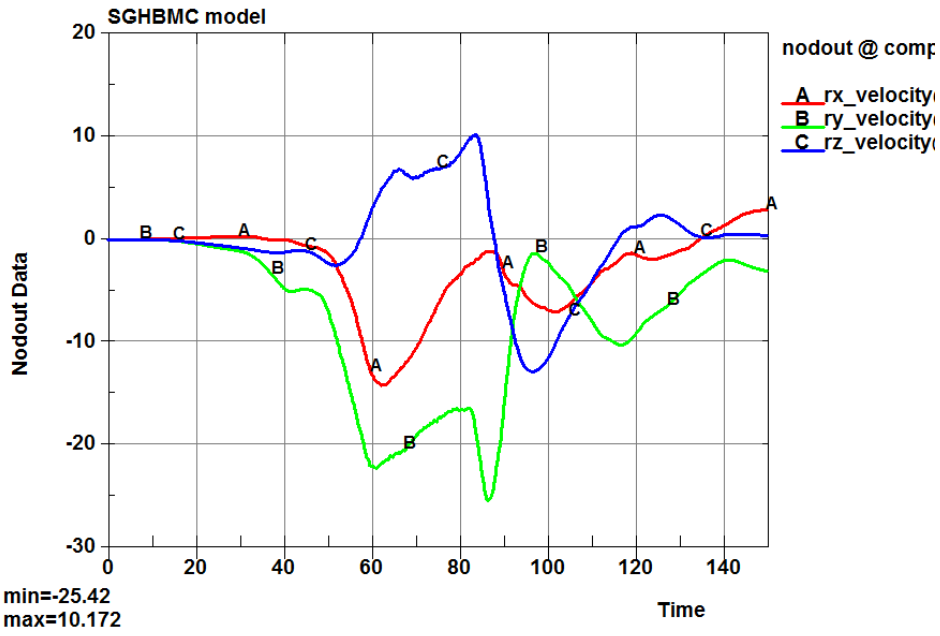

Figure C.12. FE model output for the head angular velocity components time histories for the driver near side oblique run (-20^0 PDOF) with nominal parameters.

Table C.4. Results of the driver near side oblique run with the nominal parameters.

Fab_F	Fab_MFR	Seat_F	Load_L	Sab_F	ttf	tsb	Sab_mfr	BrIC
0.5	1.0	0.5	3000	0.3	18	18	1.0	**0.58**

For the driver far side oblique run (20^0 PDOF) with nominal values of parameters the time histories of the head angular velocities are shown in Figure C.13 and the corresponding BrIC of 1.07 in

Table C.5.

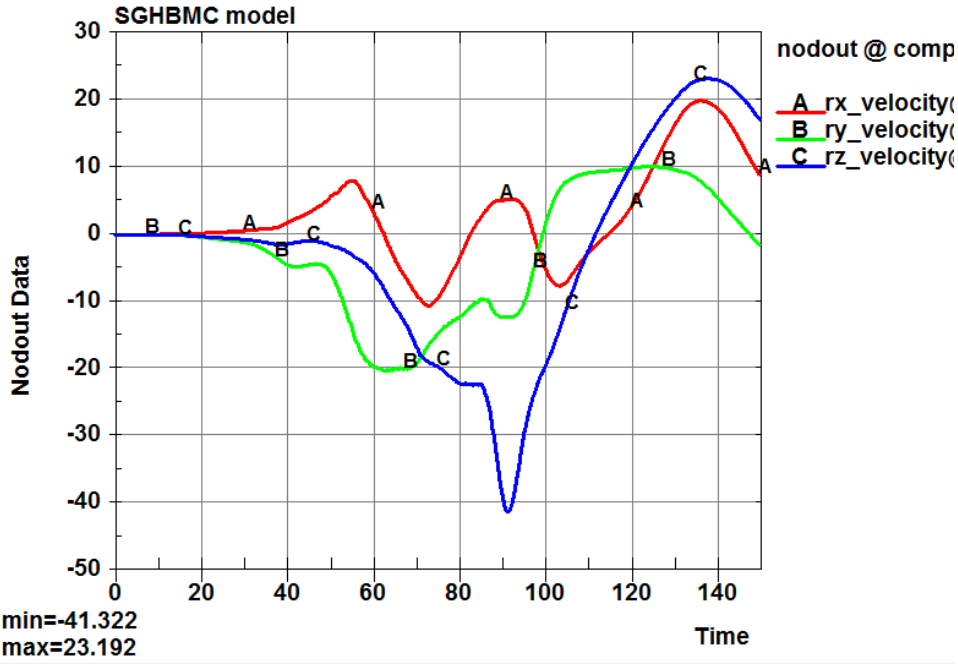

Figure C.13. FE model output for the head angular velocity components time histories for the driver far side oblique run (20^0 PDOF) with nominal parameters.

Table C.5. Results of the driver far side oblique run with the nominal parameters.

Fab_F	Fab_MFR	Seat_F	Load_L	Sab_F	ttf	tsb	Sab_mfr	BrIC
0.5	1.0	0.5	3000	0.3	18	18	1.0	**1.07**

While for frontal and near side oblique runs with nominal values of parameters, the highest angular velocity was about the y-axis (green line in Figure C.6 c) and Figure C.12), for the far side oblique run, the highest angular velocity is about the z-axis (blue line in Figure C.13).

The metamodel-based global sensitivity plot for the frontal impact is shown in Figure C.14 demonstrating that frontal airbag mass flow rate affects the values of BrIC the most (30.2%) in this test condition, followed by the frontal airbag friction (17.2%), then load limiter (14.3%), and frontal airbag firing time (10.4%). Collectively these four parameters can alter the value of BrIC by 72.1%. An example

of parameters giving low BrIC (0.38 with zero risk of any brain injury based on CSDM risk curve) and high BrIC (1.01 corresponding to 56% risk of AIS 4+ brain injury based on CSDM risk curve) in frontal impact are given in Table C.6. It should be noted that the values of parameters given in Table C.6 were selected for demonstration purposes and are just examples that give low and high values of BrIC; also, these are not the parameter values giving the lowest or highest values of BrIC. There are many different combinations of the restraint parameters that influence BrIC. For example, one could fix the values of the frontal and side airbag friction coefficients to those of nominal values and still find a set of parameters giving low and high BrIC values.

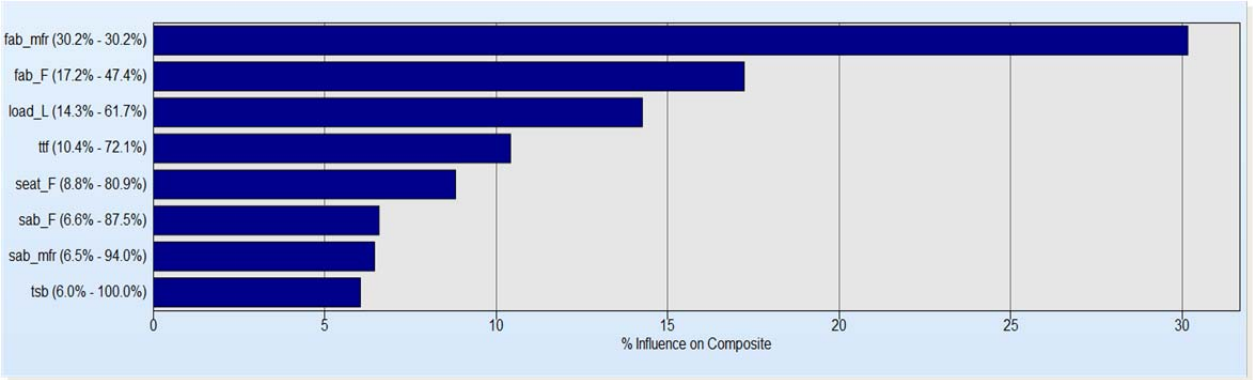

Figure C.14. Influence of all parameters given in Table C.3 on BrIC of driver in frontal impact.

Table C.6. Results of the frontal runs with parameters yielding low (0.38) BrIC and high (1.01) BrIC values.

Fab_F	Fab_MFR	Seat_F	Load_L	Sab_F	ttf	tsb	Sab_mfr	BrIC
1.84	0.85	0.1	2860	0.04	12	20	1.24	**0.38**
0.06	0.75	2.46	3075	1.58	14	25	0.97	**1.01**

For the near side driver oblique impact the metamodel-based global sensitivity plot is shown in Figure C.15. Here the most influential (over 10% influence) parameters on BrIC are: side (23.5%) and frontal (23.0%) airbags friction coefficients, followed by the load limiter (17.2%) and the frontal airbag mass flow rate (12.2%), with combined influence on BrIC of 75.9%. The friction coefficients between the airbags and the head appear to be the most influential in this test condition, and may be considered by the restraint system designer as the parameters to work on (reducing friction coefficient of the airbag fabric). However, the frontal airbag mass flow rate may be tuned along with the load limiter such to affect the values of BrIC. Table C.7 gives examples of several combinations of parameters making BrIC as small as 0.50 (corresponding to zero risk of any brain injury) and as high as 2.04 (corresponding to 99.1 % of AIS 4+ brain injury risk). Again, these are just examples of parameter sets giving extreme values of BrIC.

The designer of a restraint system must understand all the complex interactions between various parameters that influence the values of BrIC (and other injury criteria) in one direction or another to properly select a combination that would minimize overall injury risk (see below the section on optimization of the restraint systems).

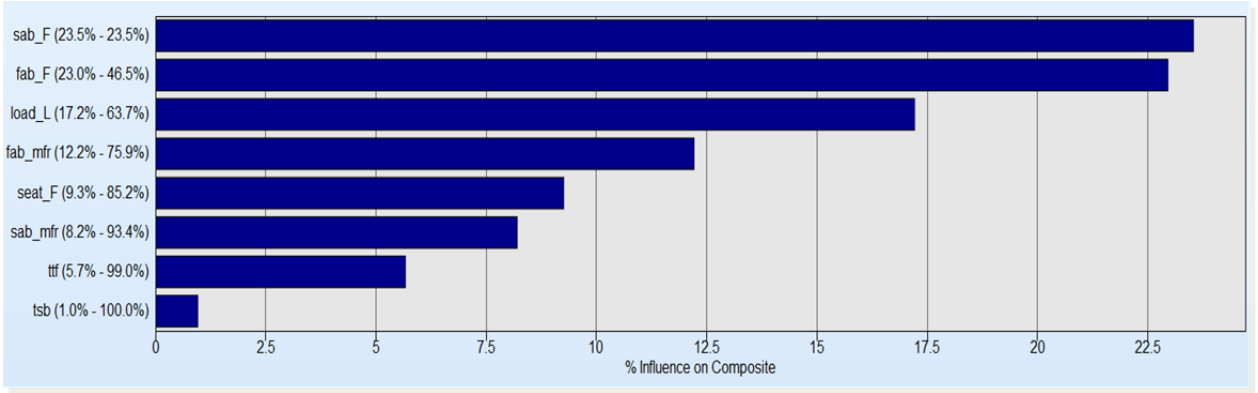

Figure C.15. Influence of all parameters given in Table C.3 on BrIC of driver in near side oblique impact.

Table C.7. Results of the near side oblique with parameters yielding low (0.50) BrIC and high (2.04) BrIC values.

Fab_F	Fab_MFR	Seat_F	Load_L	Sab_F	ttf	tsb	Sab_mfr	BrIC
0.29	1.25	2.51	1822	0.12	13.6	12	0.785	**0.50**
0.17	0.98	0.98	1050	1.2	24	17.3	1.05	**1.34**
0.22	0.78	2.94	3040	2.95	13.4	12.8	1.06	**2.04**

Finally, the metamodel-based global sensitivity plot for the driver far side oblique runs is shown in Figure C.16. In this test condition the most influential parameters affecting BrIC are: frontal airbag friction coefficient (24.5%), frontal airbag firing time (20.2%), frontal airbag mass flow rate (18.4%), and the load limiter (12.1%) collectively affecting values of BrIC by 75.2%. Note that side airbag parameters – the bottom three parameters in Figure C.16 – are not important and should be ignored; the fact they are not equal to zero is the by-product of the DOE analysis, hence only parameters with the influence greater than 10% were considered here. In the far side driver oblique impacts, the frontal airbag firing time becomes very important and the design space may be further expanded with the increased upper limit of this parameter (currently set at 25 ms – Table C.3).

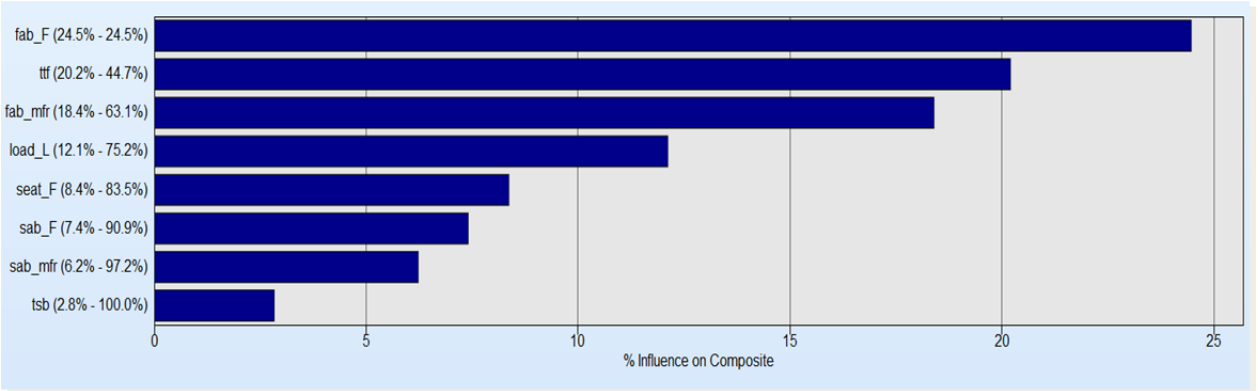

Figure C.16. Influence of all parameters given in Table C.3 on BrIC of driver in far side oblique impact.

Table C.8. Results of the far side oblique with parameters yielding low (0.62) BrIC and high (2.15) BrIC values.

Fab_F	Fab_MFR	Seat_F	Load_L	ttf	BrIC
0.322	1.11	2.92	1040	19	**0.62**
0.19	0.76	2.38	3950	23	**0.62**
2.89	0.75	0.13	1894	13	**2.15**

Despite this limitation, low values of BrIC (0.62) were obtained (these are not the lowest possible but just the values for these example parameter sets), corresponding to approximately 4% of AIS 4+ risk of brain injury (see examples in the first two rows

Table C.8). It also appears that reducing the frontal airbag mass flow rate and firing time may cause increase in BrIC values.

Table C.9 lists all the parameters affecting BrIC based on this limited DOE study (limited to the vehicle size, frontal and side airbag size, occupant size, posture, seating position, etc.) for each crash mode: frontal, near and far side driver oblique.

Table C.9. Parameters list affecting BrIC the most for each crash mode.

Frontal	Near Side	Far Side
Frontal Airbag MFR	Frontal Airbag MFR	Frontal Airbag MFR
Load Limiter	Load Limiter	Load Limiter
Frontal Airbag Friction	Frontal Airbag Friction	Frontal Airbag Friction
Frontal Airbag Firing Time	Side Airbag friction	Frontal Airbag Firing Time

Again, DOE analysis gives a general picture of the influence of various parameters on BrIC. However, it doesn't answer the question of the exact parameters values that will minimize BrIC for a given geometry of the restraint system (airbag volume), vehicle dimensions, and occupant characteristics (size, seating position, etc.). This question is analyzed in the following section.

OPTIMIZATION STUDIES

After identification of the parameters affecting BrIC with the help of DOE studies (Table C.9), it is important to demonstrate that it is possible to select a set (or a number of sets) of these parameters that minimize BrIC while keeping other injury criteria constrained to their critical values. In these optimization studies, the following constraints on injury criteria were imposed: HIC_{15} was constrained to be under 700, central chest (sternal) deflection – to 63 mm, and femur force (left and right) – to 10 kN. The objective function was BrIC itself, i.e. the study minimized BrIC subject to the four constraints listed above.

The vehicle, restraint, and occupant descriptions were given in the DOE section above and remained similar for the optimization studies (except for the optimization study #2 in which the size of the frontal airbag was increased to demonstrate the effect of increased airbag coverage on BrIC).

Instead of metamodels (see DOE section), direct simulation-based optimization was used. Genetic algorithms (GA) were used for optimization. Genetic algorithms are nature inspired search algorithms that emulate the Darwinian principle of 'survival of the fittest.' The differences between genetic algorithms and most conventional optimization methods are:

- GA does not require derivative information to drive the search of optimal points.
- While conventional methods use a single point for each iteration, GA uses a population based approach.
- GA is a global optimizer whereas conventional methods may get stuck in local optima.
- GA is a probabilistic optimization method that is, an inferior solution (that may help evolve the correct design variables structure) may also have a non-zero probability of participating in the search process.
- The computational cost of using GA may be high compared to derivative based methods.

It was also initially assumed in these optimization studies that an intelligent in-crash censoring may identify the crash mode (full frontal, near side driver oblique or far side driver oblique) within the first few milliseconds of the crash, so that separate optimizations were carried out for each crash mode. However, a single parameter set was also identified (as an example) that would work (minimize BrIC) for all crash modes.

Optimization Study #1

In this study the parameters listed in Table C.9 were varied and their range was identical to those given in Table C.3. The frontal airbag volume along with other restraint, vehicle, and occupant parameters were also kept the same as were described in the DOE studies.

The optimization history for the frontal runs is shown in Figure C.17 according to which only eight iterations were necessary to identify a global minimum for BrIC.

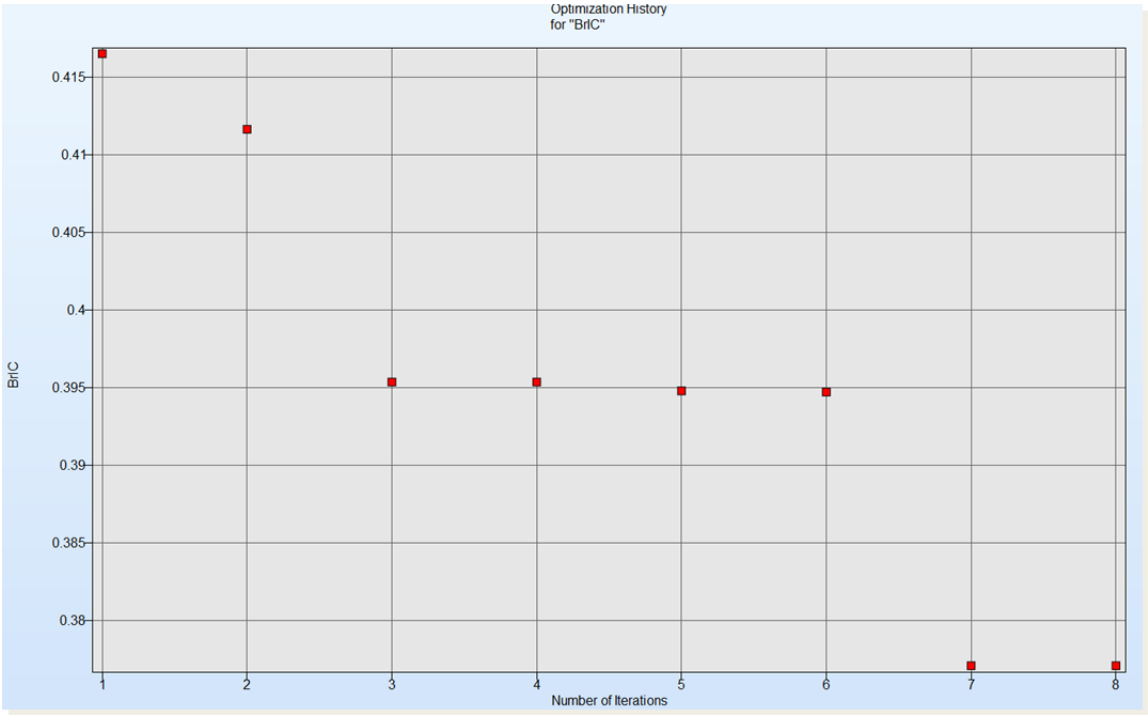

Figure C.17. Optimization history for BrIC for frontal runs.

The parallel coordinate chart for the frontal runs is given in Figure C.18. The vertical lines in Figure C.18 represent the range for each parameter varied. The names of the parameters varied are given at the bottom of the chart – first five parameters from left to right: frontal airbag friction coefficient, frontal airbag mass flow rate, frontal airbag firing time, load limiter, and side airbag friction (should be ignored in these frontal runs). The next four parameters are constraints (from left to right): left femur force, right femur force, max sternum deflection, and HIC_{15}. Finally, the response function is BrIC (rightmost parameter). The red line represent the constraint envelope, while the purple line shows the optimized value of each parameter (given in yellow rectangles). Each gray line represents result of a single run.

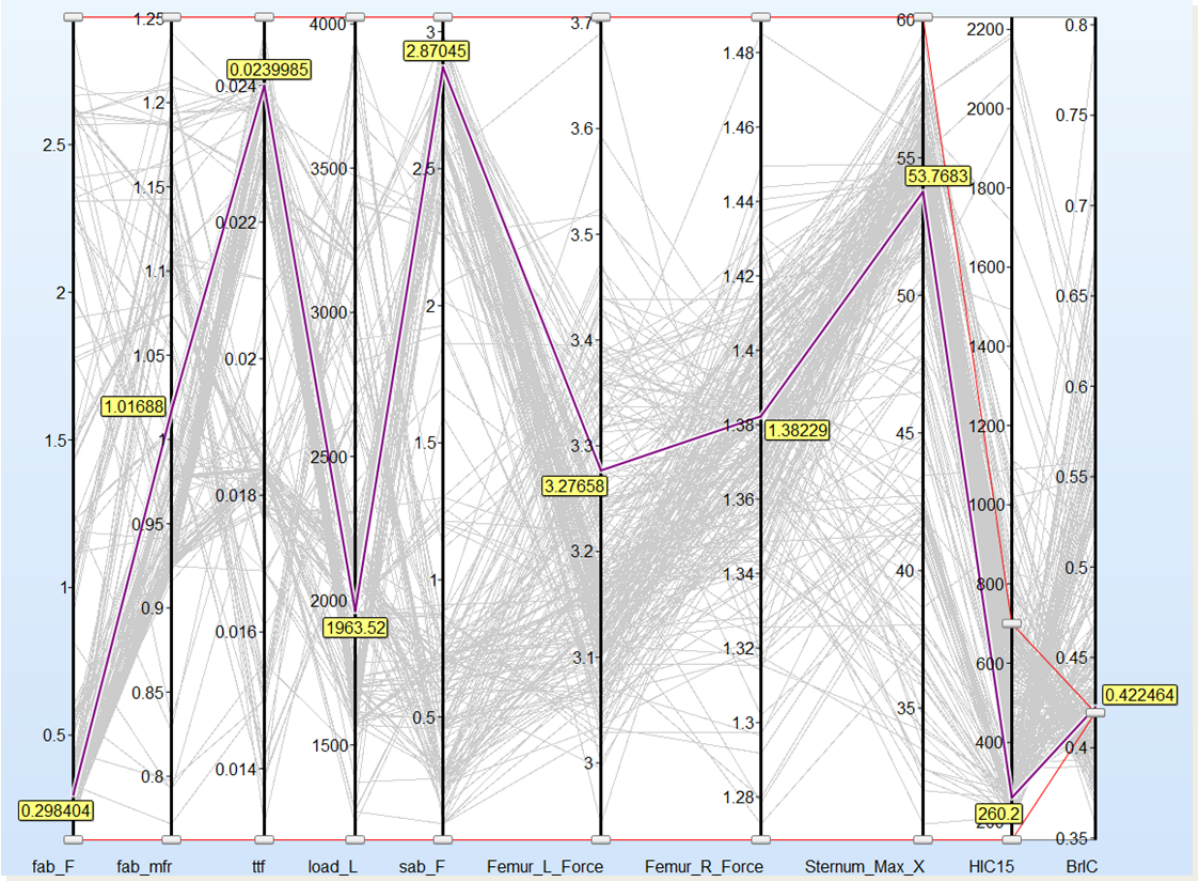

Figure C.18. Parallel coordinate chart for frontal runs.

It should be noted here that the values of constraints could be further reduced to search, for example, for the parameter sets with smaller sternal deflection and smaller BrIC. Also, the actual values here represent those measured by the simplified GHBMC model and are not directly translated to any ATD, i.e. if the optimized sternal deflection is about 54 mm for the frontal crash mode, it doesn't mean that if a model of an ATD was used instead of the GHBMC, this value would've been the same. The purpose of this exercise was to demonstrate the possibility/feasibility of reducing BrIC, while keeping other injury criteria within their constrained values. In addition, the objective function could've been redefined in a way that would minimize all the injury criteria simultaneously.

To investigate the relationships between various parameters in the frontal impact configuration, simulation based correlation matrix was plotted (Figure C.19), in which the first five columns (counted from the left) and first five rows (counted from the top) are the correlation coefficients for the investigated parameters/variables, the next seven are those of responses – four constraints and three max angular velocities, and the last column/row gives correlation coefficients for the objective function (called composite response here as it is comprised of the max angular velocities) – BrIC. The positive values in the cells at the intersection of each row and column represent positive correlation between the two parameters of interest (with increased value of one parameter, the other one increases as well). The greater the value of a correlation coefficient the more pronounced (significant) the relationship. For example, the load limiter (fourth row) and BrIC have correlation coefficient of 0.65 indicating that increasing load limiter value will increase the value of BrIC. Another example is the correlation

coefficient between BrIC and sternal deflection (-0.73), indicating that reducing sternal deflection will increase BrIC and vice-versa. In other words if a designer of a restraint system selects a parameter set that would reduce sternal deflection without the knowledge of the effect on BrIC, this could lead to increased risk of brain injuries. The opposite is true as well. Similarly, there is a negative correlation between BrIC and HIC_{15}, although not as strong as that between BrIC and sternal deflection, suggesting that reducing HIC_{15} (risk of skull fractures) will increase BrIC (risk of brain injuries). In general, the human body is a complex mechanical system and minimizing one parameter, while ignoring others, may lead to the so-called "unintended consequences" or "side effects" of such optimization. It is extremely important (as demonstrated by this example) to be aware of all the parameters affecting injury risks for various body regions. This knowledge gives a designer of restraint system the tools necessary to achieve the objective – minimize the risk of all injuries as well as the risk of "unintended consequences".

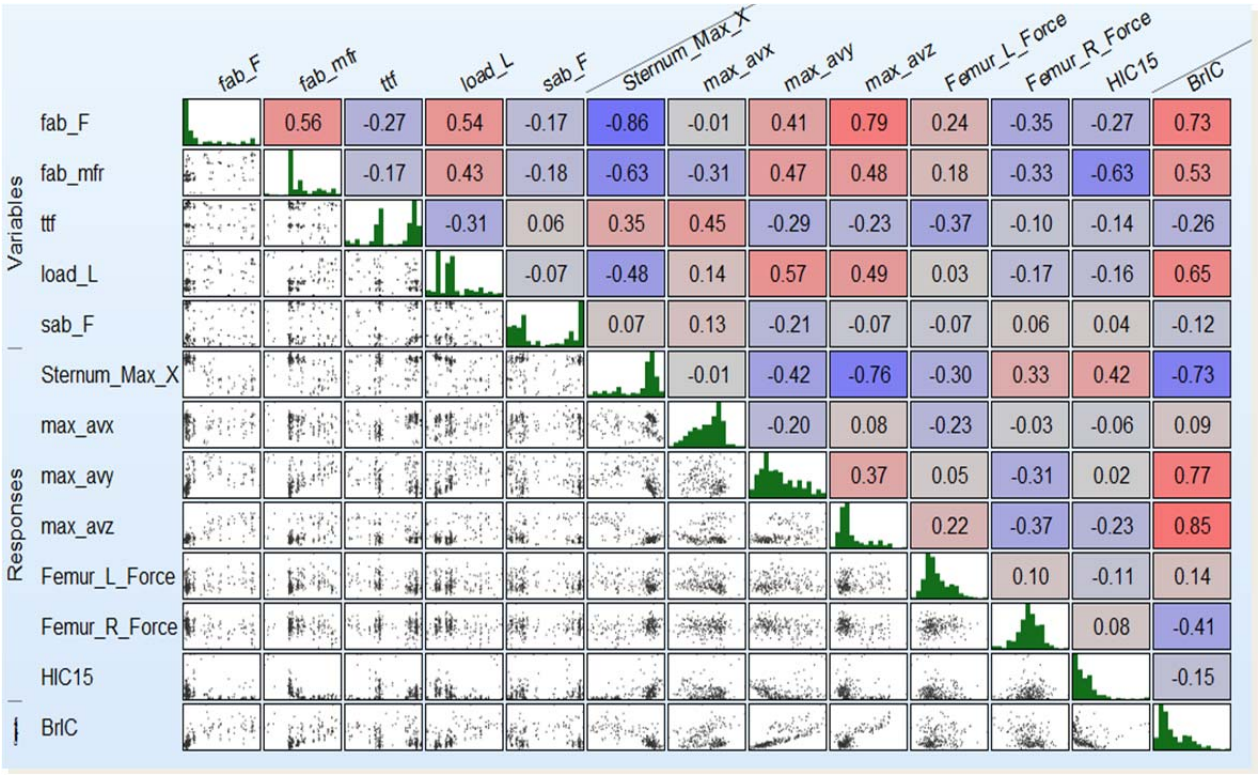

Figure C.19. Correlation matrix for frontal runs.

The relationship between HIC_{15} and BrIC (and max sternal deflection) is plotted in Figure C.20, where the inverse nature of the relationship is very clear. However, the plot also indicated that it is possible to select many different solutions with low values of both – HIC_{15} and BrIC (lower left corner of the plot) and at the same time to keep max sternal deflection to less than 40 mm (blue colored squares) in frontal crash mode as measure by the simplified GHBMC model. Exploring additional restraint design parameters in the optimization, such as steering wheel rim stiffness, etc. may offer further reduction in the values of different injury metrics.

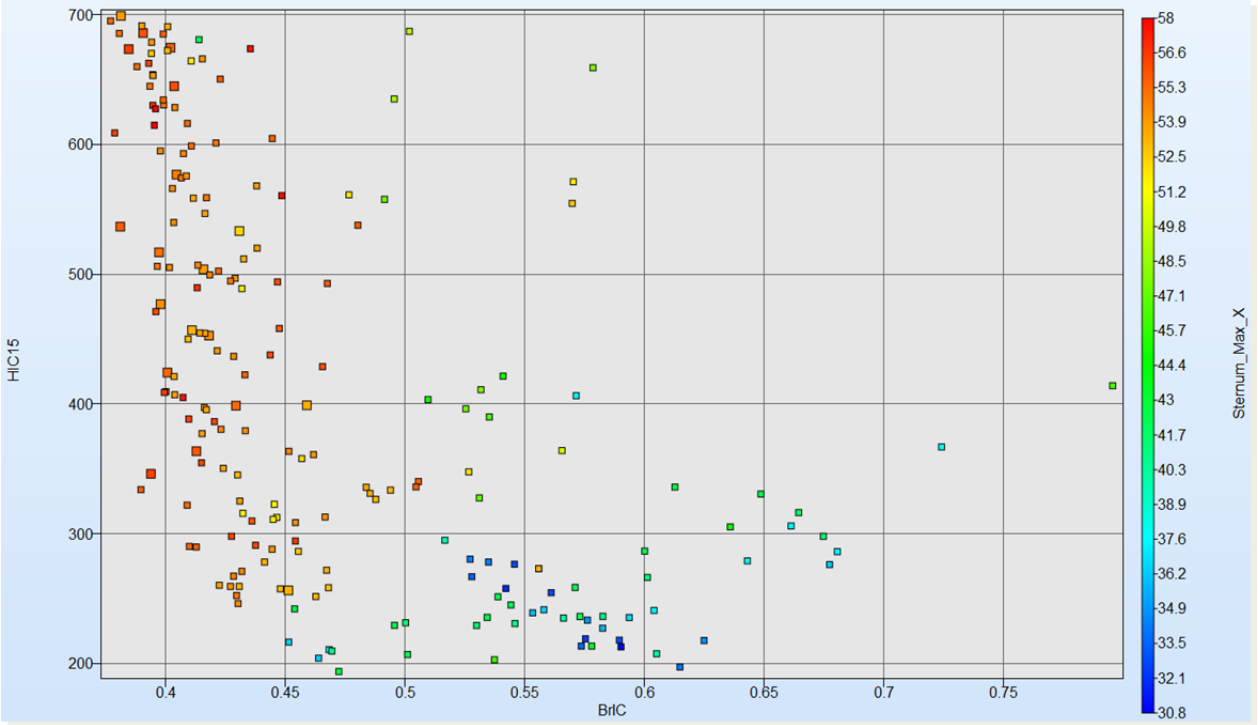

Figure C.20. Relationship between HIC_{15}, BrIC, and max sternal deflection in frontal runs (only feasible designs are shown).

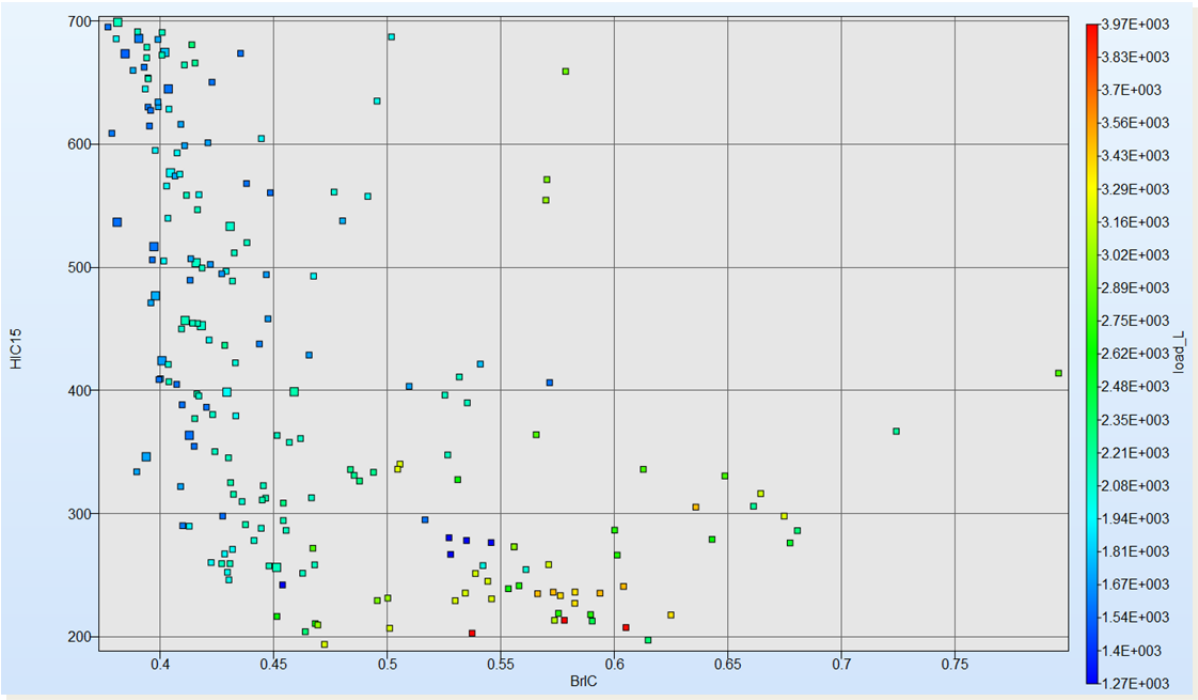

Figure C.21. Relationship between HIC_{15}, BrIC, and load limiter in frontal runs (only feasible designs are shown).

In Figure C.21 the relationship between HIC_{15}, BrIC and the load limiter is plotted indicating that low values of HIC_{15} and BrIC can be achieved simultaneously when the load limiter is set to approximately 2.0 kN.

For the near side driver oblique runs, the plots corresponding to those of the frontal runs shown in Figure C.17 through Figure C.21, are given below in Figure C.22 through Figure C.26, while those for the far side oblique runs are shown in Figure C.27 through Figure C.31.

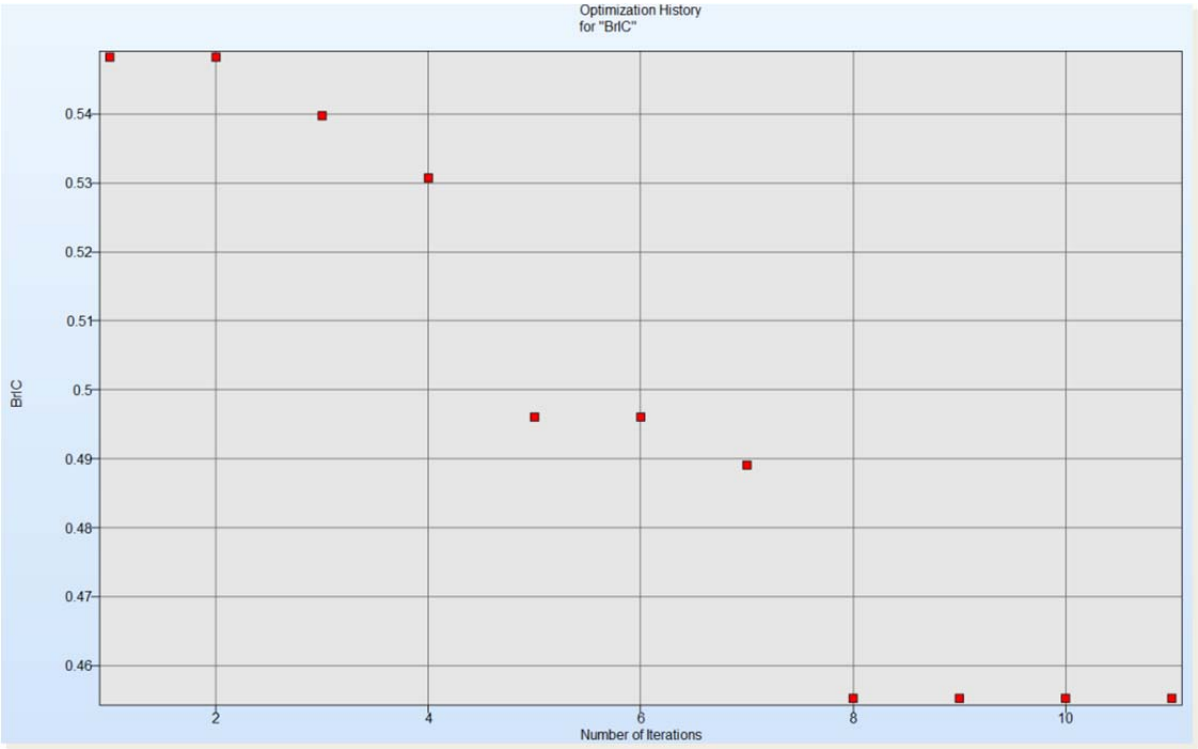

Figure C.22. Optimization history for BrIC in near side oblique runs.

The near side oblique runs converged (found global minimum for BrIC of 0.45) after 11 iterations (Figure C.22). The parallel coordinate chart for this mode (Figure C.23) shows significant increase in the right femur force compared to that in frontal crash mode (Figure C.18), while the optimized (for BrIC) max sternal deflection reduced to 43 mm. The optimized frontal airbag firing time has reduced, and the frontal airbag mass flow rate along with the load limiter force slightly increased. The correlation matrix (Figure C.24) still demonstrates negative correlation between BrIC and max sternal deflection, while that between BrIC and HIC_{15} has become positive. Another important observation is that frontal airbag mass flow rate has become significant in this crash mode demonstrating that its increase in value will reduce the value of BrIC. Figure C.25 and Figure C.26 show that it is possible to select several parameters sets to obtain low values of both HIC_{15} and BrIC (lower left corner of the charts) while keeping max sternal deflection in low 30 mm range (Figure C.25) and the load limiter in the range of 2.0 – 2.5 kN (Figure C.26).

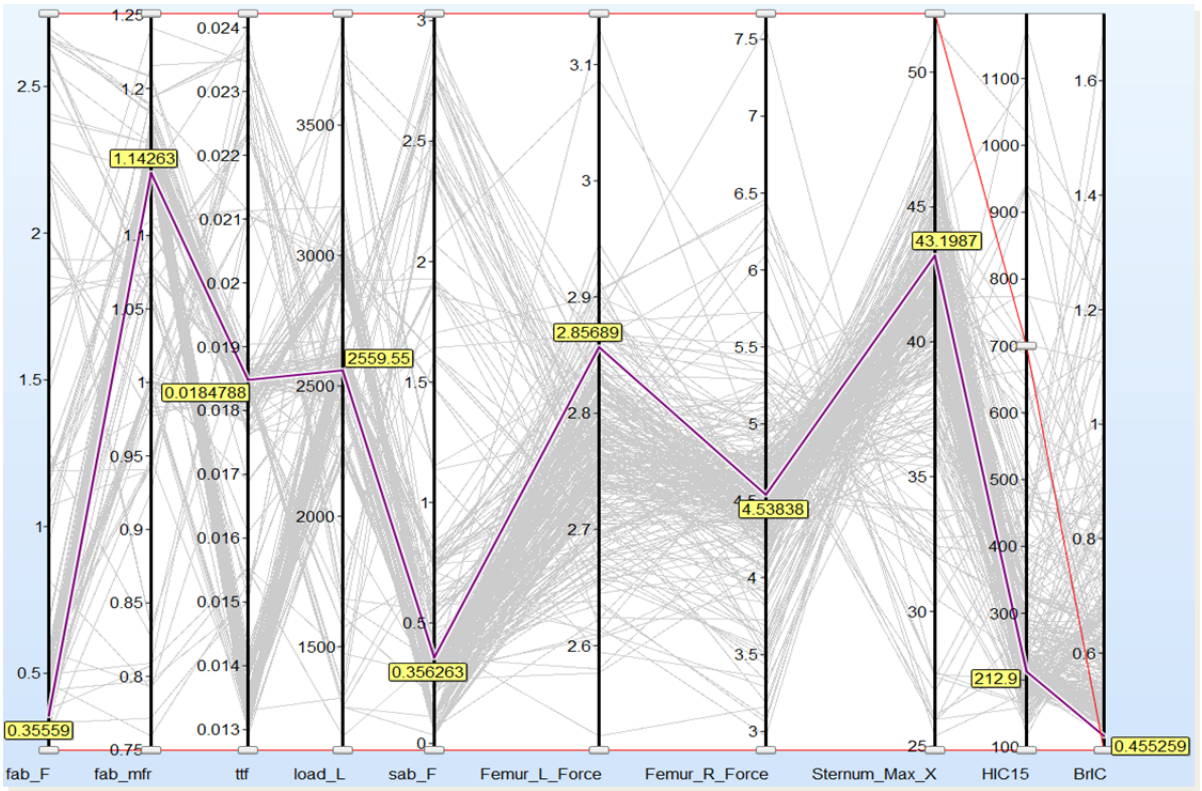

Figure C.23. Parallel coordinate chart for near side oblique runs.

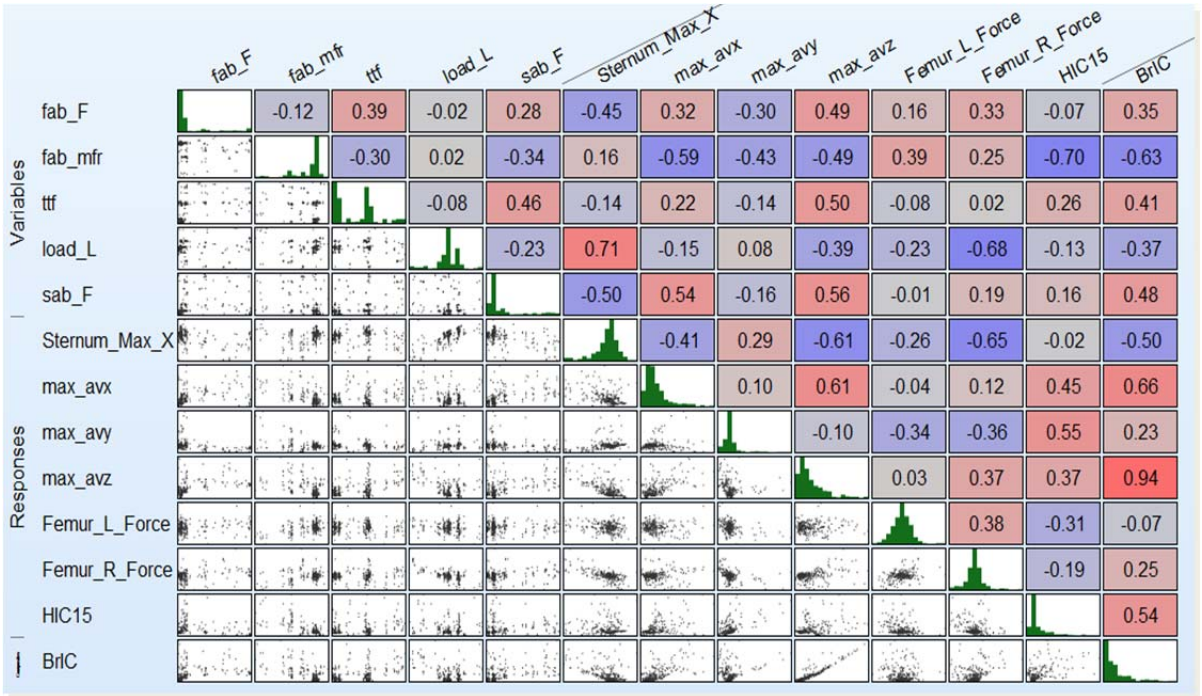

Figure C.24. Correlation matrix for near side oblique runs.

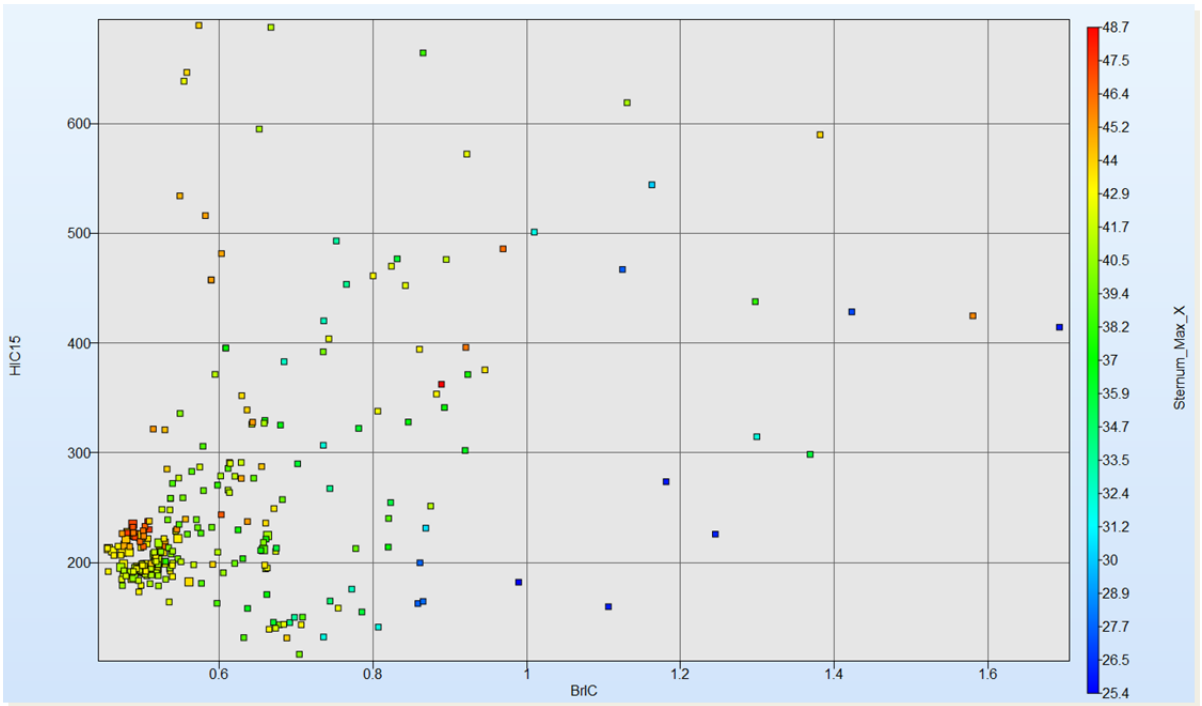

Figure C.25. Relationship between HIC_{15}, BrIC, and max sternal deflection in near side oblique runs (only feasible designs are shown).

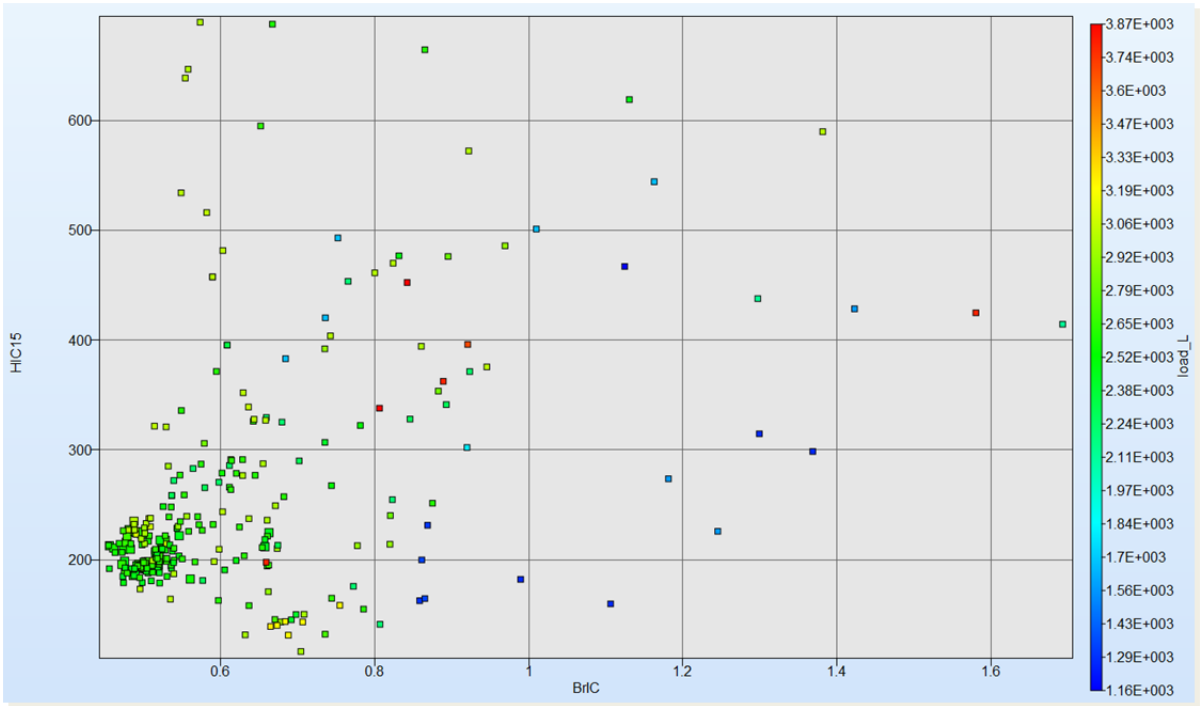

Figure C.26. Relationship between HIC_{15}, BrIC, and load limiter in near side oblique runs (only feasible designs are shown).

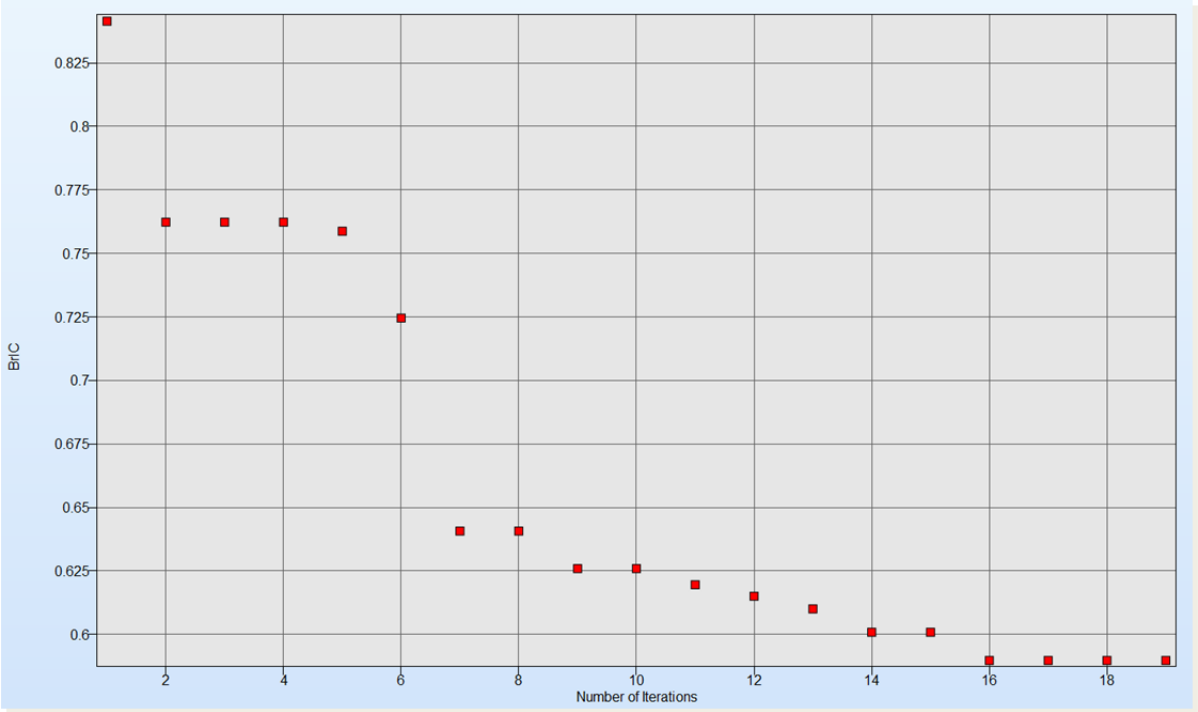

Figure C.27. Optimization history for BrIC in far side oblique runs.

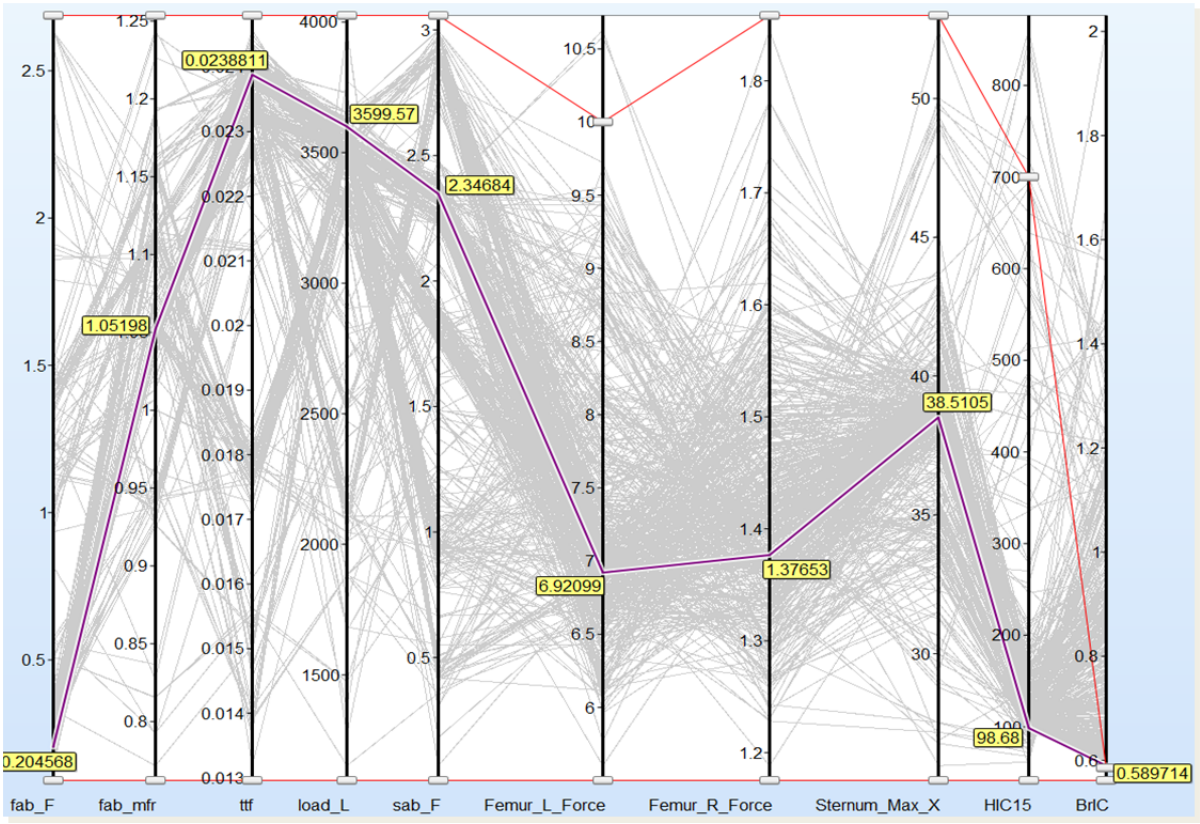

Figure C.28. Parallel coordinate chart for far side oblique runs.

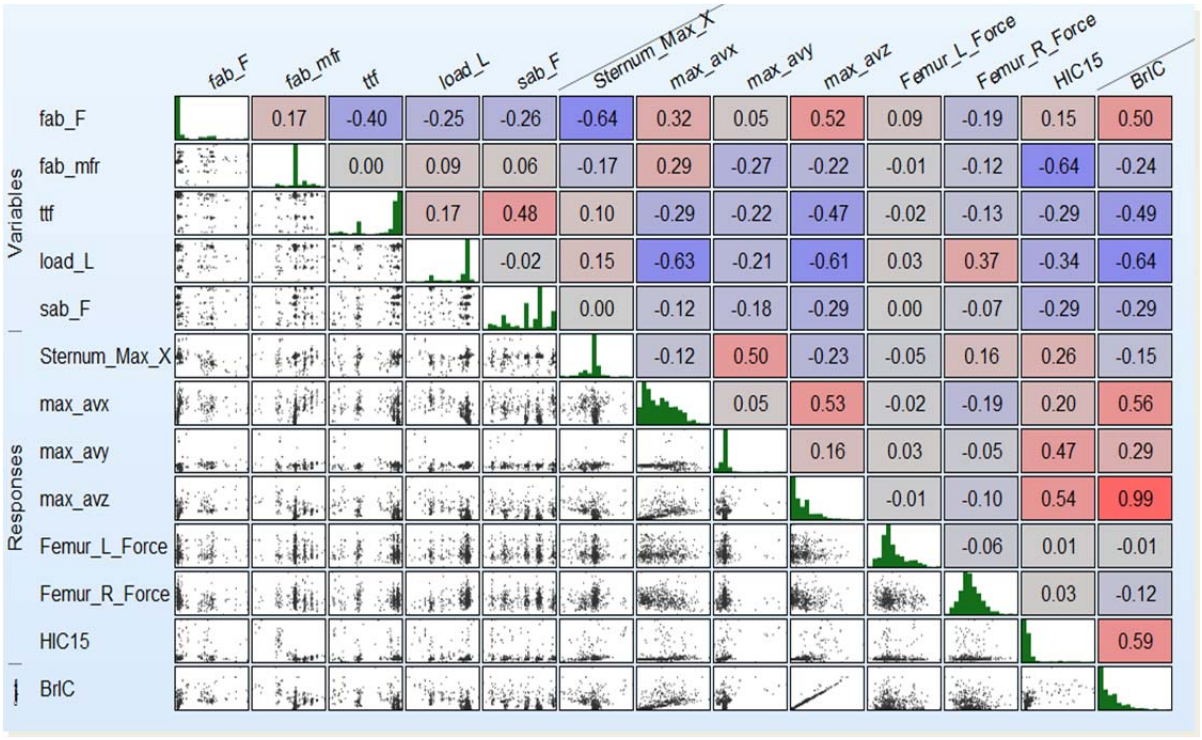

Figure C.29. Correlation matrix for far side oblique runs.

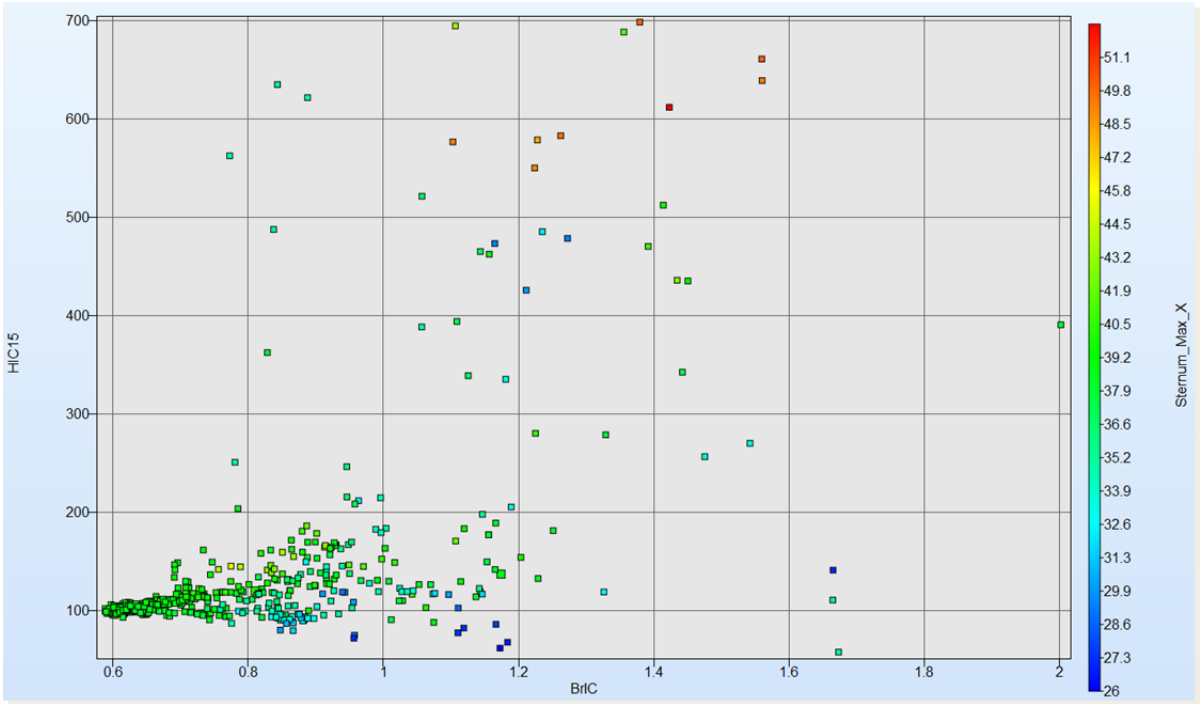

Figure C.30. Relationship between HIC_{15}, BrIC, and max sternal deflection in far side oblique runs (only feasible designs are shown).

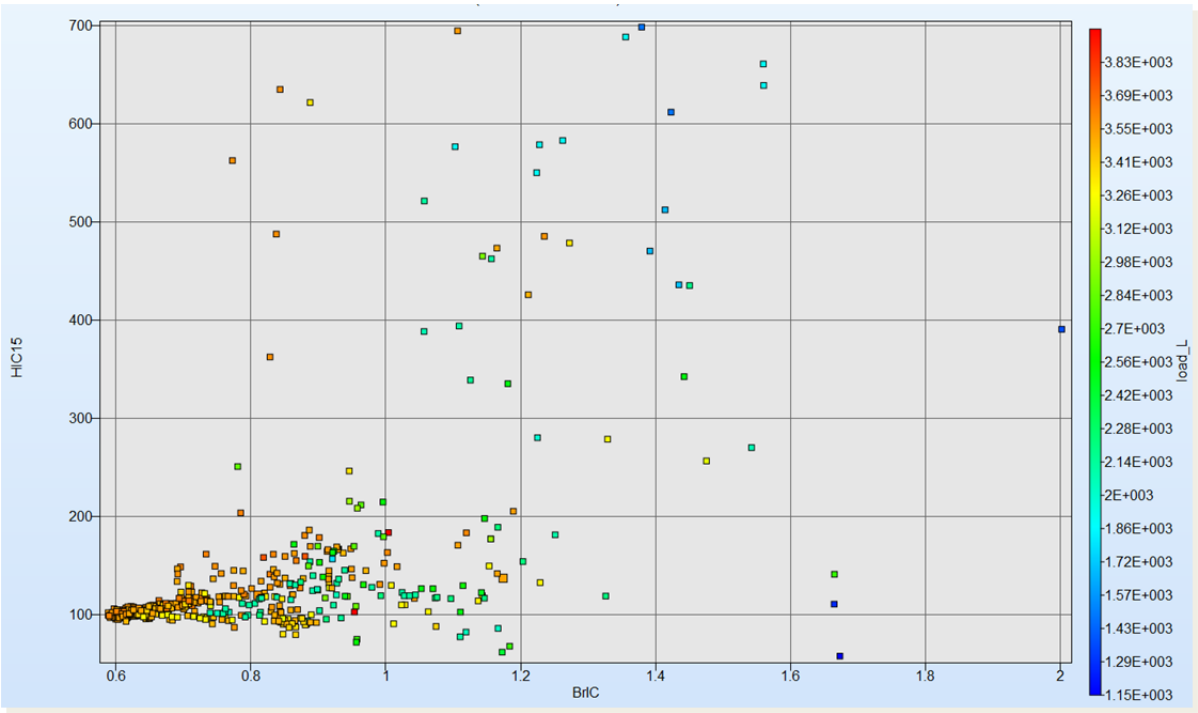

Figure C.31. Relationship between HIC_{15}, BrIC, and load limiter in far side oblique runs (only feasible designs are shown).

The optimization for BrIC in the far side oblique crash mode took the longest to converge – 19 iterations (Figure C.27) giving minimum BrIC value at just under 0.6. The parallel coordinate chart (Figure C.28) shows that for this crash mode, left femur force has significantly increased compared to that of the frontal or near side oblique crash modes. It also demonstrates that in order to keep the values of BrIC low, the load limiter force should increase to over 3.5 kN, which is the highest out the three crash modes considered in this study. Another observation from Figure C.30 is that both – HIC_{15} and max sternal deflection are the lowest here compared to those of frontal (Figure C.20) and near side driver oblique (Figure C.25) modes. This is, of course, at the expense of higher optimized value of BrIC. The simulation based correlation matrix (Figure C.29) still shows negative correlation between BrIC and max sternal deflection, albeit weaker than in the other two crash modes (correlation coefficient is -0.15). The load limiter has also a negative correlation coefficient here (compare with Figure C.21 for the frontal runs) along with the frontal airbag firing time, while correlation with HIC15 is positive (note: there were no head impacts to the instrument panel the presence of which may change correlation between HIC15 and BrIC). Figure C.30 and Figure C.31 show that there are plenty of parameter sets to choose from to obtain low values of both – HIC_{15} and BrIC, while keeping max sternal deflection in the mid 30-mm range (Figure C.30 lower left corner) and load limiter force in the range of 3.2 – 3.5 kN (Figure C.31 lower left corner).

Table C.10 lists, as an example, the values of variables for each crash mode that minimizes BrIC in this particular optimization study for this particular restraint (airbag size, etc.), vehicle (size, steering wheel assembly, etc.), and occupant (size, position, etc.) parameters.

Table C.10. Summary of the results from the optimization study #1.

Variables	Frontal (BrIC = 0.42)	Oblique - Near Side (BrIC = 0.46)	Oblique - Far Side (BrIC=0.59)
Frontal Airbag MFR	1.02	1.14	1.05
Load Limiter	1963	2559	3599
Frontal Airbag Firing Time	24	18.5	24
Frontal Airbag Friction	0.30	0.35	0.204
Side airbag Friction	N/A	0.36	N/A

In this study it was assumed that there exists an intelligent in-crash sensors system capable of detecting the PDOF of the crash within the first few milliseconds, which would give the restraint system enough time to select correct restrain system parameters (mass flow rate, load limiter, firing time, perhaps steering wheel stroke not considered in this study, etc.), examples of which are given in

Table C.10. In this example rather low values of BrIC were obtained representing zero risk of brain injuries for the full frontal and near side driver oblique crash modes and about 2.3% risk of AIS4+ brain injury in the far side crash mode. However, if such an intelligent sensor system doesn't exist, the question then becomes: is there a unique set of parameters that works for all crash modes? The best way to find such a set is to construct the objective function of the optimization process such that it minimizes BrIC for all crash modes simultaneously. However, some information can be obtained from the data presented above, from which a set of fixed parameters is selected (Table C.11) for demonstration purposes and simulations were run again at various PDOFs, results of which are given in Table C.12.

Table C.11. Fixed restraint system parameters.

Crash Pulse	Fab_F	Fab_MFR	Load_L	Sab_F	ttf
35 mph	0.35	1.14	2560	0.35	18.5

Table C.12. Injury values at different PDOF for the parameters given in Table C.11 (negative PDOF angles are for the near side driver oblique runs).

PDOF	Sternal Deflection, mm	BrIC	HIC15
0^0	53	0.50	362
-10^0	48	0.63	304
-15^0	47	0.66	248
-20^0	43	0.46	212

-25^0	41	0.62	201
-30^0	38	0.93	257
$+20^0$	40	0.82	149

Several observations can be made from Table C.12 for the fixed parameters:

1. The values of BrIC (not optimized) can be kept in a relatively low range for the near side driver oblique runs up until -25^0 PDOF; when the PDOF angle was furthered to -30^0 BrIC jumped up due to the head almost missing frontal airbag
2. The value of BrIC for the far side driver oblique run at PDOF of $+20^0$ was relatively high compared to that when optimized for just this test condition (BrIC was equal to 0.59 – see last column of
3.
4. Table C.10)
5. HIC_{15} values were relatively low with the highest value of 362 in a full frontal run – this is the crash mode in which BrIC was the lowest
6. Similarly to HIC_{15}, the highest value of the sternal deflection of 53 mm was in a full frontal run while the lowest – at -30^0 in which BrIC was the highest (0.93)

Here again, the reverse trend between BrIC and HIC_{15} (and sternal deflection) is evidenced. This means that if a restraint system is designed to minimize HIC_{15} and/or sternal deflection without the knowledge of BrIC, such design may lead to the increased risk of brain injuries. The reverse statement is true as well. However, currently restraint systems are designed without the knowledge of BrIC, which increases the risk of brain injuries as is also evidenced from the analysis of field data [See Chapter 9].

In the optimization study #1 a rather small airbag was used (50 liters) that provided limited coverage, and, as was demonstrated above, such limited coverage is insufficient to reduce BrIC values at the PDOF angles greater than -25^0 for the near side driver crash mode (and for the far side driver impact mode). To investigate how increased frontal airbag volume would affect the values of BrIC a second optimization study was conducted.

Optimization Study #2

To investigate how increased frontal airbag coverage affects BrIC, the optimization study was conducted for the near side driver oblique crash mode only with a simply scaled up frontal airbag so that its volume increased to approximately 98 liters. There are many different design solutions to increase the airbag coverage including, but not limited to: increasing the frontal airbag size (was used in this study), deploying additional airbags installed at the A-pillar (for near side driver crash mode) and/or instrument panel (for the far side driver crash mode), redesigning the shape of the frontal and side airbags with the increased coverage, developing multi-chambered airbags, etc. The purpose here was not to suggest any particular design modification, but rather to demonstrate the concept of increased frontal airbag coverage regardless of how unfeasible it may be as a "real" design solution (such as simply increasing the frontal airbag volume). Many "real" design solutions were also considered, but are outside the scope of these particular optimization studies.

Reiterating the problem statement for the optimization study #2:

1. Minimize BrIC for the near side driver oblique crash mode (PDOF = -20^0) by uniformly scaling up the volume of the frontal airbag to 98 liters
2. Keep other injury criteria to the same constraints as described in the optimization study #1
3. From all the feasible solutions of optimization (problem statement 1) find one set of parameters that would reduce the values of BrIC for any PDOF when compared to those given in Table C.12

The nominal values and the varied range of parameters are given in Table C.13. Note here that the range of friction coefficients was also reduced here, and the ranges for the frontal airbag mass flow rate and firing time were increased due to increased volume, when compared to those given in Table C.3.

Table C.13. Parameters varied in the optimization study #2 (crash pulse was kept the same as in all other studies and fixed at 35 mph).

Parameters	Nominal	Range
Frontal Airbag Friction, fab_F	0.5	0 – 1.0
Frontal Airbag Mass Flow Rate, fab_mfr	1	0.75 – 2.0
Load Limiter , load_L	3000 N	2000- 4000
Side Airbag Friction, sab_F	0.3	0 – 1.0
Frontal Airbag (firing) Time, ttf	18 ms	6- 30
Side Airbag Mass Flow Rate, sab_mfr	1	0.75 – 1.25

After the first iteration the solution converged to the BrIC value of under 0.38 (Figure C.32) and after just four iterations the optimization process stopped as the termination criterion was met. Several more iterations were kept to generate enough runs with various parameters ranges as is shown in the parallel coordinate chart (Figure C.33– gray lines). The simulation based correlation matrix and relationship between BrIC and HIC_{15} (sternal deflection and load limiter) are shown in Figure C.34 through Figure C.36.

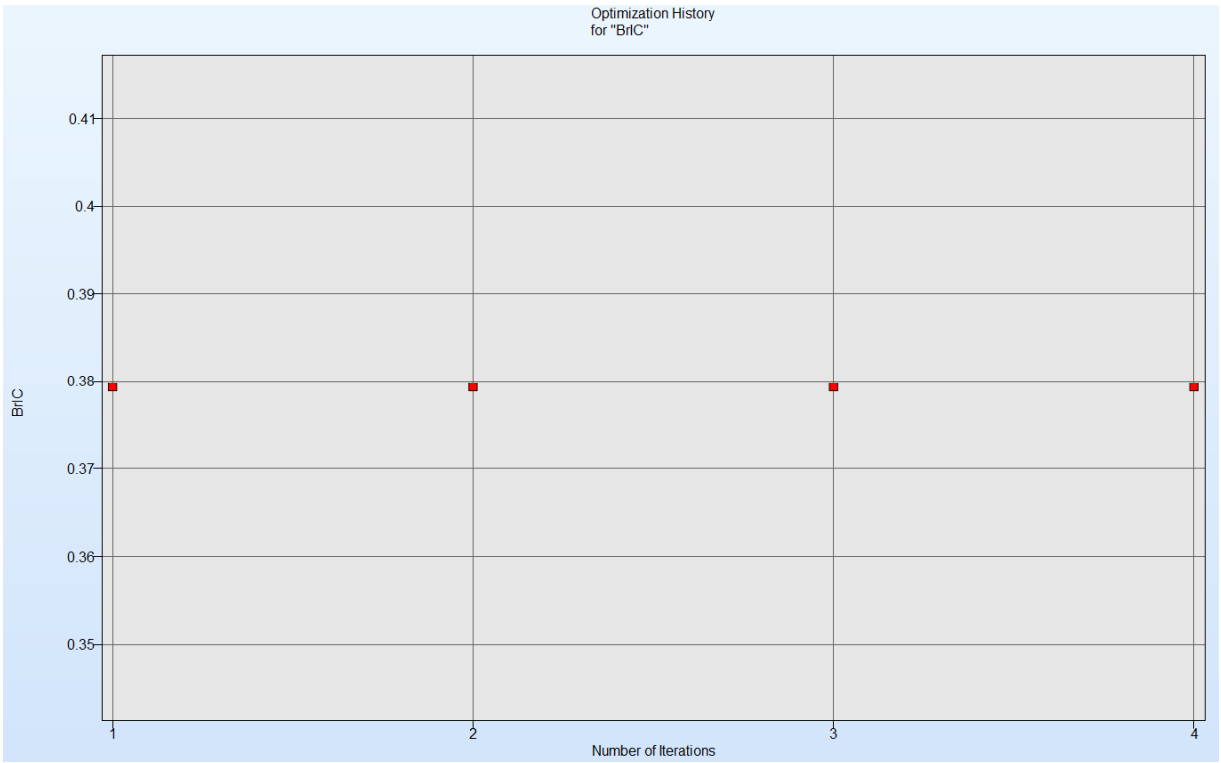

Figure C.32. Optimization history for BrIC in near side oblique runs with increased frontal airbag size.

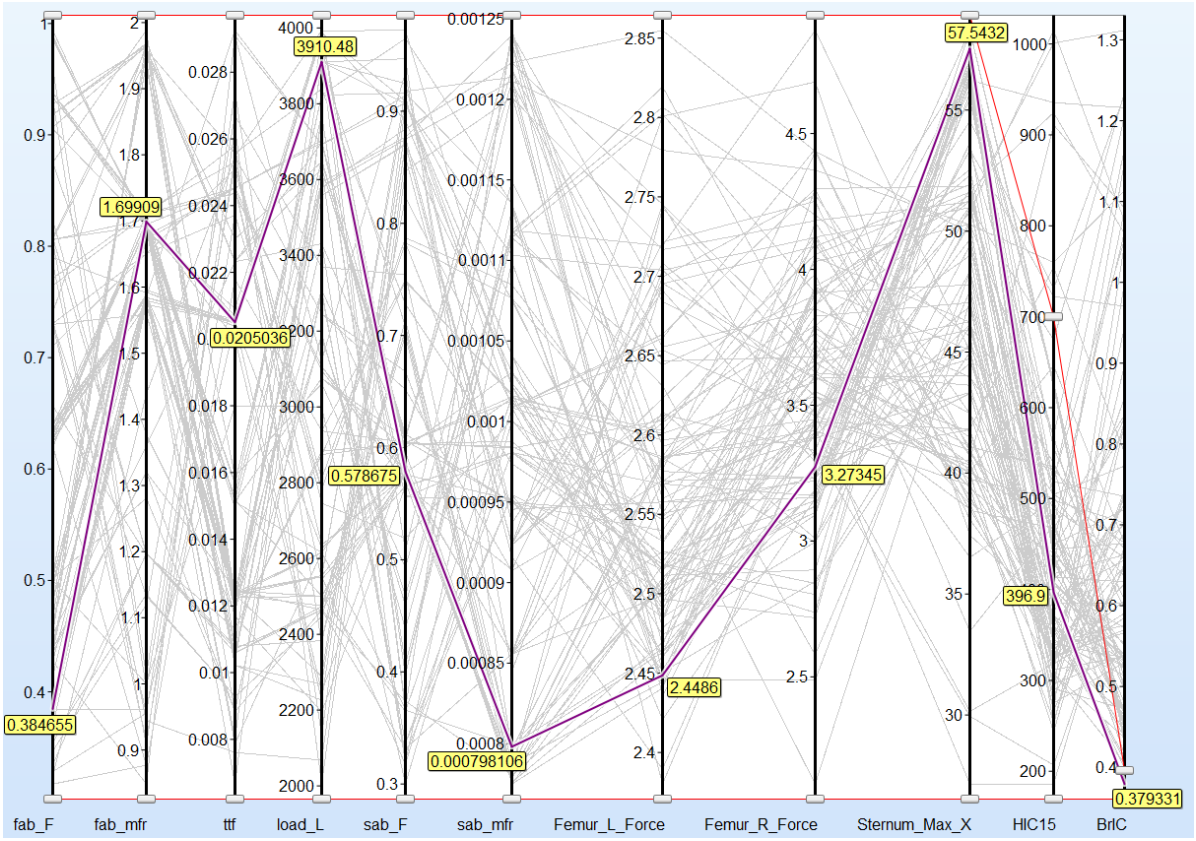

Figure C.33. Parallel coordinate chart for near side oblique runs with increased frontal airbag size.

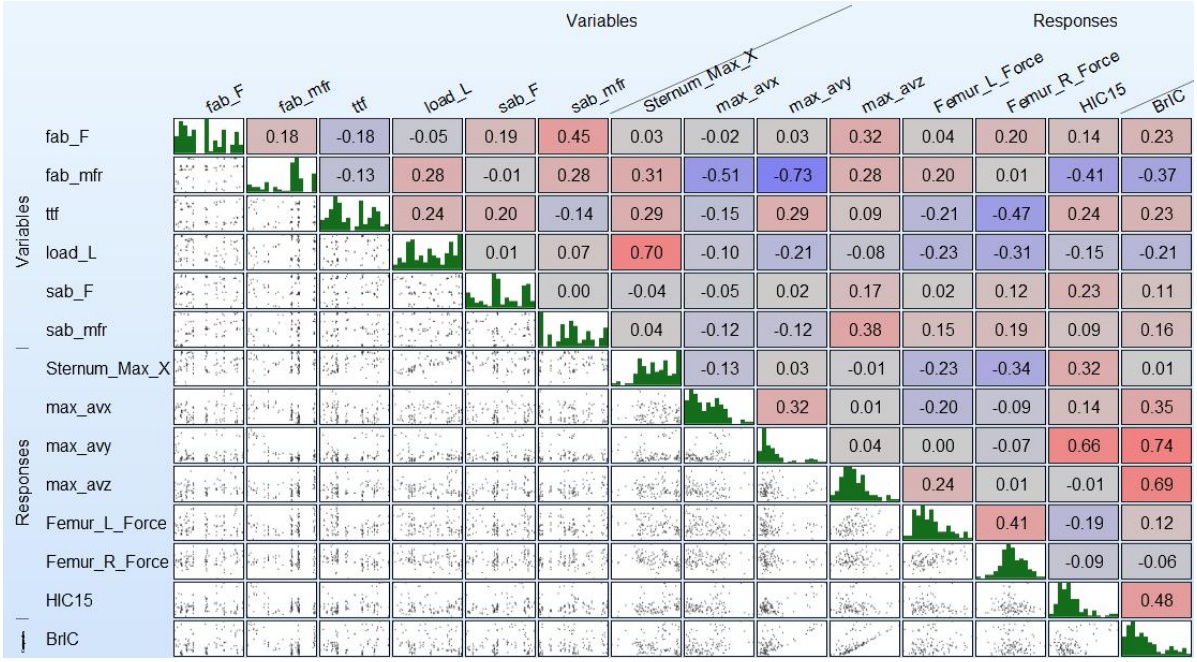

Figure C.34. Correlation matrix for near side oblique runs with increased frontal airbag size.

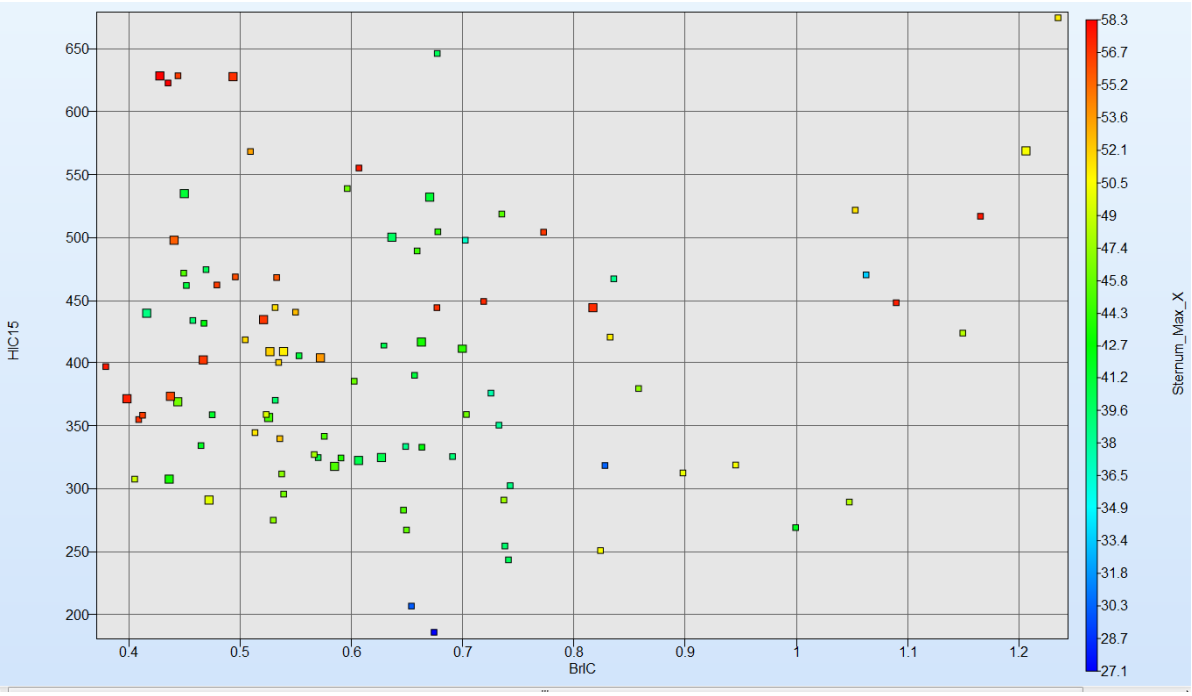

Figure C.35. Relationship between HIC_{15}, BrIC, and max sternal deflection in near side oblique runs with increased frontal airbag size (only feasible designs are shown).

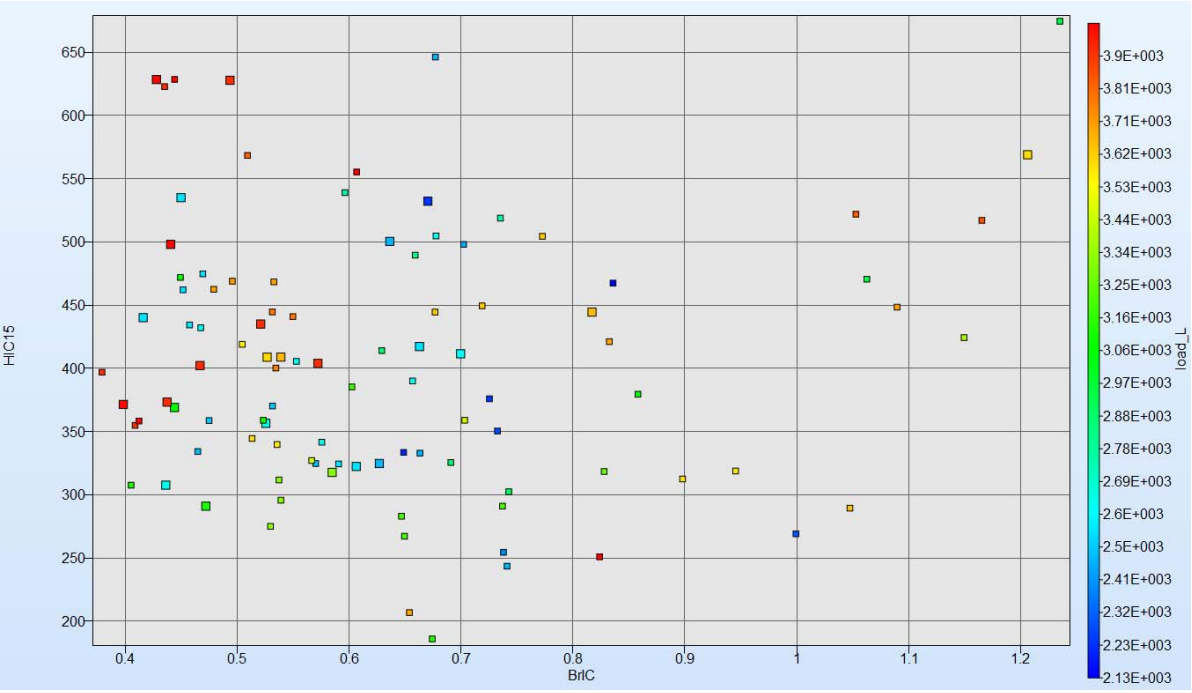

Figure C.36. Relationship between HIC_{15}, BrIC, and load limiter in near side oblique runs with increased frontal airbag size (only feasible designs are shown).

The results of the optimization are given in Table C.14 along with the parameters values. The value of BrIC now is lower than that in optimization study #1 with a 50 liter frontal airbag size. Not surprisingly, the value of HIC_{15} has increased as well as the value of the sternal deflection (similar trend as in the studies with the smaller frontal airbag). The knowledge of these trends is vital in designing future restraint systems that would offer protection from both – head/brain and chest injuries.

Table C.14. Results of the optimization near side driver oblique crash mode (PDOF = - 20^0) with increased frontal airbag size.

Crash Pulse	Fab_F	Fab_MFR	Load_L	Sab_F	Sab_MFR	ttf	Sternal Deflection	BrIC	HIC 15
35 mph	0.38	1.69	3910	0.58	0.80	20.5	**57.5**	**0.38**	**397**

Next, a single set of parameters (Table C.15) was chosen from the feasible design space (not the optimal point) and the model was exercised again with these fixed parameters at various PDOFs. The results of these simulations are shown in Table C.16.

Table C.15. Fixed restraint system parameters with increased frontal airbag size.

Crash Pulse	Fab_F	Fab_MFR	Load_L	Sab_F	Sab_MFR	ttf
35 mph	0.94	1.71	3075	0.60	1.03	15

Table C.16. Injury values at different PDOF for the parameters given in Table C.15 (negative PDOF angles are for the near side driver oblique runs) with increased frontal airbag size.

PDOF	Sternal Deflection, mm	BrIC	HIC15
0^0	45	0.38	500
-5^0	48	0.37	341
-10^0	48	0.38	426
-15^0	46	0.47	392
-20^0	46	0.44	368
-25^0	43	0.55	356
-30^0	41	0.66	450
$+20^0$	40	0.66	189

Comparing the results given in Table C.16 with that in Table C.12 for a smaller frontal airbag, it can be observed that the sternal deflection didn't change much. However, the values of BriC reduced substantially while the values of HIC_{15} increased substantially (all are still far below the 700 limit). For all PDOFs from 0^0 (full frontal crash mode) to -20^0 (near side driver oblique) the values of BrIC indicate zero risk of any brain injury with a slightly increased risk at the increased PDOFs in nears side driver oblique crash mode and the far side driver oblique crash mode. Again, this example is for demonstration purposes only and should be considered as such. However, it does demonstrate that increasing frontal airbag size/coverage decreases values of BrIC and increases values of HIC15 (which are still under the limit of 700).

APPENDIX D. Fleet Data

	VehDB TSTNO	Model Year	Make	Model	THOR Locations	Test Weight [kg]
Frontal Rigid Barrier 0 degrees Full overlap 56 km/h	09566	2016	Honda	Fit	Driver	1436
	09336	2015	Mazda	Mazda3	Driver	1599
	09567	2016	Chevrolet	Malibu	Driver	1826
	09569	2016	Nissan	Rogue	Driver	1888
	09570	2015	Toyota	Sienna	Driver	2295
	09334	2015	Toyota	Highlander	Driver	2335
	09571	2016	Ford	F150 Super crew	Driver	2485
	09568	2016	Chevrolet	Tahoe	Driver	2762
Oblique Moving Deformable Barrier 15 degrees 35% overlap 90 km/h	09572	2016	Honda	Fit	Driver, RFP	1403
	08787	2014	Mazda	Mazda3	Driver, RFP	1588
	08789	2014	Honda	Accord	Driver, RFP	1744
	08788	2014	Mazda	CX-5	Driver, RFP	1769
	08478	2014	Subaru	Forester	Driver, RFP	1803
	09573	2016	Chevrolet	Malibu	Driver, RFP	1808
	09574	2016	Nissan	Rogue	Driver, RFP	1860
	08488	2012	Volvo	S60	Driver, RFP	1936
	09585	2015	Toyota	Sienna	Driver, RFP	2272
	09481	2015	Toyota	Highlander	Driver, RFP	2306
	09587	2016	Ford	F150 Super crew	Driver, RFP	2434
	09586	2016	Chevrolet	Tahoe	Driver, RFP	2722

APPENDIX E. Thoracic Injury Criteria Source Data

Occupant Position	Environment	Restraint	Delta-V (km/h)	Age	Sex	Mass (kg)	Height (cm)	AIS 3+	PMHS BioDB	THOR BioDB	THOR Peak Res Defl (mm)	THOR PCA
Front Driver	Gold Standard	3-point standard belt	10	59	F	80	167	No		11125	12.62	1.457
				69	M	84	178	No		11126		
				60	M	81	191	No				
Front Driver	Gold Standard	3-point standard belt	40	59	F	80	167	Yes		11123	49.40	6.243
				69	M	84	178	Yes		11124		
				60	M	81	191	Yes				
Front Passenger	1997 Ford Taurus	3-point force-limited belt plus airbag	48	57	M	70	174	No	8371	11129	51.30	6.972
				69	F	53	155	Yes	8372	11130		
				72	F	59	156	Yes	8373			
				57	M	57	177	No	8374			
Front Passenger	1997 Ford Taurus	Lap belt with airbag	48	40	M	47	150	Yes*	8377	11131	30.08	3.326
				70	M	70	176	No	8378	11132		
				46	M	74	175	No	8379			
Front Passenger	1997 Ford Taurus	3-point standard belt with airbag	48	55	M	85	176	Yes	8382	11127	54.83	7.547
				69	M	84	176	Yes	8383	11128		
				59	F	79	161	Yes	8384			
Front Passenger	1997 Ford Taurus	3-point standard belt	29	49	M	58	178	No		11133	42.75	5.912
				44	M	77	172	No		11134		
				39	M	79	184	No				
Front Passenger	1997 Ford Taurus	3-point standard belt	38	44	M	77	172	No		11135	51.17	7.150
										11136		
Front Passenger	Gold Standard 1	3-point standard belt	40	76	M	70	178	Yes	9546	11117	47.73	6.857
				47	M	68	177	Yes	9547	11118		
				54	M	79	177	Yes		11119		
				49	M	76	184	Yes				
				57	M	64	175	Yes				
				72	M	81	184	Yes	11014			
				40	M	88	179	Yes	11015			
				37	M	78	180	No	11016			
Front Passenger	Gold Standard 2	3-point force-limited belt	30	59	M	68	178	No	11468	11120	26.78	3.788
				66	M	70	179	No	11469	11121		
				67	M	68	177	Yes	11509	11122		
				67	M	68	173	Yes	11510			
				74	M	70	183	No	11511			
Front Passenger	Gold Standard 3 (Near-side Oblique)	3-point force-limited belt	30	69	M	72	173	Yes	11518	11514	36	5.164
				66	M	76	172	Yes	11519	11515		
				67	M	65	177	No	11520	11516		
										11517		
Front Passenger	Far-side Oblique	3-point force-limited belt with airbag	59.5	73	M	69	180	Yes	11500	11503	53	6.475
				83	M	85	178	Yes	11501	11504		
				63	M	69	187	Yes	11502	11505		
										11506		
Rear Passenger	2004 Ford Taurus	3-point standard belt	48	51	M	55	175	Yes	9337	11143	57.96	7.999
				57	F	109	165	Yes	9338	11144		
				57	M	59	179	Yes	9339	11145		
Rear Passenger	2004 Ford Taurus	3-point force-limited belt with pretensioner	48	67	M	71	175	Yes		11140	46.66	6.520
				69	M	60	171	No		11141		
				72	M	73	175	Yes		11142		
Rear Passenger	2004 Ford Taurus	3-point inflatable force-limited belt with pretensioner	48	72	M	88	173	Yes		11137	29.66	3.790
				69	M	69	175	No		11138		
				40	M	83	186	No		11139		

APPENDIX F. Neck Injury Criteria Source Data

Table F.1. Source data for neck tension.

Specimen #	NHTSA Bio DB Test #	Study	Lab Code	Sex	Age	Peak Extension (Nm)	Rate-adjusted Extension (Nm)	Peak Tension (Nm)	Rate-adjusted Tension (Nm)	AIS 3+ Injury	AIS 2+ Injury
T22M FAOC	5272	Dibb et al. 2009	T-1	1	47	.	.	1993	2990	1	1
T23M FAOC	5312	Dibb et al. 2009	T-1	1	52	.	.	2147	3221	1	1
T24M FAOC	5354	Dibb et al. 2009	T-1	1	57	12.77	16.60	2145	3218	1	1
T25M FAOC	5954	Dibb et al. 2009	T-1	1	58	9.20	11.96	1726	2589	1	1
T26M FAOC	6018	Dibb et al. 2009	T-1	1	59	4.12	5.36	2357	3536	1	1
T27M FAOC	6135	Dibb et al. 2009	T-1	1	65	0.74	0.96	1756	2634	1	1
T28M FAOC	6070	Dibb et al. 2009	T-1	1	68	12.51	16.26	2319	3479	1	1
T29M FAOC	6310	Dibb et al. 2009	T-1	1	65	.	.	1811	2717	1	1
T31M FACG	8448	Dibb et al. 2009	T-1	1	61	18.92	24.60	2544	3816	1	1
T32M FACG	8491	Dibb et al. 2009	T-1	1	62	2.33	3.03	2761	4142	1	1
T33M FACG	8546	Dibb et al. 2009	T-1	1	57	17.95	23.34	2314	3471	1	1
T35M FACG	8658	Dibb et al. 2009	T-1	1	59	47.36	61.57	2239	3359	1	1
T36M FACG	8714	Dibb et al. 2009	T-1	1	58	23.93	31.11	2473	3710	1	1
T40M FACG	8938	Dibb et al. 2009	T-1	1	67	26.14	33.98	2112	3168	1	1
T41M FACG	8994	Dibb et al. 2009	T-1	1	53	24.67	32.07	2476	3714	1	1
T23M ECFX	5311	Duke-unpublished	T-2	1	52	1.77	2.30	308	308	0	0
T24M ECFX	5353	Duke-unpublished	T-2	1	57	7.06	9.18	310	310	0	0
T25M ECFX	5953	Duke-unpublished	T-2	1	58	4.41	4.41	305	305	0	0
T25M LAOC	5975	Duke-unpublished	T-2	1	58	0.09	0.09	295	295	0	0
T26M ECFX	6017	Duke-unpublished	T-2	1	59	6.14	6.14	305	305	0	0
T26M LAOC	6039	Duke-unpublished	T-2	1	59	0.20	0.20	300	300	0	0
T27M ECFX	6134	Duke-unpublished	T-2	1	65	5.46	5.46	307	307	0	0
T27M LAOC	6156	Duke-unpublished	T-2	1	65	0.16	0.16	302	302	0	0
T28M ECFX	6069	Duke-unpublished	T-2	1	68	5.02	5.02	308	308	0	0
T28M LAOC		Duke-unpublished	T-2	1	68	.	.	302	302	0	0
T29M ECFX	6309	Duke-unpublished	T-2	1	65	4.55	4.55	305	305	0	0
T30M ECFX	6413	Duke-unpublished	T-2	1	45	1.77	1.77	304	304	0	0
T30M LAOC	6434	Duke-unpublished	T-2	1	45	.	.	302	302	0	0
T31M ECFX	8447	Duke-unpublished	T-2	1	61	3.94	3.94	300	300	0	0
T32M ECFX	8490	Duke-unpublished	T-2	1	62	2.84	2.84	299	299	0	0
T33M ECFX	8545	Duke-unpublished	T-2	1	57	5.27	5.27	300	300	0	0
T34M ECFX	8601	Duke-unpublished	T-2	1	63	4.23	4.23	300	300	0	0
T35M ECFX	8657	Duke-unpublished	T-2	1	59	7.73	7.73	300	300	0	0
T36M ECFX	8713	Duke-unpublished	T-2	1	58	4.52	4.52	302	302	0	0
T37M ECFX	8795	Duke-unpublished	T-2	1	49	3.43	3.43	295	295	0	0
T38M ECFX	8825	Duke-unpublished	T-2	1	56	3.42	3.42	297	297	0	0
T39M ECFX	8881	Duke-unpublished	T-2	1	55	.	.	299	299	0	0
T40M ECFX	8937	Duke-unpublished	T-2	1	67	5.33	5.33	301	301	0	0
T41M ECFX	8993	Duke-unpublished	T-2	1	53	5.27	5.27	303	303	0	0
HPC14 04	6181	Pintar et al. 2005	T-3	1	63	43.00	43.00	2545	2545	0	1
HPC20 02	6221	Pintar et al. 2005	T-3	0	64	35.00	35.00	2158	2158	0	1
HPC21 02	6282	Pintar et al. 2005	T-3	0	65	41.00	41.00	3583	3583	0	1
HPC22 03	6283	Pintar et al. 2005	T-3	0	46	12.00	12.00	1524	1524	0	0
HPC28 03	8024	Pintar et al. 2005	T-3	1	63	8.00	8.00	106	106	0	0
HPC28 04	8025	Pintar et al. 2005	T-3	1	63	13.00	13.00	235	235	0	0
HPC28 05	8026	Pintar et al. 2005	T-3	1	63	92.00	92.00	2037	2037	0	1
HPC29 01	8027	Pintar et al. 2005	T-3	0	50	5.00	5.00	105	105	0	0
HPC29 02	8028	Pintar et al. 2005	T-3	0	50	11.00	11.00	232	232	0	0
HPC29 03	8029	Pintar et al. 2005	T-3	0	50	73.00	73.00	1984	1984	1	1
HPC30 02	8030	Pintar et al. 2005	T-3	1	73	3.00	3.00	115	115	0	0
HPC30 03	8031	Pintar et al. 2005	T-3	1	73	6.00	6.00	463	463	0	0
HPC30 04	8032	Pintar et al. 2005	T-3	1	73	69.00	69.00	3620	3620	1	1
HPC31 02	8033	Pintar et al. 2005	T-3	0	71	11.00	11.00	385	385	0	0
HPC31 03	8034	Pintar et al. 2005	T-3	0	71	6.00	6.00	856	856	0	0
HPC31 04	8035	Pintar et al. 2005	T-3	0	71	53.00	53.00	2254	2254	0	1
HPC32 01	8036	Pintar et al. 2005	T-3	1	72	5.00	5.00	84	84	0	0
HPC32 02	8037	Pintar et al. 2005	T-3	1	72	7.00	7.00	260	260	0	0

HPC32 03	8038	Pintar et al. 2005	T-3	1	72	44.00	44.00	1931	1931	0	1
HPC33 02	8039	Pintar et al. 2005	T-3	1	54	3.00	3.00	155	155	0	0
HPC33 03	8040	Pintar et al. 2005	T-3	1	54	8.00	8.00	351	351	0	0
HPC33 04	8041	Pintar et al. 2005	T-3	1	54	33.00	33.00	2002	2002	1	1
1	.	Yliniemi 2009	T-4	1	35	.	.	4060	4060	1	1
2	.	Yliniemi 2009	T-4	1	48	.	.	3860	3860	1	1
3	.	Yliniemi 2009	T-4	1	50	.	.	2810	2810	1	1
4	.	Yliniemi 2009	T-4	1	60	.	.	3150	3150	1	1
5	.	Yliniemi 2009	T-4	1	59	.	.	3230	3230	1	1
6	.	Yliniemi 2009	T-4	1	37	.	.	3220	3220	1	1
7	.	Yliniemi 2009	T-4	1	59	.	.	2440	2440	1	1
8	.	Yliniemi 2009	T-4	1	61	.	.	3230	3230	1	1
9	.	Yliniemi 2009	T-4	0	48	.	.	3560	3560	1	1
10	.	Yliniemi 2009	T-4	0	45	.	.	2250	2250	1	1
11	.	Yliniemi 2009	T-4	0	56	.	.	1910	1910	1	1
12	.	Yliniemi 2009	T-4	0	43	.	.	3490	3490	1	1

Table F.2. Sled data, including multiple PMHS test series conducted by UVA and PMHS and volunteer tests conducted at Naval Biodynamics Research Laboratory.

Age	Sex	Neck AIS	PMHS BioDB	THOR BioDB	THOR Peak Neck Tension (N)	THOR Peak Neck Compression (N)	THOR Peak Neck Flexion (Nm)	THOR Peak Neck Extension (Nm)	Max Nij	PMHS-equivalent Tension at max Nij	PMHS-equivalent Compression at max Nij	PMHS-equivalent Flexion at max Nij	PMHS-equivalent Extension at max Nij
59	F	0		11125	178.15	-230.99	7.87	-4.25	0.122	0.0	-124.8	4.9	0.0
69	M	0		11126									
60	M	0											
59	F	0		11123	2743.39	-476.67	22.00	-24.90	0.707	1200.7	0.0	2.3	-7.5
69	M	2		11124									
60	M	0											
57	M	0	8371	11129	1872.14	-1170.48	23.07	-20.53	0.520	899.3	0.0	0.0	-7.1
69	F	0	8372	11130									
72	F	0	8373										
57	M	0	8374										
40	M	0	8377	11131	1062.33	-939.92	8.81	-18.39	0.326	500.5	0.0	0.0	-6.8
70	M	0	8378	11132									
46	M	0	8379										
55	M	0	8382	11127	2370.62	-1668.57	12.87	-30.57	0.641	1142.0	0.0	0.0	-7.6
69	M	0	8383	11128									
59	F	0	8384										
49	M	0		11133	1388.98	-645.74	11.69	-11.12	0.359	642.4	0.0	0.0	-4.1
44	M	0		11134									
39	M	0											
44	M	0		11135	2396.56	-677.22	16.77	-13.34	0.613	1168.0	0.0	1.6	-2.3
				11136									
76	M	0	9546	11117	2134.18	-372.46	14.03	-17.90	0.565	1006.7	0.0	5.0	0.0
47	M	0	9547	11118									
54	M	0		11119									
49	M	0											
57	M	0											
72	M	0	11014										
40	M	0	11015										
37	M	0	11016										
59	M	0	11468	11120	969.16	-272.75	13.86	-10.67	0.262	447.1	0.0	2.9	0.0
66	M	2	11469	11121									
67	M	3	11509	11122									
67	M	2	11510										
74	M	0	11511										
69	M	2	11518	11514	1101.28	-102.30	8.71	-10.45	0.305	484.5	0.0	2.5	-2.4
66	M	1	11519	11515									

67	M	0	11520	11516								
				11517								
73	M	2	11500	11503	1636.40	-308.81	17.23	-13.00	0.517	697.9	0.0	7.8	-4.1
83	M	2	11501	11504								
63	M	0	11502	11505								
				11506								
51	M	2	9337	11143	3061.90	-55.88						
57	F	5	9338	11144								
57	M	3	9339	11145								
67	M	3		11140	2465.46	-697.68	23.82	-24.26	0.652	1201.7	0.0	4.7	0.0
69	M	0		11141								
72	M	0		11142								
72	M	0		11137	1671.19	-963.39	13.56	-21.29	0.435	733.5	0.0	5.0	0.0
69	M	0		11138								
40	M	0		11139								
50	M	0		10999	1083.19	-1265.96	32.77	-12.96	0.403	146.6	-46.3	18.7	0.0
51	M	0		11000								
61	F	0		11001								
51	F	2										
46	F	0										
37	M	0										
24	F	0										
59	M	0										
38	M	0										
20	M	0										
20	M	0										
20	M	0										
20	M	0										
20	M	0										

Table F.3. Source data for neck flexion and extension.

Specimen #	NHTSA Bio DB Test #	Study	Lab Code	Sex	Age	Peak Extension (Nm)	Rate-adjusted Extension (Nm)	Peak Flexion (Nm)	Rate-adjusted Flexion (Nm)	AIS 3+ Injury	AIS 2+ Injury
B19	7363	Nightingale 2007	F-1	1	69	.	.	46.20	64.68	0	0
B22	7411	Nightingale 2007	F-1	1	56	.	.	45.80	64.12	0	1
B24	7429	Nightingale 2007	F-1	1	71	.	.	33.60	47.04	0	0
B26	7441	Nightingale 2007	F-1	1	74	.	.	33.10	46.34	0	0
B28	7456	Nightingale 2007	F-1	1	69	.	.	35.00	49.00	0	0
B30	7463	Nightingale 2007	F-1	1	51	.	.	37.40	52.36	0	0
B32	7481	Nightingale 2007	F-1	1	57	.	.	36.20	50.68	1	1
B34	7499	Nightingale 2007	F-1	1	58	.	.	47.60	66.64	1	1
B23	7420	Nightingale 2007	E-1	1	65	44.80	58.24	.	.	1	1
B25	7438	Nightingale 2007	E-1	1	74	71.60	93.08	.	.	1	1
B27	7450	Nightingale 2007	E-1	1	72	56.40	73.32	.	.	1	1
B29	7459	Nightingale 2007	E-1	1	74	66.40	86.32	.	.	1	1
B31	7472	Nightingale 2007	E-1	1	64	60.80	79.04	.	.	1	1

Table F.4. Source data for neck compression.

Specimen #	NHTSA Bio DB Test #	Study	Lab Code	Sex	Age	Peak Extension (Nm)	Peak Flexion (Nm)	Peak Compression (N)	AIS 3+ Injury	AIS 2+ Injury
1	.	Panjabi et al. 1991	C-1	1	61	.	.	3200	0	0
2	.	Panjabi et al. 1991	C-1	1	61	.	.	3100	1	1
3	.	Panjabi et al. 1991	C-1	1	61	.	.	3300	1	1
4	.	Panjabi et al. 1991	C-1	1	61	.	.	3400	1	1
5	.	Panjabi et al. 1991	C-1	1	61	.	.	3500	0	1
6	.	Panjabi et al. 1991	C-1	1	61	.	.	2200	0	1

7	.	Panjabi et al. 1991	C-1	1	61	.	.	2600	0	1
8	.	Panjabi et al. 1991	C-1	1	61	.	.	3100	1	1
14	.	Carter et al. 2002	C-2	0	55	13.7	.	2632	0	1
29	.	Carter et al. 2002	C-2	1	88	80.9	.	5676	0	1
39	.	Carter et al. 2002	C-2	0	76	51.6	.	3094	0	1
41	.	Carter et al. 2002	C-2	1	91	45.6	.	3432	0	1
43	.	Carter et al. 2002	C-2	0	87	40.8	.	3036	0	1
45	.	Carter et al. 2002	C-2	0	88	34.3	.	2566	0	1
47	.	Carter et al. 2002	C-2	1	94	58.8	.	3540	0	1
49	.	Carter et al. 2002	C-2	0	86	56.9	.	3800	0	1
3	.	Carter et al. 2002	C-2	0	70	.	18.1	330	0	1
5	.	Carter et al. 2002	C-2	0	90	.	7	930	0	1
7	.	Carter et al. 2002	C-2	0	53	.	22.6	1073	0	1
8	.	Carter et al. 2002	C-2	0	34	.	23.9	542	0	1
15	.	Carter et al. 2002	C-2	1	50	.	32.2	459	0	1
17	.	Carter et al. 2002	C-2	1	61	.	37.4	486	0	1
27	.	Carter et al. 2002	C-2	0	77	.	13.8	1214	0	1
48	.	Carter et al. 2002	C-2	0	72	.	15.9	1091	0	1
2	.	Carter et al. 2002	C-2	0	78	23.477	.	3447	0	1
10	.	Carter et al. 2002	C-2	1	30	9.748	.	4110	0	1
12	.	Carter et al. 2002	C-2	1	80	8.239	.	2768	0	1
23	.	Carter et al. 2002	C-2	0	69	31.062	.	4180	0	1
28	.	Carter et al. 2002	C-2	0	84	12.704	.	2656	0	1
40	.	Carter et al. 2002	C-2	1	41	13.683	.	4755	0	1
44	.	Carter et al. 2002	C-2	0	67	7.242	.	1988	0	1
46	.	Carter et al. 2002	C-2	1	61	14.013	.	2153	0	1
N02	.	Pintar et al. 1995	C-3	0	62	.	.	3678	1	1
N03	.	Pintar et al. 1995	C-3	0	77	.	.	744	0	1
N04	.	Pintar et al. 1995	C-3	1	50	.	.	5005	0	1
N07	.	Pintar et al. 1995	C-3	1	67	.	.	4580	0	1
N09	.	Pintar et al. 1995	C-3	1	50	.	.	5179	0	1
N20	.	Pintar et al. 1995	C-3	0	29	.	.	2410	1	1
N21	.	Pintar et al. 1995	C-3	1	76	.	.	3699	1	1
N14	.	Pintar et al. 1995	C-3	0	60	.	.	3086	1	1
N17	.	Pintar et al. 1995	C-3	1	66	.	.	2732	0	1
N10	.	Pintar et al. 1995	C-3	1	59	.	.	3744	0	1
N01	.	Pintar et al. 1995	C-3	0	67	.	.	1183	0	1
N08	.	Pintar et al. 1995	C-3	1	48	.	.	3906	0	1
D40	3697	Nightingale et al. 1997	C-4	0	53	.	.	1440	1	1
D41	3695	Nightingale et al. 1997	C-4	1	69	.	.	3885	0	0
I04	.	Nightingale et al. 1997	C-4	1	63	.	.	1698	0	1
I08	3698	Nightingale et al. 1997	C-4	1	80	.	.	2918	1	1
I11	.	Nightingale et al. 1997	C-4	0	63	.	.	972	1	1
I25	.	Nightingale et al. 1997	C-4	1	59	.	.	2574	0	1
I32	.	Nightingale et al. 1997	C-4	1	78	.	.	2612	0	1
N02	3699	Nightingale et al. 1997	C-4	0	75	.	.	793	1	1
N03	4149	Nightingale et al. 1997	C-4	1	75	.	.	3509	1	1
N11	3091	Nightingale et al. 1997	C-4	1	55	.	.	2891	0	0
N13	3092	Nightingale et al. 1997	C-4	0	35	.	.	2079	0	0
N18	3094	Nightingale et al. 1997	C-4	1	.	.	.	1895	1	1
N19	3095	Nightingale et al. 1997	C-4	0	42	.	.	1037	0	1
N22	3097	Nightingale et al. 1997	C-4	1	71	.	.	2120	0	1
N24	3100	Nightingale et al. 1997	C-4	1	62	.	.	1973	0	1
N26	3069	Nightingale et al. 1997	C-4	1	65	.	.	4189	0	0
NA2	3689	Nightingale et al. 1997	C-4	1	61	.	.	2091	0	1
UK3	3691	Nightingale et al. 1997	C-4	1	62	.	.	4084	0	0
S10	.	Maiman et al. 1983	C-5	1	76	.	.	4410	1	1
S13	.	Maiman et al. 1983	C-5	1	84	.	.	2309	0	1
S16	.	Maiman et al. 1983	C-5	1	80	.	.	2936	0	1
S17	.	Maiman et al. 1983	C-5	1	65	.	.	1868	0	1
S19	.	Maiman et al. 1983	C-5	1	61	.	.	1509	0	1
S20	.	Maiman et al. 1983	C-5	1	64	.	.	7439	0	1
S6	.	Maiman et al. 1983	C-5	1	67	.	.	4500	1	1

Table F.5. Data excluded from risk curve development.

Specimen #	Study	Lab Code	Sex	Age	Reason for exclusion
B21	Nightingale et al. 2007	E-1	1	69	Fracture occurred at fixation
B33	Nightingale et al. 2007	E-1	1	69	Fracture occurred at fixation
B35	Nightingale et al. 2007	E-1	1	64	Fracture occurred at fixation
9	Panjabi et al. 1991	C-1	1	61	Pre-extended posture
10	Panjabi et al. 1991	C-1	1	61	Pre-extended posture
N05	Nightingale et al. 1997	C-4	1	36	30 degree impact surface produced non-axial compression
N21	Nightingale et al. 1997	C-4	1	61	30 degree impact surface produced non-axial compression
N23A	Nightingale et al. 1997	C-4	1	46	30 degree impact surface produced non-axial compression
N23B	Nightingale et al. 1997	C-4	1	46	30 degree impact surface produced non-axial compression
Nl3	Pintar et al. 1995	C-3	1	82	Pre-alignment produced non-axial compression
Nl8	Pintar et al. 1995	C-3	1	54	Pre-alignment produced non-axial compression
Nl9	Pintar et al. 1995	C-3	1	76	Pre-alignment produced non-axial compression
Nll	Pintar et al. 1995	C-3	1	59	Pre-alignment produced non-axial compression
N06	Pintar et al. 1995	C-3	0	68	Pre-alignment produced non-axial compression
Nl6	Pintar et al. 1995	C-3	0	64	Pre-alignment produced non-axial compression
N05	Pintar et al. 1995	C-3	0	38	Pre-alignment produced non-axial compression
Nl5	Pintar et al. 1995	C-3	0	95	Pre-alignment produced non-axial compression

APPENDIX G. Lower Extremity Injury Criteria Source Data

Table G.1. Upper tibia source data (Banglmeier et al., 1999).

Tibia Force (kN)	Mass (kg)	AIS 2+ Injury	Age	Tibia Force (kN)	Mass (kg)	AIS 2+ Injury	Age
3.7	59.1	0	83	3.8	59.1	1	83
3.8	65.9	0	82	5.8	65.9	1	82
4.3	102.7	0	48	6	59.1	1	83
4.7	65.9	0	82	6.4	81.8	1	84
5.3	81.8	0	84	6.8	61.4	1	81
5.6	61.4	0	81	7	53.2	1	80
5.8	81.8	0	84	7.5	53.2	1	80
6	69.5	0	72	7.6	69.5	1	72
6	102.7	0	48	7.9	68.2	1	72
6.4	53.2	0	80	8.1	102.7	1	48
6.4	86.4	0	60	8.2	.	1	73
6.6	90.9	0	71	9.7	86.4	1	60
7.5	68.2	0	72	10.8	90.9	1	71
7.8	.	0	73	11.5	100.9	1	63
7.9	100.9	0	63				
9.4	90.9	0	71				

Table G.2. Lower tibia source data.

Study	Tibia Fz (kN)	Height (cm)	Age	Sex	Mass (kg)	AIS 2+ Injury
Yoganandan et al. 1996	2.669	175	27	1	66	0
Yoganandan et al. 1996	10.159	175	27	1	66	0
Yoganandan et al. 1996	2.718	183	46	1	102	0
Yoganandan et al. 1996	11.454	183	46	1	102	1
Yoganandan et al. 1996	11.236	183	46	1	102	1
Yoganandan et al. 1996	4.493	180	27	1	77	0
Yoganandan et al. 1996	9.75	180	27	1	77	1
Yoganandan et al. 1996	6.227	175	55	1	82	0
Yoganandan et al. 1996	8.269	175	55	1	82	1
Yoganandan et al. 1996	2.802	180	27	1	77	0
Yoganandan et al. 1996	9.265	180	27	1	77	1
Yoganandan et al. 1996	7.815	175	55	1	82	1
Yoganandan et al. 1996	6.685	178	60	1	75	1
Yoganandan et al. 1996	5.934	178	60	1	75	1
Yoganandan et al. 1996	10.204	166	64	1	70	1
Yoganandan et al. 1996	2.749	166	64	1	70	0
Yoganandan et al. 1996	4.154	185	50	1	93	0
Yoganandan et al. 1996	7.281	185	50	1	93	0
Yoganandan et al. 1996	6.654	178	67	1	82	1
Yoganandan et al. 1996	5.529	178	67	1	82	1
Yoganandan et al. 1996	6.203	175	27	1	66	0
Yoganandan et al. 1996	7.51	175	27	1	66	0
Yoganandan et al. 1996	0.508	185	74	1	104	0
Yoganandan et al. 1996	1.162	183	58	1	73	0
Yoganandan et al. 1996	4.559	163	67	0	57	1
Yoganandan et al. 1996	4.328	163	67	0	57	1
Begeman et al. 1996	6.11	.	70	1	49	0
Begeman et al. 1996	6.99	.	70	1	49	1
Begeman et al. 1996	6.44	.	68	0	55	0
Begeman et al. 1996	6.88	.	68	0	55	1
Begeman et al. 1996	7.44	.	43	0	69	0
Begeman et al. 1996	8.65	.	43	0	69	1
Begeman et al. 1996	8.03	.	53	0	101	1
Begeman et al. 1996	8.315	.	53	0	101	0

Begeman et al. 1996	8.69	.	53	0	101	1
Begeman et al. 1996	3.43	.	63	1	82	0
Begeman et al. 1996	5.48	.	63	1	82	0
Begeman et al. 1996	4	.	52	0	53	0
Begeman et al. 1996	6.05	.	65	1	93	0
Begeman et al. 1996	5.97	.	63	1	64	0
Begeman et al. 1996	6.84	.	63	1	64	0
Begeman et al. 1996	6.26	.	65	1	69	0
Begeman et al. 1996	7.55	.	59	1	64	0
Kitagawa et al. 1998	7.801	.	68	0	.	1
Kitagawa et al. 1998	8.152	.	68	0	.	0
Kitagawa et al. 1998	8.549	.	69	0	.	1
Kitagawa et al. 1998	7.62	.	69	0	.	1
Kitagawa et al. 1998	7.11	.	59	1	.	1
Kitagawa et al. 1998	7.349	.	59	1	.	1
Kitagawa et al. 1998	7.145	.	75	0	.	1
Kitagawa et al. 1998	7.437	.	75	0	.	1
Kitagawa et al. 1998	7.779	.	83	0	.	1
Kitagawa et al. 1998	7.759	.	83	0	.	1
Kitagawa et al. 1998	6.738	.	69	0	.	1
Kitagawa et al. 1998	5.737	.	69	0	.	1
Kitagawa et al. 1998	8.654	.	75	1	.	1
Kitagawa et al. 1998	8.803	.	75	1	.	1
Kitagawa et al. 1998	9.108	.	70	0	.	1
Kitagawa et al. 1998	7.091	.	70	0	.	1
Funk et al. 2002	4.106	163	67	0	63.6	1
Funk et al. 2002	4.463	178	47	1	52.3	1
Funk et al. 2002	2.574	160	74	0	60	1
Funk et al. 2002	3.827	160	74	0	60	1
Funk et al. 2002	4.685	163	67	0	63.6	1
Funk et al. 2002	7.349	168	42	0	71.4	1
Funk et al. 2002	6.854	170	59	1	47.7	1
Funk et al. 2002	3.221	168	62	0	52.3	1
Funk et al. 2002	4.801	170	59	1	47.7	1
Funk et al. 2002	4.644	168	62	0	52.3	1
Funk et al. 2002	6.334	191	67	1	80.5	1
Funk et al. 2002	5.829	191	67	1	80.5	1
Funk et al. 2002	5.506	188	65	1	84.1	1
Funk et al. 2002	5.824	188	65	1	84.1	1
Funk et al. 2002	5.185	175	67	1	70.5	1
Funk et al. 2002	6.248	175	67	1	73.6	1
Funk et al. 2002	9.312	173	57	1	74.5	1
Funk et al. 2002	3.912	178	72	0	66.8	1
Funk et al. 2002	8.606	173	62	1	75.9	1
Funk et al. 2002	7.486	163	74	0	78.2	1
Funk et al. 2002	5.577	160	41	0	89.5	1
Funk et al. 2002	5.875	163	74	0	78.2	1
Funk et al. 2002	8.87	173	62	1	75.9	1
Funk et al. 2002	5.525	170	71	1	87.7	1
Funk et al. 2002	2.846	157	65	0	46.8	1
Funk et al. 2002	4.302	145	69	0	57.3	1
Funk et al. 2002	10.837	178	51	1	84.1	1
Funk et al. 2002	2.94	157	65	0	46.8	1
Funk et al. 2002	3.835	145	69	0	57.3	1
Funk et al. 2002	10.55	178	51	1	84.1	1
Funk et al. 2002	2.205	163	67	0	63.6	0
Funk et al. 2002	5.887	160	63	0	55.9	0
Funk et al. 2002	5.263	175	67	1	70.5	0
Funk et al. 2002	4.159	175	67	1	73.6	0

Table G.3. Bending moment source data.

Study	Test #	Sex	Moment (Nm)	Mass (kg)
Nyquist et al. 1985	116	M	176	57
Nyquist et al. 1985	117	M	326	68
Nyquist et al. 1985	118	M	395	68
Nyquist et al. 1985	121	F	302	53
Nyquist et al. 1985	122	F		53
Nyquist et al. 1985	123	M	453	82
Nyquist et al. 1985	124	M	287	82
Nyquist et al. 1985	125	M	182	73
Nyquist et al. 1985	126	M	224	73
Nyquist et al. 1985	127	M	237	79
Nyquist et al. 1985	128	M	312	99
Nyquist et al. 1985	129	M	349	99
Nyquist et al. 1985	132	M	264	45
Nyquist et al. 1985	133	M	402	45
Nyquist et al. 1985	134	M	287	57
Nyquist et al. 1985	135	M	324	84
Nyquist et al. 1985	145	M	424	79
Nyquist et al. 1985	146	F	315	75
Nyquist et al. 1985	147	M	431	84
Nyquist et al. 1985	148	F	254	75
Nyquist et al. 1985	152	F	274	68
Nyquist et al. 1985	153	F	246	68
Schreiber et al. 1998	48-R	M	205*	61.3
Schreiber et al. 1998	1001-L	M	212*	58.9
Schreiber et al. 1998	73-R	F	213*	57.2
Schreiber et al. 1998	48-L	M	239	61.3
Schreiber et al. 1998	73-L	F	242	57.2
Schreiber et al. 1998	1002-R	F	259	57.9
Schreiber et al. 1998	74-L	F	266*	50.3
Schreiber et al. 1998	50-L	F	319*	46.7
Schreiber et al. 1998	1006-L	F	329*	80.4
Schreiber et al. 1998	50-R	F	371	46.7
Schreiber et al. 1998	1006-R	F	372	80.4
Schreiber et al. 1998	1004-L	F	388*	59.9
Schreiber et al. 1998	1000-L	M	388*	104
Schreiber et al. 1998	68-R	M	424	72.6
Schreiber et al. 1998	1010-R	F	440	73.9
Schreiber et al. 1998	1005-R	M	445	73.6
Schreiber et al. 1998	1000-R	M	458	105
Schreiber et al. 1998	1003-L	M	482*	69.5
Schreiber et al. 1998	69-R	M	534	90.3
Schreiber et al. 1998	1004-R	F	535	59.9
Schreiber et al. 1998	1003-R	M	577	69.5
Untariou et al. 2008	.	.	171	.
Untariou et al. 2008	.	.	173	.
Untariou et al. 2008	.	.	193	.
Untariou et al. 2008	.	.	196	.
Untariou et al. 2008	.	.	198	.
Untariou et al. 2008	.	.	213	.
Untariou et al. 2008	.	.	238	.
Untariou et al. 2008	.	.	241	.
Untariou et al. 2008	.	.	242	.
Untariou et al. 2008	.	.	246	.
Untariou et al. 2008	.	.	267	.
Untariou et al. 2008	.	.	273	.
Untariou et al. 2008	.	.	276	.
Untariou et al. 2008	.	.	286	.
Untariou et al. 2008	.	.	320	.
Untariou et al. 2008	.	.	320	.
Untariou et al. 2008	.	.	320	.
Untariou et al. 2008	.	.	324	.

Untariou et al. 2008	.	.	333	.
Untariou et al. 2008	.	.	333	.

*Not used in risk function formulation due to unknown equivalent moment from axial load

APPENDIX H. Field Data Charts

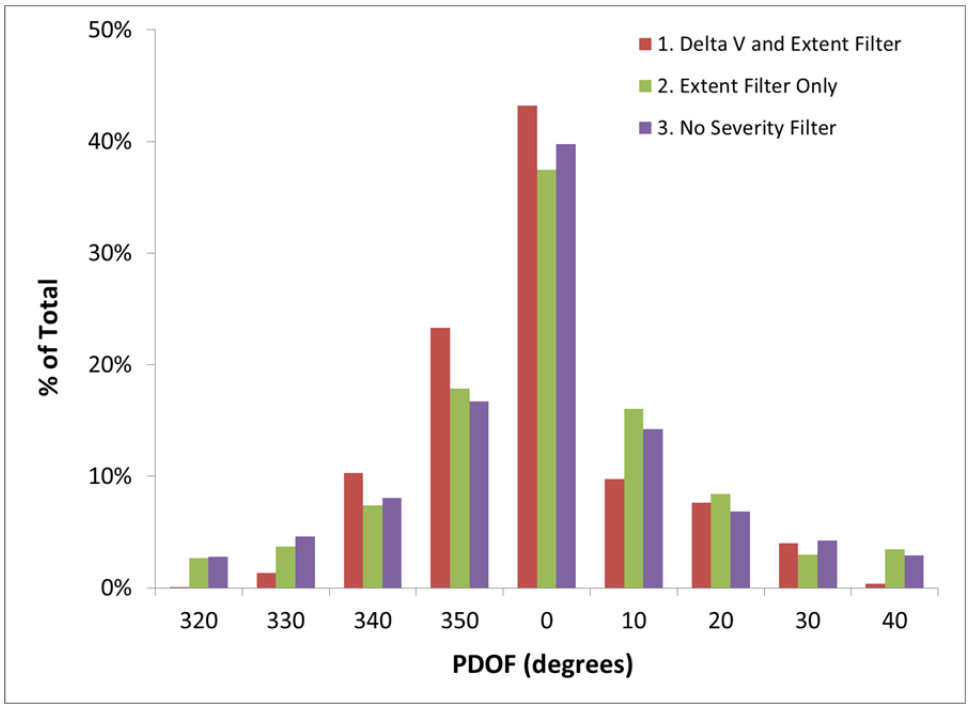

Figure H.1. PDOF for frontal crashes in 2000-2014 NASS-CDS using same filters as used for Table 9.3.

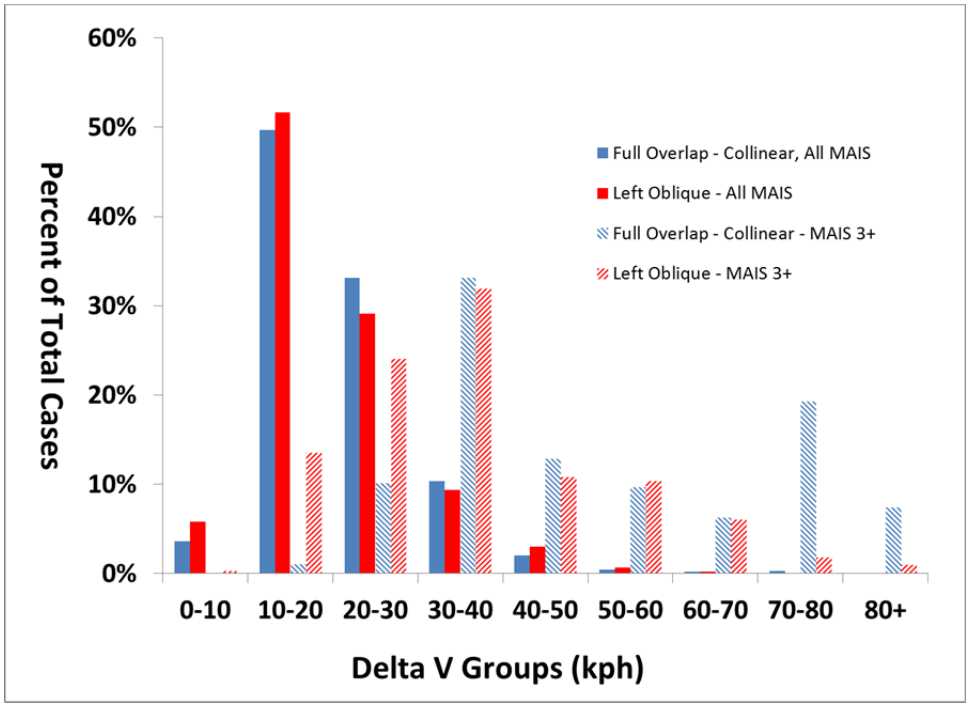

Figure H.2. Delta V distribution for different frontal crash types.

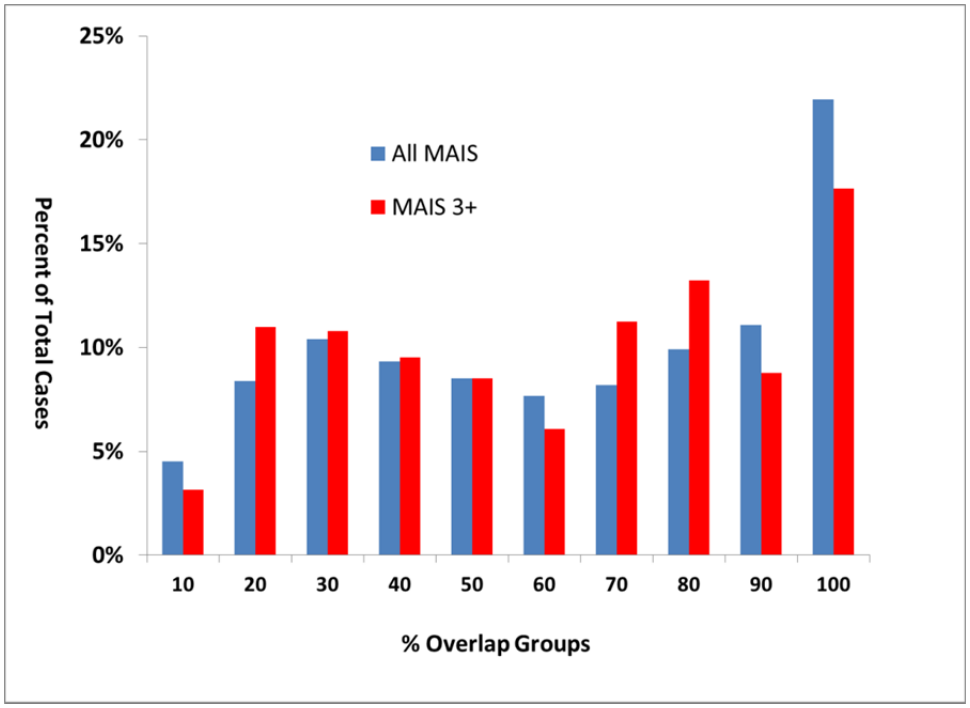

Figure H.3. Percent overlap for frontal crashes.

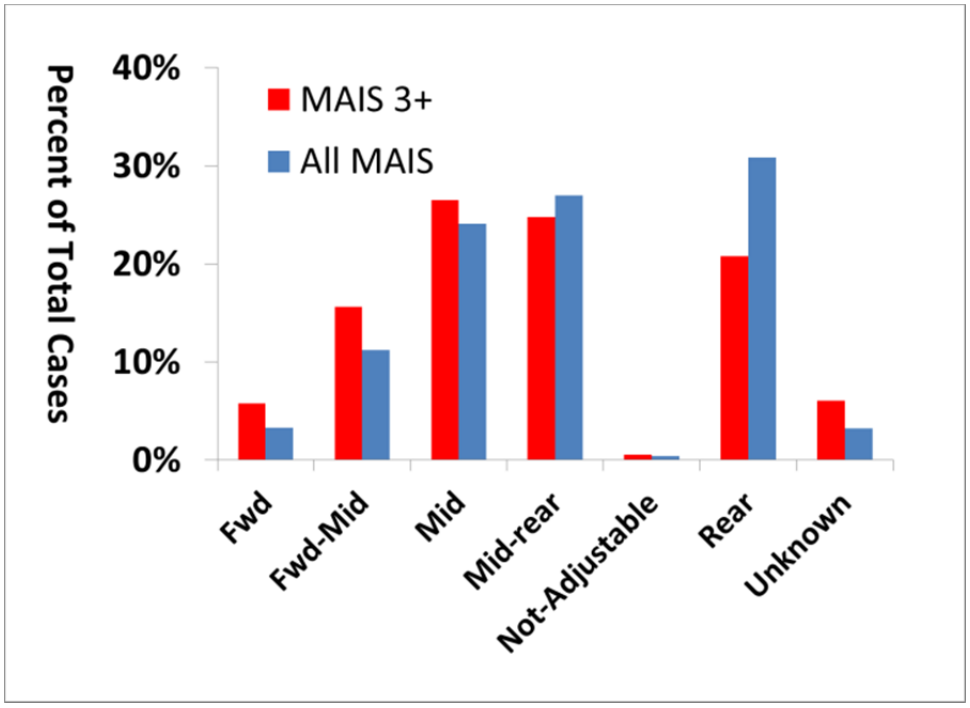

Figure H.4. Driver seat track position in frontal crashes, NASS-CDS 2000-2014.

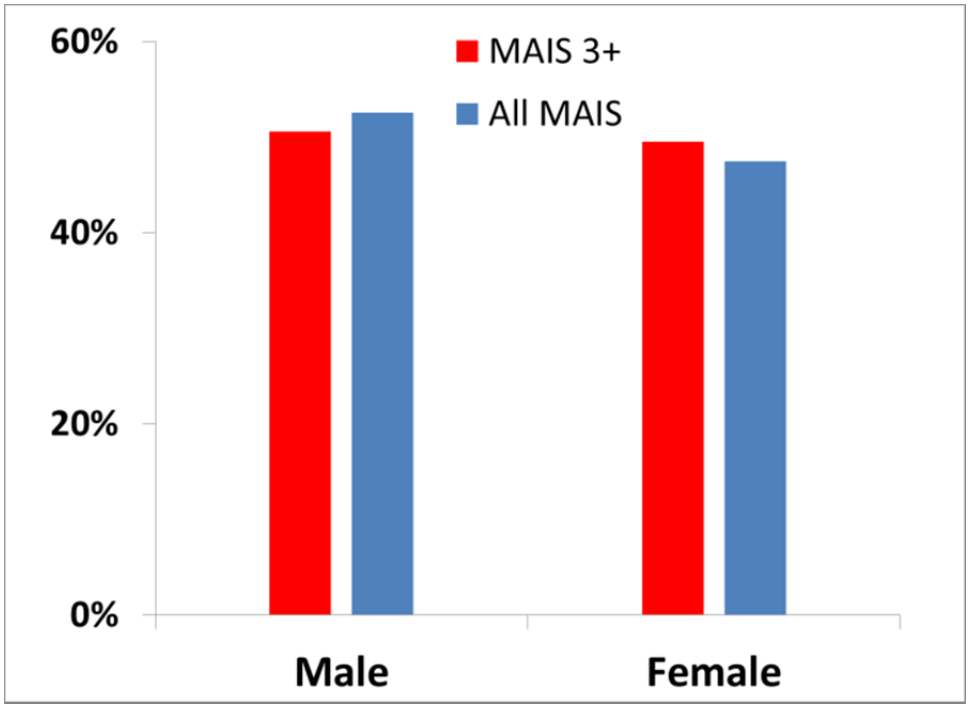

Figure H.5. Driver gender in frontal crashes, NASS-CDS 2000-2014.

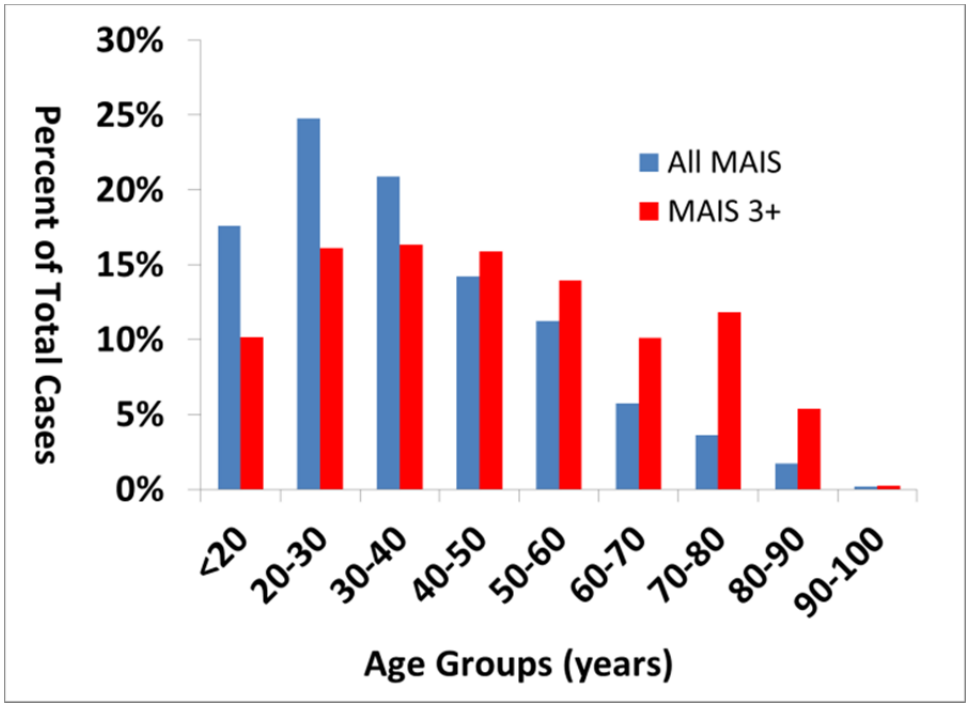

Figure H.6. Driver age in frontal crashes, NASS-CDS 2000-2014.

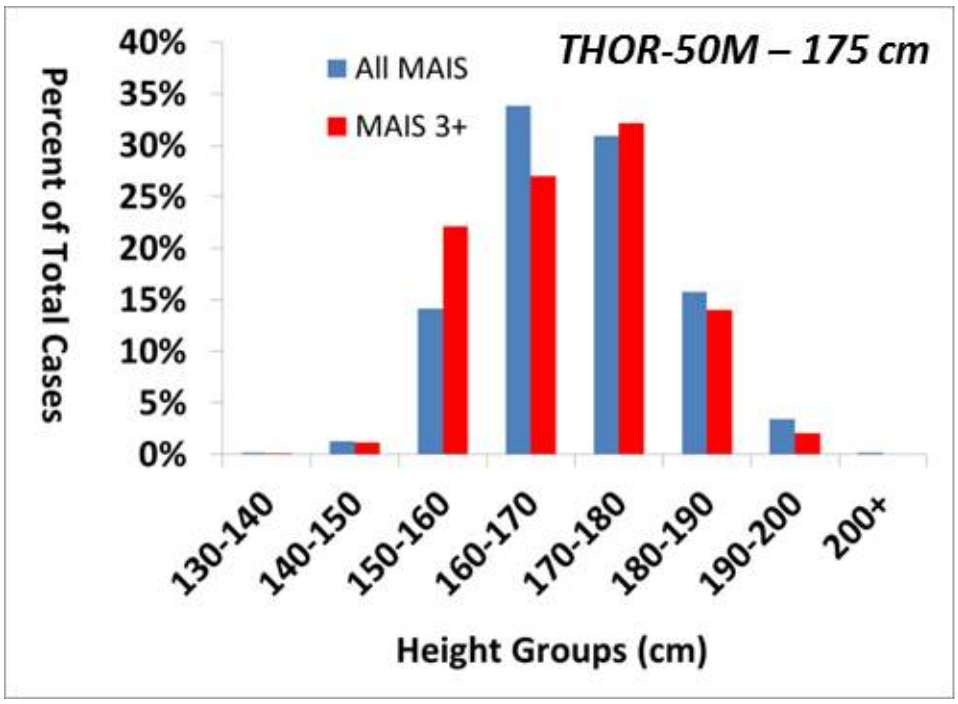

Figure H.7. Driver height in frontal crashes, NASS-CDS 2000-2014.

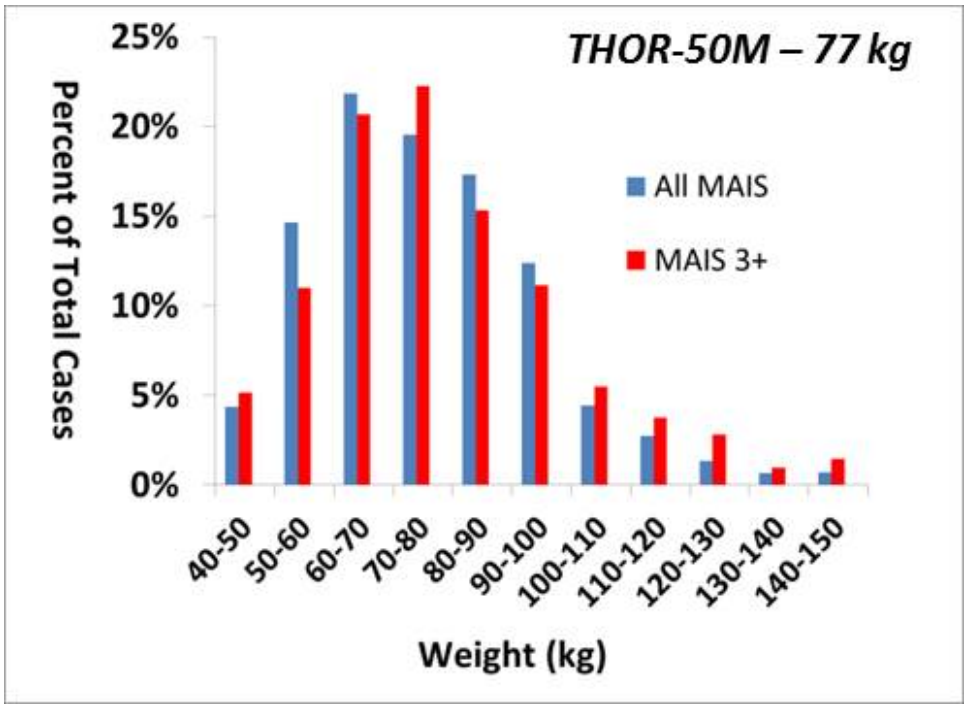

Figure H.8. Driver weight in frontal crashes, NASS-CDS 2000-2014.

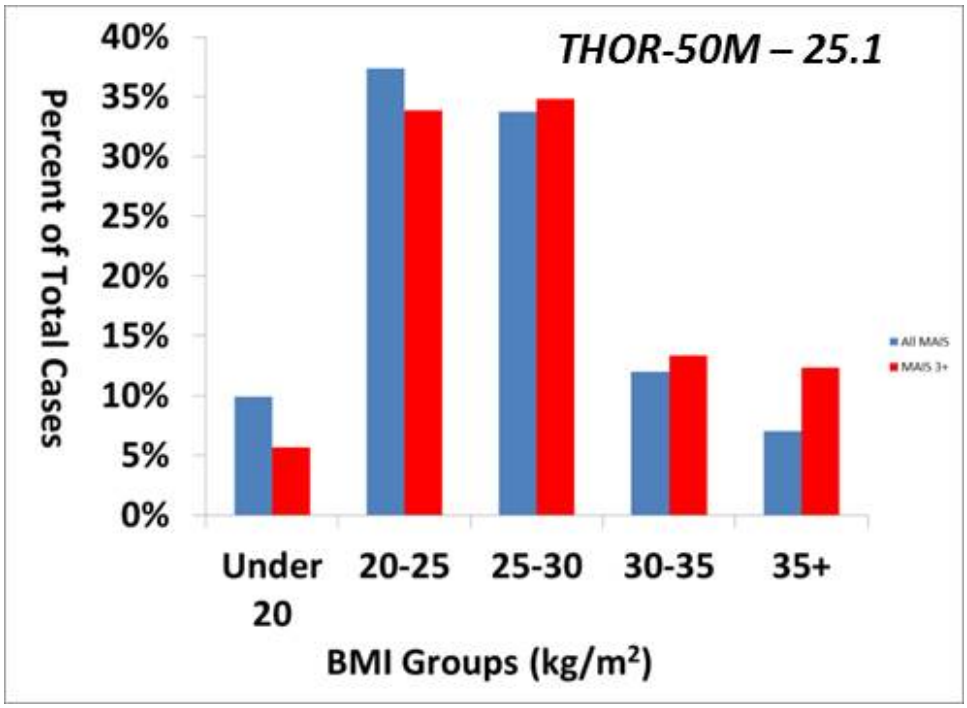

Figure H.9. Driver BMI in frontal crashes, NASS-CDS 2000-2014.